CARBON NANOTUBE THIN FILMS AS FLEXIBLE SUBSTRATES FOR THE SUPPORT OF INORGANIC NANOSTRUCTURES

CARBON NANOTUBE THIN FILMS AS FLEXIBLE SUBSTRATES FOR THE SUPPORT OF INORGANIC NANOSTRUCTURES

By

GREGOR LAWSON

M.Sc. (University of Strathclyde, Glasgow) 2004

A Thesis

Submitted to the School of Graduate Studies

In Partial Fulfillment of the Requirements

For the Degree of

Doctor of Philosophy

in

Chemistry

McMaster University

DOCTOR OF PHILOSOPHY (2010) McMASTER UNIVERSITY

(Chemistry) Hamilton, Ontario

TITLE:	Carbon Nanotube Thin Films as Flexible Substrates for the Support of Inorganic Nanostructures
AUTHOR:	Gregor Lawson, M.Sc. (University of Strathclyde, Glasgow)
SUPERVISOR:	Professor Alex Adronov
NUMBER OF PAGES:	xxiii, 229

Abstract

Carbon nanotubes (CNTs) are arguably the most widely studied material within the field of nanotechnology. The impressive physical and electronic properties of these materials have led to their investigation in a diverse range of applications. In recent years, the deposition of inorganic nanoparticles upon the surface of CNTs has received much attention. Research within this field has been driven by the desire to develop new composite materials exhibiting novel electronic, optical, and catalytic properties. In addition to the decoration of individual nanotubes, several groups have also investigated the use of CNT thin films as scaffolds for the assembly of inorganic nanostructures as well as other secondary components, including polymers and biomaterials. Nanotube films exhibit a number of physical properties that make them suitable for such applications, displaying impressive electrical conductivity, flexibility, and thermal stability while also possessing a high surface area upon which chemical modification can be conducted.

This thesis presents work that demonstrates the potential of CNT thin films as flexible conductive scaffolds for the support of a variety of inorganic nanostructures. Procedures are described for the preparation of SWNT-Au nanoparticle composite films that, as subsequently demonstrated, are suitable substrates for the growth of III-V semiconductor nanowires using gas-source molecular beam epitaxy. At the time of writing, the majority of published research within this field focused upon the preparation of SWNT composite films containing spherical metallic or semiconductor nanoparticles. In contrast, the growth of semiconductor nanowires upon nanotube thin films had not been explored. The work described in this thesis therefore represents the development of a novel composite material that combines the flexibility of CNT films with the unique optoeletronic properties exhibited by semiconductor nanowires. The development of functional electronic devices incorporating these materials is also discussed, as is the extension of the methods developed to investigate novel composite materials that combine other inorganic nanostructures with carbon based substrates.

Acknowledgements

There have been many people at McMaster University who have been instrumental to my success in the PhD program. First, I would like to thank my supervisor Dr. Alex Adronov for his ongoing guidance and encouragement. I am extremely grateful for all the opportunities that he has provided by accepting me as a student within his research group.

Special thanks to the members of my committee, Dr. Harald Stöver and Dr. Robert Pelton, for their insight and helpful contributions to my research, as well as to Dr. Brian McCarry for his interest and advice.

The work presented in this thesis would not have been possible were it not for the contributions and assistance of many hard-working and talented individuals. I would like to thank all of the researchers with whom I have had the privilege of collaborating: Dr.Michael Brook, Dr. Ferdinand Gonzaga, Dr. Ray LaPierre, Parsian Mohseni, Dr. Geoffrey Ozin, and Jordan Thomson. I would also like to acknowledge all of the facilities staff at McMaster, particularly Frank Gibbs, Steve Kornic, Brad Robinson, Glynis de Silveira, Chris Butcher, Julia Huang, Fred Pearson and Steve Koprich, who all went over and above the call of duty in helping me with my work.

Thank you to all the members of the Adronov group, both past and present, for their support and advice over the last five years. In particular I would like to acknowledge Greg Bahun, Matt Parrott and Rahima Benhabbour, who quickly brought me up to speed when I arrived at McMaster, and helped to prepare me for life in graduate school. I would also like to thank members of the Brook, Stöver, Vargas-Baca and Saravanamuttu groups

for their help and friendship, which made my time in the PhD program all the more enjoyable.

On a personal note, I would like to thank my parents, Bob and Evelyn Lawson, my brother, Malcolm, the Thompson family and last but not least my fiancé, Laura. I am grateful for their continued support.

Table of Contents **Page**

Chapter 2: Au–carbon nanotube composites from self-reduction of Au^{3+} upon poly(ethylene imine) functionalized SWNT thin films 60

Chapter 5: Growth of III-V Semiconductor NWs upon Highly Ordered Pyrolytic Graphite 143

List of Figures and Schemes

List of Figures **Page**

Chapter 1: Overview of carbon nanotube chemistry, thin film fabrication and applications 1

Chapter 2: Au–carbon nanotube composites from self-reduction of Au^{3+} upon poly(ethylene imine) functionalized SWNT thin films 60

List of Schemes Page

List of Tables Page

List of Abbreviations

ATRP	Atom Transfer Radical Polymerization
CNT	Carbon Nanotube
CVD	Chemical Vapour Deposition
DCM	Dichloromethane
DMF	Dimethyl Formamide
DNA	Deoxyribonucleic Acid
DTAB	Dodecyltrimethyl Ammonium Bromide
EBSD	Electron Backscatter(ed) Diffraction
EDXS	Electrodispersive X-ray Spectroscopy
EPD	Electrophoretic Deposition
FIB	Focused Ion Beam
GO	Graphene Oxide
GS	Gas Source
HA	Hydroxyapetite
HAADF	High Angle Annular Dark Field
HiPCO	High-Pressure Carbon Monoxide
HOPG	Highly Ordered Pyrolytic Graphite
LbL	Layer-by-Layer
LED	Light Emitting Diode
ITO	Indium-Tin-Oxide

List of Abbreviations (Continued)

MBE	Molecular Beam Epitaxy
MCC	Molecular Metal Chalcogenide
MOCVD	Metal Organic Chemical Vapour Deposition
MWNT	Multi-Walled Carbon Nanotube
NMP	Nitroxide Mediated Radical Polymerization
NP	Nanoparticle
NW	Nanowire
PABS	Poly-*m*-Aminobenzene Sulfonic Acid
PDDA	Poly(diallyldimethylammonium chloride)
PDMS	Polydimethyl Siloxane
PE-CVD	Plasma-Enhanced Chemical Vapor Deposition
PEI	Polyethylene Imine
PET	Poly(ethylene terephthalate)
PL	Photoluminescence
PSS	Polystyrene Sulfonate
PTFE	Polytetrafluoroethylene
PV	Photovoltaic
PVP	Polyvinylpyrrolidone
PXRD	Powder X-Ray Diffraction
RAFT	Reversible Addition Fragmentation Chain-Transfer Polymerization

List of Abbreviations (Continued)

RIE	Reactive Ion Etching
RTA	Rapid Thermal Anneal
SAD	Selective Area Diffraction
SDBS	Sodium Dodecyl Benzeze Sulfonate
SDS	Sodium Dodecyl Sulfate
SEM	Scanning Electron Microscopy
SEED	Substrate-Enhanced Electroless Deposition
SWNT	Single-Walled Carbon Nanotube
TEM	Transmission Electron Microscopy
TGA	Thermogravimetric Analysis
THF	Tetrahydrofuran
VLS	Vapour-Liquid-Solid
VSS	Vapour-Solid-Solid
XPS	X-ray Photoelectron Spectroscopy
YAG	Yttrium Aluminium Garnet
ZB	Zinc Blende

Chapter 1: Overview of carbon nanotube chemistry, thin film fabrication and applications

Abstract

Carbon nanotubes (CNTs) are perhaps the most widely researched material within the field of nanotechnology. The impressive and unique physical properties of CNTs has led to their investigation in a wide range of applications, including the development of high performance composites, synthetic biomaterials, photovoltaic devices and light emitting diodes. This work has been enabled, in part, by the rich and varied chemistry that has been developed for the modification of CNTs. Attachment of small molecules and polymers to the surface of nanotubes, using both covalent and non-covalent approaches, has been shown to aid the efficient dispersion of these materials within both aqueous and organic solvents. Consequently, homogeneous thin films of CNTs can be fabricated using a variety of low-cost solution based techniques such as spin casting, spray coating, and vacuum filtration. The high aspect ratio of CNTs enables the preparation of films which are conductive despite being thin enough to allow optical transparency. Additionally, films are highly flexible, have a large surface area, and exhibit excellent stability towards both high temperatures and chemical treatment. This unique combination of properties makes CNT thin films excellent candidates for investigation as structural supports for the assembly of secondary materials, such as polymers, biomaterials and inorganic particles.

1.1. Introduction

1.1.1. Allotropes of carbon

Carbon is the 15th most abundant element in earth's crust and 2nd most abundant within the human body. The stability of carbon-carbon bonding, and consequent catenation properties of carbon, is the foundation that supports the construction of large organic molecules in nature from which all life on our planet is composed. Carbon can exist in several allotropic forms, the structure and bonding of which influence both the physical properties and chemical reactivity of the bulk materials. The most common allotropes of carbon are naturally occurring amorphous carbon, graphite and diamond. Additionally, newer allotropes, in the form of fullerenes and carbon nanotubes, have been discovered relatively recently, and can be prepared via synthetic methods.

Graphite is the most thermodynamically stable form of carbon at regular temperatures and atmospheric pressure. The ideal structure of graphite consists of sheets of sp^2 hybridized carbon atoms arranged in a planar hexagonal lattice, such that each carbon atom is bonded to three others. The fourth valence electron of each carbon atom is delocalized through the extended π conjugated network of the planar lattice giving rise to conductivity in the direction of the basal plane. Within graphite, sheets are layered in ABAB (α-graphite) or ABCABC arrangements (β-graphite). Spacing between carbon atoms in consecutive layers (3.35 Å) is greater than that within the hexagonal lattice (1.42 Å). This structural anisotropy is reflected by the physical properties of graphite, including mechanical strength, electrical conductivity and thermal conductivity. Graphite can, for example, be readily cleaved parallel to the direction of the basal plane, while force applied perpendicular may result in cracking or delamination of layers.

In diamond all carbon atoms are sp^3 hybridized, with each atom bonded to four nearest neighbours in a tetrahedral arrangement that yields a cubic unit cell. All carbon-carbon bonds within the crystal are equivalent (1.54 Å). The high strength of these bonds is reflected in the properties of diamond, which exhibits the highest hardness of any known bulk material. Unlike graphite, diamond contains no delocalized electrons and exhibits negligible conductivity. Longsdaleite is a lesser known allotrope of carbon that has been found to exist in nature. Longsdaleite exhibits a structure similar to diamond in which each carbon atom is bonded to four others in a tetrahedral arrangement. These tetrahedral units are however layered in such a way as to produce a hexagonal wurtzite type lattice as opposed to a cubic lattice structure.

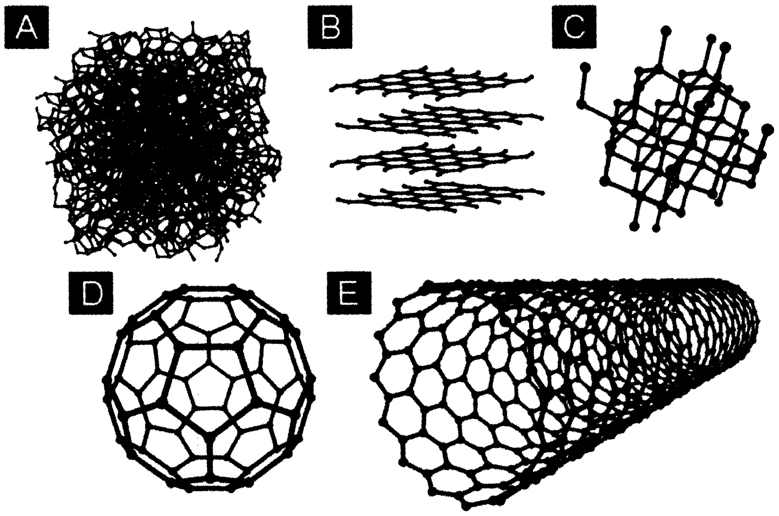

Figure 1.1. Allotropes of carbon; (A) amorphous carbon, (B) α-graphite, (C) diamond, (D) fullerenes (C_{60}), (E) carbon nanotubes.[1]

Table 1.1. Physical and structural properties of diamond and α-graphite[2]

Property	α-Graphite	Diamond
C-C bond length / Å	1.42	1.54
Density /g cm	2.266	3.514
Hardness / Mohs	< 1	10
MP / K	4100 ±100 (at 9 kbar)	4100 ±100 (at 200 kbar)
Refractive Index, *n* (546 nm)	2.15 (basal), 1.81 (c-axis)	2.41
P / Ohm cm	~ 0.4×10^{-5} (basal), ~ 0.2 (c-axis)	~ 10^{15}

1.1.2. Fullerenes

In 1985, the discovery of a new allotrope of carbon, C_{60}, was reported by a group of researchers at Rice University, led by Harry Kroto and Richard Smalley.[3] It was shown that vaporization of graphite using laser irradiation or electric arcs under helium flow resulted in the formation of polyhedral carbon clusters composed of an even number of atoms. The most stable of these was C_{60}, the structure of which was determined to be a hollow sphere 6.83 Å in diameter where the carbon framework of the molecule is comprised of 20 six-membered rings and 12 five-membered rings, similar to a soccer ball. Here, it is the curvature, introduced by the presence of five-membered rings that enables the formation of a spherical closed cage. Other structurally similar compounds were subsequently isolated, including C_{70} and C_{90}. This new family of molecular carbon compounds was given the name fullerenes, due to their resemblance to geodesic dome structures commonly associated with the designs of American architect Richard Buckminster Fuller. Methods for gram scale synthesis of fullerenes, and their separation by chromatographic methods, were subsequently developed[4-6] enabling commercial production and initiating an almost unprecedented surge of research. In 1996 Smalley, Kroto and Curl received the Noble Prize in Chemistry for the discovery of fullerenes and the determination of their structure, recognizing the tremendous impact that this work had made upon modern science.

One property of fullerenes that sets them aside from other more common allotropes of carbon is their reactivity. The widespread study of fullerenes and examination of their potential in a diverse range of fields including as photovoltaics, organic electronics[7] and biomedicinal applications,[8, 9] has been facilitated in part, by the wealth of reactions that may be conducted upon these molecules. The spherical shape of fullerenes induces a considerable amount of strain and fullerenes are consequently less thermodynamically stable than planar graphite. The non-planar nature of fullerenes does not permit carbon atoms to exist in true sp^2 hybridization. The π orbitals of fullerenes therefore exhibit partial s character, making fullerenes somewhat electronegative.[10] Covalent derivatization of fullerenes has been demonstrated using a wide variety of procedures including nucleophilic and radical addition reactions, cycloaddition reactions, halogenation, hydrogenation and metal complex formation.[10-12] The π system of fullerenes is also known to interact strongly with other aromatic molecules allowing supramolecular functionalization with a variety of materials.[13]

1.1.3. Carbon nanotubes

Carbon nanotubes (CNTs), the ‘newest’ or most recently discovered allotrope of carbon, are arguably the most widely studied materials within the field of nanotechnology. The structure of CNTs resembles a graphene sheet that has been rolled so that the edges connect forming a hollow cylinder, each end of which is capped by a hemispherical half fullerene structure.[14, 15] There has been some discussion as to when CNTs were first discovered and by whom.[15-17] In the majority of literature, the first reported synthesis is credited to Iijima[18, 19] who, in a paper published in 1991,[18] described the preparation of CNTs by electric-arc vapourization of graphite in the presence of a metal catalyst. Thirteen years earlier however in 1978 Wiles and Abrahamson reported the observation that carbon fibres, 4 nm in diameter, formed upon a graphite electrode following low current arcing under a nitrogen atmosphere. These fibers were subsequently characterized, and shown to exhibit a structure similar to what we now call CNTs.[20] Similar descriptions of high aspect ratio carbon fibers were also reported by Oberlin and Endo in work published in 1976.[21] With this in mind, it does not seem accurate to refer to Iijma's work as the 'first discovery'. Nonetheless, Iijama does deserve the credit for determining the structure of CNTs, popularizing CNT research, and drawing the attention of researchers worldwide to these remarkable materials.

CNTs exist in one of two varieties; single-walled CNTs (SWNTs), which exhibit the basic structure described with diameters ranging from 0.7 to 2 nm, and multi-walled CNTs (MWNTs), which contain several concentric cylinders. The internal diameter of MWNTs is approximately 5 nm while the external diameter is dependant upon the number of concentric tubes present and can be as large as 100 nm. Spacing between tubes in MWNTs is approximately equal that of the interlayer spacing of sheets in bulk graphite (3.41Å). Over the years, several techniques have been developed for the gram scale synthesis of CNTs including arc-discharge, laser ablation, chemical vapour deposition and high pressure gas-phase methods.[15,22] The structure, length and diameter of CNTs varies depending upon the method used for synthesis as well as additional factors, including the nature of the carbon source and the metal catalyst employed. Current commercial techniques for nanotube synthesis allow the production of both single-walled and multi-walled varieties with lengths ranging from several microns up to the centimetre scale.

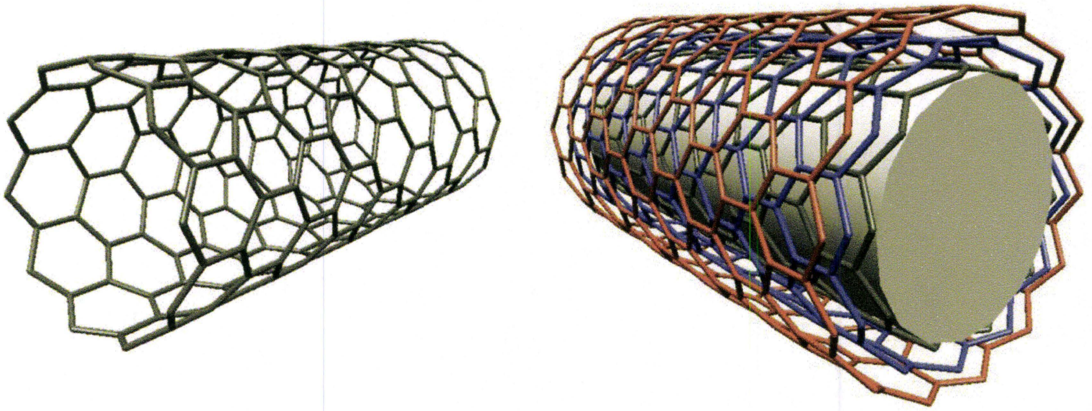

Figure 1.2. Schematic showing the structure of a SWNT (left) and MWNT (right). The innermost tube of the MWNT has been filled for the purposes of visual clarity.

1.1.3.1. Properties of CNTs

Since the publication of Iijima's paper in 1991, the field of nanotube research has expanded at an incredible rate.[15, 23] Today, this research encompasses almost every facet of modern science, from fundamental investigations of structure-property relationships, to the development of advanced CNT based devices.[23-29] The primary driving force behind this research is the unique fundamental properties of CNTs, which have captured the attention of researchers working in a wide variety of disciplines from chemistry and physics to engineering, materials science, and medicine. CNTs are, for example, amongst the strongest materials ever reported. They exhibit a Young's modulus of 1.2 TPa and a tensile strength that is approximately 100 times that of steel.[14] Additionally, CNTs have a very low density (~1.4 g cm^{-3}). This combination of properties makes CNTs ideal candidates as reinforcing agents in polymers, and the development on nanotube composites has accordingly been widely studied.[15, 30-32] Nanotubes also exhibit a high specific surface area, high aspect ratio, impressive electrical properties, flexibility, and stability to both high temperatures and chemical treatment.

Table 1.2. Properties of single-walled carbon nanotubes[30]

Property	
Diameter / nm	0.7 - 2
Young's Modulus / TPa*	0.32 – 1.47
Tensile Strength / GPa	63
Resistivity / μOhm cm **	0.1-100
Thermal Conductivity / W/m K***	35 – 200
Density / g cm^{-3}	~1.4
Cost / $ (US) g^{-1}	~200

* diameter dependent ** chirality dependent *** strongly affected by bundling

With regard to electrical properties[33-37] CNTs can be either metallic, semiconducting or low bandgap semiconductors. The specific properties of an individual nanotube is dependent upon both the tube diameter and chirality, a term that refers to the orientation of the hexagonal carbon lattice structure with respect to the tube circumference. The chirality of a CNT can be classified in reference to a 2D planar graphene sheet, as shown in Figure 1.3. Here, a lattice vector, $C = (ma_1 + na_2)$, can be defined that joins any two chosen atoms on the planar sheet, where a_1 and a_2 are the two vectors of the graphene unit cell ($a_1 = a_2 = 2.461$ Å) and m and n are integers defining the magnitude of the lattice vector. A chiral angle (θ), associated with this vector can be similarly defined. If the graphene sheet is rolled in such a way that the two ends of the lattice vector connect, then the circumference of a nanotube is formed. Individual CNTs can therefore be identified using lattice vector indices (m,n), which provide information regarding both the chirality and diameter of the tubes.[38]

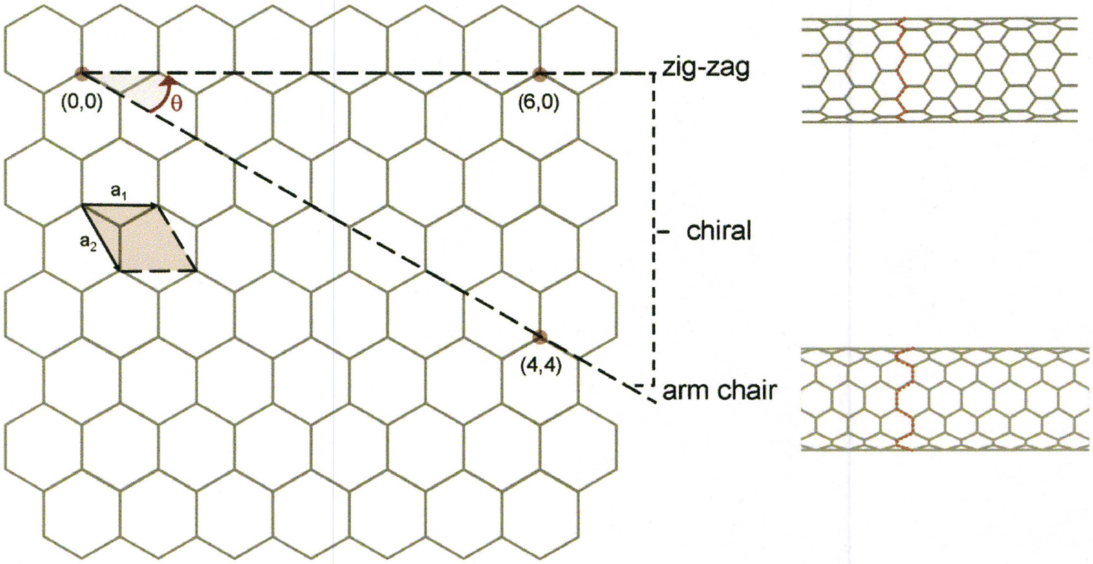

Figure 1.3. Schematic showing a hexagonal graphene lattice and lattice vectors used to define the chirality of CNTs

When both indices are equal in value ((m, m), (θ = 0º)), the resulting nanotubes are termed 'armchair tubes' due to the arrangement of carbon atoms around the tube's circumference. These tubes are known to exhibit metallic conductivity, a property that results from efficient overlap of electronic states along the length of the tube's axis. In contrast, (m, 0) nanotubes, for which θ = 30º are referred to as 'zig-zag' tubes. Overlap of electronic states is less efficient for this conformation and the resulting nanotubes behave as low band-gap semiconductors. Both 'arm-chair' and 'zig-zag' structures are achiral, having at least one rotational axis of symmetry. For all other indices ($0° < \theta < 30°$), chiral nanotubes are formed, and these also exhibit semiconductor behaviour.[14]

At present, all known methods of nanotube synthesis yield samples with some variation in diameter, length, and chirality. Commercial samples of CNTs therefore typically contain a mix of both metallic and semiconducting tubes. This has been problematic in applications that require nanotubes exhibiting specific electronic properties. Methods for the efficient purification of CNTs and sorting of nanotube chiralities are therefore highly desirable and have been studied by a number of groups. Recent advances, using methods such as ultracentrifugation,[39-47] show promise in allowing the separation of nanotubes by chirality. Commercial availability of specific nanotube chiralities that can be selected to suit specific niche applications recently became a reality and will no doubt become more widespread as this technology matures.

1.1.3.2. Challenges within the field of CNT research

If the full potential of CNTs is to be developed there are several challenges that must first be overcome. Perhaps the greatest of these relates to the purity of commercially available nanotube samples. At present, CNTs purchased from commercial suppliers contain a number of impurities that result from the methods used for their production. These include carbon based byproducts, such as amorphous carbon and fullerenes, as well as metallic nanoparticles (NPs), which are employed as catalysts during nanotube synthesis. A number of procedures have been developed for the purification of CNTs, although typically these involve the use of harsh oxidative treatments that can damage the nanotube structure and diminish the very properties researchers would hope to exploit. The improvement of nanotube purity, through modification of synthesis techniques and development of milder non-destructive post synthetic treatments currently remains a subject of ongoing research. CNTs are also quite expensive. At the time of writing, the cost of SWNTs was approximately $200 / g, approximately 5.6 times that of gold. If CNT based technology is to become commercialized to the extent that has been predicted, new lower-cost methods for CNT production will also be required.

1.1.3.3. Chemical functionalization of CNTs

Another problem that any researcher working with CNTs will undoubtedly encounter is their absolute lack of solubility in practically all organic and aqueous solvents. Unmodified CNTs form large bundles that are held together by Van der Waals interactions, originating from the tube's extended pi-conjugated framework.[15, 48] This impedes the homogeneous dispersion of CNTs within solution and throughout host materials. The effects of bundling upon the processability of CNTs is a significant issue, especially when considering the potential commercialization of nanotube based technology. Fortunately, many developments have been made in recent years that utilize chemistry to overcome the problem of CNT dispersability.[48-51] Modification of CNTs with small molecules and polymers, through supramolecular attachment and covalent sidewall coupling, has been shown to allow the formation of stable dispersions of carbon nanotubes in aqueous and organic solvents allowing for effective solution phase processing and incorporation within composite materials.[52]

Within literature, the behaviour of modified carbon nanotubes in various solvents is commonly described in terms of solubility. A solution is however technically defined as a thermodynamically stable mixture containing two or more components within a single phase. As some of the techniques utilized for the modification of carbon nanotubes yield not only individual nanotubes but also nanotube bundles modified solely upon their exterior, and covalently crosslinked nanotubes, the use of the term solubility to describe the interaction of these materials with a solvent phase is not truly accurate. Such materials may be better described as colloidal dispersions, where the dispersed phase consists of modified nanotube bundles or nanotube-polymer aggregates. Certain modification techniques, such as the non-covalent functionalization of carbon nanotubes with conjugated polymers (described in section 1.1.3.4.2) are however highly efficient in enabling the debundling of carbon nanotubes. The use of these techniques, in combination with high speed centrifugation, can produce mixtures containing primarily individual debundled nanotubes dispersed homogeneously within a solvent phase. These materials could therefore be viewed as solutions rather than colloidal dispersions.

1.1.3.3.1. Covalent approaches

In CNT chemistry, covalent functionalization refers to any process by which the chemical structure of CNTs is altered to introduce a small molecule, polymer or functional group. Initial work within this field, reported by Haddon and Smalley, involved the use of oxidative treatment to introduce carboxylic acid groups to the tubes surface.[53, 54] When exposed to strong oxidative conditions, such as refluxing in nitric acid, defect sites can be introduced to the structure of CNTs. These can take several forms, including the opening of end caps or generation of holes within the nanotube sidewall. Following prolonged exposure, tubes will eventually be broken apart forming smaller fragments that resemble short open-ended nanotubes. Multiple functional groups, mainly of the carboxylic acid variety, are consequently introduced at the location of these defect sites. Acid shortened tubes display increased solubility in a number of solvents. The presence of carboxylic acid functionalities also enables the attachment of small molecules or polymers through amidation and esterification reactions,[55] in addition to which non-covalent functionalization through electrostatic interactions has also been explored.[56] This technique has consequently been used to functionalize CNTs with a wide range of molecules.[57-62] Acid treatment offers the additional incentive of removing some metallic impurities present within CNTs. The high degree of damage incurred to the tube structure does, however, have a detrimental effect on both the mechanical and electrical properties of CNTs.

Since this initial work, the number of reactions available for the functionalization of CNTs has increased significantly. The reactivity of CNTs originates in part from the significant strain imposed by the curvature of the nanotube upon the sp^2 hybridized carbon atoms that make up the tube's framework.[48, 51, 63] The energy barrier for addition reactions is relatively low due to the strain relief that results from conversion of these carbon atoms to sp^3 hybridization. This strain enhanced reactivity is similar to that described previously for fullerenes. Much of the chemistry that has been utilized for the derivatization of CNTs has been developed using the wealth of reactions previously established for the chemical modification of fullerenes and graphite surfaces.

Several reactions commonly employed for the covalent modification of CNTs, are shown in Scheme 1.1.[51, 64, 65] Each of these reactions may be used to produce nanotubes bearing multiple functional groups that can subsequently be utilized for secondary coupling reactions. In recent years the topic of CNT chemistry has been reviewed extensively in the literature. Reviews by Prato[64] and others offer an excellent comprehensive view of work within this field that readers are encouraged to refer to for further information.

Scheme 1.1. Examples of reactions that enable the covalent modification of CNTs. [51, 64, 65] (A) 1,3-dipolar cycloaddition with azomethine ylide (B) arylation via diazonium species (C) nitrene cycloaddition (D) nucleophilic addition (E) Bingel reaction (F) addition of carboxyalkyl radical

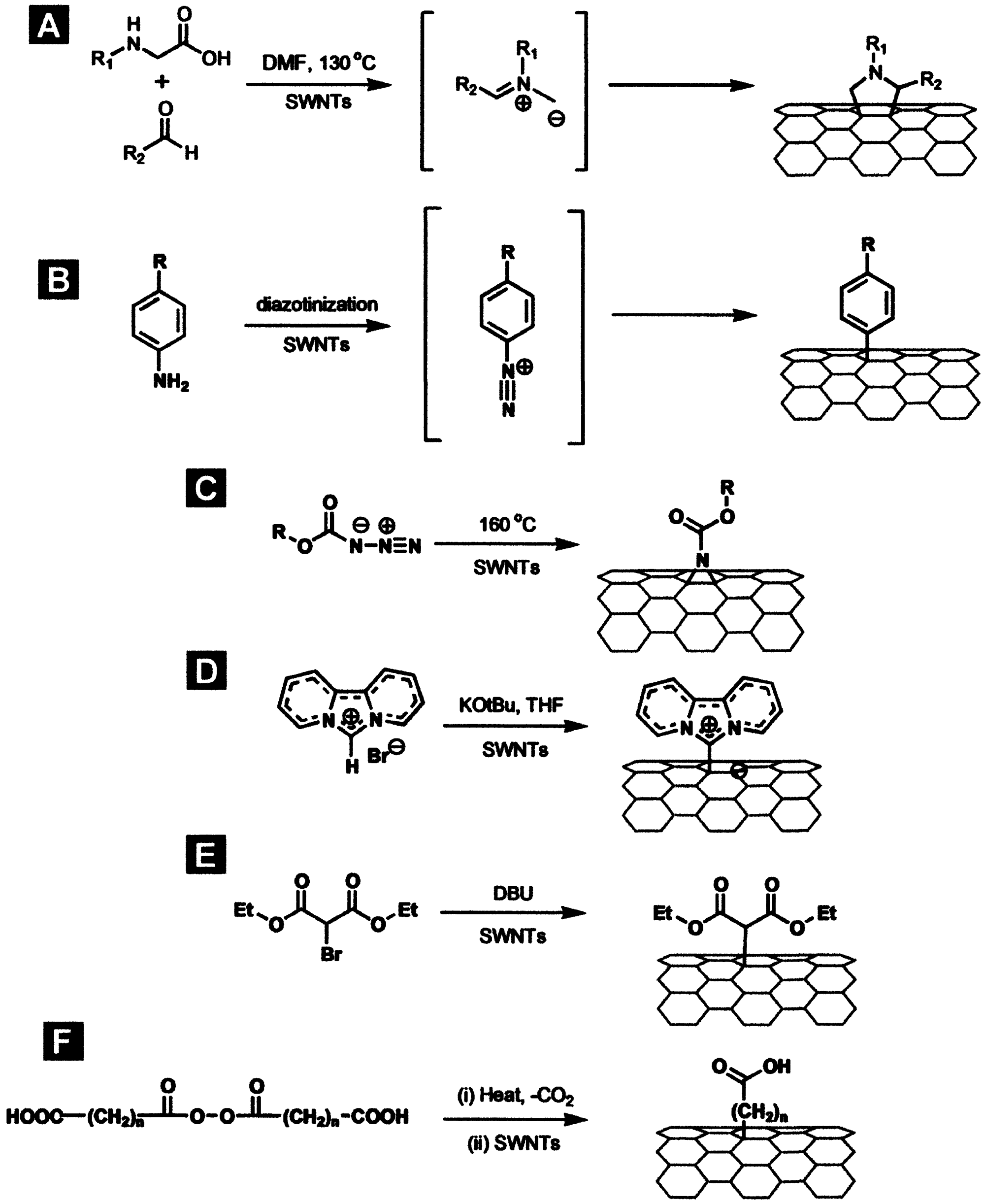

A number of highly reactive species, including carbenes[54, 65], nitrenes[66-68], azomethine ylides,[69, 70] and radicals[71, 72] have all been shown to undergo direct reaction with the surface of CNTs. In many examples, these species can be generated in-*situ* by thermal or photochemical decomposition of an appropriate precursor molecule. An example of one such reaction is the addition of an aryl radical generated in-*situ* from a diazonium species.[73-77] This reaction is simple, robust, and offers a means by which a variety of functional groups can be introduced to the surface of CNTs. As such, it is an important tool in the work of many nanotube chemists.

The first reported functionalization of nanotubes using diazonium salts was conducted by electrochemical reduction upon a CNT thin film electrode.[64, 78] This work was inspired in part by existing electrochemical methods for the derivatization of graphite and glassy carbon surfaces.[79-81] It was later shown that diazonium salt species dispersed in water reacted efficiently with CNTs at room temperature and in the absence of an electrochemical driving force, yielding a high degree of functionalization, equal to approximately one functional group for every nine carbon atoms.[82] Tour and coworkers have speculated that the reaction proceeds by donation of an electron from a CNT to a diazonium compound, resulting in the formation of dinitrogen, an aryl radical, and a CNT radical cation. The aryl radical subsequently reacts by radical-radical coupling to form a covalent bond with the nanotube surface.[74] Interestingly, studies determined that under controlled conditions, diazonium compounds react almost exclusively with metallic type tubes,[83] supporting the hypothesis that electron transfer from the CNT is a requirement for reaction with diazonium species. The generation of diazonium species in-*situ*, by reaction of a suitable aniline derivative with isoamyl nitrite in the presence of CNTs was also shown to result in a high degree of functionalization. This reaction has also been shown to proceed in a variety of solvents, both organic[76] and aqueous,[77] as well as in solvent free conditions,[73] demonstrating the potential for large-scale derivatization of CNTs with a variety of functional groups including carboxylic acids, esters, nitro groups, and halides. Additionally it has recently been shown that sequential functionalization reactions can be conducted that allow the introduction of multiple different functional groups to the nanotube surface.[75]

1.1.3.3.2. Non-covalent approaches

Although covalent modification has proven highly efficient for the functionalization of CNTs and their dispersion within solution, the effect of structural modification upon nanotube properties is an inherent disadvantage of this approach. Conversion of carbon atoms to sp^3 hybridization disrupts electronic band structure of CNTs and ultimately diminishes their conductivity. For this reason, methods enabling the efficient non-covalent functionalization of CNTs are highly desirable. Provided that interactions are sufficiently strong, adsorption of molecules upon the surface of nanotubes can disrupt the close knit packing of CNT bundles and facilitate the dispersion of nanotubes within solution. The primary advantage of this approach is that it allows the derivatization of CNTs and their effective dispersion without compromising the nanotube's structural integrity or conductive properties. This is of particular significance in research focusing upon the incorporation of CNTs within electrical devices such as sensors, photovoltaics, and field-emission displays.

One family of molecules that has been successfully employed for the non-covalent functionalization of CNTs is amphiphilic surfactants, among which the most widely used is sodium dodecyl sulfate (SDS).[53, 84-87] The structure of SDS consists of a hydrophilic sulfonate group attached to a hydrophobic alkyl chain. In aqueous solution SDS forms micelles in which, the anionic head groups are located at the surface, in contact with water molecules, while the hydrophobic tail sections aggregate within the micelle core. In the presence of CNTs, the alkyl chain of SDS is adsorbed onto the surface of the CNTs through hydrophobic interactions.[88] As a result of this interaction, nanotubes become functionalized with a high density of negatively charged sulfate groups, which are directed outwards into aqueous solution such that the nanotube is effectively encapsulated within an SDS micelle. Electrostatic repulsion between sulfate groups upon the nanotube surfaces inhibits aggregation and consequently nanotube dispersions in SDS solution remain stable for a period of several months. In addition to SDS a variety of other ionic surfactants have also been investigated for the solubilization of CNTs including sodium dodecyl benzeze sulfonate (SDBS) and dodecyltrimethyl ammonium bromide (DTAB).[87, 89]

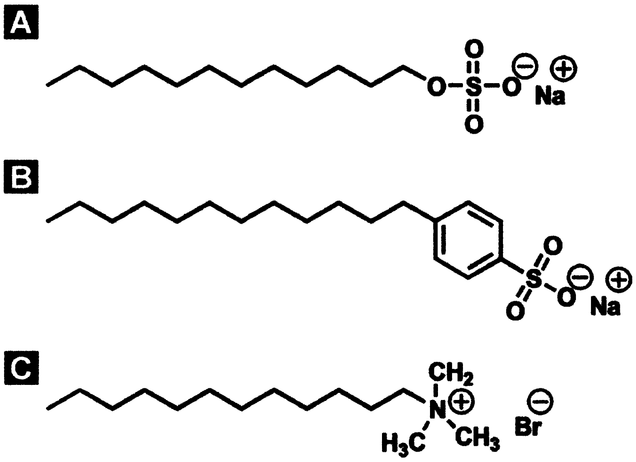

Figure 1.4. Examples of amphiphilic surfactants utilized for solubilization of CNTs in aqueous solution; (A) sodium dodecyl sulfate (SDS), (B) sodium dodecyl benzene sulfonate (SDBS), and (C) dodecyltrimethyl ammonium bromide (DTAB).

In addition to amphiphilic surfactants, an assortment of polyaromatic compounds have been shown to undergo strong binding with the surface of CNTs, aiding their dispersion within solution. Here, the adsorption of polyaromatics results from π-π stacking interactions with the graphitic lattice structure of the nanotube surface, as indicated by quenching of fluorescence and a bathochromatic shift in the UV adsorption of the complexed molecule. Examples of suitable polyaromatics include pyrene,[90-93] anthracene,[94, 95] porphyrin[96-98] and phthalocyanine[99] derivatives, bearing a variety of functional groups.[100] In the case of pyrene, it has been shown that the binding affinity with the nanotube surface is sufficiently strong to allow anchoring of macromolecules, including proteins.[93, 101]

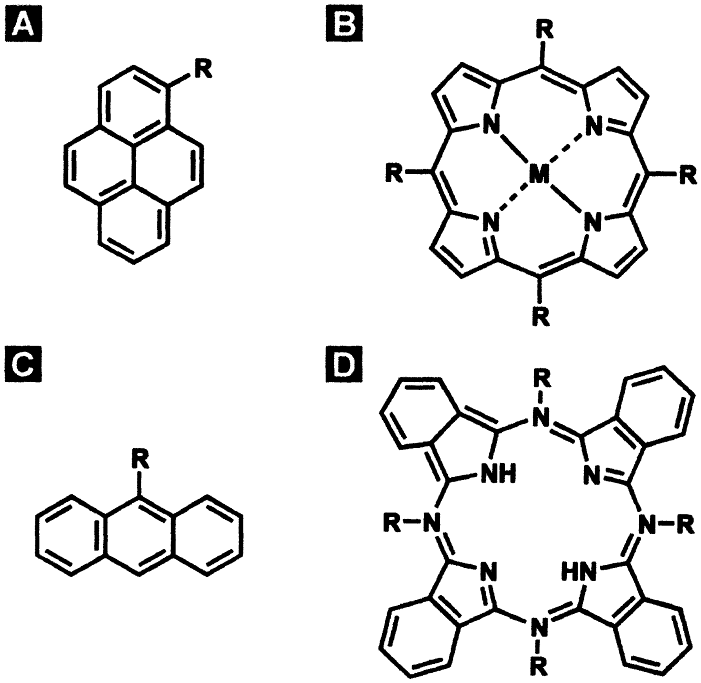

Figure 1.5. Examples of polyaromatic compounds utilized for solubilization of CNTs in aqueous solution, (A) pyrene (B) porphyrins (C) anthracene and (D) phthalocyanine.

1.1.3.4. Polymer Chemistry of CNTs

A large amount of research has also been conducted upon the functionalization of CNTs with macromolecules, using both covalent and non-covalent chemistry.[55] Functionalization of CNTs using macromolecules offers several advantages in comparison to similar chemistry utilizing small molecules. First, due to their size, polymers offer a means by which a large number of functional groups may be attached to a single CNT. Polymer functionalized CNTs can therefore display dramatic changes in solubility relative to nanotubes functionalized with comparable small molecules, even when a lower grafting density is observed. Second, modern polymer chemistry incorporates numerous well-established techniques that allow for precise control over polymer molecular weight, polydispersity, composition and architecture. As such, the preparation of polymers exhibiting practically any desired structure, property, or functionality can be obtained. Additionally, variation of polymer structure, and consequently of physical properties, can be achieved with minimal variation to experimental procedures. Systematic adjustment of factors such as feedstock ratio or concentration of initiator can be utilized to prepare a series of polymers exhibiting a range of physical properties.

1.1.3.4.1. Covalent Approaches

Covalent functionalization of nanotubes with polymers can be divided into two approaches; grafting-from and grafting-to. The grafting-from approach involves the attachment of functional groups to the surface of nanotubes from which polymerization may be initiated. Grafting-from polymer functionalization of CNTs has been reported using a variety of techniques including atom transfer radical polymerization (ATRP),[67, 102] nitroxide mediated radical polymerization (NMP),[103, 104] and reversible addition fragmentation chain-transfer polymerization (RAFT).[105, 106] This approach generally yields high grafting density, although control of polymer molecular weight can potentially be problematic. In contrast, the grafting-to approach involves attachment of pre-formed polymer chains to the surface of pristine CNTs or to suitable functional groups previously introduced upon the nanotube surface. This method offers the advantage of allowing full characterization of polymer chains prior to grafting and therefore a high degree of control over polymer molecular weight. Steric effects may however limit the grafting density obtained using this approach. A diverse range of reactions have been utilized for the attachment of polymer chains to the surface of CNTs, including radical chemistry,[72] acid-defect chemistry, [60, 107] click chemistry,[108] and cycloaddition reactions.[66, 67]

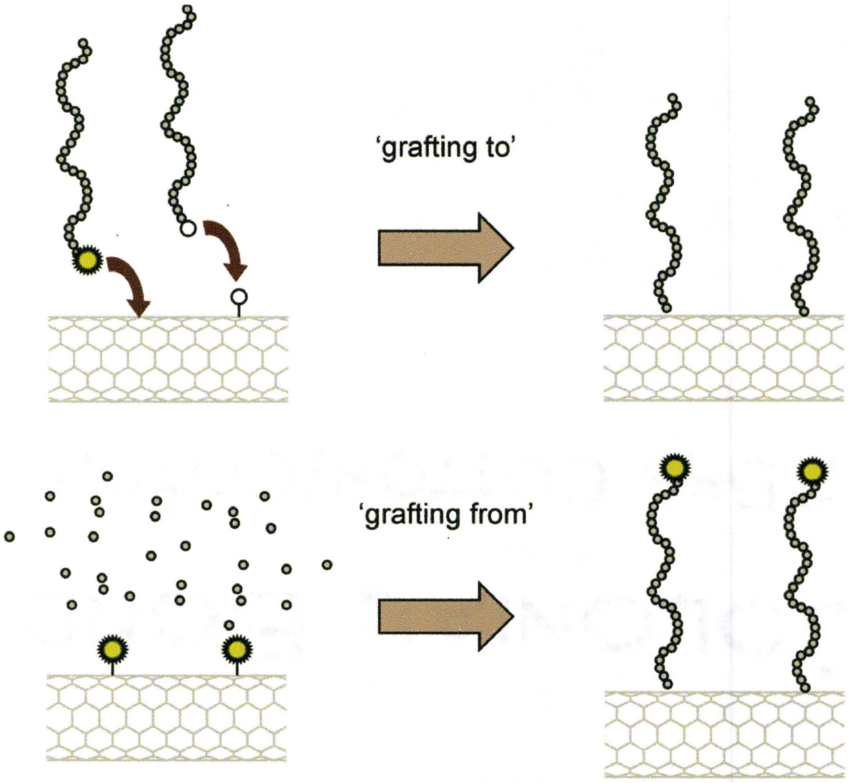

Figure 1.6. Schematic representing the two different approaches for polymer functionalization of CNTs.

1.1.3.4.2. Non-Covalent Approaches

The non-covalent functionalization of CNTs using macromolecules has also been studied using a wide range of synthetic polymers and bio-macro molecules.[55, 100] As with supramolecular attachment of small molecules to CNTs, the adsorption of polymers to the nanotubes surface is generally a result of hydrophobic or π-π stacking interactions. Additionally, the use of electrostatic interactions between carboxyl functionalizaed CNTs and cationic polyelectrolytes has also been investigated.[109, 110] As mentioned previously, ionic surfactants can be utilized for the dispersion of CNTs in solution enabled by the adsorption of hydrophobic alkyl chains to the nanotube surface. Likewise, amphiphilic block polymers have also been shown to interact with the surface of CNTs in a similar manner.[111, 112] Here, hydrophobic blocks can interact strongly with the surface of the tube, while hydrophilic sections are directed outwards into solution. The solvent employed must exhibit properties such that it cannot effectively solubilize the hydrophobic section, promoting interaction the CNT surface, while acting as a good solvent for the other block, enabling efficient dispersion in solution. In addition to interacting with solvent molecules, polymer chains provide steric stabilization that disrupts bundling of CNTs and prevents reaggregation. Examples of block copolymers that have been used for this purpose include poly(ethylene oxide)-block-poly(propylene oxide)-block-poly(-ethylene oxide), and poly(styrene)-block-poly(t-butyl acrylate). Additionally, commercially available surfactants including the Pluronics series and Triton X have proven highly efficient in allowing the dispersion of CNTs in water.[87, 113, 114]

Other polymers, such as polyvinylpyrrolidone (PVP) have been shown to wrap around CNTs in a helical manner, aiding their dispersion in aqueous solution.[115] This arrangement minimizes both the conformational strain experienced by the polymer and the area of the hydrophobic CNT surface that is in contact with solution. In the case of PVP, the hydrophobic backbone of the polymer adheres to the nanotube surface while polar pyrrolidone groups are in contact with surrounding water molecules. A number of pyrrolidinone and polystyrene based polymers and copolymers, including polystyrene sulfonate (PSS), have also been shown to interact with CNTs in a similar manner. Single stranded DNA has been shown to adopt a helical wrapping arrangement around CNTs. Here however it is the hydrophobic nucleotides that interact with the surface of the tubes, through π-π stacking interactions, while the hydrophilic sugar backbone is directed out towards solution.[47, 116]

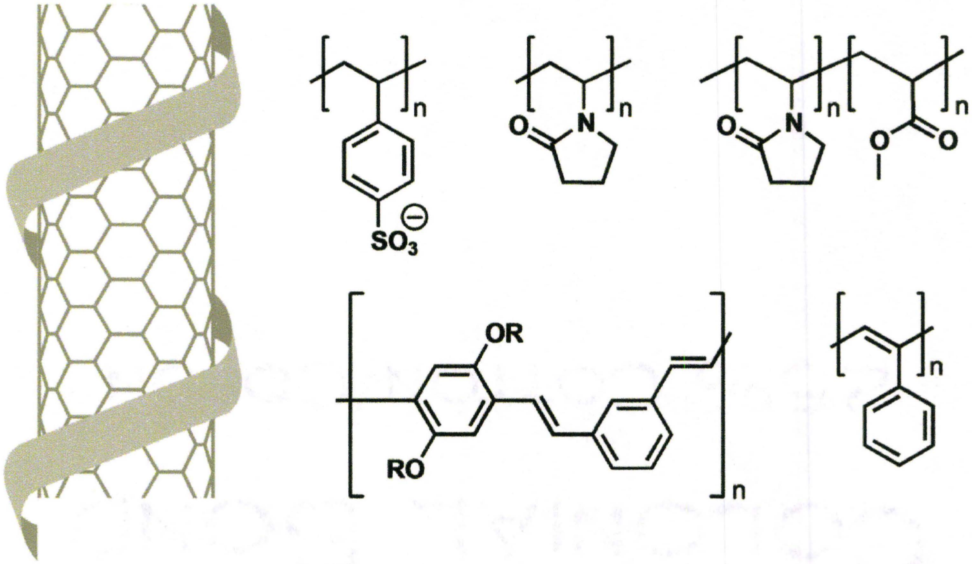

Figure 1.7. Schematic representing the helical wrapping of a polymer around a SWNT and some examples of polymers known to adopt this arrangement.

With regard to non-covalent functionalization of CNTs utilizing π-π stacking interactions, the size of polymers and consequently their high degree of functionality, can be exploited to enable multivalent binding that increases the strength of polymer-CNT interactions relative to structurally comparable small molecules. This is exemplified by polymers containing multiple polyaromatic units, such as pyrene and porphyrins. Jérôme and coworkers reported the preparation of a methyl methacyrylate based copolymer containing multiple pyrene groups located upon side-chain functionalities.[117] In this work, the solubility of nanotubes functionalized with pyrene containing polymers in several organic solvents was shown to improve with increasing pyrene content. This approach has subsequently been extended to investigate a range of random and block copolymers of varying composition.[118, 119]

In addition to polymers functionalized with small polyaromatic molecules, the use of π-conjugated polymers has also proven to be highly effective for the functionalization and dispersion of CNTs in both aqueous and organic solvents. Conjugated polymers have been widely studied in recent years due to their promising optical and conductive properties. The dispersion of CNTs within conjugated polymers has been widely investigated as a means of improving the conductivity of these materials. Electronic interaction between conjugated polymers and the π-system of CNTs has been shown to exist in a number of examples, allowing the occurrence of energy transfer.[120-124] Such behaviour is of particular significance in the development of nanotube based photovoltaic devices. Examples of conjugated polymers that have proven effective in the non-covalent functionalization of CNTs including poly(m-phenylenevinylene) and poly(phenylacetylene), which are known to adopt a helical wrapping arrangement around the nanotube,[125-129] as well as polyphenylene, polyfluorene, poly(phenyleneethynylene), and poly(polphyrin) structures that align in a non-helical fashion along the tube's axis.[98, 120, 130, 131] In both cases, orientation of conjugated polymers occurs in such a way as to maximize polymer-CNT interactions without compromising polymer conjugation. The rigidity of conjugated polymers can also strongly influence the conformation that is adopted.

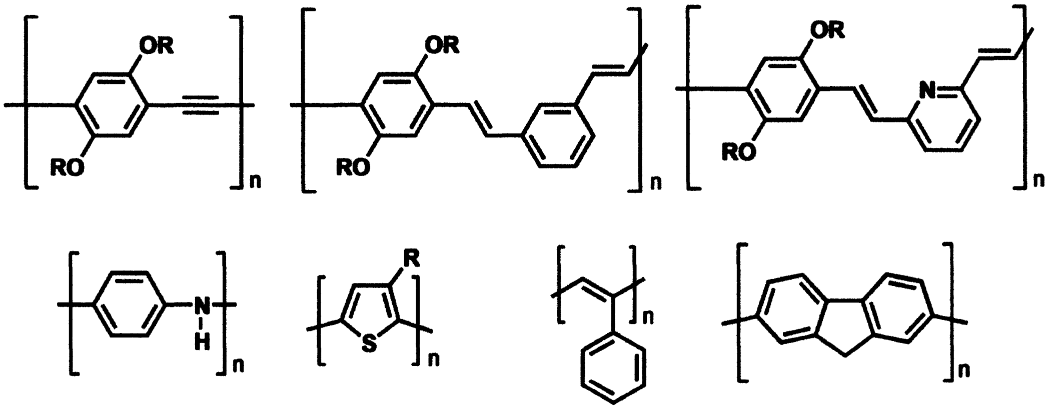

Figure 1.8. Conjugated polymers that have been investigated for the non-covalent functionalization of CNTs.

1.1.3.5. Functionalization of CNTs with inorganic nanoparticles

The preparation and characterization of metallic and semiconductor nanoparticles (NPs) has received immense attention in recent years.[132-135] It is known that the properties and reactivity of materials can alter radically when their physical dimensions are reduced from bulk to the nanometer scale. Nanoparticles composed of various metals, alloys, and semiconductor materials have been shown to display unique and advantageous optical, electrical, magnetic and catalytic properties. This has led to their investigation in a range of applications including energy storage and catalysis as well as to their incorporation as active components within electronic devices, such as chemical sensors, light-emitting diodes, and solar cells.

In 1994, Ajayan and coworkers published the first reported preparation of a CNT-metal NP composite.[136] In this work, CNTs decorated with Ru nanoparticles were prepared by high temperature reduction under hydrogen of an organometallic Ru precursor compound, which was adsorbed upon the nanotube surface. The composite materials prepared were shown to display impressive and selective catalytic activity in liquid-phase hydrogenation reactions. The high surface area, conductivity, and stability of CNTs make them ideal materials for investigation as structural supports in a range of applications including heterogeneous catalysis and chemical sensors. It is therefore no surprise that, following this initial report, the deposition of inorganic nanoparticles upon the surface of CNTs has been widely investigated.[137-140]

Literature methods for the preparation of CNT-nanoparticle composites are both varied and numerous, but can generally be divided into two categories. The first of these involves the adsorption of preformed nanoparticles, either directly upon the nanotube surface or to some suitable functional group introduced by chemical modification. The second approach involves the in-*situ* formation of nanoparticles on the surface of CNTs.

This can be achieved by using a variety of techniques, including, but not limited to, electrodeposition, vapour deposition, and chemical or thermal reduction of metal salts.

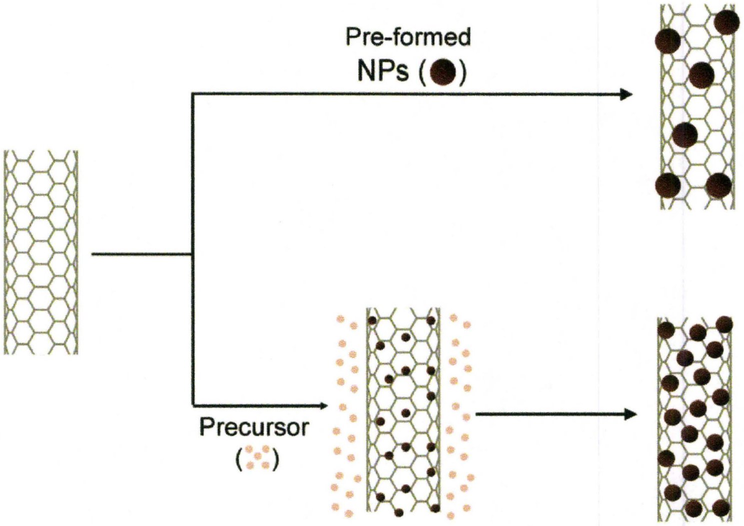

Figure 1.9. Schematic representing different methodologies for functionalization of CNTs with metallic nanoparticles, where precursors can be either a salt, organometallic compound, or metal vapour.

1.1.3.5.1. Attachment of preformed particles

Attachment of preformed nanoparticles to CNTs has been widely investigated using a variety of techniques, both covalent and non-covalent. One inherent advantage to this approach is that it allows for the characterization of nanoparticles prior to attachment, and therefore enables accurate control over the dimensions of nanoparticles, which will strongly influence the properties of any composite material that is formed. The simplest approach by which preformed particles may be attached to CNTs exploits hydrophobic interactions between ligands surrounding the nanoparticle and the surface of the CNT.[141,

[142] Rahman and coworkers demonstrated that alkanethiol ligands forming a protective monolayer on the surface of Au NPs will adsorb on the hydrophobic surface of CNTs following mixing in dichloromethane, leading to the attachment of Au NPs in relatively high density.[141] As an added benefit, the presence of alkyl chains on the nanotube surface was shown to influence the solubilities of the resulting composite material.

Alternatively, the introduction of functional groups, through covalent and non-covalent chemistry, to the surface of nanotubes can be used to promote strong interactions with a variety nanoparticles (Figure 1.10).[137-140] This has been achieved using groups such as thiols,[143-146] thioethers,[147] and amines,[148] which bind directly to the surface of NPs, as well groups such as carboxylic acids, which can bind indirectly through supramolecular interactions with ligands present upon the NP's surface.[149, 150] In cases where electrostatic interactions are employed to anchor nanoparticles, the density of nanoparticles that can be successfully attached will depend upon the charge density on the surface of the CNTs. One manner in which high charge density can be introduced is by functionalizing CNTs with a suitable polyelectrolyte. Acid treated CNTs, contain a large number of carboxylic acid surface functionalities, allowing adsorption of cationic polyelectrolytes such as poly(diallyldimethylammonium chloride) (PDDA).[151-153] Positively charged polymer modified nanotubes can subsequently bind with negatively charged nanoparticles, resulting in high-density coverage. CNTs modified with anionic polycations such as poly(styrene sulfonate) have also been investigated, where nanoparticles bearing a positive charge were subsequently bound to the nanotube surface.[56]

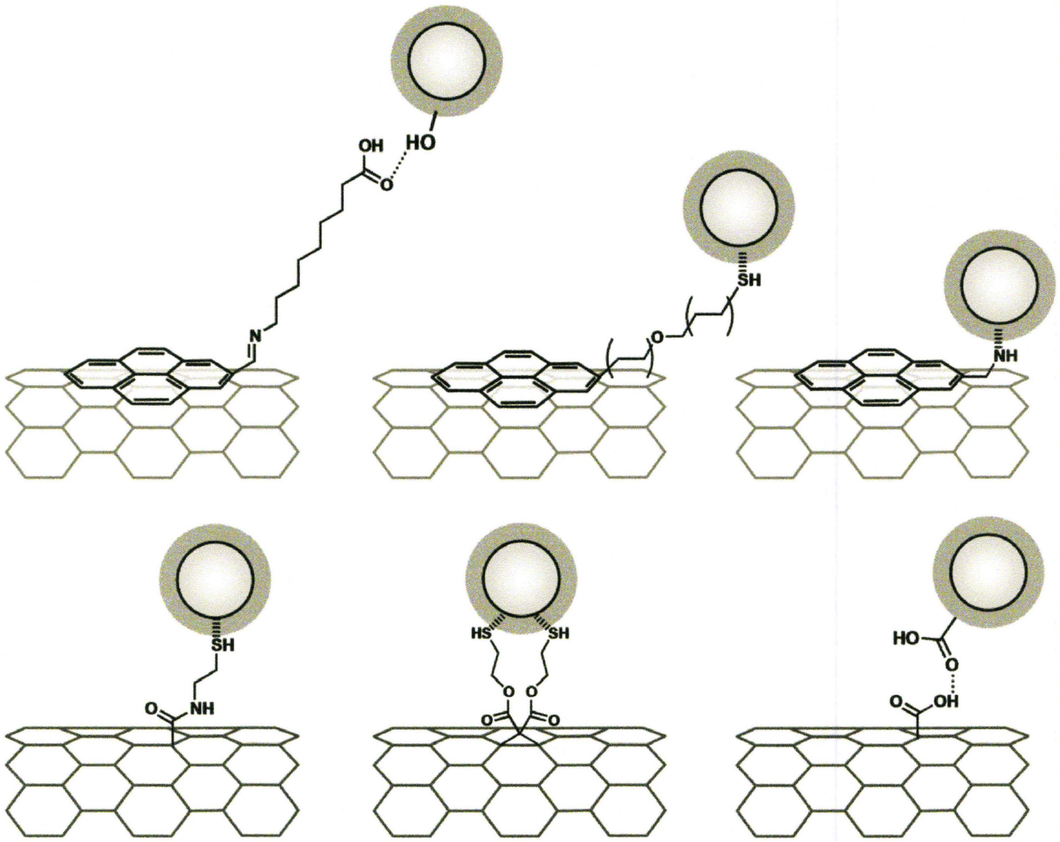

Figure 1.10. Schematic representing different approaches for the attachment of preformed nanoparticles to chemically modified CNTs.

1.1.3.5.2. In-*situ* formation of nanoparticles

The in-*situ* formation of nanoparticles upon the surface of CNTs has been reported, using a variety of techniques, including electrodeposition,[154-156] vapour deposition,[157] and reduction of metal salts through either chemical or thermal means.[139, [158-161] The simplest of these approaches involved reduction of a metal salt, using a suitable reducing agent, in the presence of CNTs. Here, particles are adsorbed upon the CNT surface where they are held through weak Van der Waals interactions. Lordi and coworkers noted that Pt nanoparticles produced by in-*situ* reduction of K_2PtCl_4 using ethylene glycol, adhered to the tube surface at sites where carboxylic acids or other functional groups had been introduced by oxidative treatment.[162] A number of groups have similarly reported the use of covalent modification, with small molecules,[144, 163, 164] polymers,[165] and dendrimers[166] as a means of introducing functional groups that can provide preferential sites for nanoparticle nucleation and adsorption. In many examples chemical modification offers the additional incentive of increasing nanotube dispersability within solution. The resulting debundling of nanotubes increases the surface area upon which nanoparticle deposition can occur. This is of particular significance in applications such as catalysis, where a high surface area support is desirable.

In addition to covalent modification, non-covalent approaches have also been employed for the functionalization of nanotubes with compounds allowing the in-*situ* formation of nanoparticles. As mentioned previously, electrostatic interactions can be employed to functionalize nanotubes with polyelectrolytes that can subsequently bind with charged nanoparticles. Dong and coworkers reported a novel method for the preparation of CNT-Au nanoparticle composites in which polyethylene imine (PEI) functions as both a surfactant, allowing the dispersion of CNTs in solution, and reducing agent for the formation of Au nanoparticles.[167] Here, acid treated MWNTs, containing carboxylic acid functional groups, were functionalized with PEI by sonication in aqueous solution. During this process PEI, which is a polycation, was adsorbed upon the surface of the negatively charged nanotubes. Addition of $HAuCl_4$ followed by mild heating resulted in the formation of Au NPs, the size and density of which could be altered by adjusting the ratio of PEI to $HAuCl_4$.

Another particularly significant finding, with regard to the decoration of CNTs with nanoparticles, was the observation reported by Dai and coworkers that some metal salts can undergo spontaneous electroless reduction in the presence of CNTs.[168] Here, the authors propose that a redox reaction occurs, in which the CNTs act as an electron donor. Provided that the metal cation exhibits a redox potential higher than that of CNTs then formation of nanoparticles can occur. Qu et al. later reported the development of a technique dubbed Substrate-Enhanced Electroless Deposition (SEED), which allows the decoration of nanotubes with nanoparticles composed of metals with redox potentials lower than CNTs.[169] This procedure operates by a galvanic displacement mechanism whereby nanotubes deposited upon a metal substrate function as a cathode for the reduction of metal cations in solution while the substrate upon which the nanotubes are located operates as an anode at which metal atoms are oxidized to form cations. This technique allows the deposition of any metallic nanoparticle upon the surface of CNTs provided the redox potential of the substrate is appropriately lower than the metal which is to be deposited.

1.1.3.6. CNT Thin Films

In recent years, great interest has developed within the field of nanotube research surrounding the fabrication and characterization of CNT thin films. These films, which resemble 2D interpenetrating non-woven networks of nanotubes, have been shown to exhibit properties making them of interest in a number of potential applications. For example, nanotube films display very low percolation values, a result of the nanotube's high aspect ratio. Consequently, films of CNTs can be prepared that, while thin enough to allow optically transparency, display conductivity that is suitable for device applications. At present devices such as light emitting diodes and solar cells typically contain transparent electrodes composed of either Indium-Tin-Oxide (ITO) or thin layers of materials such as copper or aluminium. These materials are deposited using techniques such as electron beam evaporation, vapour phase deposition and sputtering. In addition to being costly, these procedures often involve the use of high temperatures, which may prevent deposition upon substrates exhibiting a low melting point, such as organic polymers. ITO, the most commonly used material for the production of transparent electrodes, is also expensive, due to the limited supply of indium. The shape and flexibility of electronic devices is currently limited by the use of ITO, which is relatively brittle.

Recently, CNT thin films have been shown to exhibit conductivity and optical transparency approaching that of ITO,[170] while also displaying superior flexibility.[171] It is therefore believed that CNT thin films offer a commercially viable alternative to ITO in electronic device applications such as chemical sensors, light-emitters[172-175] and photovoltaics,[176, 177] particularly in applications where a high degree of flexibility is required. CNT films can be fabricated using a variety of methods, including chemical vapour deposition, spin,[178] dip,[179] and rod coating,[180] casting,[171, 181-183] spraying,[184-189] electrodeposition,[190] layer by layer deposition, hydroentangling,[191] flash drying,[192] and vacuum filtration.[43, 193-197] Of these techniques, it is solution based processing methods that display the greatest potential in the development of new commercial technology. Not only do these approaches offer significant economic advantages but the ability to fabricate CNT films at room temperature also allows the deposition of films upon flexible polymeric substrates and incorporation of temperature-sensitive materials such as enzymes and biopolymers. Additionally, recent work has shown that advances in the purification of CNTs and sorting of nanotube chiralities[39-46] can been applied in conjunction with solution based processing methods to prepare CNT films in which the ratio of metallic to semiconducting tubes and therefore the electronic properties of the film can be finely controlled.[41, 44, 198-200] Doping of CNT films using post fabrication chemical treatments can also be employed to influence the film's conductivity.

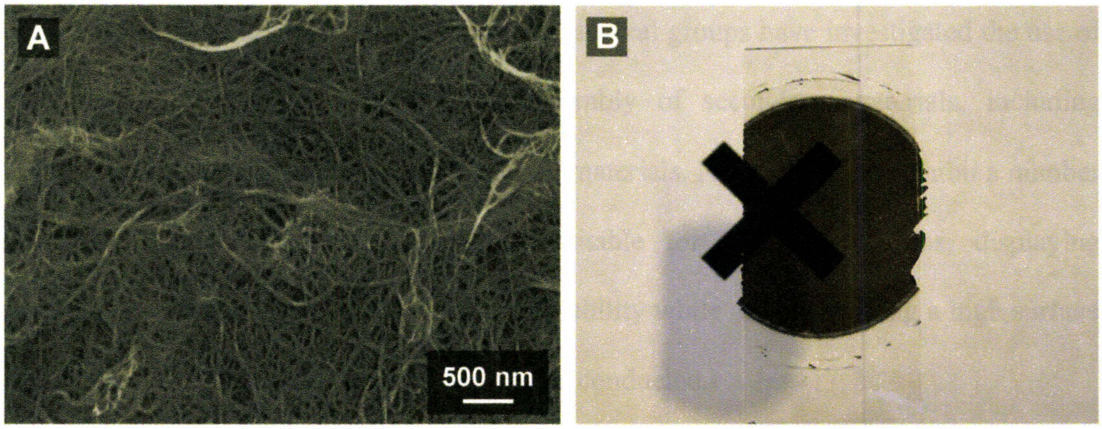

Figure 1.11. Planar SEM of a SWNT thin films (A) and photograph of an optically transparent SWNT film supported upon a glass microscopy slide (B)

In order for homogeneous thin films to be formed using these solution-based methods, CNTs must first be efficiently dispersed in solution. Generally this has been achieved through sonication of CNTs in aqueous solutions containing a surfactant, such as SDS or Triton-X, or in organic solutions containing low molecular weight amines. Alternatively, the functionalization of nanotubes using polymers and small molecules has also been employed.[201] A number of groups have reported the preparation of polymer-CNT composite films using this approach. In addition to aiding nanotube dispersability in solution, chemical modification, prior to film fabrication, offers a means by which properties such as the functionality, surface charge, and hydrophilicity of nanotube films may be influenced and consequently tailored to suit specific applications.

1.1.3.6.1. CNT films as scaffolds

In addition to electronics applications, several groups have investigated the use of CNT thin films as scaffolds for the assembly of secondary materials, including polymers,[202] inorganic nanostructures, and biomaterials. Nanotube films exhibit a number of physical properties that make them suitable for such applications, displaying impressive strength, flexibility, and thermal stability while also possessing a high surface area upon which chemical modification can be conducted.

1.1.3.6.2. Biomaterials

Research surrounding the use of CNT films as scaffolds, is arguably most highly developed with regard to the support and assembly of biomaterials[203]. Several reports have been published in recent years that detail the biocompatibility of CNTs and nanotube based composite materials.[204] The potential of CNTs in a range of bio-medicinal applications, such as drug delivery devices, biosensors, and synthetic biomaterials, is currently under investigation.[203, 205]

In 2000, Mattson et al. reported the growth of embryonic rat neurons upon films of MWNTs that were drop cast from a dispersion in ethanol upon glass substrates coated with poly(ethylene imine).[206] This work represented the first use of CNTs in a neuroscience application. Nanotubes were selected as a substrate for neuronal growth because of their strength, flexibility, conductivity and potential for chemical modification. Additionally nanotubes are non-biodegradable, and display negligible change in conductivity under harsh conditions. Researchers have speculated that these properties make CNTs potentially suitable for in vivo implants such as neural prosthetics or extracellular scaffolds for the treatment of brain and spinal cord injuries, where the conductive properties of CNTs would potentially allow for sensing of neurotransmitters and direct electrical stimulation of neurons.[207-209] While the work of Mattson et al. showed that neurons could indeed be successfully grown upon films of unmodified MWNTs, it was also noted that neurite branching of increased complexity was observed upon films of MWNTs which had been modified using 4-hydroxynoneal. This work therefore not only identified CNT films as substrates for neuronal growth but also highlighted the potential advantages of chemical modification within this field. Several other studies have subsequently been published further characterizing the growth of cells upon CNT films, which were either unfunctionalized[210-212] or functionalized using small molecules.[213]

The first example of neuronal growth upon a polymer functionalized CNT substrate was reported by Hu et al.[207] In this work, acid chloride chemistry was used to prepare MWNTs covalently functionalized with poly-*m*-aminobenzene sulfonic acid (PABS) and ethylene diamine. These molecules were selected for study because the functional groups they contain allowed the modification of nanotube surface charge. Studies involving hippocampal neuronal cultures indicated that MWNT films carrying a positive surface charge resulted in neurites grown to longer lengths, if not with increased density or with a higher degree of branching. These results confirmed that polymer functionalization of CNTs could be exploited to influence neurite outgrowth and branching processes.

Since these initial studies, several research groups have investigated the use of CNT thin films functionalized by covalent and non-covalent means as substrates for the growth of a variety of cells. Notable contributions to this field have been made by Kotov and coworkers who utilized non-covalent functionalization of CNTs with polyelectrolytes, to prepare nanotube films using layer-by-layer assembly. The authors speculate that this approach could be amended to allow the incorporation of drugs or proteins within nanotube-polymer composites, which could further aid neurite outgrowth and differentiation upon these substrates.[214]

In addition the use of CNT films as substrates for neuronal growth there have also been reports of their use in bone tissue integration and tissue engineering applications.[215-218] Haddon and co-workers reported the use of SWNTs covalently functionalized with PABS as a scaffold for artificial bone growth.[219] The authors state that the high strength and low density of CNTs make them suitable for use in the fabrication of artificial bone materials. Additionally it is noted that the diameter of SWNTs is similar to that of a collagen fibril triple helix and may therefore resemble the in vivo environment of hydroxyapatite (HA) crystallization. As with this group's previous work, detailing the use of nanotube films as substrates for neuronal growth,[207] polymer functionalized nanotubes were prepared using acid chloride chemistry. PABS functionalized nanotubes were subsequently dispersed in aqueous solutions from which thin films were prepared by spray coating upon a heated glass substrates. Following incubation in solutions containing $CaCl_2$ and Na_2HPO_4, microscopy studies revealed the formation of well-aligned plate like HA crystals upon the surface of the nanotube films.

1.1.3.6.3. Inorganic materials

The use of CNT films as scaffolds for the support of inorganic materials has also been investigated. The majority of work within this field involves the preparation of CNT films containing metallic, organometallic, or semiconductor nanoparticles. As mentioned previously, CNTs display a high surface area and exhibit exceptional thermal and chemical stability. These properties make CNTs excellent candidates for the structural support of catalytic nanoparticles. Additionally, electronic interactions between semiconductor quantum dots and CNTs has been shown to result in effective charge transfer properties.[149] It is therefore believed that these materials may potentially find application as active components in optoelectric devices such as solar cells.

Several approaches have been developed for the preparation of CNT films containing inorganic NPs. These include; (i) the deposition of CNTs from solution that have been decorated with NPs by some prior treatment, (ii) the co-deposition of CNTs and preformed NPs from solution, (iii) post-fabrication deposition of preformed nanoparticles upon CNT thin films, and (iv) post-fabrication formation of NPs directly upon the surface of a CNT film. A schematic representing these various approaches is shown in Figure 1.12. Table 1.3 summarizes some of the techniques previously reported for the preparation of CNT-NP composite films.

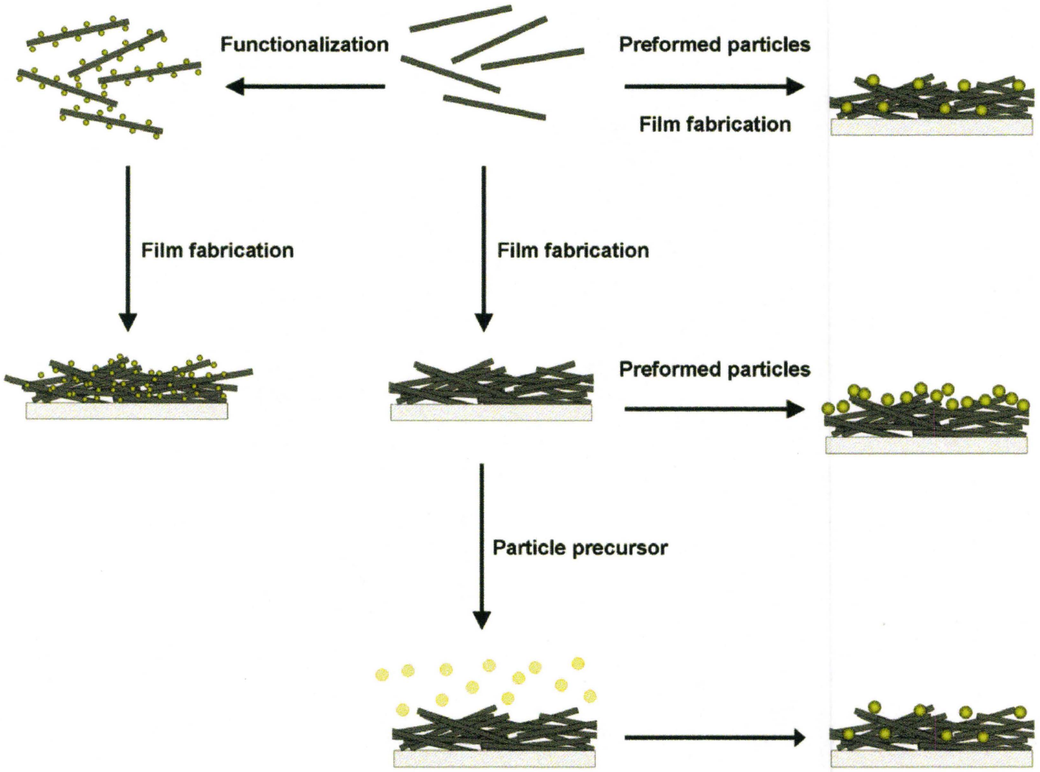

Figure 1.12. Schematic representing different approaches for the preparation of CNT-Inorganic NP composite films

One of the most commonly used methods for the preparation of CNT films containing inorganic materials is electrophoretic deposition (EPD), a technique in which charged colloids or molecules are deposited from solution onto the surface of a conductive substrate under the influence of an electric field. Compared to other surface modification techniques such as electron beam evaporation and sputtering, EPD is a relatively cheap and simple approach. Additionally, electrodeposition can be conducted at room temperature and is therefore compatible with temperature sensitive materials such as organic polymers and biomaterials. There are two different approaches by which CNT-inorganic composite films can be prepared using EPD. In the first approach, CNTs are deposited at the same time as either preformed NPs or in the presence of an appropriate precursor compound that forms NPs in-*situ* through electrochemical reaction at the electrode's surface. This approach has been used for the preparation of CNT films containing NPs composed of Ag,[220] ZnO,[221] MnO,[222, 223] and Prussian Blue.[224] In order for CNTs to be deposited using EPD they must first be modified to introduce some charged functional group. This can be achieved through acid treatment, covalent sidewall coupling, or non-covalent functionalization, as outlined previously. Alternatively, CNT films can be fabricated through some other means, such as drop casting or vacuum filtration, and subsequently used as electrodes for the deposition of a secondary material by EPD. Composite films containing a variety of materials including Au,[225-227] Sn,[228] and nickel hexacyanoferrates[229] have been prepared in this manner. Bui and coworkers recently demonstrated the patterning of Au NPs upon SWNT films by combining this approach with the use of a polymeric photoresist.[225] Several groups have also reported the use of EPD in the preparation of SWNT-polyaniline composite modified electrodes. It was shown that these materials could subsequently be utilized for the electrochemical reduction of H_2PtCl_2 producing Pt NP decorated films exhibiting promising electrocatalytic activity.[230-232]

Table 1.3. Examples of CNT composite films incorporation inorganic nanoparticles

NP	Film Fabrication	NP Deposition	Cited Application
Au[225-227, 233-237]	Vacuum filtration, Spray coating Spin coating Rod casting Drop casting LbL deposition	Electrodeposition Ionic liquid assisted sonochemical method Codeposited LbL deposition Thermal reduction Chemical deposition	SERS Sensors Fuel cells Transparent electrode materials Electrocatalysis Optoelectronic devices
Ag[220, 238]	Drop casting Spin coating Electrodeposition	Codeposited Thermal reduction	Chemical sensors Electrode materials
Pt[230-232]	Electrodeposition with PANI	Electrodeposition	Electrocatalysis
PtM alloys[239, 240] (M = Ru, Au, Pd)	Rod casting – ionic liquid composite gel	Ultrasonic Electrodeposition	Biosensors Electrocatalysis
Sn[228]	Vacuum filtration	Cofiltration Electrodeposition	Supercapacitors Fuel cells Sensors
ZnO[221, 241]	Vacuum filtration Drop casting Electrodeposition	Drop casting Adsorption Electodeposition	Solar cells
TiO_2[242, 243]	Electrodeposition	Casting	Solar cells
Fe_2O_3[244]	Spray coating	Codesposition	Supercapacitors
Silica[245]	LbL deposition	Sol gel chemistry	Separation
Organometallics [224, 229, 246, 247]	Drop casting Electrodeposition LbL depsoition	Electrodeposition Chemical deposition	Therapeutic biomaterials Ion exchange materials Bio-sensors

In addition to EPD several other approaches for the preparation of CNT-inorganic NP composite films has also been reported. These include layer-by-layer deposition,[234, 235] co-filtration,[228] and thermal reduction.[238] Jung and coworkers reported the preparation of SWNT-Au NP composite films via electroless reduction of a gold salt solution upon thin films of unmodified SWNTs.[233] In this work thin films were fabricated by vacuum filtration of a SWNT dispersion in SDS solution. Following removal of SDS, by repeated washing with deionized water, the films were transferred to poly(ethylene terephthalate) (PET) substrates and immersed in a solution of $HAuCl_4$ in water/ethanol for varying lengths of time. Following this procedure, Au NPs were introduced to the surface of SWNT thin films. It was demonstrated that Au modified films displayed a two-fold increase in conductivity, while retaining their impressive optical transparency, making them excellent candidates for use as transparent electrodes in devices such as light emitting diodes and solar cells. The authors speculate that electron donation from SWNTs during Au cation reduction results in p type doping, which consequently increases the conductivity of the SWNT thin films.

As mentioned previously, the vast majority of CNT-inorganic composite films reported in literature contain either a metallic or semiconductor component that is present in the form of nanoparticles. One recent exception can be found in the work of Chhowalla and coworkers, who reported the hydrothermal growth of zinc oxide nanowires upon a thin film of SWNTs.[248] In this work, SWNT thin films, prepared using vacuum filtration, were transferred to PET substrates and immersed within nitric acid, generating hydrophilic functionalities upon the CNT's surface. Saturation of films with zinc acetate dihydrate solution and subsequent thermal annealing treatment was employed to introduce ZnO NPs in high density upon the films surface. Incubation of these ZnO modified films within zinc nitrate hexahydrate solution at 90°C resulted in the formation of ZnO NWs, with diameters of between 30 and 60 nm in diameter and length of up to 400 nm. A bulk heterojunction type device was constructed by spin coating a layer of poly(4-hexylthiophene) upon a SWNT-ZnO NW composite film. This device was shown to display a photoconversion efficiency of 0.65%. Although the authors cite the flexibility of CNT films as an advantage over conventional substrates, the performance of the device when bent was not directly addressed in this publication.

1.1.4. Graphene

Graphene consists of a single sheet of carbon atoms exhibiting a hexagonal lattice structure. A huge amount of interest has recently arisen regarding the potential of graphene in the development of conductive materials for use in electronic device applications.[249] This research has been inspired by the observation that individual graphene sheets display impressive electronic properties that result from the confinement of electrons within a single two-dimensional plane.[250] Recent developments enabling solution based synthesis and processing of graphene has influenced the extent of research within this field.[251-253] Previously, graphene could only be prepared by mechanical cleavage of graphite, epitaxial growth, or the thermal reduction of silicon carbide.[254] These techniques are not amenable to either large scale production or the preparation of chemically modified graphene. It has been shown that the chemical oxidation of graphite powder can be used to produce graphene oxide (GO) containing multiple hydrophilic functionalities that enable dispersion and exfoliation of individual sheets within aqueous solution[255, 256] and some organic solvents.[257, 258] Thin films of GO can subsequently be prepared using low cost solution based techniques.[259-262] Reduction of GO by chemical or thermal treatment[263-267] can then be used to produce highly conductive graphene thin films. In the case of chemical reduction, this step can also be conducted in solution prior to film fabrication. Graphene thin films exhibit several advantageous properties that are similar to those of CNT thin films including low resistivity, impressive flexibility, thermal stability and optical transparency.[253] The applications for which graphene thin films display promise are therefore the same as those previously investigated for nanotube thin films. Although graphene research is still in its relative infancy and much work must still be conducted for properties such as conductivity and processability to be optimized, a tremendous amount of research has already been published detailing the use of graphene thin films as transparent electrode materials[253, 268-271] and within electronic devices such as solar cells and chemical sensors.[272] A number of groups have also reported the functionalization of GO with small molecules,[273-276] polymers,[277-279] and inorganic nanoparticles[272, 280-285] using methods comparable to those discussed previously for the modification of CNTs. One significant advantage that graphene offers over CNTs, when considering electronic device applications, is the relatively low cost by which it can be produced. With this in mind, it is perceivable that, in coming years, the use of graphene will potentially surpass that of CNTs in research focusing upon the development of flexible electronic devices.

1.2. Summary

Despite their relatively recent discovery, the immense interest surrounding CNTs has led to rapid development of a wide array of techniques allowing their modification with small molecules, polymers, and inorganic particles. The potential of CNTs has been investigated in many different applications. Understandably, CNT research is much better developed within certain fields than others. The goal of this thesis is to investigate the potential of CNT thin films as flexible conductive substrates for the support of inorganic materials. To date the majority of work within this field has focused upon the decoration of CNT thin films with discrete metallic nanoparticles. The development of more complex nanostructured architectures incorporating nanotube thin films has not been widely investigated. Several novel techniques are described in this work, which enable preparation of SWNT-inorganic composite films, where inorganic components include Au nanoparticle clusters, and semiconductor nanowires prepared by both gas phase epitaxy and solution based processes. The fabrication of functional electronic devices incorporating these novel composite materials and the expansion of techniques developed to include other carbon materials is also discussed.

1.3. References

(1) M. Strock Eight Allotropes of Carbon, wikipedia.org/wiki/File:Eight_Allotropes_of_Carbon.png

(2) N. N. Greenwood and A. Earnshaw, *Chemistry of the Elements*. 2nd ed.; Butterworth-Heinemann: 1997.

(3) H. W. Kroto, A. W. Allaf and S. P. Balm. *Chem Rev* **1991,** 91, (6), 1213-1235.

(4) W. Kratschmer, L. D. Lamb, K. Fostiropoulos and D. R. Huffman. *Nature* **1990,** 347, (6291), 354-358.

(5) N. I. Alekseyev and G. A. Dyuzhev. *Carbon* **2003,** 41, (7), 1343-1348.

(6) J. B. Howard, J. T. Mckinnon, Y. Makarovsky, A. L. Lafleur and M. E. Johnson. *Nature* **1991,** 352, (6331), 139-141.

(7) D. M. Guldi, B. M. Illescas, C. M. Atienza, M. Wielopolskia and N. Martin. *Chem Soc Rev* **2009,** 38, (6), 1587-1597.

(8) Z. Markovic and V. Trajkovic. *Biomaterials* **2008,** 29, (26), 3561-3573.

(9) N. F. Steinmetz, V. Hong, E. D. Spoerke, P. Lu, K. Breitenkamp, M. G. Finn and M. Manchester. *J. Am. Chem. Soc.* **2009,** 131, (47), 17093-+.

(10) A. Hirsch. *Fullerenes and Related Structures* **1999,** 199, 1-65.

(11) F. Diederich and C. Thilgen. *Science* **1996,** 271, (5247), 317-323.

(12) F. Wudl. *J. Mater. Chem.* **2002,** 12, (7), 1959-1963.

(13) F. Diederich and M. Gomez-Lopez. *Chem Soc Rev* **1999,** 28, (5), 263-277.

(14) H. J. Dai. *Surf Sci* **2002,** 500, (1-3), 218-241.

(15) M. Terrones. *Annu. Rev. Mater. Res.* **2003,** 33, 419-501.

(16) M. Monthioux and V. L. Kuznetsov. *Carbon* **2006,** 44, (9), 1621-1623.

(17) G. G. B. Wildgoose, C.E.; Compton, R.G. *Small* **2006,** 2, (2), 182-193.

(18) S. Iijima. *Nature* **1991,** 354, (6348), 56-58.

(19) S. Iijima and T. Ichihashi. *Nature* **1993,** 364, (6439), 737-737.

(20) J. Abrahamson, P. G. Wiles and B. L. Rhoades. *Carbon* **1999,** 37, (11), 1873-1874.

(21) A. Oberlin, M. Endo and T. Koyama. *J Cryst Growth* **1976,** 32, (3), 335-349.

(22) P. Nikolaev, M. J. Bronikowski, R. K. Bradley, F. Rohmund, D. T. Colbert, K. A. Smith and R. E. Smalley. *Chem Phys Lett* **1999,** 313, (1-2), 91-97.

(23) R. H. Baughman, A. A. Zakhidov and W. A. de Heer. *Science* **2002,** 297, (5582), 787-792.

(24) J. Kong, N. R. Franklin, C. W. Zhou, M. G. Chapline, S. Peng, K. J. Cho and H. J. Dai. *Science* **2000,** 287, (5453), 622-625.

(25) E. Bekyarova, M. Davis, T. Burch, M. E. Itkis, B. Zhao, S. Sunshine and R. C. Haddon. *J. Phys. Chem. B* **2004,** 108, (51), 19717-19720.

(26) J. Sippel-Oakley, H. T. Wang, B. S. Kang, Z. C. Wu, F. Ren, A. G. Rinzler and S. J. Pearton. *Nanotechnology* **2005,** 16, (10), 2218-2221.

(27) S. J. Tans, A. R. M. Verschueren and C. Dekker. *Nature* **1998,** 393, (6680), 49-52.

(28) A. Bachtold, P. Hadley, T. Nakanishi and C. Dekker. *Physica E* **2003,** 16, (1), 42-46.

(29) K. Kostarelos, A. Bianco and M. Prato. *Nat Nanotechnol* **2009,** 4, (10), 627-633.
(30) J. N. Coleman, U. Khan, W. J. Blau and Y. K. Gun'ko. *Carbon* **2006,** 44, (9), 1624-1652.
(31) J. N. Coleman, U. Khan and Y. K. Gun'ko. *Adv. Mater.* **2006,** 18, (6), 689-706.
(32) M. T. Byrne and Y. K. Gun'ko. *Adv. Mater.* **2009,** 21, 1-17.
(33) W. A. Deheer, A. Chatelain and D. Ugarte. *Science* **1995,** 270, (5239), 1179-1180.
(34) N. Hamada, S. Sawada and A. Oshiyama. *Phys Rev Lett* **1992,** 68, (10), 1579-1581.
(35) R. Saito, M. Fujita, G. Dresselhaus and M. S. Dresselhaus. *Appl. Phys. Lett.* **1992,** 60, (18), 2204-2206.
(36) R. Saito, M. Fujita, G. Dresselhaus and M. S. Dresselhaus. *Phys. Rev. B* **1992,** 46, (3), 1804-1811.
(37) J. W. G. Wildoer, L. C. Venema, A. G. Rinzler, R. E. Smalley and C. Dekker. *Nature* **1998,** 391, (6662), 59-62.
(38) E. Kymakis, I. Alexandou and G. A. J. Amaratunga. *Synthetic Met.* **2002,** 127, (1-3), 59-62.
(39) A. G. Rinzler. *Nat Nanotechnol* **2006,** 1, (1), 17-18.
(40) A. Nish, J. Y. Hwang, J. Doig and R. J. Nicholas. *Nat Nanotechnol* **2007,** 2, (10), 640-646.
(41) M. S. Arnold, A. A. Green, J. F. Hulvat, S. I. Stupp and M. C. Hersam. *Nat Nanotechnol* **2006,** 1, (1), 60-65.
(42) R. Martel. *Acs Nano* **2008,** 2, (11), 2195-2199.
(43) D. Chattopadhyay, L. Galeska and F. Papadimitrakopoulos. *J Am Chem Soc* **2003,** 125, (11), 3370-3375.
(44) Y. Maeda, S. Kimura, M. Kanda, Y. Hirashima, T. Hasegawa, T. Wakahara, Y. F. Lian, T. Nakahodo, T. Tsuchiya, T. Akasaka, J. Lu, X. W. Zhang, Z. X. Gao, Y. P. Yu, S. Nagase, S. Kazaoui, N. Minami, T. Shimizu, H. Tokumoto and R. Saito. *J Am Chem Soc* **2005,** 127, (29), 10287-10290.
(45) B. Zhou, Y. Lin, D. E. Hill, W. Wang, L. M. Veca, L. W. Qu, P. Pathak, M. J. Meziani, J. Diaz, J. W. Connell, K. A. Watson, L. F. Allard and Y. P. Sun. *Polymer* **2006,** 47, (15), 5323-5329.
(46) W. Wang, K. A. S. Fernando, Y. Lin, M. J. Meziani, L. M. Veca, L. Cao, P. Zhang, M. M. Kimani and Y. P. Sun. *J Am Chem Soc* **2008,** 130, (4), 1415-1419.
(47) M. Zheng, A. Jagota, M. S. Strano, A. P. Santos, P. Barone, S. G. Chou, B. A. Diner, M. S. Dresselhaus, R. S. McLean, G. B. Onoa, G. G. Samsonidze, E. D. Semke, M. Usrey and D. J. Walls. *Science* **2003,** 302, (5650), 1545-1548.
(48) A. Hirsch. *Angew Chem Int Ed* **2002,** 41, (11), 1853-1859.
(49) J. L. Bahr and J. M. Tour. *J. Mater. Chem.* **2002,** 12, (7), 1952-1958.
(50) S. Banerjee, T. Hemraj-Benny and S. S. Wong. *Adv. Mater.* **2005,** 17, (1), 17-29.
(51) S. Niyogi, M. A. Hamon, H. Hu, B. Zhao, P. Bhowmik, R. Sen, M. E. Itkis and R. C. Haddon. *Accounts of Chemical Research* **2002,** 35, (12), 1105-1113.
(52) Y. Huang, X. F. Duan, Q. Q. Wei and C. M. Lieber. *Science* **2001,** 291, (5504), 630-633.

(53) J. Liu, A. G. Rinzler, H. J. Dai, J. H. Hafner, R. K. Bradley, P. J. Boul, A. Lu, T. Iverson, K. Shelimov, C. B. Huffman, F. Rodriguez-Macias, Y. S. Shon, T. R. Lee, D. T. Colbert and R. E. Smalley. *Science* **1998,** 280, (5367), 1253-1256.
(54) J. Chen, M. A. Hamon, H. Hu, Y. S. Chen, A. M. Rao, P. C. Eklund and R. C. Haddon. *Science* **1998,** 282, (5386), 95-98.
(55) G. J. C. Bahun, F.; Homenick, C.M.; Lawson, G.; Zhu, J.;Adronov, A., The Polymer Chemistry of Carbon Nanotubes. In *Chemistry of Carbon Nanotubes*, V. A. B. Basiuk, E.V.; , Ed. American Scientific Publishers: in press.
(56) B. Kim and W. M. Sigmund. *Langmuir* **2004,** 20, (19), 8239-8242.
(57) H. Q. Peng, L. B. Alemany, J. L. Margrave and V. N. Khabashesku. *J. Am. Chem. Soc.* **2003,** 125, (49), 15174-15182.
(58) Y. P. Sun, W. J. Huang, Y. Lin, K. F. Fu, A. Kitaygorodskiy, L. A. Riddle, Y. J. Yu and D. L. Carroll. *Chem. Mater.* **2001,** 13, (9), 2864-2869.
(59) J. E. Riggs, Z. X. Guo, D. L. Carroll and Y. P. Sun. *J. Am. Chem. Soc.* **2000,** 122, (24), 5879-5880.
(60) Y. P. Sun, K. F. Fu, Y. Lin and W. J. Huang. *Accounts of Chemical Research* **2002,** 35, (12), 1096-1104.
(61) C. Dwyer, M. Guthold, M. Falvo, S. Washburn, R. Superfine and D. Erie. *Nanotechnology* **2002,** 13, (5), 601-604.
(62) G. H. Jiang, L. Wang, C. Chen, X. C. Dong, T. Chen and H. J. Yu. *Mater Lett* **2005,** 59, (16), 2085-2089.
(63) K. Mylvaganam and L. C. Zhang. *J. Phys. Chem. B* **2004,** 108, (39), 15009-15012.
(64) D. Tasis, N. Tagmatarchis, A. Bianco and M. Prato. *Chem Rev* **2006,** 106, (3), 1105-1136.
(65) M. Holzinger, O. Vostrowsky, A. Hirsch, F. Hennrich, M. Kappes, R. Weiss and F. Jellen. *Angew Chem Int Ed* **2001,** 40, (21), 4002-+.
(66) M. Holzinger, J. Steinmetz, D. Samaille, M. Glerup, M. Paillet, P. Bernier, L. Ley and R. Graupner. *Carbon* **2004,** 42, (5-6), 941-947.
(67) S. H. Qin, D. Q. Qin, W. T. Ford, D. E. Resasco and J. E. Herrera. *Macromolecules* **2004,** 37, (3), 752-757.
(68) M. Holzinger, J. Abraha, P. Whelan, R. Graupner, L. Ley, F. Hennrich, M. Kappes and A. Hirsch. *J. Am. Chem. Soc.* **2003,** 125, (28), 8566-8580.
(69) V. Georgakilas, N. Tagmatarchis, D. Pantarotto, A. Bianco, J. P. Briand and M. Prato. *Chem Commun* **2002**, (24), 3050-3051.
(70) D. Pantarotto, C. D. Partidos, R. Graff, J. Hoebeke, J. P. Briand, M. Prato and A. Bianco. *J. Am. Chem. Soc.* **2003,** 125, (20), 6160-6164.
(71) M. S. P. Shaffer and K. Koziol. *Chem Commun* **2002**, (18), 2074-2075.
(72) Y. Q. Liu, Z. L. Yao and A. Adronov. *Macromolecules* **2005,** 38, (4), 1172-1179.
(73) C. A. Dyke and J. M. Tour. *J. Am. Chem. Soc.* **2003,** 125, (5), 1156-1157.
(74) C. A. Dyke, M. P. Stewart, F. Maya and J. M. Tour. *Synlett* **2004**, (1), 155-160.
(75) J. J. Stephenson, J. L. Hudson, A. D. Leonard, B. K. Price and J. M. Tour. *Chem. Mater.* **2007,** 19, (14), 3491-3498.
(76) J. L. Bahr and J. M. Tour. *Chem. Mater.* **2001,** 13, (11), 3823-+.
(77) B. K. Price and J. M. Tour. *J. Am. Chem. Soc.* **2006,** 128, (39), 12899-12904.

(78) J. L. Bahr, J. P. Yang, D. V. Kosynkin, M. J. Bronikowski, R. E. Smalley and J. M. Tour. *J. Am. Chem. Soc.* **2001,** 123, (27), 6536-6542.
(79) P. Allongue, M. Delamar, B. Desbat, O. Fagebaume, R. Hitmi, J. Pinson and J. M. Saveant. *J. Am. Chem. Soc.* **1997,** 119, (1), 201-207.
(80) B. Ortiz, C. Saby, G. Y. Champagne and D. Belanger. *J Electroanal Chem* **1998,** 455, (1-2), 75-81.
(81) C. Saby, B. Ortiz, G. Y. Champagne and D. Belanger. *Langmuir* **1997,** 13, (25), 6805-6813.
(82) C. A. Dyke and J. M. Tour. *Nano Lett.* **2003,** 3, (9), 1215-1218.
(83) M. S. Strano, C. A. Dyke, M. L. Usrey, P. W. Barone, M. J. Allen, H. W. Shan, C. Kittrell, R. H. Hauge, J. M. Tour and R. E. Smalley. *Science* **2003,** 301, (5639), 1519-1522.
(84) B. Vigolo, A. Penicaud, C. Coulon, C. Sauder, R. Pailler, C. Journet, P. Bernier and P. Poulin. *Science* **2000,** 290, (5495), 1331-1334.
(85) Y. X. Zhou, L. B. Hu and G. Gruner. *Appl. Phys. Lett.* **2006,** 88, (12), 123109.
(86) M. J. O'Connell, S. M. Bachilo, C. B. Huffman, V. C. Moore, M. S. Strano, E. H. Haroz, K. L. Rialon, P. J. Boul, W. H. Noon, C. Kittrell, J. P. Ma, R. H. Hauge, R. B. Weisman and R. E. Smalley. *Science* **2002,** 297, (5581), 593-596.
(87) V. C. Moore, M. S. Strano, E. H. Haroz, R. H. Hauge, R. E. Smalley, J. Schmidt and Y. Talmon. *Nano Lett.* **2003,** 3, (10), 1379-1382.
(88) C. Richard, F. Balavoine, P. Schultz, T. W. Ebbesen and C. Mioskowski. *Science* **2003,** 300, (5620), 775-778.
(89) J. Y. Shin, T. Premkumar and K. E. Geckeler. *Chem-Eur J* **2008,** 14, (20), 6044-6048.
(90) Y. Tomonari, H. Murakami and N. Nakashima. *Chem-Eur J* **2006,** 12, (15), 4027-4034.
(91) N. Nakashima, Y. Tomonari and H. Murakami. *Chem Lett* **2002,** (6), 638-639.
(92) N. Nakashima, Y. Tanaka, Y. Tomonari, H. Murakami, H. Kataura, T. Sakaue and K. Yoshikawa. *J. Phys. Chem. B* **2005,** 109, (27), 13076-13082.
(93) F. J. Gomez, R. J. Chen, D. W. Wang, R. M. Waymouth and H. J. Dai. *Chem Commun* **2003,** (2), 190-191.
(94) T. G. Hedderman, S. M. Keogh, G. Chambers and H. J. Byrne. *J. Phys. Chem. B* **2004,** 108, (49), 18860-18865.
(95) J. Zhang, J. K. Lee, Y. Wu and R. W. Murray. *Nano Lett.* **2003,** 3, (3), 403-407.
(96) H. Murakami, T. Nomura and N. Nakashima. *Chem Phys Lett* **2003,** 378, (5-6), 481-485.
(97) D. M. Guldi, H. Taieb, G. M. A. Rahman, N. Tagmatarchis and M. Prato. *Adv. Mater.* **2005,** 17, (7), 871-+.
(98) F. Y. Cheng, S. Zhang, A. Adronov, L. Echegoyen and F. Diederich. *Chem-Eur J* **2006,** 12, (23), 6062-6070.
(99) X. B. Wang, Y. Q. Liu, W. F. Qiu and D. B. Zhu. *J. Mater. Chem.* **2002,** 12, (6), 1636-1639.
(100) D. A. Britz and A. N. Khlobystov. *Chem Soc Rev* **2006,** 35, (7), 637-659.

(101) R. J. Chen, Y. G. Zhang, D. W. Wang and H. J. Dai. *J. Am. Chem. Soc.* **2001,** 123, (16), 3838-3839.

(102) Z. L. Yao, N. Braidy, G. A. Botton and A. Adronov. *J. Am. Chem. Soc.* **2003,** 125, (51), 16015-16024.

(103) M. Dehonor, K. Varlot-Masenelli, A. Gonzalez-Montiel, C. Gauthier, J. Y. Cavaille, H. Terrones and M. Terrones. *Chem Commun* **2005**, (42), 5349-5351.

(104) X. D. Zhao, X. H. Fan, X. F. Chen, C. P. Chai and Q. F. Zhou. *J Polym Sci Pol Chem* **2006,** 44, (15), 4656-4667.

(105) C. Y. Hong, Y. Z. You and C. Y. Pan. *Chem. Mater.* **2005,** 17, (9), 2247-2254.

(106) G. Y. Xu, W. T. Wu, Y. S. Wang, W. M. Pang, P. H. Wang, G. R. Zhu and F. Lu. *Nanotechnology* **2006,** 17, (10), 2458-2465.

(107) K. A. S. Fernando, Y. Lin and Y. P. Sun. *Langmuir* **2004,** 20, (11), 4777-4778.

(108) H. M. Li, F. O. Cheng, A. M. Duft and A. Adronov. *J. Am. Chem. Soc.* **2005,** 127, (41), 14518-14524.

(109) B. Kim, H. Park and W. M. Sigmund. *Langmuir* **2003,** 19, (6), 2525-2527.

(110) B. Kim and W. M. Sigmund. *Langmuir* **2003,** 19, (11), 4848-4851.

(111) R. Shvartzman-Cohen, E. Nativ-Roth, E. Baskaran, Y. Levi-Kalisman, I. Szleifer and R. Yerushalmi-Rozen. *J. Am. Chem. Soc.* **2004,** 126, (45), 14850-14857.

(112) R. Shvartzman-Cohen, Y. Levi-Kalisman, E. Nativ-Roth and R. Yerushalmi-Rozen. *Langmuir* **2004,** 20, (15), 6085-6088.

(113) R. Rastogi, R. Kaushal, S. K. Tripathi, A. L. Sharma, I. Kaur and L. M. Bharadwaj. *J Colloid Interf Sci* **2008,** 328, (2), 421-428.

(114) M. S. Strano, V. C. Moore, M. K. Miller, M. J. Allen, E. H. Haroz, C. Kittrell, R. H. Hauge and R. E. Smalley. *J. Nanosci. Nanotechnol.* **2003,** 3, (1-2), 81-86.

(115) M. J. O'Connell, P. Boul, L. M. Ericson, C. Huffman, Y. H. Wang, E. Haroz, C. Kuper, J. Tour, K. D. Ausman and R. E. Smalley. *Chem Phys Lett* **2001,** 342, (3-4), 265-271.

(116) M. Zheng, A. Jagota, E. D. Semke, B. A. Diner, R. S. Mclean, S. R. Lustig, R. E. Richardson and N. G. Tassi. *Nat Mater* **2003,** 2, (5), 338-342.

(117) P. Petrov, F. Stassin, C. Pagnoulle and R. Jerome. *Chem Commun* **2003,** (23), 2904-2905.

(118) G. J. Bahun, C. Wang and A. Adronov. *J Polym Sci Pol Chem* **2006,** 44, (6), 1941-1951.

(119) X. D. Lou, R. Daussin, S. Cuenot, A. S. Duwez, C. Pagnoulle, C. Detrembleur, C. Bailly and R. Jerome. *Chem. Mater.* **2004,** 16, (21), 4005-4011.

(120) F. Y. Cheng, P. Imin, S. Lazar, G. A. Botton, G. de Silveira, O. Marinov, J. Deen and A. Adronov. *Macromolecules* **2008,** 41, (24), 9869-9874.

(121) J. Chen, H. Y. Liu, W. A. Weimer, M. D. Halls, D. H. Waldeck and G. C. Walker. *J. Am. Chem. Soc.* **2002,** 124, (31), 9034-9035.

(122) D. M. Guldi, G. M. A. Rahman, F. Zerbetto and M. Prato. *Accounts of Chemical Research* **2005**.

(123) G. M. A. Rahman, D. M. Guldi, R. Cagnoli, A. Mucci, L. Schenetti, L. Vaccari and M. Prato. *J. Am. Chem. Soc.* **2005,** 127, (28), 10051-10057.

(124) J. Mao, Q. Liu, X. Lv, Z. F. Liu, Y. Huang, Y. F. Ma, Y. S. Chen and S. G. Yin. *J. Nanosci. Nanotechnol.* **2007,** 7, (8), 2709-2718.
(125) A. B. Dalton, C. Stephan, J. N. Coleman, B. McCarthy, P. M. Ajayan, S. Lefrant, P. Bernier, W. J. Blau and H. J. Byrne. *J. Phys. Chem. B* **2000,** 104, (43), 10012-10016.
(126) B. McCarthy, J. N. Coleman, R. Czerw, A. B. Dalton, M. I. H. Panhuis, A. Maiti, A. Drury, P. Bernier, J. B. Nagy, B. Lahr, H. J. Byrne, D. L. Carroll and W. J. Blau. *J. Phys. Chem. B* **2002,** 106, (9), 2210-2216.
(127) D. W. Steuerman, A. Star, R. Narizzano, H. Choi, R. S. Ries, C. Nicolini, J. F. Stoddart and J. R. Heath. *J. Phys. Chem. B* **2002,** 106, (12), 3124-3130.
(128) B. Z. Tang and H. Y. Xu. *Macromolecules* **1999,** 32, (8), 2569-2576.
(129) W. Z. Yuan, J. Z. Sun, Y. Q. Dong, M. Haussler, F. Yang, H. P. Xu, A. J. Qin, J. W. Y. Lam, Q. Zheng and B. Z. Tang. *Macromolecules* **2006,** 39, (23), 8011-8020.
(130) F. Y. Cheng, P. Imin, C. Maunders, G. Botton and A. Adronov. *Macromolecules* **2008,** 41, (7), 2304-2308.
(131) F. Y. Cheng and A. Adronov. *Chem-Eur J* **2006,** 12, (19), 5053-5059.
(132) A. Roucoux, J. Schulz and H. Patin. *Chem Rev* **2002,** 102, (10), 3757-3778.
(133) M. C. Daniel and D. Astruc. *Chem Rev* **2004,** 104, (1), 293-346.
(134) Y. N. Xia, P. D. Yang, Y. G. Sun, Y. Y. Wu, B. Mayers, B. Gates, Y. D. Yin, F. Kim and Y. Q. Yan. *Adv. Mater.* **2003,** 15, (5), 353-389.
(135) T. K. Sau, A. L. Rogach, F. Jackel, T. A. Klar and J. Feldmann. *Adv. Mater.* **2009,** 21, Final page numbers not assigned.
(136) J. M. Planeix, N. Coustel, B. Coq, V. Brotons, P. S. Kumbhar, R. Dutartre, P. Geneste, P. Bernier and P. M. Ajayan. *J. Am. Chem. Soc.* **1994,** 116, (17), 7935-7936.
(137) G. G. Wildgoose, C. E. Banks and R. G. Compton. *Small* **2006,** 2, (2), 182-193.
(138) V. G. Georgakilas, D.; Tzitzios, V.; Pasquato, L.; Guldi, D.M.; Prato, M. *J. Mater. Chem.* **2007,** 17, 2679 - 2694.
(139) X. H. Peng, J. Y. Chen, J. A. Misewich and S. S. Wong. *Chem Soc Rev* **2009,** 38, (4), 1076-1098.
(140) D. Eder. *Chem Rev* **2008.**
(141) G. M. A. Rahman, D. M. Guldi, E. Zambon, L. Pasquato, N. Tagmatarchis and M. Prato. *Small* **2005,** 1, (5), 527-530.
(142) A. V. Ellis, K. Vjayamohanan, R. Goswaimi, N. Chakrapani, L. S. Ramanathan, P. M. Ajayan and G. Ramanath. *Nano Lett.* **2003,** 3, (3), 279-282.
(143) L. Liu, T. X. Wang, J. X. Li, Z. X. Guo, L. M. Dai, D. Q. Zhang and D. B. Zhu. *Chem Phys Lett* **2003,** 367, (5-6), 747-752.
(144) J. Shi, Z. Wang and H. L. Li. *J Nanopart Res* **2006,** 8, (5), 743-747.
(145) B. R. Azamian, K. S. Coleman, J. J. Davis, N. Hanson and M. L. H. Green. *Chem Commun* **2002**, (4), 366-367.
(146) R. Zanella, E. V. Basiuk, P. Santiago, V. A. Basiuk, E. Mireles, I. Puente-Lee and J. M. Saniger. *J. Phys. Chem. B* **2005,** 109, (34), 16290-16295.
(147) K. S. Coleman, S. R. Bailey, S. Fogden and M. L. H. Green. *J. Am. Chem. Soc.* **2003,** 125, (29), 8722-8723.
(148) Y. Y. Ou and M. H. Huang. *J. Phys. Chem. B* **2006,** 110, (5), 2031-2036.

(149) D. M. Guldi, G. M. A. Rahman, V. Sgobba, N. A. Kotov, D. Bonifazi and M. Prato. *J. Am. Chem. Soc.* **2006,** 128, (7), 2315-2323.
(150) L. Han, W. Wu, F. L. Kirk, J. Luo, M. M. Maye, N. N. Kariuki, Y. H. Lin, C. M. Wang and C. J. Zhong. *Langmuir* **2004,** 20, (14), 6019-6025.
(151) K. Y. Jiang, A. Eitan, L. S. Schadler, P. M. Ajayan, R. W. Siegel, N. Grobert, M. Mayne, M. Reyes-Reyes, H. Terrones and M. Terrones. *Nano Lett.* **2003,** 3, (3), 275-277.
(152) A. Carrillo, J. A. Swartz, J. M. Gamba, R. S. Kane, N. Chakrapani, B. Q. Wei and P. M. Ajayan. *Nano Lett.* **2003,** 3, (10), 1437-1440.
(153) C. Gao, C. D. Vo, Y. Z. Jin, W. W. Li and S. P. Armes. *Macromolecules* **2005,** 38, (21), 8634-8648.
(154) D. J. Guo and H. L. Li. *Electrochem Commun* **2004,** 6, (10), 999-1003.
(155) T. M. Day, P. R. Unwin, N. R. Wilson and J. V. Macpherson. *J. Am. Chem. Soc.* **2005,** 127, (30), 10639-10647.
(156) T. M. Day, P. R. Unwin and J. V. Macpherson. *Nano Lett.* **2007,** 7, (1), 51-57.
(157) H. Z. Zhang, J. S. Qiu, C. H. Liang, Z. L. Li, X. N. Wang, Y. P. Wang, Z. C. Feng and C. Li. *Catal Lett* **2005,** 101, (3-4), 211-214.
(158) P. Chen, X. Wu, J. Lin and K. L. Tan. *J. Phys. Chem. B* **1999,** 103, (22), 4559-4561.
(159) V. Georgakilas, D. Gournis, V. Tzitzios, L. Pasquato, D. M. Guldi and M. Prato. *Journal of Materials Chemistry* **2007,** 17, (26), 2679-2694.
(160) B. Xue, P. Chen, Q. Hong, J. Y. Lin and K. L. Tan. *J. Mater. Chem.* **2001,** 11, (9), 2378-2381.
(161) C. Pham-Huu, N. Keller, V. V. Roddatis, G. Mestl, R. Schlogl and M. J. Ledoux. *Phys. Chem. Chem. Phys.* **2002,** 4, (3), 514-521.
(162) V. Lordi, N. Yao and J. Wei. *Chem. Mater.* **2001,** 13, (3), 733-737.
(163) L. Q. Jiang and L. Gao. *Carbon* **2003,** 41, (15), 2923-2929.
(164) L. M. Guo and Z. Q. Peng. *Langmuir* **2008,** 24, (16), 8971-8975.
(165) M. J. Moghaddam, S. Taylor, M. Gao, S. M. Huang, L. M. Dai and M. J. McCall. *Nano Lett.* **2004,** 4, (1), 89-93.
(166) X. Lu and T. Imae. *J. Phys. Chem. C* **2007,** 111, (6), 2416-2420.
(167) X. G. Hu, T. Wang, X. H. Qu and S. J. Dong. *J. Phys. Chem. B* **2006,** 110, (2), 853-857.
(168) H. C. Choi, M. Shim, S. Bangsaruntip and H. J. Dai. *J. Am. Chem. Soc.* **2002,** 124, (31), 9058-9059.
(169) L. T. Qu and L. M. Dai. *J. Am. Chem. Soc.* **2005,** 127, (31), 10806-10807.
(170) R. Jung, H. S. Kim, Y. Kim, S. M. Kwon, H. S. Lee and H. J. In. *J Polym Sci Pol Phys* **2008,** 46, (12), 1235-1242.
(171) N. Saran, K. Parikh, D. S. Suh, E. Munoz, H. Kolla and S. K. Manohar. *J. Am. Chem. Soc.* **2004,** 126, (14), 4462-4463.
(172) R. A. Hatton, A. J. Miller and S. R. P. Silva. *J Mater Chem* **2008,** 18, (11), 1183-1192.
(173) D. H. Zhang, K. Ryu, X. L. Liu, E. Polikarpov, J. Ly, M. E. Tompson and C. W. Zhou. *Nano Lett* **2006,** 6, (9), 1880-1886.

(174) J. Li, L. Hu, L. Wang, Y. Zhou, G. Gruner and T. J. Marks. *Nano Lett* **2006,** 6, (11), 2472-2477.
(175) E. C.-W. Ou, L. Hu, G. C. R. Raymond, O. K. Soo, J. Pan, Z. Zheng, Y. Park, D. Hecht, G. Irvin, P. Drzaic and G. Gruner. *Acs Nano* **2009,** 3, (8), 2258-2264.
(176) A. D. Pasquier, H. E. Unalan, A. Kanwal, S. Miller and M. Chhowalla. *Appl Phys Lett* **2005,** 87, (20), -.
(177) S. Chaudhary, H. W. Lu, A. M. Muller, C. J. Bardeen and M. Ozkan. *Nano Lett* **2007,** 7, (7), 1973-1979.
(178) M. A. Meitl, Y. X. Zhou, A. Gaur, S. Jeon, M. L. Usrey, M. S. Strano and J. A. Rogers. *Nano Lett* **2004,** 4, (9), 1643-1647.
(179) M. H. A. Ng, L. T. Hartadi, H. Tan and C. H. P. Poa. *Nanotechnology* **2008,** 19, (20), -.
(180) B. Dan, G. C. Irvin and M. Pasquali. *Acs Nano* **2009,** 3, (4), 835-843.
(181) C. S. Du, J. Yeh and N. Pan. *J Mater Chem* **2005,** 15, (5), 548-550.
(182) T. V. Sreekumar, T. Liu, S. Kumar, L. M. Ericson, R. H. Hauge and R. E. Smalley. *Chem Mater* **2003,** 15, (1), 175-178.
(183) V. Bocharova, A. Kiriy, U. Oertel, M. Stamm, F. Stoffelbach, R. Jerome and C. Detrembleur. *J Phys Chem B* **2006,** 110, (30), 14640-14644.
(184) S. Kazaoui, N. Minami, R. Jacquemin, H. Kataura and Y. Achiba. *Phys Rev B* **1999,** 60, (19), 13339-13342.
(185) M. Kaempgen, G. S. Duesberg and S. Roth. *Appl Surf Sci* **2005,** 252, (2), 425-429.
(186) C. S. S. Sangeeth, M. Jaiswal and R. Menon. *J Appl Phys* **2009,** 105, (6), -.
(187) H. Z. Geng, K. K. Kim, K. P. So, Y. S. Lee, Y. Chang and Y. H. Lee. *J Am Chem Soc* **2007,** 129, (25), 7758-+.
(188) J. E. Trancik, S. C. Barton and J. Hone. *Nano Lett* **2008,** 8, (4), 982-987.
(189) K. A. Watson, S. Ghose, D. M. Delozier, J. G. Smith and J. W. Connell. *Polymer* **2005,** 46, (7), 2076-2085.
(190) Y. Abe, R. Tomuro and M. Sano. *Adv Mater* **2005,** 17, (18), 2192-2194.
(191) X. W. Zhang. *Adv Mater* **2008,** 20, (21), 4140-+.
(192) L. Hu, G. Gruner, J. Jenkins and C. J. Kim. *J Mater Chem* **2009,** 19, (32), 5845-5849.
(193) Z. C. Wu, Z. H. Chen, X. Du, J. M. Logan, J. Sippel, M. Nikolou, K. Kamaras, J. R. Reynolds, D. B. Tanner, A. F. Hebard and A. G. Rinzler. *Science* **2004,** 305, (5688), 1273-1276.
(194) F. Hennrich, S. Lebedkin, S. Malik, J. Tracy, M. Barczewski, H. Rosner and M. Kappes. *Phys Chem Chem Phys* **2002,** 4, (11), 2273-2277.
(195) S. Malik, H. Rosner, F. Hennrich, A. Bottcher, M. M. Kappes, T. Beck and M. Auhorn. *Phys Chem Chem Phys* **2004,** 6, (13), 3540-3544.
(196) H. E. Unalan, G. Fanchini, A. Kanwal, A. Du Pasquier and M. Chhowalla. *Nano Lett* **2006,** 6, (4), 677-682.
(197) B. B. Parekh, G. Fanchini, G. Eda and M. Chhowalla. *Appl Phys Lett* **2007,** 90, (12), -.
(198) Y. Miyata, K. Yanagi, Y. Maniwa and H. Kataura. *J Phys Chem C* **2008,** 112, (10), 3591-3596.

(199) J. L. Blackburn, T. M. Barnes, M. C. Beard, Y. H. Kim, R. C. Tenent, T. J. McDonald, B. To, T. J. Coutts and M. J. Heben. *Acs Nano* **2008,** 2, (6), 1266-1274.
(200) Y. Maeda, M. Hashimoto, S. Kaneko, M. Kanda, T. Hasegawa, T. Tsuchiya, T. Akasaka, Y. Naitoh, T. Shimizu, H. Tokumoto, J. Lu and S. Nagase. *J Mater Chem* **2008,** 18, (35), 4189-4192.
(201) A. Anson-Casaos, J. M. Gonzalez-Dominguez, E. Terrado and M. T. Martinez. *Carbon* **2010,** 48, (5), 1480-1488.
(202) C. Z. Meng, C. H. Liu and S. S. Fan. *Electrochem Commun* **2009,** 11, (1), 186-189.
(203) E. Bekyarova, Y. C. Ni, E. B. Malarkey, V. Montana, J. L. McWilliams, R. C. Haddon and V. Parpura. *J Biomed Nanotechnol* **2005,** 1, (1), 3-17.
(204) A. Bianco and M. Prato. *Adv Mater* **2003,** 15, (20), 1765-1768.
(205) F. S. Lu, L. R. Gu, M. J. Meziani, X. Wang, P. G. Luo, L. M. Veca, L. Cao and Y. P. Sun. *Adv. Mater.* **2009,** 21, (2), 139-152.
(206) M. P. Mattson, R. C. Haddon and A. M. Rao. *J Mol Neurosci* **2000,** 14, (3), 175-182.
(207) H. Hu, Y. C. Ni, V. Montana, R. C. Haddon and V. Parpura. *Nano Lett* **2004,** 4, (3), 507-511.
(208) T. I. Chao, S. H. Xiang, C. S. Chen, W. C. Chin, A. J. Nelson, C. C. Wang and J. Lu. *Biochem Bioph Res Co* **2009,** 384, (4), 426-430.
(209) E. Jan and N. A. Kotov. *Nano Lett* **2007,** 7, (5), 1123-1128.
(210) V. Lovat, D. Pantarotto, L. Lagostena, B. Cacciari, M. Grandolfo, M. Righi, G. Spalluto, M. Prato and L. Ballerini. *Nano Lett* **2005,** 5, (6), 1107-1110.
(211) A. Mazzatenta, M. Giugliano, S. Campidelli, L. Gambazzi, L. Businaro, H. Markram, M. Prato and L. Ballerini. *J Neurosci* **2007,** 27, (26), 6931-6936.
(212) X. Zhang, S. Prasad, S. Niyogi, A. Morgan, M. Ozkan and C. S. Ozkan. *Sensor Actuat B-Chem* **2005,** 106, (2), 843-850.
(213) A. V. Liopo, M. P. Stewart, J. Hudson, J. M. Tour and T. C. Pappas. *J Nanosci Nanotechno* **2006,** 6, (5), 1365-1374.
(214) N. W. S. Kam, E. Jan and N. A. Kotov. *Nano Lett* **2009,** 9, (1), 273-278.
(215) B. S. Harrison and A. Atala. *Biomaterials* **2007,** 28, (2), 344-353.
(216) L. P. Zanello, B. Zhao, H. Hu and R. C. Haddon. *Nano Letters* **2006,** 6, (3), 562-567.
(217) X. Tu, C. M. Skinner, X. Chen and W. Zhao. *Materials Research Society Symposium Proceddings* **2007,** 1018, EE04-09.
(218) X. K. Zhang, X. F. Wang, Q. H. Lu and C. L. Fu. *Carbon* **2008,** 46, (3), 453-460.
(219) B. Zhao, H. Hu, S. K. Mandal and R. C. Haddon. *Chem Mater* **2005,** 17, (12), 3235-3241.
(220) T. Casagrande, G. Lawson, H. Li, J. Wei, A. Adronov and I. Zhitomirsky. *Mater Chem Phys* **2008,** 111, (1), 42-49.
(221) F. Vietmeyer, B. Seger and P. V. Kamat. *Adv. Mater.* **2007,** 19, (19), 2935-+.
(222) Y. H. Wang and I. Zhitomirsky. *Langmuir* **2009,** 25, (17), 9684-9689.
(223) J. Li and I. Zhitomirsky. *J Mater Process Tech* **2009,** 209, (7), 3452-3459.

(224) D. Du, M. H. Wang, Y. H. Qin and Y. H. Lin. *J. Mater. Chem.* **2010,** 20, (8), 1532-1537.
(225) M. P. N. Bui, S. Lee, K. N. Han, X. H. Pham, C. A. Li, J. Choo and G. H. Seong. *Chem Commun* **2009**, (37), 5549-5551.
(226) C. G. Hu, Y. Ding, Y. Ji, J. Xu and S. Hu. *Carbon* **2010,** 48, 1345-1352.
(227) D. R. Kauffman, D. C. Sorescu, D. P. Schofield, B. L. Allen, K. D. Jordan and A. Star. *Nano Lett.* **2010,** 10, (3), 958-963.
(228) J. H. Lee, B. S. Kong, S. B. Yang and H. T. Jung. *J Power Sources* **2009,** 194, (1), 520-525.
(229) Y. H. Lin and X. L. Cui. *J. Mater. Chem.* **2006,** 16, (6), 585-592.
(230) Z. Wang, Z. Z. Zhu, J. Shi and H. L. Li. *Appl. Surf. Sci.* **2007,** 253, (22), 8811-8817.
(231) G. Wu, L. Li, J. H. Li and B. Q. Xu. *J Power Sources* **2006,** 155, (2), 118-127.
(232) J. Shi, D. J. Guo, Z. Wang and H. L. Li. *J Solid State Electr* **2005,** 9, (9), 634-638.
(233) B. S. Kong, D. H. Jung, S. K. Oh, C. S. Han and H. T. Jung. *J Phys Chem C* **2007,** 111, (23), 8377-8382.
(234) T. Wang, X. G. Hu and S. J. Dong. *J. Mater. Chem.* **2007,** 17, (39), 4189-4195.
(235) J. Kim, S. W. Lee, P. T. Hammond and Y. Shao-Horn. *Chem. Mater.* **2009,** 21, (13), 2993-3001.
(236) F. Xiao, F. Q. Zhao, J. W. Li, L. Q. Liu and B. Z. Zeng. *Electrochim Acta* **2008,** 53, (26), 7781-7788.
(237) H. Park, J. Kim, B. G. Choi, S. M. Jo, D. Y. Kim, W. H. Hong. and S. Jang. *Carbon* **2010,** 48, 1325-1330.
(238) H. Acharya, J. Sung, H. Shin, S. Y. Park, B. G. Min and C. Park. *React Funct Polym* **2009,** 69, (7), 552-557.
(239) F. Xiao, F. Q. Zhao, D. P. Mei, Z. R. Mo and B. Z. Zeng. *Biosens Bioelectron* **2009,** 24, (12), 3481-3486.
(240) F. Xiao, F. Q. Zhao, Y. F. Zhang, G. P. Guo and B. Z. Zeng. *J. Phys. Chem. C* **2009,** 113, (3), 849-855.
(241) D. Wei, H. E. Unalan, D. X. Han, Q. X. Zhang, L. Niu, G. Amaratunga and T. Ryhanen. *Nanotechnology* **2008,** 19, (42), -.
(242) A. Kongkanand, R. M. Dominguez and P. V. Kamat. *Nano Lett.* **2007,** 7, (3), 676-680.
(243) P. Brown, K. Takechi and P. V. Kamat. *J. Phys. Chem. C* **2008,** 112, (12), 4776-4782.
(244) X. Zhao, C. Johnston and P. S. Grant. *J. Mater. Chem.* **2009,** 19, (46), 8755-8760.
(245) J. H. Rouse, P. T. Lillehei, J. Sanderson and E. J. Siochi. *Chem. Mater.* **2004,** 16, (20), 3904-3910.
(246) S. P. Wang, L. M. Lu, M. H. Yang, Y. Lei, G. L. Shen and R. Q. Yu. *Anal Chim Acta* **2009,** 651, (2), 220-226.
(247) T. Baumgartner, W. Bergmans, T. Karpati, T. Neumann, M. Nieger and L. Nyulaszi. *Chem-Eur J* **2005,** 11, (16), 4687-4699.
(248) H. E. Unalan, P. Hiralal, D. Kuo, B. Parekh, G. Amaratunga and M. J. Chhowalla. *J. Mater. Chem.* **2008,** 18, 5909-5912.

(249) D. Li and R. B. Kaner. *Science* **2008,** 320, (5880), 1170-1171.
(250) M. Freitag. *Nat Nanotechnol* **2008,** 3, (8), 455-457.
(251) C. E. Hamilton, J. R. Lomeda, Z. Z. Sun, J. M. Tour and A. R. Barron. *Nano Lett.* **2009,** 9, (10), 3460-3462.
(252) Y. Hernandez, V. Nicolosi, M. Lotya, F. M. Blighe, Z. Y. Sun, S. De, I. T. McGovern, B. Holland, M. Byrne, Y. K. Gun'ko, J. J. Boland, P. Niraj, G. Duesberg, S. Krishnamurthy, R. Goodhue, J. Hutchison, V. Scardaci, A. C. Ferrari and J. N. Coleman. *Nat Nanotechnol* **2008,** 3, (9), 563-568.
(253) G. Eda, G. Fanchini and M. Chhowalla. *Nat Nanotechnol* **2008,** 3, (5), 270-274.
(254) K. V. Emtsev, A. Bostwick, K. Horn, J. Jobst, G. L. Kellogg, L. Ley, J. L. McChesney, T. Ohta, S. A. Reshanov, J. Rohrl, E. Rotenberg, A. K. Schmid, D. Waldmann, H. B. Weber and T. Seyller. *Nat Mater* **2009,** 8, (3), 203-207.
(255) W. S. Hummers and R. E. Offeman. *J. Am. Chem. Soc.* **1958,** 80, 1339.
(256) Y. Si and E. T. Samulski. *Nano Lett.* **2008,** 8, (6), 1679-1682.
(257) J. I. Paredes, S. Villar-Rodil, A. Martinez-Alonso and J. M. D. Tascon. *Langmuir* **2008,** 24, (19), 10560-10564.
(258) S. Park, J. H. An, I. W. Jung, R. D. Piner, S. J. An, X. S. Li, A. Velamakanni and R. S. Ruoff. *Nano Lett.* **2009,** 9, (4), 1593-1597.
(259) L. J. Cote, F. Kim and J. Huang. *J. Am. Chem. Soc.* **2008,** ASAP.
(260) X. L. Li, G. Y. Zhang, X. D. Bai, X. M. Sun, X. R. Wang, E. Wang and H. J. Dai. *Nat Nanotechnol* **2008,** 3, (9), 538-542.
(261) J. T. Robinson, M. Zalalutdinov, J. W. Baldwin, E. S. Snow, Z. Q. Wei, P. Sheehan and B. H. Houston. *Nano Lett.* **2008,** 8, (10), 3441-3445.
(262) S. Biswas and L. T. Drzal. *Nano Lett.* **2009,** 9, (1), 167-172.
(263) V. C. Tung, M. J. Allen, Y. Yang and R. B. Kaner. *Nat Nanotechnol* **2009,** 4, (1), 25-29.
(264) S. Stankovich, D. A. Dikin, R. D. Piner, K. A. Kohlhaas, A. Kleinhammes, Y. Jia, Y. Wu, S. T. Nguyen and R. S. Ruoff. *Carbon* **2007,** 45, (7), 1558-1565.
(265) X. B. Fan, W. C. Peng, Y. Li, X. Y. Li, S. L. Wang, G. L. Zhang and F. B. Zhang. *Adv. Mater.* **2008,** 20, (23), 4490-4493.
(266) D. Li, M. B. Muller, S. Gilje, R. B. Kaner and G. G. Wallace. *Nat Nanotechnol* **2008,** 3, (2), 101-105.
(267) W. Gao, L. B. Alemany, L. J. Ci and P. M. Ajayan. *Nat Chem* **2009,** 1, (5), 403-408.
(268) X. Wang, L. J. Zhi and K. Mullen. *Nano Lett.* **2008,** 8, (1), 323-327.
(269) H. A. Becerril, J. Mao, Z. Liu, R. M. Stoltenberg, Z. Bao and Y. Chen. *Acs Nano* **2008,** 2, (3), 463-470.
(270) J. B. Wu, M. Agrawal, H. A. Becerril, Z. N. Bao, Z. F. Liu, Y. S. Chen and P. Peumans. *Acs Nano* **2010,** 4, (1), 43-48.
(271) J. B. Wu, H. A. Becerril, Z. N. Bao, Z. F. Liu, Y. S. Chen and P. Peumans. *Appl. Phys. Lett.* **2008,** 92, (26), -.
(272) J. Lu, I. Do, L. T. Drzal, R. M. Worden and I. Lee. *Acs Nano* **2008,** 2, (9), 1825-1832.

(273) J. R. Lomeda, C. D. Doyle, D. V. Kosynkin, W. F. Hwang and J. M. Tour. *J. Am. Chem. Soc.* **2008,** 130, (48), 16201-16206.
(274) Y. X. Xu, H. Bai, G. W. Lu, C. Li and G. Q. Shi. *J. Am. Chem. Soc.* **2008,** 130, (18), 5856-+.
(275) S. Stankovich, R. D. Piner, S. T. Nguyen and R. S. Ruoff. *Carbon* **2006,** 44, (15), 3342-3347.
(276) Y. Y. Liang, D. Q. Wu, X. L. Feng and K. Mullen. *Adv. Mater.* **2009,** 21, (17), 1679-+.
(277) S. Stankovich, R. D. Piner, X. Q. Chen, N. Q. Wu, S. T. Nguyen and R. S. Ruoff. *J. Mater. Chem.* **2006,** 16, (2), 155-158.
(278) S. Stankovich, D. A. Dikin, G. H. B. Dommett, K. M. Kohlhaas, E. J. Zimney, E. A. Stach, R. D. Piner, S. T. Nguyen and R. S. Ruoff. *Nature* **2006,** 442, (7100), 282-286.
(279) N. I. Kovtyukhova, P. J. Ollivier, B. R. Martin, T. E. Mallouk, S. A. Chizhik, E. V. Buzaneva and A. D. Gorchinskiy. *Chem. Mater.* **1999,** 11, (3), 771-778.
(280) R. Muszynski, B. Seger and P. V. Kamat. *J. Phys. Chem. C* **2008,** 112, (14), 5263-5266.
(281) T. Cassagneau and J. H. Fendler. *J. Phys. Chem. B* **1999,** 103, (11), 1789-1793.
(282) G. Williams, B. Seger and P. V. Kamat. *Acs Nano* **2008,** 2, (7), 1487-1491.
(283) R. S. Sundaram, C. Gomez-Navarro, K. Balasubramanian, M. Burghard and K. Kern. *Adv. Mater.* **2008,** 20, (16), 3050-3053.
(284) C. Xu, X. Wang and J. W. Zhu. *J. Phys. Chem. C* **2008,** 112, (50), 19841-19845.
(285) S. Villar-Rodil, J. I. Paredes, A. Martinez-Alonso and J. M. D. Tascon. *J. Mater. Chem.* **2009,** 19, (22), 3591-3593.

Chapter 2: Au–carbon nanotube composites from self-reduction of Au^{3+} upon poly(ethylene imine) functionalized SWNT thin films

Gregor Lawson, Ferdinand Gonzaga, Julia Huang, Glynis de Silveira, Michael A. Brook, Alex Adronov

Reproduced by permission of The Royal Society of Chemistry

J. Mater. Chem., **2008,** (14), 1694-1702, DOI: 10.1039/b715277a

The work detailed in this chapter was carried out in collaboration with Dr. Ferdinand Gonzaga and Dr. Michael A. Brook (Department of Chemistry and Brockhouse Institute of Materials Research, McMaster University, Hamilton, Ontario). Nanotube functionalization, characterization and composite film preparation was conducted by Gregor Lawson. All electron microscopy analysis was conducted by Dr. Ferdinand Gonzaga with the exception of focused ion beam experiments, conducted by Julia Huang (Canadian Centre for Electron Microscopy, McMaster University, Hamilton, Ontario).

Abstract

A simple method for the production of carbon nanotube thin films containing Au nanoparticles is described. SWNTs functionalized with highly branched poly(ethylene imine) (Mn = 10 kDa) could be easily dispersed in aqueous solution (180 mg L^{-1}), allowing for the formation of homogeneous thin films by vacuum filtration. These films were subsequently functionalized with Au nanoparticle clusters by in-situ reduction of $HAuCl_4$ under mild conditions in the absence of additional reducing agents. Using thermogravimetric analysis, it was determined that poly(ethylene imine) functionalized SWNTs contained 17 wt% polymer, which amounts to one polymer chain for every 2600 carbon atoms within the nanotubes. Incubating these films in aqueous $HAuCl_4$ solutions resulted in a high density, uniform distribution of Au nanoparticle clusters along the film surface. In addition, using transmission electron microscopy (TEM) and focused ion beam (FIB) milling within a scanning electron microscope (SEM), nanoparticles were found to be embedded at various depths throughout the film. SEM was employed to determine Au nanoparticle diameter and distribution. The average diameter of the Au clusters could be controlled in the range of 50 to 550 nm.

2.1. Introduction

In recent years, there has been immense interest surrounding carbon nanotubes due to the unique structure and physical properties of these nanomaterials, as well as their prospective applications in a wide variety of fields.[1] The conductive properties of nanotubes have led to the investigation of their potential in the construction of electronic devices such as chemical sensors,[2-6] field emission devices,[7-9] and solar cells.[10, 11] The formation of nanotube–nanoparticle composites represents a significant sub-discipline within the field of nanotube research as materials of this nature potentially offer a wide range of novel electronic, optical, magnetic and catalytic properties.[12, 13] Preparation of carbon nanotube-gold nanoparticle composites has been reported by a variety of different methods, where interaction between the surface of carbon nanotubes and gold nanoparticles has been achieved by adsorption to thiol functionalities,[14, 15] hydrophobic interactions,[16-18] and direct electroless reduction of gold cations by carbon nanotubes.[19-21] Recently, Jung and coworkers reported the electroless reduction of gold cations upon single-walled carbon nanotube (SWNT) thin films fabricated by vacuum filtration.[22] It was shown that the resulting gold nanoparticle-containing SWNT films displayed good optical transparency and increased electrical conductivity compared to unmodified SWNT films.

The preparation of thin, free-standing carbon nanotube films has attracted significant attention in recent years.[23] A number of techniques for the preparation of nanotube films of varying thickness have been reported, including spin coating,[24] casting,[25-28] spraying,[29, 30] Langmuir-Blodgett film formation,[31] layer-by-layer (LbL) assembly with polyelectrolytes,[32-34] electrodeposition,[35] and vacuum filtration.[36-40] Of these, vacuum filtration offers the simplest means by which homogeneous carbon nanotube films may be produced with excellent and reproducible control of film thickness.[37, 38] Typically, this procedure involves filtration of a carbon nanotube suspension in aqueous solution containing a surfactant, such as SDS or Triton-X, through a porous membrane. It has long been known that carbon nanotubes functionalized with polymers or small molecules can form stable dispersions in both aqueous and organic solvents compared to pristine nanotubes,[41] which allows the formation of homogeneous thin films by vacuum filtration without additional surfactant.[42] Considering the wide variety of polymers that can now be introduced to the surface of carbon nanotubes,[41, 43] it should be possible to use the vacuum filtration approach to produce polymer functionalized nanotube films containing multiple reactive groups that can subsequently be utilized for further derivatization, such as the introduction of metal nanoparticles.

Poly(ethylene imine) (PEI) is highly hydrophilic and has previously been utilized for the functionalization of carbon nanotubes yielding composite materials that can be easily dispersed in aqueous solution.[44] PEI is also known to act as a reducing and stabilizing agent in the production of inorganic nanoparticles.[45-51] Hu and coworkers reported fabrication of Au/CNT composite materials in solution through in-situ reduction of $HAuCl_4$ by MWNTs that were non-covalently functionalized with PEI.[52] Although this work demonstrated high Au nanoparticle densities on the surface of MWNTs, the resulting composites exhibited large-scale aggregation of particles, forming a nearly continuous shell around MWNTs after prolonged deposition times, which precludes any potential for nanoparticle addressability. In addition, thin films of these materials were not prepared. Here, we demonstrate a simple method for the production of SWNT films containing individually separated Au nano-clusters in high density. Upon covalent functionalization of SWNTs with PEI, sufficient dispersability was achieved to allow the formation of homogeneous thin films, which could subsequently be decorated with Au nanoparticles by in-situ reduction of $HAuCl_4$ in water. The resulting composite materials exhibit a high-density of Au nano-clusters upon SWNT films, and thus differ greatly from previously reported examples involving non-covalently functionalized MWNTs in solution.[52] The nanoparticle-loaded films produced using this technique may be suitable for a range of electronics, materials, and catalysis applications, and could potentially be used in conjunction with recently developed PDMS-based transfer printing techniques to allow controlled deposition and micropatterning of CNT/Au composite materials upon a number of substrates.[53, 54]

2.2. Results and Discussion

2.2.1. Preparation and characterization of PEI functionalized SWNTs

The SWNTs used in this study were produced by the HiPCO process (Carbon Nanotechnologies Inc.) and were used without further purification. Benzoic acid functionalized SWNTs were produced using the previously reported diazotization and coupling reaction in water (Scheme 2.1).[55] This was followed by reaction with thionyl chloride to produce acid chloride functionalized SWNTs that were subsequently reacted with highly branched PEI (Mn = 10 kDa). To prevent crosslinking of nanotubes during the amidation reaction, a large excess of PEI was used. Efficient stirring also proved to be crucial in preventing the crosslinking of nanotubes. Polymer functionalized nanotubes were washed repeatedly with water and DMF to remove all traces of unbound PEI. The resulting functionalized nanotubes could be easily dispersed in aqueous solution yielding highly stable suspensions (180 mg L^{-1}).

Scheme 2.1. Preparation of PEI functionalized SWNTs; (i) SWNT, 4-aminobenzoic acid, isoamyl nitrite, H_2O, 60°C, 18 h (ii) thionyl chloride, DMF, 0°C - RT, 4 h; (iii) PEI, dichloromethane, 0 – 55°C, 24h

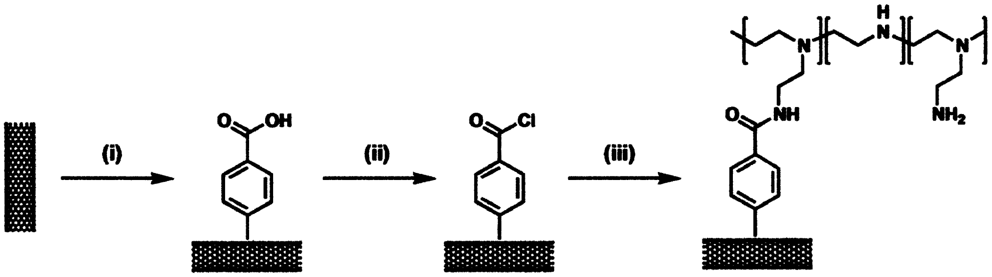

Information regarding the degree of functionalization and structural integrity of modified SWNTs was obtained using Raman spectroscopy. The spectrum of pristine SWNTs, shown in Figure 2.1.A, exhibits characteristic radial breathing ($\omega_r \approx 250$ cm^{-1}) and tangential ($\omega_t \approx 1{,}590$ cm^{-1}) modes in addition to a relatively low intensity disorder band ($\omega_d \approx 1{,}290$ cm^{-1}). This latter mode is indicative of the presence of sp^3-hybridized carbons within the nanotube framework. The intensity of the disorder band increased significantly following benzoic acid functionalization, suggesting that a number of carbon atoms in the nanotube framework underwent conversion from sp^2 to sp^3 hybridization. This observation confirmed that benzoic acid functionalization has proceeded successfully. Following reaction with PEI, there was no apparent increase in the intensity of the disorder band, indicating that no further hybridization of carbon atoms in the nanotube framework had occurred. This implies that grafting of PEI to SWNTs occurred only at benzoic acid groups previously introduced on the nanotube surface.

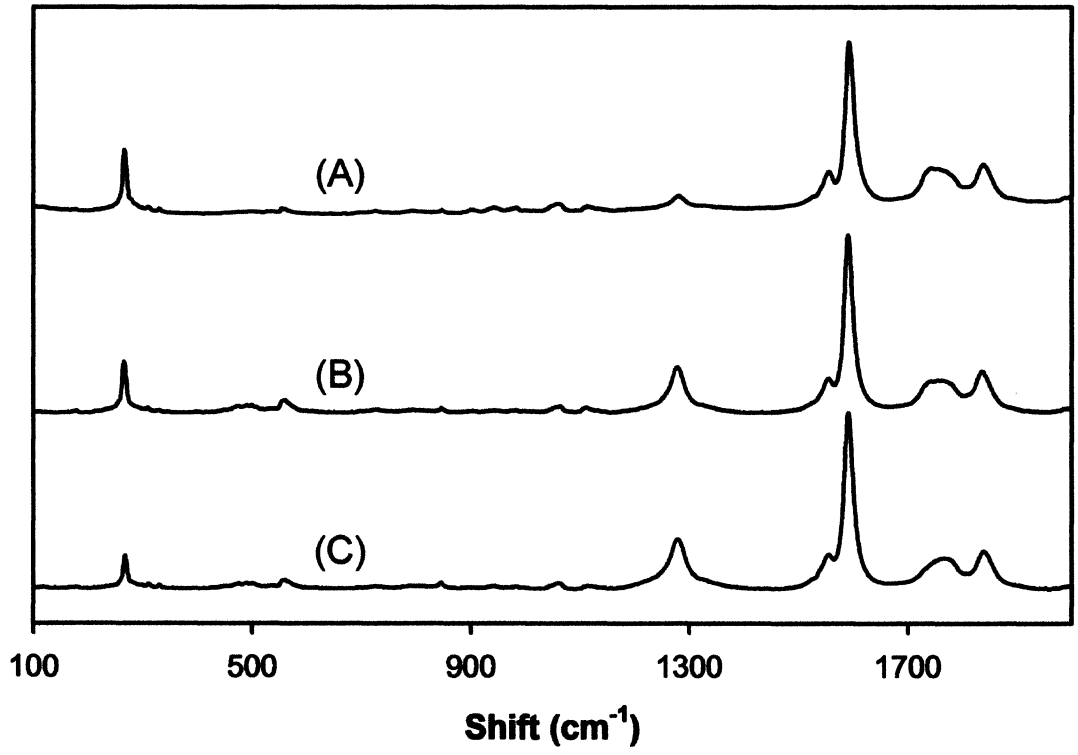

Figure 2.1. Raman Spectra of pristine SWNTs (A), benzoic acid functionalized SWNTs (B), and PEI functionalized SWNTs (C).

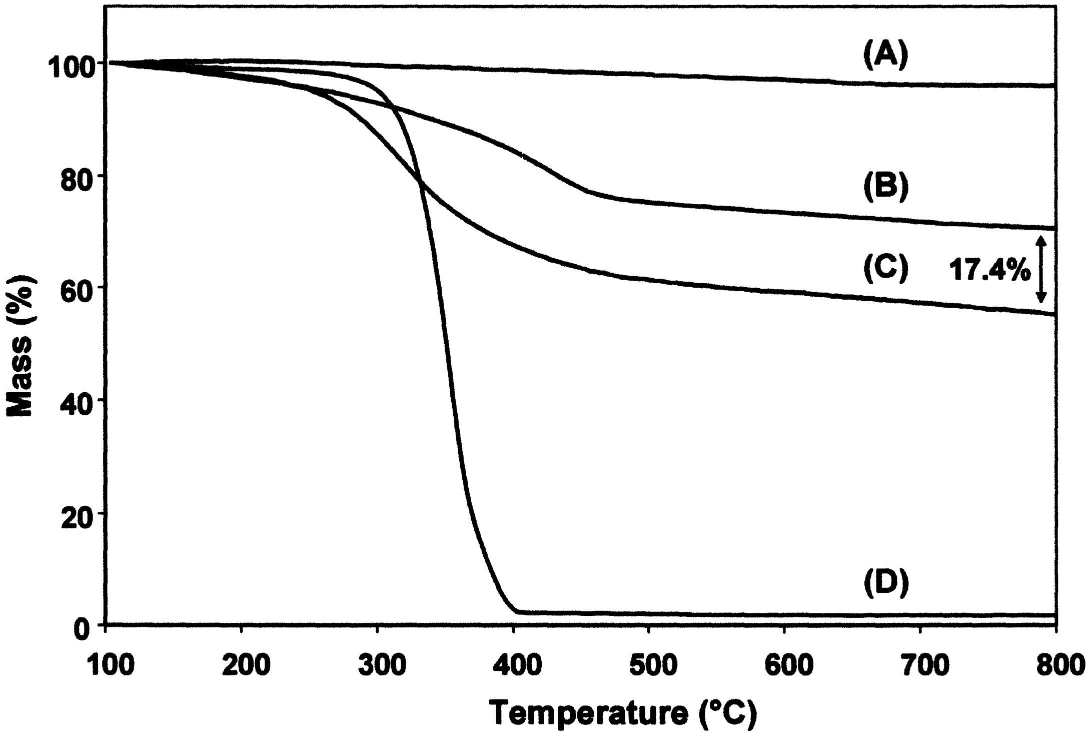

Figure 2.2. TGA plot of pristine SWNTs (A), benzoic acid functionalized SWNTs (B), PEI functionalized SWNTs (C), and PEI (Mn = 10 kDa) (D).

The degree of functionalization of modified SWNTs was quantified using thermogravimetric analysis (TGA) (Figure 2.2). Pristine SWNTs exhibit a small mass loss when heated under Argon to 800°C. When heated using the same temperature profile, benzoic acid functionalized SWNTs displayed a mass loss of 23.4%, centered at a temperature of 390°C. Taking the molecular weight of the benzoic acid groups into account, the degree of functionalization was determined to be approximately equal to 1 functional group for every 31 carbon atoms within the nanotube. In the case of PEI functionalized SWNTs, a further mass loss of 17.4% was attributed to decomposition of polymer, corresponding to the introduction of approximately one polymer chain for every 2,600 carbon atoms within the nanotube. The decomposition temperature of PEI upon functionalized SWNTs, taken from the point of 50% decomposition, was determined to be 330°C. This value agrees favorably with that obtained for pure PEI (350°C). It is possible that the earlier onset of polymer degradation observed for functionalized SWNTs in comparison to pure PEI may result from the high thermal conductivity of the nanotubes.

2.2.2. Fabrication of PEI functionalized SWNT thin films

PEI functionalized SWNT films were prepared using the vacuum filtration method. Polymer functionalization enables the preparation of stable nanotube dispersions and allows homogeneous films to be formed using vacuum filtration without the addition of surfactants such as SDS. Dilute solutions of polymer functionalized SWNTs were prepared by dispensing 10 mg of PEI functionalized SWNTs in 20 mL of distilled H_2O by sonication (20 minutes). This dispersion was then centrifuged for 20 minutes at 2570g and allowed to stand for 48 hours, after which the supernatant was transferred to a flask and diluted by addition of 80 mL of distilled water. The resulting dilute solution was filtered through a 200 nm pore diameter PTFE membrane, taking care to avoid the formation of bubbles. The film was washed with distilled water (250 mL) and diethyl ether (250 mL), then dried in a vacuum oven for 48 hours (55°C). For the purposes of this work, films were kept intact upon the filtration membranes, due to the additional mechanical support that they provided. However, these films could be peeled away from the membrane to produce free standing thin films, or they could be transferred to a suitable substrate if required.[37] Using 3D optical profilometry, the thickness of PEI functionalized nanotube films was determined to be approximately 2 μm. In addition to PEI functionalized SWNT films, pristine SWNTs were cast into thin films by filtration of a nanotube dispersion in 1% SDS solution, according to literature procedures, to provide a control sample lacking PEI.[53, 54] As an additional control sample, SWNT films containing non-covalently bound PEI were prepared by filtration of pristine nanotubes dispersed in 5 wt% PEI solution.

2.2.3. Reduction of $HAuCl_4$ upon PEI functionalized SWNT thin films

Reduction of $HAuCl_4$ upon the surface of PEI functionalized SWNT thin films was conducted by submersing nanotube films, supported upon PTFE filtration membranes, in aqueous solutions of $HAuCl_4$ (0.5 – 2 mM) and heating to 60°C for between 30 and 120 minutes. Films were then removed from solution and washed repeatedly with distilled water and acetone to remove traces of residual $HAuCl_4$, followed by drying under a flow of nitrogen. Following this treatment, gold could be seen deposited upon the surface of the polymer functionalized nanotube films. Under the same reaction conditions, pristine SWNT films displayed a similar change in appearance. The amount of gold deposited was however significantly lower than was observed for PEI functionalized SWNT films. When this process was repeated, using films containing PEI that was not covalently bound to the surface of SWNTs, the $HAuCl_4$ solution turned from yellow to red shortly after heating, indicating the formation of gold nanoparticles in solution (Figure 2.3). When films were removed and washed, no significant change in the appearance of the film was observed. Under these conditions, it is believed that PEI leeches from the film into solution where it reduces gold cations and stabilizes the growth.

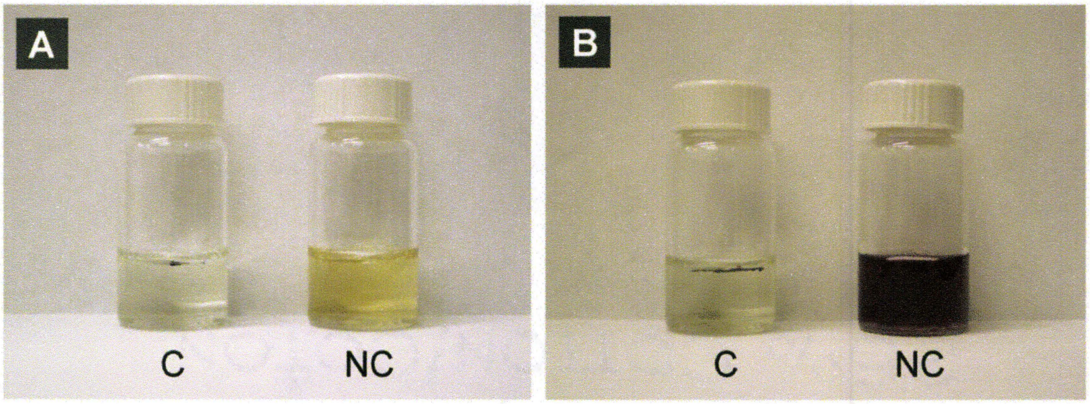

Figure 2.3. Photographs of vials containing 0.5 mM $HAuCl_4$ solution and films of SWNTs functionalized with PEI by covalent (C) and non covalent (NC) approaches. Photo (A) was taken 5 minutes after films were added to the solution. Photo (B) was taken following 30 min of heating at 60°C.

It is known that carbon nanotubes may spontaneously reduce metal ions in solution by direct redox reaction.[19, 20] However, as pristine SWNT films prepared in this work contain no additional reducing or stabilizing agents, they were expected to display lower density of gold functionalization than films containing PEI. SDS, the surfactant used in the fabrication of pristine SWNT films, is known to act as a stabilizing agent in the production of gold nanoparticles,[56-58] and has previously been utilized in the functionalization of MWNTs with gold nanoparticles in solution.[59] For the purposes of our control experiments, it was therefore vital that pristine SWNT films contained no traces of residual surfactant.

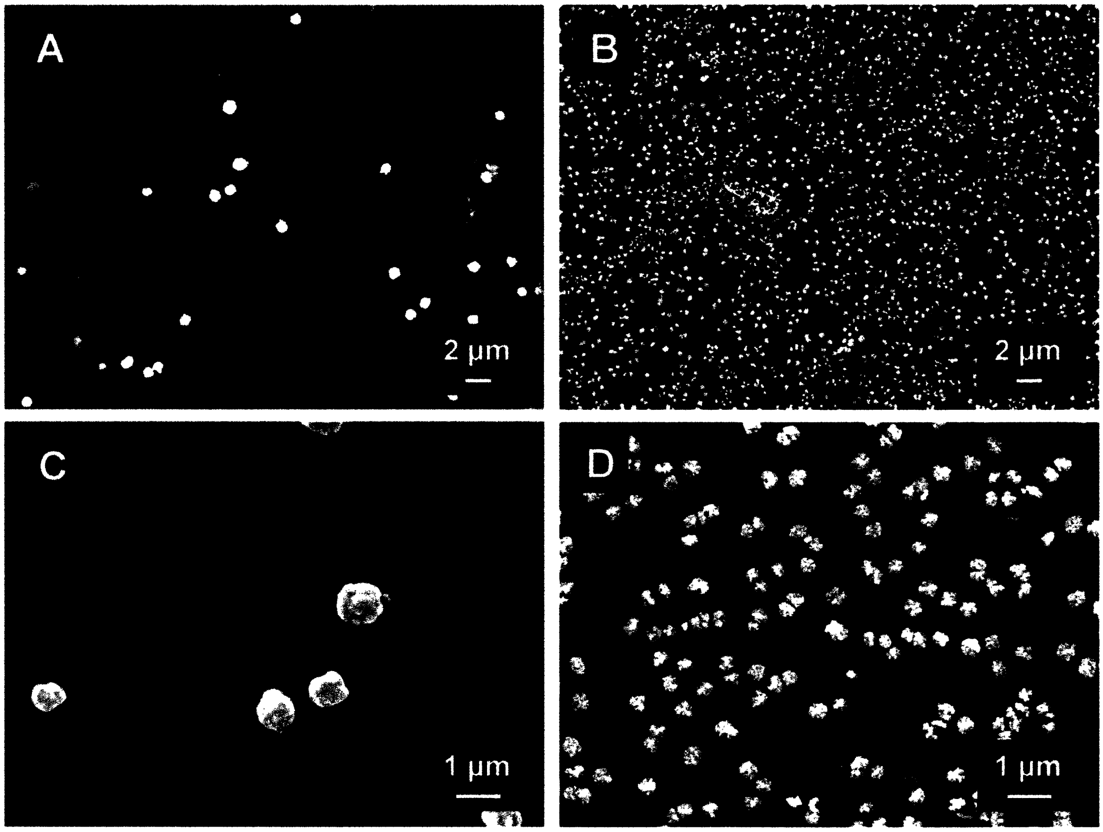

Figure 2.4. SEM image of unmodified (A and C) and PEI functionalized (B and D) SWNT films following immersion and heating at 60°C in 0.5 mM $HAuCl_4$ solution for 30 minutes.

Pristine nanotube films used in this work were washed with approximately 4 L of distilled water to ensure the complete removal of SDS. In addition, Jung and coworkers[22] previously reported the functionalization of pristine carbon nanotube films with gold nanoparticles by in-situ reduction of $HAuCl_4$ (0.5 – 2 mM) in 50% ethanol. Under certain conditions, alcohols are known to act as reducing agents in the formation of gold nanoparticles,[58, 60] and a recent report by Li et al. demonstrated that ethanol potentially plays an important role in the mechanism of electroless reduction of metal ions upon the surface of carbon nanotubes[61]. We have therefore chosen to conduct our experiment in doubly distilled water to ensure that the effects of PEI functionalization may be observed without interference from any other reducing agents.

Following treatment in $HAuCl_4$, films were transferred from the PTFE membrane support to carbon tape and imaged using scanning electron microscopy (SEM). Untreated pristine nanotube films resemble randomly oriented two dimensional interpenetrated networks of nanotube bundles. Figure 2.4 shows images of pristine and PEI functionalized SWNTs films following immersion and heating in 0.5 mM $HAuCl_4$ solution for 30 min. It can be seen that, in both cases, the films are covered with gold nanoparticle clusters. In addition, some larger aggregates are also observed in regions of high density. Nanoparticle clusters are located both at the surface and also appear to be embedded below the surface of the film. These films differ significantly from composite materials produced by in-situ reduction of $HAuCl_4$ in solution by non-covalently functionalized MWNTs as reported by Hu and co-workers.[52]

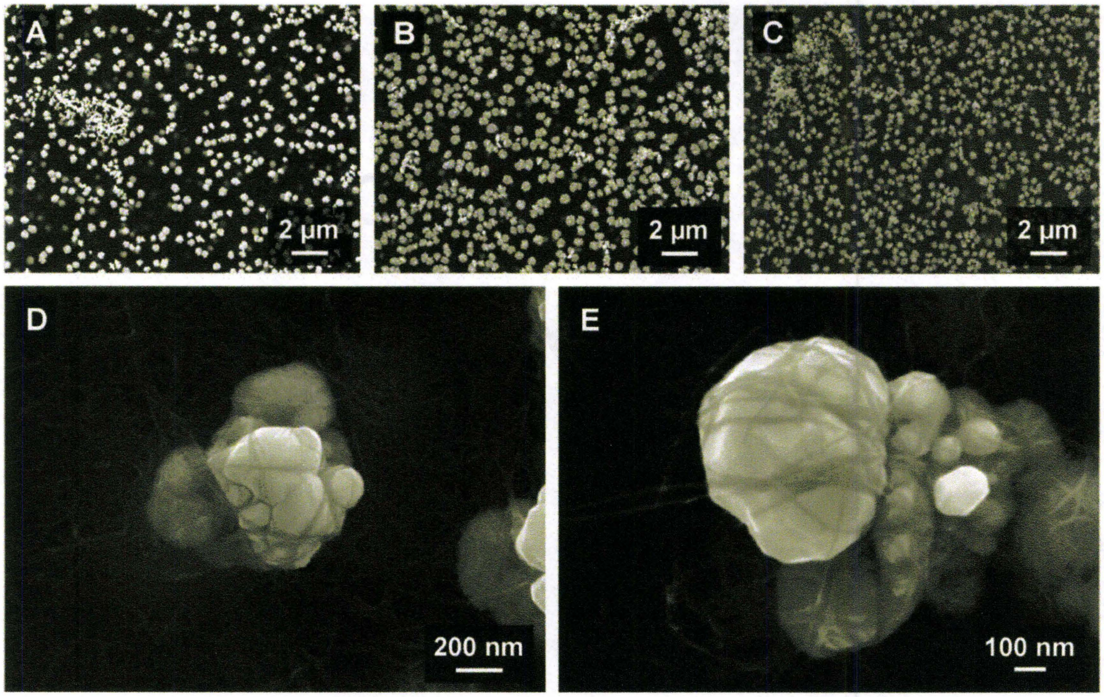

Figure 2.5. SEM images of PEI functionalized SWNT films following immersion and heating at 60°C in 0.5 mM $HAuCl_4$ solution for 30 minutes (A), 60 minutes (B), and 120 minutes (C). Images (D) and (E) correspond to samples from the same films following immersion and heating at 60°C for 30 minutes in 1.0 mM and 2.0 mM $HAuCl_4$ solutions respectively.

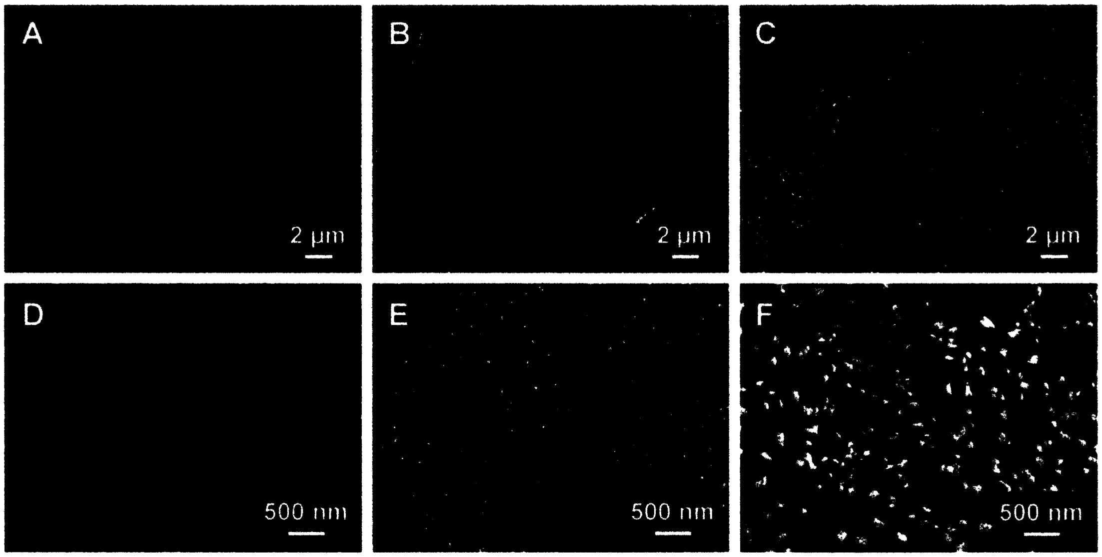

Figure 2.6. SEM images of PEI functionalized SWNT films following immersion in 0.5 mM $HAuCl_4$ solution at room temperature for 1 min (A and D), 2 min (B and E) and 5 min (C and F).

In this previous example, nanowires consisting of MWNTs coated with interconnected Au nanoparticles were obtained. We propose that the close proximity of PEI functionalized nanotubes in densely packed thin films enables the reduction of gold ions into discrete nanoparticles that are stabilized in the form of small clusters by the nanotube-bound PEI, but do not coat individual nanotubes, as shown in Figures 2.4 and 2.5 Electrodispersive X-ray Spectroscopy (EDXS) was utilized to confirm the presence of metallic gold (see Appendices, Figure 2.I.1). In the case of PEI functionalized SWNT films, the density of nanoparticles was significantly greater than that observed for films of unmodified SWNTs. The average diameter of gold clusters was also significantly smaller when formed upon PEI functionalized nanotube films, relative to unmodified SWNTs

(Table 2.1). The effect of reaction time upon Au nanoparticle cluster size and distribution was also investigated. In Figure 2.5, SEM images, a, b, and c, show PEI functionalized nanotube films submersed in 0.5 mM $HAuCl_4$ solution for 30 minutes, 1 hour, and 2 hours, respectively.

Table 2.1. Average nanoparticle cluster diameter of unmodified and PEI functionalized SWNT films following immersion in 0.5 mM $HAuCl_4$ solution.

Time (Min)	Temp. (°C)	Pristine[a] (nm)	PEI f-SWNT[b] (nm)
1	25	-	53 ± 10
2	25	-	59 ± 10
5	25	-	140 ± 20
30	60	972 ± 110	448 ± 50
60	60	1015 ± 100	542 ± 50
120	60	944 ± 130	407 ± 50

a Average values taken from a minimum of 15 measurements, b Average values taken from a minimum of 25 measurements

At high magnification, gold clusters that penetrate the film surface can be observed, which are caged and seemingly held in place by nanotube bundles running over the face of the clusters. Based on a visual, qualitative analysis of this SEM data, it was speculated that small, discrete gold nanoparticles first formed upon PEI functionalized SWNTs within the films, and later aggregated to form larger clusters, as shown in Figure 2.5. D and E. It was therefore postulated that at much shorter reaction times, smaller individual particles might be observed within the nanotube films. Figure 2.6 shows SEM images of films that were submersed in 0.5 mM $HAuCl_4$ solution at room temperature for periods of 1, 2, and 5 minutes. After one minute (Figure 2.6, A and D), nanoparticles approximately 50 nm in diameter were observed upon the surface of nanotube bundles in addition to some smaller nanoparticles. After two minutes (Figure 2.6, B and E), the average nanoparticle diameter increased to approx. 60 nm while the density of nanoparticles seemed to decrease. Smaller nanoparticles were no longer observable, suggesting that aggregation of particles had begun. In films submersed in $HAuCl_4$ solutions for five minutes, irregularly shaped nanoparticles were observed that resemble the larger clusters obtained at longer reaction times. In addition to the aggregation effect described above, it is possible that nanoparticles continue to grow as a result of diffusion and reduction of gold cations from solution.

Films containing PEI that was not covalently bound to the surface of nanotubes were also characterized using SEM. Following treatment in $HAuCl_4$ solution, films were shown to contain a high density of discrete Au nanoparticles, the diameter of which is smaller than those observed in films of covalently functionalized SWNTs. The presence of smaller discrete nanoparticles may be due to an increase in the percentage of PEI present within these films. It is, however, likely that these nanoparticles are formed by a different process. When films are placed in solution, unbound PEI is released from the film. In solution, free PEI acts to reduce $HAuCl_4$ forming Au nanoparticles that are subsequently deposited upon the nanotube film. Soaking these films in distilled water overnight led to aggregation of nanoparticles, possibly as a result of further loss of PEI from the film into solution.

Figure 2.7. SEM images (A) and (B) correspond to SWNT films containing unbound PEI following immersion and heating at 60°C for 1 hour in $HAuCl_4$ solution having a concentration of 0.5 mM. Image (C) is of the same sample following submersion in distilled water overnight.

The distribution of gold nanoparticles within the nanotube films was studied using TEM. In samples which had undergone immersion in 0.5 mM $HAuCl_4$ solution for 1 minute at room temperature (Figure 2.8, A and B), gold nanoparticle clusters were shown to be located primarily upon the films surface. The size and distribution of these clusters is in agreement with the images obtained using SEM. At higher magnification smaller gold nanoparticles can also be seen, embedded at various depths within the film. At short reaction times, the growth of nanoparticles within the film is likely hindered by the rate of diffusion of gold cations. In addition, the structure of the carbon nanotube film may also prevent the rapid aggregation of these nanoparticles and formation of nanoparticle clusters. In the case of samples which have undergone immersion in 0.5 mM $HAuCl_4$ solution for 1 hour at 60°C (Figure 2.8, C and D) large nanoparticle clusters are located throughout the film. Few discrete nanoparticles are observed in these samples suggesting that clusters within the film form by aggregation in a manner similar to those upon the film's surface.

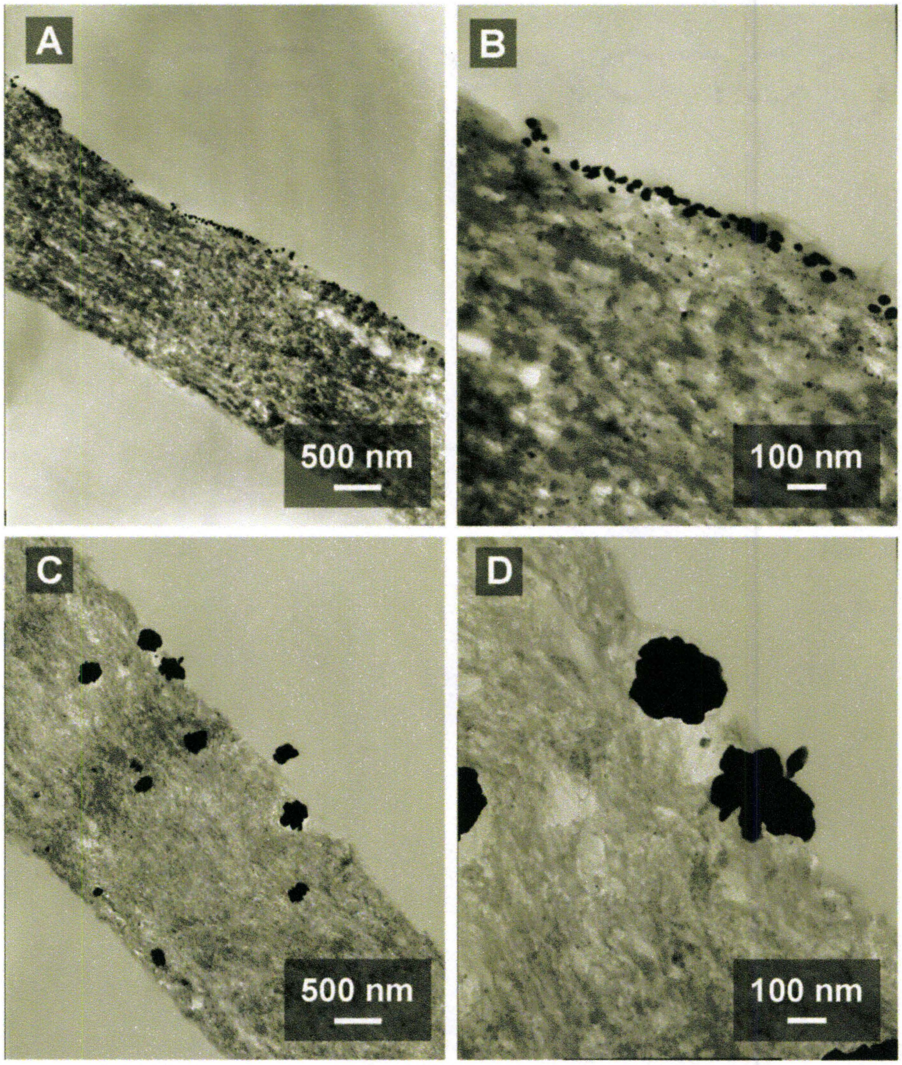

Figure 2.8. TEM images of PEI functionalized SWNT films following immersion in 0.5 mM $HAuCl_4$ solution at room temperature for 1 minute (A and B) and at 60°C for 60 minutes (C and D)

Images of the film's cross section were obtained using Focused Ion Beam–SEM. Figure 2.9.A shows PEI functionalized nanotube films which have undergone room temperature immersion in $HAuCl_4$ solution for 1 minute. In agreement with data obtained from TEM images, it was observed that gold nanoparticle clusters are located predominantly upon the surface of these nanotube films. Smaller discrete nanoparticles, located at various depths throughout the film, are also observed. Cross sectional images reveal the films to have a porous layered structure. It is proposed that the presence of free volume within these films allows the internal diffusion and aggregation of nanoparticles which is observed at longer reaction times (Figure 2.9.B).

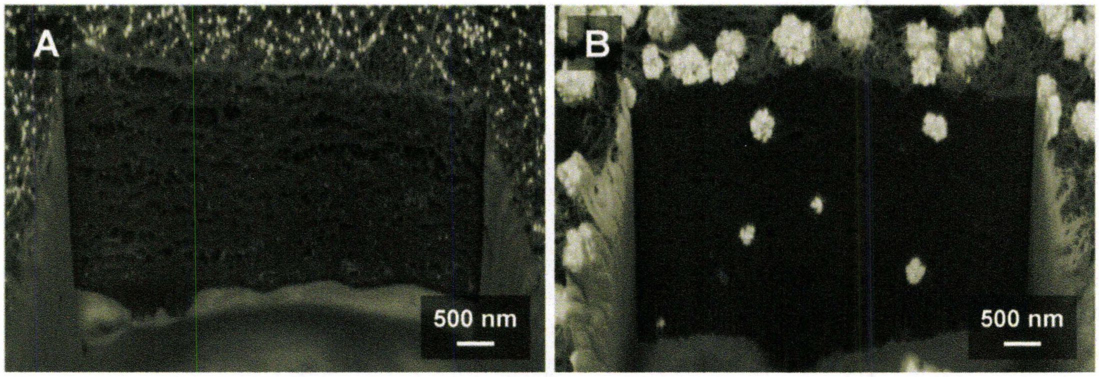

Figure 2.9. FIB-SEM images of PEI functionalized SWNT films following immersion in 0.5 mM $HAuCl_4$ solution at room temperature for 1 minute (A) and at 60°C for 60 minutes (B).

2.3. Conclusion

We have shown that polymer functionalization of carbon nanotubes allow the preparation of highly stable nanotube dispersions in aqueous solution, enabling the formation of homogeneous thin films containing multiple active functional groups that can subsequently be utilized for further reaction. PEI functionalized SWNT films were prepared by vacuum filtration in the absence of additional surfactants. Decoration of films with gold nanoparticle clusters was achieved by in-situ reduction of gold cations under mild conditions in the absence of additional reducing agents. Nanoparticle size and density was controlled by adjustment of reaction time. In the absence of PEI, nanoparticle density was shown to be greatly reduced, indicating that the PEI tethered to the nanotube surface does play an important role in the formation of Au nanoparticles. The work reported here paves the way for further investigation of metal reduction on the nanotube film surface, which will lead to new composite materials that will potentially be suitable for a range of applications within nanotube-based electronics and catalysis.

2.4. Experimental

2.4.1. General

Single-walled carbon nanotubes were purchased from Carbon Nanotechnologies, Inc. (Houston, TX). SWNTs were produced by the HiPCO process and were used as received. All other reagents and solvents were obtained from commercial suppliers and used without any prior treatment. Laser Raman spectroscopy was performed on a Bruker

RFS 100 instrument equipped with a YAG laser and a Ge high-sensitivity detector. Thermogravimetric analysis (TGA) was carried out on a NETZSCH STA 409 PC instrument, heating from 0°C to 800°C at a constant rate of 5°C per minute under argon. All absorbance measurements were made using a Cary 50 Bio UV-Visible Spectrophotometer. Optical profilometry was performed on a Veeco WYKO NT1100 Optical Profiling System. SEM imaging was performed using a JEOL JSM-7000F scanning electron microscope, equipped with a Schottky type field emission gun filament, with nanotube films attached to carbon tape upon SEM stubs. Electrodispersive X-ray spectroscopy was conducted using an Oxford instruments INCA Energy Dispersive Spectrometer (EDXS) X-ray microanalysis system equipped with HKL Electron Backscatter(ed) Diffraction (EBSD) system. TEM imaging was performed using a JEOL JEM 1299 EX TEMSCAN transmission electron microscope (JEOL, Peabody, MA, USA) operated at an accelerating voltage of 80 kV. For cross-section analysis, pieces of Au-loaded SWNT films were embedded in spur resin before microtomy (60-80 nm thickness). The cuts were then transfer onto carbon-coated TEM grids and imaged with the same TEM. Filtrations were carried out using VWR filtration apparatus with stainless steel support screen and Sartorius PTFE membranes (4.7 cm diameter, 200 nm pore size). Nanotube samples were dispersed in solvent using a Branson 1510 bath sonicator. Nanotube dispersions in solvent were centrifuged using a Beckman Coulter Allegra X-22 Centrifuge set at 2570g for 20 minutes.

2.4.2. Measurement of SWNT-PEI conjugate concentration

A vial containing poly(ethylene imine)-functionalized SWNTs (10 mg) and distilled water (20 mL) was sonicated for 15 minutes. The vial was then centrifuged at 2570 g for 20 minutes and subsequently allowed to stand for 48 hours, after which the supernatant was removed and diluted with distilled water to appropriate concentrations for UV/vis absorption measurement. The specific extinction coefficient at 500 nm ($0.0103\ L\ mg^{-1}\ cm^{-1}$)[62] was used to calculate the concentration of the functionalized full-length SWNTs .

2.4.3. Preparation of Benzoic Acid functionalized SWNTs

250 mg pristine SWNTs and 150 mL distilled water were added to a 250 mL round bottomed flask. Nanotubes were dispersed by sonication (45 minutes). 8.00 g of 4-aminobenzoic acid (58 mmol, 2.8 equiv/mol. carbon) was added to the flask, followed by 4.00 mL of isoamylnitrite (30 mmol, 1.4 equiv/mol. carbon). The flask was equipped with a reflux condenser and heated to 80°C for 18 hours, after which the nanotubes were isolated by filtration through a PTFE membrane (200 nm pore size) and washed with DMF until the filtrate became colorless. DMF was removed by washing with diethyl ether, and the product was dried in a vacuum oven (50°C) for 48 h.

2.4.4. Preparation of PEI functionalized SWNTs

Benzoic acid functionalized SWNTs (8.9 mg) were dispersed in 20 mL anhydrous DMF and stirred at 0°C under a constant flow of nitrogen. Thionyl chloride (1.5 mL, 20.56 mmol) was added slowly and reaction temperature was raised to room temperature and allowed to stir for 4 hours. Acyl chloride functionalized tubes were obtained by filtration through a PTFE membrane (200 nm pore size) and washed (anhydrous DCM, 250 mL) to remove excess thionyl chloride. Nanotubes were immediately dispersed in 50 mL anhydrous DCM and added slowly to a solution of PEI (9.0 g, Mw = 10 kDa) in 100 mL anhydrous DCM at 0°C. The reaction was allowed to stir overnight at room temperature under nitrogen, after which the temperature was slowly raised to 55°C over a period of 4 hours. The resulting nanotubes were isolated by filtration through a PTFE membrane (200 nm pore size) and washed with DMF (750 mL), water (500 mL) and diethyl ether (250 mL). 5.6 g (63 wt%) soluble polymer functionalized SWNTs were obtained using this procedure.

2.4.5. Fabrication of PEI functionalized SWNT thin films

A vial containing Poly(ethylene imine)-functionalized SWNTs (10 mg) and distilled water (20 mL) was sonicated for 15 minutes. The vial was then centrifuged at 2570 g for 20 minutes and subsequently allowed to stand for 48 hours, after which the supernatant was transferred to an Erlenmeyer flask and diluted by addition of approximately 80 mL distilled water. This dilute solution was filtered through a PTFE membrane (200 nm pore size). The SWNT film produced by this process was then washed with distilled water (250 mL) and diethyl ether (250 mL). The film was then dried in vacuo (50°C, 48 hours) during which time it remained intact upon the filtration membrane.

2.4.6. Fabrication of non-covalently functionalized PEI / SWNT thin films

A flask containing SWNTs (20 mg) and 500 mL 5 wt% PEI solution in distilled water was sonicated at room temperature for 30 minutes. The resulting dispersion was centrifuged at 2570g for 20 minutes, and allowed to stand for 48 hours after which the supernatant was removed and transferred to an Erlenmeyer flask. This solution was subsequently filtered through a PTFE membrane (200 nm pore size). The film was then dried in vacuo (50°C, 48 hours) during which time films remained upon the filtration membrane.

2.4.7. Fabrication of unmodified SWNT thin films

A flask containing SWNTs (20 mg) and 500 mL of a 1 wt% SDS solution in distilled water was sonicated at room temperature for 30 minutes. The resulting dispersion was centrifuged at 2570 g for 20 minutes, and allowed to stand for 48 hours, after which the supernatant was removed and transferred to an Erlenmeyer flask. This process was repeated until 1 L of CNT / SDS solution was obtained. This solution was subsequently filtered through a PTFE membrane (200 nm pore size). The SWNT film produced by this process was then washed with distilled water (4 L) and diethyl ether (250 mL). The film was then dried in vacuo (50°C, 48 hours) during which time it remained intact upon the filtration membrane.

2.4.8. Reduction of $HAuCl_4$ upon SWNT thin films

A section of SWNT thin film supported upon PTFE filtration membrane having dimensions approximately equal to 1 cm^2 was placed in a 20 mL glass vial and submersed in 0.5 mM $HAuCl_4$ solution. The vial was heated to 60°C for a period of 30 minutes after which the film was removed and washed repeatedly with water and acetone to remove traces of excess $HAuCl_4$. Films were dried under nitrogen gas.

2.5. References

(1) M. Terrones. *Annu. Rev. Mater. Res.* **2003,** 33, 419-501.

(2) J. Kong, N. R. Franklin, C. W. Zhou, M. G. Chapline, S. Peng, K. J. Cho and H. J. Dai. *Science* **2000,** 287, (5453), 622-625.

(3) E. Bekyarova, M. Davis, T. Burch, M. E. Itkis, B. Zhao, S. Sunshine and R. C. Haddon. *J. Phys. Chem. B* **2004,** 108, (51), 19717-19720.

(4) J. Sippel-Oakley, H. T. Wang, B. S. Kang, Z. C. Wu, F. Ren, A. G. Rinzler and S. J. Pearton. *Nanotechnology* **2005,** 16, (10), 2218-2221.

(5) A. Star, T. R. Han, V. Joshi, J. C. P. Gabriel and G. Gruner. *Adv. Mater.* **2004,** 16, (22), 2049-2052.

(6) O. A. Kuzmych, B. L.; Star, A. . *Nanotechnology* **2007**, 1-7.

(7) S. J. Tans, A. R. M. Verschueren and C. Dekker. *Nature* **1998,** 393, (6680), 49-52.

(8) A. Bachtold, P. Hadley, T. Nakanishi and C. Dekker. *Physica E* **2003,** 16, (1), 42-46.

(9) R. H. Baughman, A. A. Zakhidov and W. A. de Heer. *Science* **2002,** 297, (5582), 787-792.

(10) D. M. Guldi, G. M. A. Rahman, M. Prato, N. Jux, S. H. Qin and W. Ford. *Angew Chem Int Ed* **2005,** 44, (13), 2015-2018.

(11) B. J. Landi, R. P. Raffaelle, S. L. Castro and S. G. Bailey. *Prog. Photovoltaics* **2005,** 13, (2), 165-172.

(12) V. G. Georgakilas, D.; Tzitzios, V.; Pasquato, L.; Guldi, D.M.; Prato, M. *J. Mater. Chem.* **2007,** 17, 2679 - 2694.

(13) G. G. B. Wldgoose, C.E.; Compton, R.G. *Small* **2006,** 2, (2), 182-193.

(14) L. Liu, T. X. Wang, J. X. Li, Z. X. Guo, L. M. Dai, D. Q. Zhang and D. B. Zhu. *Chem Phys Lett* **2003,** 367, (5-6), 747-752.

(15) J. Shi, Z. Wang and H. L. Li. *J Nanopart Res* **2006,** 8, (5), 743-747.

(16) A. V. Ellis, K. Vjayamohanan, R. Goswaimi, N. Chakrapani, L. S. Ramanathan, P. M. Ajayan and G. Ramanath. *Nano Lett.* **2003,** 3, (3), 279-282.

(17) G. M. A. Rahman, D. M. Guldi, E. Zambon, L. Pasquato, N. Tagmatarchis and M. Prato. *Small* **2005,** 1, (5), 527-530.

(18) L. Han, W. Wu, F. L. Kirk, J. Luo, M. M. Maye, N. N. Kariuki, Y. H. Lin, C. M. Wang and C. J. Zhong. *Langmuir* **2004,** 20, (14), 6019-6025.

(19) H. C. Choi, M. Shim, S. Bangsaruntip and H. J. Dai. *J. Am. Chem. Soc.* **2002,** 124, (31), 9058-9059.

(20) D. S. Kim, T. Lee and K. E. Geckeler. *Angew Chem Int Ed* **2006,** 45, (1), 104-107.

(21) L. T. Qu and L. M. Dai. *J. Am. Chem. Soc.* **2005,** 127, (31), 10806-10807.

(22) B. S. Kong, D. H. Jung, S. K. Oh, C. S. Han and H. T. Jung. *J. Phys. Chem. C* **2007,** 111, (23), 8377-8382.

(23) G. Gruner. *J. Mater. Chem.* **2006,** 16, (35), 3533-3539.

(24) M. A. Meitl, Y. X. Zhou, A. Gaur, S. Jeon, M. L. Usrey, M. S. Strano and J. A. Rogers. *Nano Lett.* **2004,** 4, (9), 1643-1647.

(25) C. S. Du, J. Yeh and N. Pan. *J. Mater. Chem.* **2005,** 15, (5), 548-550.

(26) T. V. Sreekumar, T. Liu, S. Kumar, L. M. Ericson, R. H. Hauge and R. E. Smalley. *Chem. Mater.* **2003,** 15, (1), 175-178.

(27) N. Saran, K. Parikh, D. S. Suh, E. Munoz, H. Kolla and S. K. Manohar. *J. Am. Chem. Soc.* **2004,** 126, (14), 4462-4463.

(28) V. Bocharova, A. Kiriy, U. Oertel, M. Stamm, F. Stoffelbach, R. Jerome and C. Detrembleur. *J. Phys. Chem. B* **2006,** 110, (30), 14640-14644.

(29) S. Kazaoui, N. Minami, R. Jacquemin, H. Kataura and Y. Achiba. *Phys. Rev. B* **1999,** 60, (19), 13339-13342.

(30) M. Kaempgen, G. S. Duesberg and S. Roth. *Appl. Surf. Sci.* **2005,** 252, (2), 425-429.

(31) Y. Kim, N. Minami, W. Zhu, S. Kazaoui, R. Azumi and M. Matsumoto. *Synthetic Met.* **2003,** 135, (1-3), 747-748.

(32) A. Mamedov, D. M. Guldi, M. Prato and N. A. Kotov. *Abstr. Pap. Am. Chem. S.* **2002,** 223, U409-U409.

(33) H. Ko, C. Y. Jiang, H. Shulha and V. V. Tsukruk. *Chem. Mater.* **2005,** 17, (10), 2490-2493.

(34) M. Olek, J. Ostrander, S. Jurga, H. Mohwald, N. Kotov, K. Kempa and M. Giersig. *Nano Lett.* **2004,** 4, (10), 1889-1895.

(35) Y. Abe, R. Tomuro and M. Sano. *Adv. Mater.* **2005,** 17, (18), 2192-2194.

(36) L. Hu, D. S. Hecht and G. Gruner. *Nano Lett.* **2004,** 4, (12), 2513-2517.

(37) Z. C. Wu, Z. H. Chen, X. Du, J. M. Logan, J. Sippel, M. Nikolou, K. Kamaras, J. R. Reynolds, D. B. Tanner, A. F. Hebard and A. G. Rinzler. *Science* **2004,** 305, (5688), 1273-1276.

(38) F. Hennrich, S. Lebedkin, S. Malik, J. Tracy, M. Barczewski, H. Rosner and M. Kappes. *Phys. Chem. Chem. Phys.* **2002,** 4, (11), 2273-2277.

(39) S. Malik, H. Rosner, F. Hennrich, A. Bottcher, M. M. Kappes, T. Beck and M. Auhorn. *Phys. Chem. Chem. Phys.* **2004,** 6, (13), 3540-3544.

(40) H. E. Unalan, G. Fanchini, A. Kanwal, A. Du Pasquier and M. Chhowalla. *Nano Lett.* **2006,** 6, (4), 677-682.

(41) G. J. C. Bahun, F.; Homenick, C.M.; Lawson, G.; Zhu, J.;Adronov, A., The Polymer Chemistry of Carbon Nanotubes. In *Chemistry of Carbon Nanotubes*, V. A. B. Basiuk, E.V.; , Ed. American Scientific Publishers, **2008,** 191-206.

(42) M. J. O'Connell, P. Boul, L. M. Ericson, C. Huffman, Y. H. Wang, E. Haroz, C. Kuper, J. Tour, K. D. Ausman and R. E. Smalley. *Chem Phys Lett* **2001,** 342, (3-4), 265-271.

(43) C. M. L. Homenick, G.; Adronov, A. . *Polymer Reviews* **2007,** 47, (2), 265-290.

(44) I. Yamaguchi and T. Yamamoto. *Mater Lett* **2004,** 58, (5), 598-603.

(45) L. M. Bronstein, S. N. Sidorov, A. Y. Gourkova, P. M. Valetsky, J. Hartmann, M. Breulmann, H. Colfen and M. Antonietti. *Inorg Chim Acta* **1998,** 280, (1-2), 348-354.

(46) M. J. Richardson, J. H. Johnston and T. Borrmann. *Eur J Inorg Chem* **2006,** (13), 2618-2623.

(47) P. L. Kuo, C. C. Chen and M. W. Jao. *J. Phys. Chem. B* **2005,** 109, (19), 9445-9450.

(48) C. Note, S. Kosmella and J. Koetz. *Colloids Surf A* **2006,** 290, (1-3), 150-156.

(49) X. P. Sun, S. J. Dong and E. K. Wang. *Polymer* **2004,** 45, (7), 2181-2184.

(50) P. L. Kuo, W. F. Chen, H. Y. Huang, I. C. Chang and S. A. Dai. *J. Phys. Chem. B* **2006,** 110, (7), 3071-3077.

(51) J. Sun and L. Gao. *J Electroceram* **2006,** 17, (1), 91-94.

(52) X. G. Hu, T. Wang, X. H. Qu and S. J. Dong. *J. Phys. Chem. B* **2006,** 110, (2), 853-857.

(53) Y. X. Zhou, L. B. Hu and G. Gruner. *Appl. Phys. Lett.* **2006,** 88, (12), 123109.

(54) D. H. Zhang, K. Ryu, X. L. Liu, E. Polikarpov, J. Ly, M. E. Tompson and C. W. Zhou. *Nano Lett.* **2006,** 6, (9), 1880-1886.

(55) B. K. Price and J. M. Tour. *J. Am. Chem. Soc.* **2006,** 128, (39), 12899-12904.

(56) J. P. Deng, W. C. Shih and C. Y. Mou. *Chemphyschem* **2005,** 6, (10), 2021-2025.

(57) J. P. Deng, C. H. Wu, C. H. Yang and C. Y. Mou. Langmuir **2005,** 21, (19), 8947-8951.

(58) K. Barbour, M. Ashokkumar, R. A. Caruso and F. Grieser. J. Phys. Chem. B **1999,** 103, (43), 9231-9236.

(59) M. N. Zhang, L. Su and L. Q. Mao. Carbon **2006,** 44, (2), 276-283.

(60) M. Quinn and G. Mills. J Phys Chem-Us **1994,** 98, (39), 9840-9844.

(61) P. J. Li, Y. Chai, X. L. Zhou, Q. F. Zhang and J. L. Wu. Fuller Nanotub Car N **2005,** 13, (4), 377-383.

(62) Y. Q. Liu, Z. L. Yao and A. Adronov. Macromolecules **2005,** 38, (4), 1172-1179.

Chapter 3: Growth and Characterization of GaAs Nanowires on Carbon Nanotube Composite Films

Parsian K. Mohseni, Gregor Lawson, Christophe Couteau, Gregor Weihs, Alex Adronov and Ray R. LaPierre,

This chapter has been reproduced in part with permission from *Nano Letters,* **2008,** 8 (11), 4075–4080, **DOI:** 10.1021/nl802003m

Work detailed in this chapter was carried out in collaboration with Parsian K. Mohsini and Dr. Ray LaPierre (Department of Engineering Physics and Centre for Emerging Device Technology, McMaster University, Hamilton, Ontario). Both Gregor Lawson and Parsian K. Mohseni contributed equally to the experimental planning and writing of this work. Composite film preparation and characterization was conducted by Gregor Lawson. Nanowire growth and characterization was conducted by Parsian K. Mohseni.

Abstract

Poly(ethylene imine) functionalized carbon nanotube thin films, prepared using the vacuum filtration method, were decorated with Au nanoparticles by in-situ reduction of $HAuCl_4$ under mild conditions. These Au nanoparticles were subsequently employed for the growth of GaAs nanowires (NWs) by the vapor-liquid-solid process in a gas source molecular beam epitaxy system. The process resulted in the dense growth of GaAs NWs monolithically integrated across the entire surface of the single-walled nanotube (SWNT) films. The NWs, which were orientated in a variety of angles with respect to the SWNT films, ranged in diameter between 20 to 200 nm, with heights up to 2.5 μm. Transmission electron microscopy analysis of the NW-SWNT interface indicated that NW growth was initiated upon the surface of the nanotube composite films. Photoluminescence characterization of a single NW specimen showed high optical quality. Rectifying, asymmetric current-voltage behavior was observed from contacted NW ensembles and attributed to the core-shell pn-junction within the NWs.

3.1. Introduction

Compound semiconductor nanowires have generated significant interest in recent years, due in part to their active role in electronic devices such as single-electron transistors, light-emitting diodes[1, 2] and biosensors. It has been predicted that the use of III-V NWs in solar cell applications will result in improved photoconversion efficiency several times greater than that of current commercial technology, due to the high carrier efficiency afforded by these materials.

There are a number of different approaches by which semiconductor NWs can be produced,[3, 4] of which the most popular and well established is perhaps metal particle assisted nanowire growth. This technique is extremely versatile, having been used in conjunction with a variety of source materials and substrates as well as numerous growth techniques including chemical vapor deposition,[5, 6] molecular beam epitaxy[7, 8] and laser assisted catalytic growth.[9-12] Metal assisted nanowire growth is generally accepted to proceed via the vapour-liquid-solid (VLS) mechanism[8, 13, 14] which was first proposed in 1964 by Wagner and Ellis for the growth of micrometer sized Si whiskers by chemical vapour deposition.[14] The mechanism has subsequently been applied to a range of systems including the growth of III-V semiconductor nanowires.[12, 15] Following this mechanism, gas species impinging upon the substrate are selectively adsorbed upon the surface of metal nanoparticles, which exhibit a large accommodation coefficient in comparison to the substrate material. Diffusion of gas species into the metal particles results in the formation of a eutectic metal alloy which is a liquid at the NW growth temperature. Following supersaturation of the seed particle, nucleation of growth species subsequently occurs at the liquid-solid interface resulting in localized epitaxial film growth and, under a continuous supply of growth species from the vapour phase, the formation of single-crystal nanowires. In recent years, there has been some discussion as to whether or not metal alloy particles exist in the liquid phase at the temperatures employed for nanowire growth. It has been argued that under certain conditions metal-alloy nanoparticles remain solid during the growth process and that nanowires are therefore formed through a vapour-solid-solid mechanism.[16] At present, the exact mechanism by which several species of nanowire are formed remains a topic of ongoing discussion.[8, 16-18]

Molecular beam epitaxy (MBE) is an ultra-high vacuum technique in which evaporated atoms or molecules are provided in the vapor phase from multiple sources directed towards a heated substrate.[19] The adsorption of these species upon the substrate and their subsequent interactions results in nucleation and epitaxial film growth. The use of ultrahigh vacuum in MBE ensures that the growth chamber is free of species which may contaminate the film. MBE is therefore a suitable technique for the fabrication of high purity crystalline films. A number of different sources are used in modern MBE systems including resistively heated effusion cells and organometallic or hydride gas sources. These sources are equipped with shutters which allow the molecular beam flux to be switched 'on' and 'off' rapidly by physically blocking the source, preventing growth species from reaching the substrate. By controlling the flux from each individual effusion cell in this manner the composition of films prepared by MBE may be carefully controlled with a high degree of accuracy. This allows for the deposition of ultrathin films and incorporation of abrupt changes in film composition such as variations in dopant type or concentration. With respect to semiconductor NWs, the use of MBE in conjunction with metal particle assisted nanowire growth provides a means by which nanowire architecture can be controlled with a high degree of accuracy. This allows for the fabrication of nanowires exhibiting hetero-epitaxial and core shell arrangements[20] that have been shown to display promise with regard to obtaining high charge carrier efficiency.[21]

Growth of semiconductor NWs using GS-MBE is typically conducted upon single crystalline substrates, such as wafers composed of Si or GaAs.[20] The long range order present in materials of this kind provides a template for nucleation of growth species, and as such can promote the establishment of an epitaxial relationship between NWs and the underlying substrate, enabling the preparation of aligned NW arrays. Additionally, these materials are stable at the high temperatures required for NW growth. For GaAs, NW growth is generally conducted within the range of 470 to 570°C. [22] The high temperatures required for NW growth using MBE rules out the use of substrates such as organic polymers which undergo thermal degradation at elevated temperatures.

As mentioned previously, CNTs are known to exhibit exceptional thermal stability.[23-25] Additionally, CNTs display excellent flexibility, can be prepared using low cost techniques, and have been shown to display low resistivity, making them of interest in the fabrication of electronic devices. Previously, it has been reported CNT thin films can be employed as p-type Ohmic contacts within GaN-based LEDs resulting in contact resistances lower than that observed using conventional metallic contacts.[26] CNT thin films are therefore excellent candidates for use as flexible conducting substrates for growth of semiconductor NWs. Although CNTs have been demonstrated as templates for the assembly of various supplementary nanostructures,[27-29] little consideration has been made to date with regard to their integration with single crystal semiconductor NWs, over macroscopic scales.

In the previous chapter, we described a simple method for the preparation of single-walled nanotube (SWNT) thin films decorated with Au nanoparticle clusters.[30] Here, we report that these composite films may be employed as conductive substrates for the formation of III-V semiconductor NWs by metal-particle assisted nanowire growth in a gas source molecular beam epitaxy (GS-MBE) system. Although several groups have previously reported the use of carbon nanotubes as scaffolds for the assembly of nanomaterials, at the time this work was originally published the growth of compound semiconductor nanowires upon carbon nanotube thin films had, to the best of our knowledge, never been investigated. This work therefore represented the development of a truly novel nanohybrid material combining the optoelectronic properties of GaAs NWs with the impressive flexibility and conductivity of CNT films.

3.2. Results and Discussion

SWNTs used in this work were purchased from Carbon Nanotechnologies, Inc. (Houston, TX). The SWNTs were produced by the HiPCO process and used as received. SWNT films decorated with Au nanoparticles were prepared using the procedure described in the previous chapter.[30] To obtain nanoparticles having diameters suitable for NW growth, films were submersed in 0.5 mM $HAuCl_4$ solution for one minute at room temperature. After films had been washed to remove traces of $HAuCl_4$, they were dried under nitrogen and removed from the Teflon membrane support. Films were subsequently transferred to Si wafers having dimensions of approximately 1 cm^2, using methods previously detailed in literature[31] and subjected to a rapid thermal anneal (RTA) treatment at 550°C for 10 minutes, under nitrogen ambient.

Following thermal annealing, the Si substrate upon which the Au-SWNT composite film was attached, was indium mounted to a sample holder and transferred to the GS-MBE growth chamber. Prior to growth initiation, the samples were heated to the growth temperature of 550°C under an As_2 overpressure. In the GS-MBE system, group III species (Ga) were supplied as monomers from a heated solid elemental effusion cell while the group V species were supplied as dimers (As_2) from a hydride (AsH_3) gas cracker operating at 950°C. NW growth was initiated by opening the Ga effusion cell shutter, preset to yield a nominal two-dimensional film growth rate of 1 μm/hr under a constant V/III flux ratio of 1.5. For the purposes of this study, two distinct NW architectures were studied (groups A and B). Group A NWs were strictly composed of nominally undoped GaAs, while group B NWs were composed of pn-junction core-shell heterostructures. The core-shell structures consisted of an n-doped GaAs core surrounded by a p-doped GaAs shell. For the group A sample, nominally undoped NWs were grown for 30 minutes. In the case of the group B sample, a primary GaAs layer was grown over a 15 minute period, nominally n-doped with Te to a concentration of 10^{18} cm^{-3}. Next, a secondary GaAs layer was deposited for 15 minutes, nominally p-doped with Be to a concentration of 10^{18} cm^{-3}. Doping concentrations were calibrated using previous depositions of GaAs epilayers on GaAs (100) substrates. For both group A and group B NWs, the growth was terminated, after a total period of 30 minutes, by closing the shutter to the Ga cell and allowing the samples to cool down from the growth temperature under an As_2 overpressure.

Figure 3.1 shows planar SEM images of SWNT-Au composite films before and after the RTA annealing treatment. Covalent modification of SWNTs by PEI-functionalization results in the conversion of numerous carbon atoms within the framework of nanotubes to sp^3 hybridization. Thermal annealing of PEI-functionalized SWNT films induces decomposition of the functional groups attached to the surface of the nanotubes and results in partial restoration of the nanotube electronic structure and conductivity.[32] Furthermore, an annealing treatment ensures removal of volatile organic matter that might otherwise contaminate the MBE chamber used for semiconductor NW growth. Following this treatment, irregularly shaped Au-nanoparticle clusters were found to re-form into smaller, discrete nanoparticles having an average diameter of approximately 38 nm as shown in Figure 3.1.B. Typically, following thermal annealing an increase in nanoparticle diameter may be expected due to migration and aggregation of individual nanoparticles. It was speculated that irregularly shaped Au clusters exhibit fractal like structures containing some free volume. These clusters are sufficiently large that migration does not occur to any significant degree during high temperature annealing and clusters instead re-form, with the exclusion of free volume, to yield compact spherical particles that exhibit smaller diameters than the starting clusters.

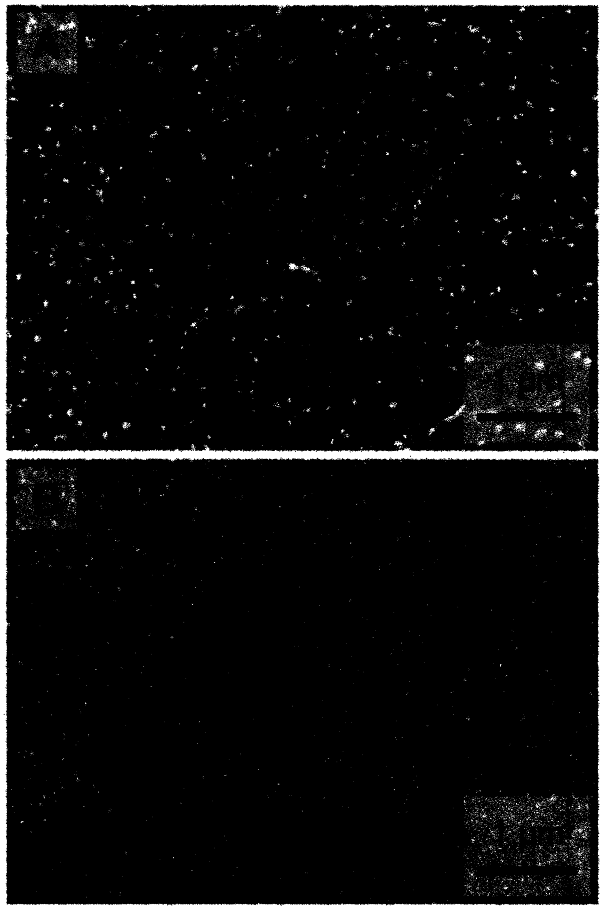

Figure 3.1. Planar SEM image of SWNT-Au composite film (A) before and (B) after annealing treatment. Bright spots indicate Au particles.

SEM analysis in Figure 3.2 indicated that the as-grown samples from group A exhibited dense NW growth over the entire span of the Au-functionalized SWNT films. Similar results were obtained from the group B sample. In comparison to the vertically oriented growth of NWs on Si (111) or GaAs (111)B substrates,[20, 33] NWs grown on SWNT substrates were observed to be oriented in a variety of angles with respect to the growth surface. This can be understood by considering the well-established premise that

NWs preferentially assemble in the thermodynamically favorable <0001> or <111> directions, for wurtzite and zincblende crystal structures, respectively.[20, 34] However, in the case of the present study, the growth surface lacks long range spatial periodicity, which is necessary for epitaxial orientation of the NWs, due to the random stacking arrangement of single-walled CNTs in the composite film.

Predominantly, both group A and group B NWs were of characteristic tapered or "pencil-shaped" morphologies, with heights up to 2.5 μm and average full-width at half-maximum diameters of roughly 100 nm. The tapered NW morphology is attributed to sidewall diffusion-limited radial growth, as previously reported.[33] The simultaneous occurrence of layer-by-layer radial deposition and Au-nanoparticle-based axial growth results in the core-shell architecture of the NWs.[20] A two-dimensional GaAs film, formed concurrently with the NWs, is evident in Figure 3.2.B above the SWNT substrate. Prior growths on single crystalline Si substrates indicated two-dimensional film thicknesses of 120 nm.[20] In comparison, the present growth resulted in deposition of a thicker film layer of approximately 450 nm on average, probably as a consequence of shorter adatom diffusion lengths on the rough surface of the SWNT films.

Figure 3.2.C shows a tilted SEM view of an area specifically manipulated to demonstrate the flexibility of a SWNT film containing NWs. It is particularly remarkable that the NWs studied in this project maintained their structural integrity after bending, contorting, rolling, and folding of the underlying flexible substrate, over macroscopic scales.

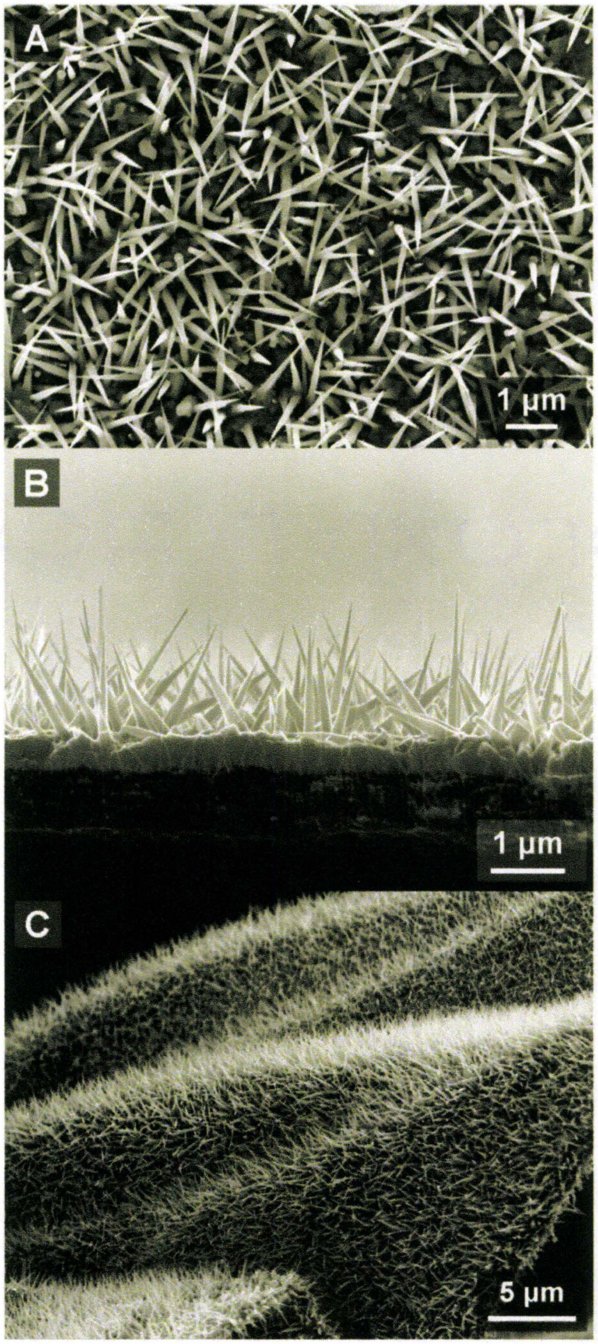

Figure 3.2. (A) Planar, (B) cross-sectional, and (C) tilted view SEM images of as-grown samples containing GaAs NWs on CNT composite films.

Structural analysis of numerous single NWs from both group A and group B samples was carried out by TEM. Figure 3.3.A shows a TEM image of a Group A NW that is representative of the structure and morphology of practically all NWs grown on the CNT films. Figure 3.3.B reveals a magnified image of the identical NW in Figure 3.3.A. Contrast stripes intersecting the NWs indicated the presence of intermittent stacking faults. A selective area diffraction pattern obtained on the <2-1-10> zone axis of a defect-free NW segment, shown in the inset of Figure 3.3.A, confirmed a wurtzite crystal structure with wires growing along the <0001> direction. Consistent with previous experiments involving hetero- and homo-epitaxially grown NWs,[20, 35] the stacking faults studied in the present case appeared as atomic layers arranged in a zincblende structure, amongst defect-free wurtzite segments. The Au-nanoparticle at the NW tip provides evidence for growth according to the VLS mechanism.

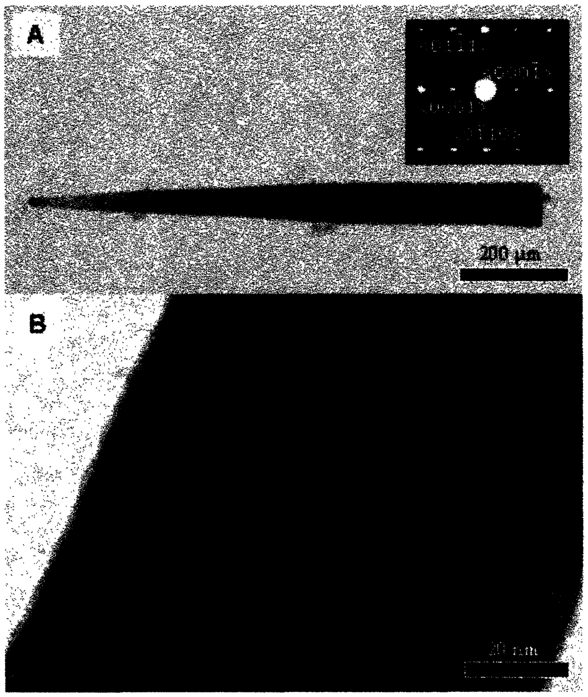

Figure 3.3. (A) TEM image of a single NW. Inset shows the SAD pattern, indicative of the wurtzite structure and <0001> growth direction. (B) Magnified TEM view of stacking faults visible along the NW length.

A point of interest is the nature of the growth surface. Due to the simultaneous deposition of a GaAs film during NW assembly, the NW/CNT interface becomes buried during the growth process. To investigate the NW/CNT interface, thin lamellae were prepared via FIB, allowing for the analysis of small cross-sectional windows where the internal NW structure, GaAs film, and CNT-composite substrate can be examined in a single specimen. In Figure 3.4.A TEM image is shown of a lamella removed from the as-grown sample. The coating surrounding the NW in Figure 3.4 is simply a carbon layer deposited during the sample preparation, as a protective envelope. Stacking faults can be seen throughout the entire length of the NW including the portion buried within the 2-D GaAs film. This observation leads to the argument that the initial NW nucleation process occurred at the CNT/Au interface. As the diameter of the Au nanoparticles is considerably greater than that of a single CNT, each nanoparticle is located upon a unique site which spans several randomly oriented underlying CNTs. Although the initial GaAs island nucleation can occur over a single CNT, the formation of the initial GaAs layer at the CNT/Au interface, nonetheless, extends over multiple CNTs. Therefore, it remains unclear, at present, whether growth is epitaxially initiated. Additionally, a GaAs film grows simultaneously between the NWs, but appears to play a negligible role in the NW growth process. Due to the intimate contact between the NWs, 2-D film, and CNTs, the role of the planar GaAs layer is of importance to the electrical conduction pathways of this system, as discussed later.

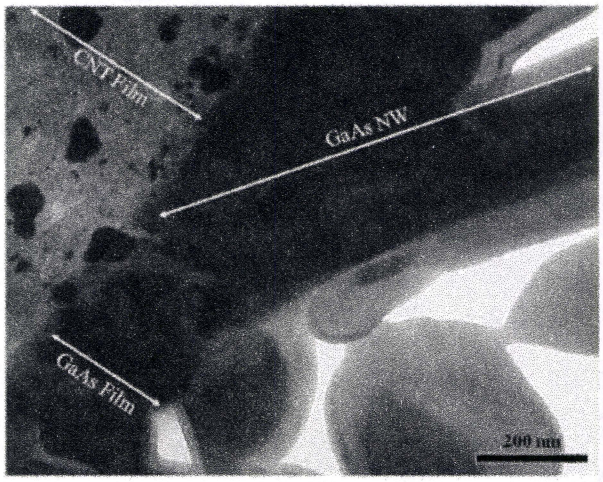

Figure 3.4. Cross-sectional TEM image of interfaces between NW, GaAs film, and CNT substrate. The extension of stacking faults within the GaAs film, localized to the lateral extent of the visible NW, indicates NW growth from the CNT surface.

Micro-photoluminescence studies were conducted on single NWs placed on SiO_2 substrates. A typical μ-PL spectrum is shown in Figure 3.5 for a group A NW. Here, a single peak with 12.5 meV linewidth is obtained at 7 K, centered at 1.51 eV. The inset of Figure 3.5 shows a plot of the experimental shift in μ-PL peak energy with increasing temperature. The expected temperature dependence of the bandgap is plotted in the inset as a solid line according to the Varshni curve of bulk GaAs.[36] The agreement between the measured values and the Varshni expression indicates that the PL emission may be attributed to band-related recombination transitions within the undoped GaAs NW.[36] Agreement between the measured values and the expected trend also illustrates the high crystallinity, purity, and optical quality of the NWs, making these materials promising for use in optoelectronic device applications.

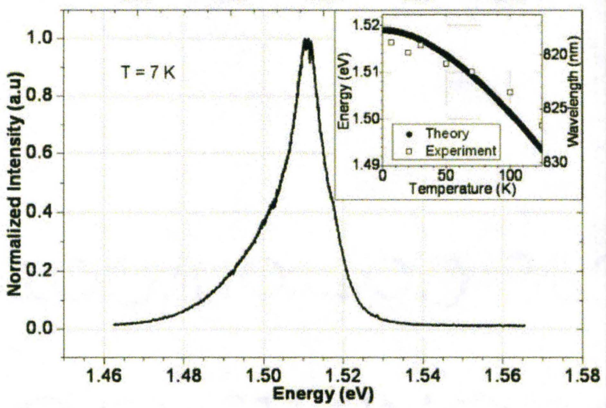

Figure 3.5. Single NW μ-PL spectrum at 7 K. Inset plots the measured PL peak energy with increasing temperature as compared to the theoretical bulk GaAs Varshni curve.

The group A and B samples were further processed for electrical characterization. The main intent in the processing procedure was to ensure intimate electrical contact with the Au-capped NW tips, while avoiding a possible short-circuit pathway through the planar growth region. SEM images of the sample, at various processing steps employed in the device fabrication, are shown in Figure 3.6. First, the entire sample was coated with a SiO_x layer (step A) formed through plasma-enhanced chemical vapor deposition (PE-CVD). This layer provides a conformal insulating shell across all NWs and the surface of the GaAs film, approximately 100 nm in thickness. Next, a polymer layer (S-1808 photoresist) was spin-cast over the oxide-coated NWs (step B). After a 1 min oxygen-plasma reactive ion etching (RIE) treatment, the top-most layers of the spin-on-polymer were removed to expose the oxidized NW tips (step C). At this point, the sample underwent a wet etch in a 10:1 buffered HF solution to remove the thin SiO_x cap at the

NW tips (step D). A second, more prolonged, RIE treatment occurred next, etching the remaining photoresist from the surface of the NWs. As seen in Figure 3.6.E, after this processing step, the planar GaAs layer and the body of the NWs remained insulated by the oxide layer, while the NW tips are exposed. Thus, once a Ti/Pt/Au top contact layer was deposited (step F), the intended pathway for electron flow is through the NWs to the SWNT film.

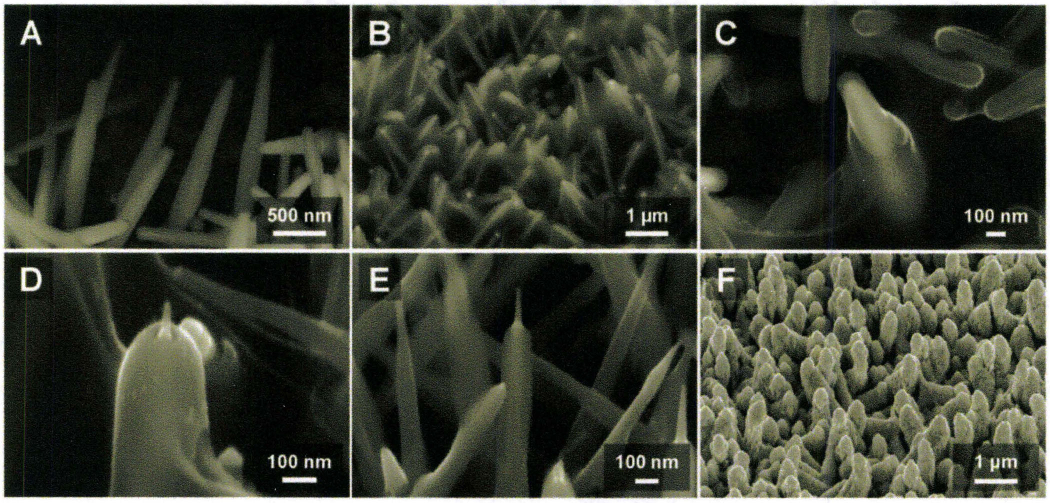

Figure 3.6. Processing steps in device fabrication: (A) PE-CVD deposition of 100 nm SiO_x layer to coat NWs and planar growth layer. (B) Coating of oxidized NWs with spin-cast polymer (S1808 photoresist) layer. (C) Partial O_2-plasma RIE of polymer layer for exposure of oxidized NW tips. (D) Buffered HF wet etch treatment for the exposure of bare NW tips. (E) Full O_2-plasma RIE for the removal of remaining polymer layer. (F) Deposition of Ti/Pt/Au top contact, followed by RTA treatment.

To study the electrical behavior of the fabricated devices and to establish the role of Be and Te as dopants, a Ti/Pt/Au layer was deposited by electron-beam evaporation on both group A (undoped GaAs NWs) and group B (pn-junction core-shell NWs) samples. Prior to measurement, the samples were treated at 400°C for 30 seconds, to produce an Ohmic contact at the contact/NW interface. Figure 3.7 shows the current-voltage (I-V) characteristics of a bare SWNT film (post RTA), a device fabricated using group A NWs, and a device fabricated using group B NWs, under an applied bias of -2 V to 2 V.

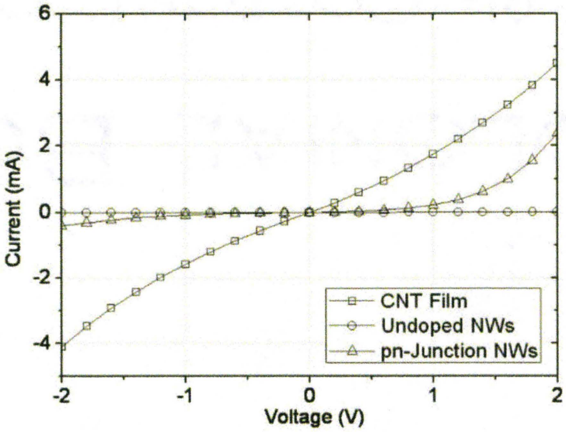

Figure 3.7. I-V characteristics of purified CNT film, prior to NW deposition (squares), fabricated devices containing undoped NWs (circles), and fabricated devices containing pn-junction NWs (triangles). Asymmetric rectification in group B devices is indicative of diode-type behaviour from the pn-junction NWs.

It is worthy to note that the SWNT film exhibited a conductive behavior prior to growth. From the I-V curve (square data points), SWNT films revealed a sheet resistance of roughly 68 Ω/sq (resistivity of 6.81×10^{-3} Ω·cm) after being subjected to an annealing process. This value is in agreement with SWNT composite film resistances previously reported[31, 37, 38] and is comparable to sheet resistances measured in commercial ITO films.[37] The observed rectifying behaviour is attributed to Schottky barriers formed between the CNT film and probe tips.[39] The undoped NWs (group A samples, circular data points) demonstrated a high resistivity of roughly 5900 Ω·cm. In contrast, the curve obtained from sample B containing pn-junction NWs (triangular data points) exhibited asymmetric rectification. Although the specific contribution of the CNT/GaAs interface quality to the electrical behaviour observed remains a matter of continued investigation, the observation of diode-type behavior in group B devices, while not in group A devices, demonstrated the rectifying properties exhibited by the pn-junction NWs. Similar results were reproducibly obtained from at least 15 different contacts on each sample. Furthermore, pn-junction GaAs NWs grown on GaAs and Si substrates, processed and contacted in same approach discussed above, yielded forward bias currents within the same order of magnitude as those grown on CNT composite films. This behavior opens the door to possible applications of these hybrid device architectures in a variety of applications, including photovoltaics, light-emitting diodes, and sensors.

3.3. Conclusions

In summary, a novel material combination involving GaAs NWs grown on Au-functionalized SWNT composite films is reported. Au-nanoparticles on the surface of the SWNT sheets act as atomic sinks, collecting gas-phase adatoms supplied in a GS-MBE system and accommodating NW growth according to the VLS mechanism. As-grown

NWs were oriented in a variety of angles on the SWNT surface and grew along the <0001> direction with wurtzite crystal structure. TEM analysis conducted on the NW/SWNT interface confirmed initiation of growth on the SWNT surface. Micro-PL characterization of a single NW specimen confirmed high optical quality. Electrically contacted pn-junction NWs exhibited rectifying behaviour, while undoped NWs showed high resistivity. Thus, a proof-of-concept potential for an emerging class of optoelectronic devices integrated with a conductive, flexible, and low-cost substrate as an alternative to conventional ITO is demonstrated. Similarly, CNT films are expected to accommodate VLS growth of alternative compound semiconductor material groups. Future efforts will focus on large-scale core-shell NW-based photovoltaics on carbon-nanotube composite fabric.

3.4. Experimental

3.4.1. General

SWNT-Au composite films were prepared using procedures outlined in the previous chapter. To obtain nanoparticles having diameters suitable for NW growth, PEI functionalized SWNT thin films were submersed in 0.5 mM $HAuCl_4$ solution for one minute at room temperature. After films had been washed to remove traces of $HAuCl_4$, they were dried under nitrogen and removed from the Teflon membrane support. Absorbance measurements were made using a Cary 50 Bio UV-Visible Spectrophotometer. Filtrations were carried out using VWR filtration apparatus with stainless steel support screen and Sartorius PTFE membranes (4.7 cm diameter, 200 nm pore size). Nanotube samples were dispersed in solvent using a Branson 1510 bath sonicator. Nanotube dispersions were centrifuged using a Beckman Coulter Allegra X-22 Centrifuge. The orientation, morphology, and density of the as-grown samples were investigated using a JEOL JSM-7000 scanning electron microscope (SEM) and a Carl Zeiss SMT NVision 40 dual-beam microscope, in secondary-electron mode. The latter, equipped with focused ion beam (FIB) capability, was used in the preparation of lamellae for cross-sectional transmission electron microscopy (TEM) using a Philips CM12 microscope and a JEOL 2010F high-resolution transmission electron microscope (HR-TEM). For analysis of a single NW specimen, the as-grown samples were subjected to a 60 second ultra-sonication process in a small volume of de-ionized water after which suspended NWs were deposited on a holey carbon-coated copper grid. Similarly, single NWs were dispersed on an oxidized-Si substrate for micro-photoluminescence (μ-PL) characterization in a continuous flow helium cryostat at 7 K. Excitation was provided using a laser centered at 532 nm at a power of 80 μW. Excitation and μ-PL collection were achieved through an objective allowing for an excitation spot of roughly 2 μm diameter. PL was resolved by a 75 cm grating spectrometer and detected by a liquid nitrogen-cooled Si charge-coupled device camera.

3.4.2. Transfer of SWNT-Au composite film to Si substrate

The surface of a (111) silicon wafer, having dimesions of approximately 1 cm^2, was wet using distilled water. A SWNT-Au composite film was placed upon the wet surface and a teflon fitration membrane subsequently placed on top of the film. This assembly was transferred to a vice and pressure was applied, taking care not to crack the silicon substrate. The sample was then heated at 50°C under vacuum for 15 minutes after which the sample was removed from the vice and the teflon filter carefully peeled back, leaving the nanotube film firmly attached to the substrate. Films were subsequently treated using a rapid thermal annealling process (550°C, 10 minutes, N_2 atmosphere).

3.4.3. Growth of GaAs nanowires

A GS-MBE system was employed for NW growths in which Ga monomers were supplied from a solid elemental effusion cell and a hydride (AsH_3) gas cracker operating at 950°C acted as a source of As_2 dimers. Prior to NW growth, a degas procedure was performed within the MBE chamber, heating to 300°C for 15 minutes under vacuum followed by an inductively coupled hydrogen plasma treatment (10 minutes, 550°C), under As_2 overpressure. NW growth was initiated by opening the Ga cell shutter. During the growth process, the substrate temperature and V/III flux ratio were maintained at 550°C and 1.5 respectively yielding a nominal GaAs growth rate of 1 μmhr^{-1}. NW growth was terminated by closing the shutter of the Ga effusion cell, following which samples were cooled under As_2 overpressure.

In this study, two different groups of GaAs NWs were prepared. Group A NWs were prepared to exhibit a pn-junction within a coaxial architecture, containing a Te doped n-GaAs core and Be doped p-GaAs shell. Each segment of the group A wires was grown over a period of 15 minutes, resulting in a total growth time of 30 minutes. NWs in group B were, in contrast, composed entirely of Te doped n-GaAs. Again, the total growth time for these wires was 30 minutes. In both growths, nominal dopant concentrations were maintained at 4×10^{18} cm^{-3} for Te in both group A and group B wires and at 5×10^{18} cm^{-3} for Be in group A wires. These values were based upon previous calibrations of epitaxial films on GaAs (100) substrates.

3.5. References

(1) H. A. Nilsson, T. Duty, S. Abay, C. Wilson, J. B. Wagner, C. Thelander, P. Delsing and L. Samuelson. *Nano Lett.* **2008,** 8, (3), 872-875.

(2) M. S. Gudiksen, L. J. Lauhon, J. Wang, D. C. Smith and C. M. Lieber. *Nature* **2002,** 415, (6872), 617-620.

(3) Y. N. Xia, P. D. Yang, Y. G. Sun, Y. Y. Wu, B. Mayers, B. Gates, Y. D. Yin, F. Kim and Y. Q. Yan. *Adv. Mater.* **2003,** 15, (5), 353-389.

(4) K. S. Shankar and A. K. Raychaudhuri. *Mat Sci Eng C-Bio S* **2005,** 25, (5-8), 738-751.

(5) T. I. Kamins, R. S. Williams, D. P. Basile, T. Hesjedal and J. S. Harris. *J. Appl. Phys.* **2001,** 89, (2), 1008-1016.

(6) S. K. Lim, M. J. Tambe, M. M. Brewster and S. Gradecak. *Nano Lett.* **2008,** 8, (5), 1386-1392.

(7) C. Chatillon, F. Hodaj and A. Pisch. *J Cryst Growth* **2009,** 311, (14), 3598-3608.

(8) V. G. Dubrovskii, N. V. Sibirev, G. E. Cirlin, J. C. Harmand and V. M. Ustinov. *Phys. Rev. E* **2006,** 73, (2), 021603-10.

(9) X. F. Duan and C. M. Lieber. *J. Am. Chem. Soc.* **2000,** 122, (1), 188-189.

(10) A. M. Morales and C. M. Lieber. *Science* **1998,** 279, (5348), 208-211.

(11) X. F. Duan, J. F. Wang and C. M. Lieber. *Appl. Phys. Lett.* **2000,** 76, (9), 1116-1118.

(12) X. F. Duan and C. M. Lieber. *Adv. Mater.* **2000,** 12, (4), 298-302.

(13) B. A. Wacaser, K. A. Dick, J. Johansson, M. T. Borgstrom, K. Deppert and L. Samuelson. *Adv. Mater.* **2009,** 21, (2), 153-165.

(14) R. S. Wagner and W. C. Ellis. *Appl. Phys. Lett.* **1964,** 4, 89-90.

(15) K. Hiruma, M. Yazawa, K. Haraguchi, K. Ogawa, T. Katsuyama, M. Koguchi and H. Kakibayashi. *J. Appl. Phys.* **1993,** 74, (5), 3162-3171.

(16) A. I. Persson, M. W. Larsson, S. Stenstrom, B. J. Ohlsson, L. Samuelson and L. R. Wallenberg. *Nat Mater* **2004,** 3, (10), 677-681.

(17) K. A. Dick, K. Deppert, L. S. Karlsson, L. R. Wallenberg, L. Samuelson and W. Seifert. *Adv Funct Mater* **2005,** 15, (10), 1603-1610.

(18) J. C. Harmand, G. Patriarche, N. Pere-Laperne, M. N. Merat-Combes, L. Travers and F. Glas. *Appl. Phys. Lett.* **2005,** 87, (20), 203101-3.

(19) M. Ohring, *The Materials Science of Thin Films*. Accademic Press, Inc.: 1992.

(20) P. K. Mohseni, C. Maunders, G. A. Botton and R. R. LaPierre. *Nanotechnology* **2007,** 18, (44), 445304-6.

(21) L. J. Lauhon, M. S. Gudiksen and C. M. Lieber. *Philos T Roy Soc A* **2004,** 362, (1819), 1247-1260.

(22) M. Tchernycheva, J. C. Harmand, G. Patriarche, L. Travers and G. E. Cirlin. *Nanotechnology* **2006,** 17, (16), 4025-4030.

(23) K. Metenier, S. Bonnamy, F. Beguin, C. Journet, P. Bernier, M. L. de La Chapelle, O. Chauvet and S. Lefrant. *Carbon* **2002,** 40, (10), 1765-1773.

(24) K. M. Liew, C. H. Wong, X. Q. He and M. J. Tan. *Phys. Rev. B* **2005,** 71, (7), 075424-6.

(25) M. Yudasaka, T. Ichihashi, D. Kasuya, H. Kataura and S. Iijima. *Carbon* **2003,** 41, (6), 1273-1280.

(26) K. Lee, Z. Wu, Z. Chen, F. Ren, S. J. Pearton and A. G. Rinzler. *Nano Lett.* **2004,** 4, (5), 911-914.

(27) S. H. Jo, D. Banerjee and Z. F. Ren. *Appl. Phys. Lett.* **2004,** 85, (8), 1407-1409.

(28) Y. Zhang and H. J. Dai. *Appl. Phys. Lett.* **2000,** 77, (19), 3015-3017.

(29) B. H. Juarez, C. Klinke, A. Kornowski and H. Weller. *Nano Lett.* **2007,** 7, (12), 3564-3568.

(30) G. Lawson, F. Gonzaga, J. Huang, G. de Silveira, M. A. Brook and A. Adronov. *J. Mater. Chem.* **2008,** 18, (14), 1694-1702.

(31) Z. C. Wu, Z. H. Chen, X. Du, J. M. Logan, J. Sippel, M. Nikolou, K. Kamaras, J. R. Reynolds, D. B. Tanner, A. F. Hebard and A. G. Rinzler. *Science* **2004,** 305, (5688), 1273-1276.

(32) J. Cabana and R. Martel. *J. Am. Chem. Soc.* **2007,** 129, (8), 2244-2245.

(33) C. Chen, M. C. Plante, C. Fradin and R. R. LaPierre. *J. Mater. Res.* **2006,** 21, (11), 2801-2809.

(34) J. Johansson, B. A. Wacaser, K. A. Dick and W. Seifert. *Nanotechnology* **2006,** 17, (11), S355-S361.

(35) D. M. Cornet, V. G. M. Mazzetti and R. R. LaPierre. *Appl. Phys. Lett.* **2007,** 90, (1), 013116-3.

(36) V. Swaminathan and A. T. Macrander, *Materials Aspects of GaAs and InP Based Structures*. Prentice Hall: 1991.

(37) N. Saran, K. Parikh, D. S. Suh, E. Munoz, H. Kolla and S. K. Manohar. *J. Am. Chem. Soc.* **2004,** 126, (14), 4462-4463.

(38) B. S. Kong, D. H. Jung, S. K. Oh, C. S. Han and H. T. Jung. *J. Phys. Chem. C* **2007,** 111, (23), 8377-8382.

(39) Y. Liu, Z. Y. Zhang, Y. F. Hu, C. H. Jin and L. M. Peng. *J. Nanosci. Nanotechnol.* **2008,** 8, (1), 252-258.

Chapter 4: Hybrid GaAs-nanowire carbon nanotube flexible photovoltaics

Work detailed in this chapter was carried out in collaboration with Parsian K. Mohsini and Dr. Ray LaPierre (Department of Engineering Physics and Centre for Emerging Device Technology, McMaster University, Hamilton, Ontario). Both Gregor Lawson and Parsian K. Mohseni contributed equally to the experimental planning and writing of this work. Composite film preparation and characterization was conducted by Gregor Lawson. Nanowire growth, device fabrication and characterization was conducted by Parsian K. Mohseni.

Abstract

A simple method is described for the preparation of carbon nanotube (CNT) composite films containing Au nanoparticles, which act as adatom collection agents promoting the growth of core-shell pn-junction GaAs nanowires (NWs), according to the vapour-liquid-solid mechanism. This approach for composite film formation requires no covalent modification, and therefore ensures that the electronic properties of CNTs are not compromised. GaAs NWs obtained are randomly aligned with respect to the CNT substrate in a densely packed arrangement. Nano-hybrid films, incorporating coaxial GaAs NWs as the active, light-harvesting medium are used in the fabrication of photovoltaic cells, exhibiting conversion efficiencies up to 0.32%. Doping experiments confirm that conduction is not dominated by Schottky barriers at contact interfaces. The NW/CNT solar cells are shown to retain function following bending up to a curvature radius of 12.5 mm, illustrating the potential of these novel materials in flexible device applications.

4.1. Introduction

One-dimensional structures play a unique role in the landscape of nanometer-scale science and engineering. In this realm, semiconductor nanowires (NWs) and carbon nanotubes (CNTs) have attracted interest by demonstrating quantum mechanical phenomena and integration within a new generation of electronic and photonic devices.[1] Furthermore, the combination of semiconducting nanowires or carbon nanotubes with more mature functional materials, such as thin films and polymers, has demonstrated enhanced functionality and improved device performance.[2-6]

Of particular significance is the solar energy conversion potential possessed by semiconductor NWs. This stems from a variety of factors including their inherent light-trapping capabilities, as NW ensembles allow for improved optical absorption, in comparison to their thin film or textured-surface counterparts.[7] There is particular interest in coaxial pn-junction nanowires where, for example, a p-doped core is surrounded by an n-doped shell. With this geometry, charge carriers are efficiently separated by the coaxial pn-junction across the nanowire diameter, d, which can be smaller than the carrier diffusion length, thereby promoting high efficiency collection of photogenerated carriers.[8] Recently, numerous efforts have demonstrated the photovoltaic (PV) capabilities of semiconductor NWs, based on Si,[9-12] III-V,[13, 14] and II-VI[15-17] materials. As NWs can easily be integrated with a variety of functional substrates, fabrication of mechanically flexible, NW-based optoelectronic devices has attracted considerable attention[18] and remains a matter of continual importance.

In Chapter 3 we reported that single walled carbon nanotube (SWNT) composite films decorated by Au nanoparticles can be employed as substrates for the assembly of III-V semiconductor NWs,[19] according to the vapour-liquid-solid (VLS) mechanism.[20-22] In this prior work, thin films of poly(ethylene imine) (PEI) functionalized carbon nanotubes (CNTs), prepared using the vacuum filtration method,[23-25] were decorated with Au nanoparticles by in-situ reduction of $HAuCl_4$ under mild conditions.[26] These SWNT-Au composite films were subsequently used as substrates for the growth of GaAs NWs in a gas source molecular beam epitaxy (GS-MBE) system. Following this procedure, randomly aligned NWs were obtained in high density across the entire surface of the SWNT substrates. Characterization of these NWs, using TEM and micro-photoluminescence, revealed them to be of high purity and optical quality. This work therefore represented the development of a novel nano-hybrid material that combines the optoelectronic properties of GaAs NWs with the impressive flexibility and conductivity of CNT films and, as such, displays apparent potential in the development of flexible, lightweight electronic devices such as photovoltaics, light emitting diodes, and sensors.

In this chapter it is demonstrated that these hybrid nano-materials can indeed be used in the fabrication of photovoltaic cells, wherein coaxial pn-junction GaAs NWs act as the active medium for energy conversion, while the underlying CNT films simultaneously serve as robust, flexible electrodes. Additionally, we outline a simplified method for the preparation of SWNT-Au composite substrates which requires no covalent modification of CNTs, greatly reducing the time required for composite film fabrication and also ensuring the retention of the CNTs electrical properties.

4.2. Results and discussion

Single-walled carbon nanotubes were purchased from Carbon Nanotechnologies, Inc. (Houston, TX). SWNTs were produced by the HiPCO process and were used as received. Full details of procedures employed for the preparation of SWNT-Au composite films are included in the Experimental section of this chapter. The Au nanoparticles were prepared using the well established citrate reduction method,[27-29] which results in near mono-disperse particles. Deposition of Au nanoparticles was achieved by filtration of a dilute nanoparticle solution through a thin film of unmodified SWNTs, prepared by vacuum filtration of a SWNT dispersion in aqueous surfactant solution. CNT thin films, such as those prepared in this work, resemble a random finely-interpenetrating network of nanotube bundles. The porous microstructure of these films makes them ideal candidates for use as high efficiency fibrous filtration membranes. Several groups have investigated the potential of CNTs in separation and filtration applications.[30-37] Although much of this work has focused upon the use of aligned CNT arrays, Lipowicz and coworkers reported the effective removal of fine airborne particulate, having dimension as small as 50 nm, using thin films composed solely of randomly aligned multi-walled CNTs.[32]

The current approach for the fabrication of SWNT-Au substrates offers several advantages over the previously reported in-situ reduction method.[26] Covalent modification of carbon nanotubes, which was necessary in our previous work, results in conversion of numerous carbon atoms within the framework of the CNTs to sp^3 hybridization, disrupting the π system of the CNTs and significantly diminishing their electrical conductivity.[38] It is expected that the use of unfunctionalized SWNTs, in our modified procedure, will allow for the structure and electronic properties of the CNTs to not be compromised in any way during film fabrication. As the modified approach requires few synthetic steps, the time required for the preparation of each composite film is greatly reduced. In addition, the current procedure allows for fine control over the size and polydispersity of Au nanoparticles deposited on the nanotube surface.

Following fabrication, composite films were cut into small sections having dimensions of approximately 5 x 10 mm, removed from the filtration membranes and transferred,[23] Au nanoparticle side up, to copper substrates. Copper was arbitrarily chosen as a rigid, conductive, and GS-MBE compatible support material to which the CNT films could easily be transferred for subsequent NW growth or later removed. These samples were then thermally annealed at 550°C for 10 minutes in nitrogen ambient, ensuring the removal of volatile organic matter which could potentially contaminate the MBE chamber during NW growth.

Figure 4.1 shows planar SEM images of SWNT-Au composite film samples before (A) and after (B) thermal annealing at 550°C for 10 minutes in nitrogen ambient. Prior to the thermal anneal, Au nanoparticles have an average diameter of 30 ± 5 nm. This value increases to 38 ± 6 nm following the annealing procedure, as a result of the migration and coalescence of a small fraction of Au nanoparticles at elevated temperatures. It can however be seen, from the SEM images in Figure 4.1, that large scale aggregation of Au nanoparticles does not occur during this process. The density of Au nanoparticles upon the surface of annealed composite films, which was also determined using SEM, ranged between 20 and 86 nanoparticles per 1 μm^2, with an average density of 50 nanoparticles per 1 μm^2 (Appendices, Figure 4.I.1).

Cross-sectional images of these films were obtained after focused ion beam (FIB) milling. A trench cut within a SWNT-Au composite film, which has not undergone thermal annealing, is shown in Figure 4.1.C. In this image, Au nanoparticles are observed to be located predominantly upon the film's surface. Some Au nanoparticles can also be seen in low density within the structure of the nanotube film. The presence of Au nanoparticles within the film is not unexpected, given the film's porous microstructure and the dimensions of Au nanoparticles used in this work. In addition to Au nanoparticles, clusters of iron were also detected, embedded within the nanotube film. These clusters, which appear as bright regions in the SEM image having dimensions on the scale of 10s to 100s of nanometers, are impurities present in the commercially-purchased nanotube sample used in this work (Fe catalyst from SWNT synthesis). Figure 4.1.D illustrates a similar trench produced by FIB milling of a sample that has been annealed at 550°C. From these images it was determined that the distribution of Au nanoparticles throughout our SWNT-Au composite films is not significantly altered by the annealing process.

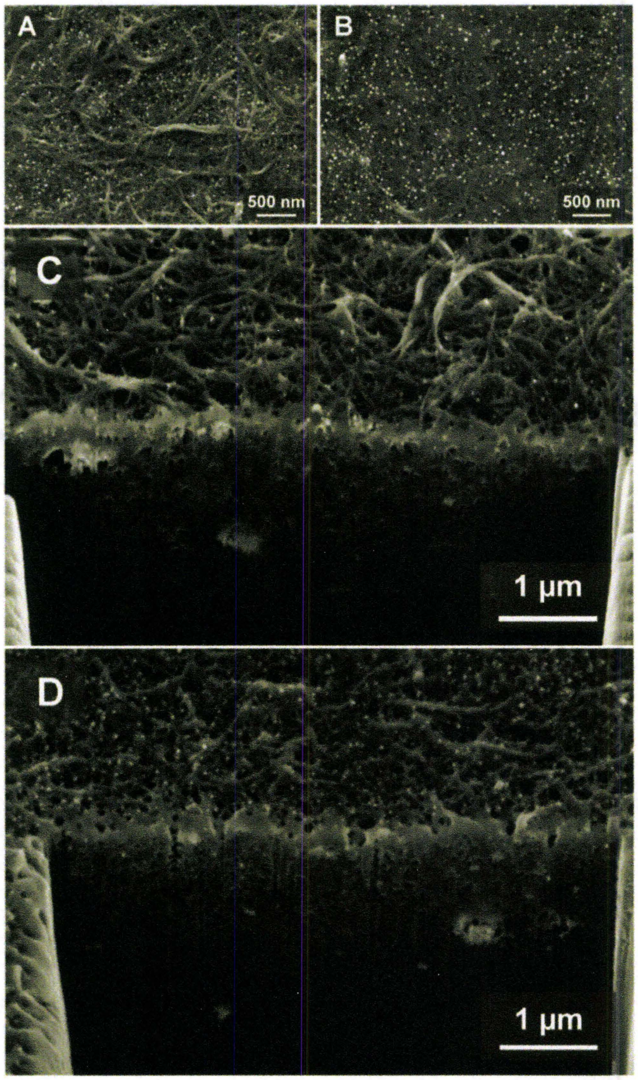

Figure 4.1. Planar SEM images of a SWNT-Au thin film, before (A) and after (B) rapid thermal annealing at 550°C for 10 minutes under nitrogen, and tilted SEM cross-sectional images of trenches milled within SWNT-Au films before (C) and after (D) the same annealing procedure.

The SEM images of group A NWs, shown in Figure 4.2, reveal dense NW growth with no preferred NW orientation (similar results were obtained from group B NWs). The random alignment of NWs relative to the substrate surface was previously attributed to the random manner in which SWNT bundles comprising the underlying film are situated.[19] As determined from sample sets of over 100 single specimens, the NWs have an average full-width at half-length diameter of roughly 100 nm and heights up to 3.5 μm. The highly tapered morphology is a trademark of diffusion limited sidewall growth and is anticipated for GS-MBE growths under the growth conditions employed.[19, 39]

As outlined in the Experimental section, solar cell fabrication was carried out through a process designed to effectively exploit NWs as the active, energy conversion medium. A schematic representation of the final device structure, showing a single NW for clarity, is depicted in Figure 4.3. In light of recent reports on the inhomogeneity of dopant profiles in semiconductor NWs[40, 41] and the anticipated incongruity in dopant incorporation between the (100) surface of the doping calibration sample and the (111) surfaces of the nanowires, the degree of uniformity in the dopant distributions within the samples discussed here remains a matter for further scrutiny. Nonetheless, a clear distinction can be made between group A NWs (those containing a pn-junction in a core-shell homostructure) and group B NWs (those intentionally highly n-doped).

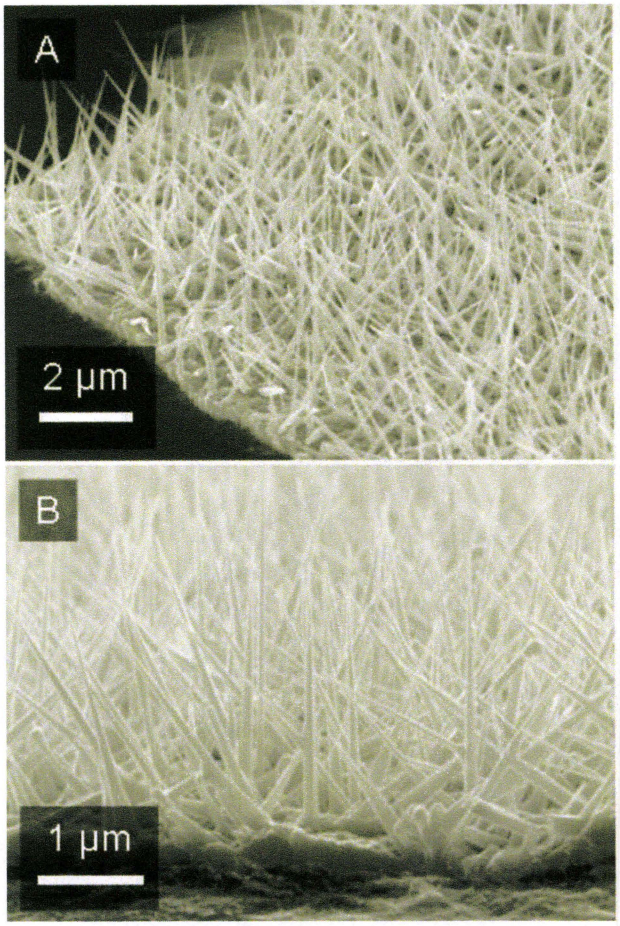

Figure 4.2. 45° tilted view (A) and cross-sectional (B) SEM image of as-grown group A NW samples. Densely packed NWs are grown at various orientations with a highly tapered morphology. Similar results were obtained from group B NW samples.

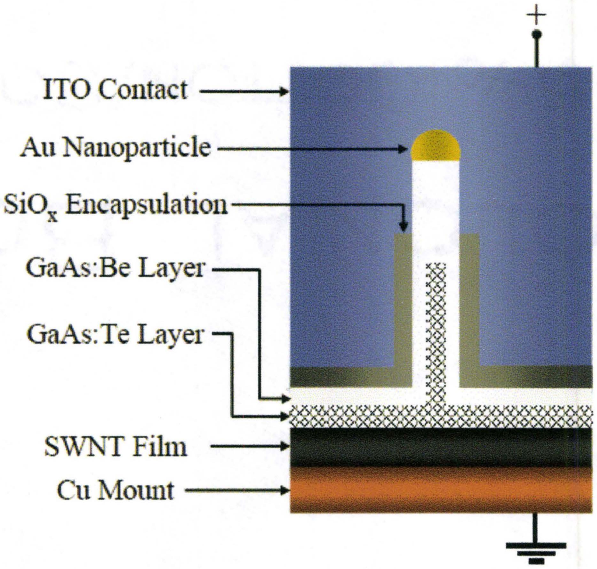

Figure 4.3. Schematic representation of group A NW solar cell, showing biasing conditions. The NW bases and planar GaAs film are electrically isolated from the ITO top contact. The CNT substrate simultaneously serves as the growth surface and backside contact.

Upon fabrication, the photovoltaic response of the NW solar cells was measured. Figure 4.4 shows the fourth quadrant current-voltage characteristics of an ensemble of ITO contacted group A NWs, under dark (black, circular data points) and 2.6 Sun illumination (red, square data points) conditions. A clear photovoltaic response is evident, attributed to the sum contribution of all contacted NWs in the contact area. Although varying efficiency values were measured from different contact dots, likely due to different numbers of NWs contacted by each dot and small growth temperature variances across the sample leading to slightly dissimilar NW structures, each contact dot exhibited reproducible efficiencies. The optimal efficiency curve, shown in Figure 4.4, was characterized by a short circuit current, $I_{SC} = 43.1\ \mu A$ (equivalently, $J_{SC} = 8.57\ mA/cm^2$ for the 800 μm diameter contact dot), an open circuit voltage, $V_{OC} = 0.32$ V, a maximum power, $P_{max} = 42.3\ \mu W$, a fill factor of 30.8%, and a maximum conversion efficiency of 0.32%. No such conversion response was evident in group B NWs (n-doped NWs) contacted with the transparent conductive oxide layer, indicating that the PV effect was due to the pn-junctions in group A NWs.

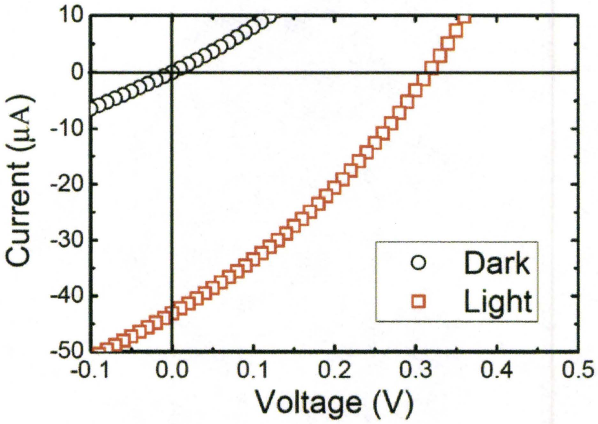

Figure 4.4. Current-voltage curve of group A NWs, with ITO top contacts, under dark and 2.6 Sun illumination. Group B NWs demonstrated no such photo-response.

In comparison, previously reported ensemble contacted NW-based solar cells [9, 10, 13, 14, 42, 43] have demonstrated maximum measured conversion efficiencies ranging between 0.1% to 4.5%. For example, coaxial p-n Si nanowire cells grown by the vapor-liquid-solid (VLS) process gave an efficiency of 0.1% on stainless steel substrates.[9] Si nanowire cells on glass substrates formed by wet electroless etching yielded efficiencies of 4.4%.[10] Coaxial p-n Si nanowire cells grown by the vapor-liquid-solid (VLS) process gave an efficiency of <1% on Si substrates.[42] An efficiency of 0.1% was reported for

VLS-grown Si nanowires on multicrystalline Si thin films on glass.[43] A single GaAs nanowire cell was recently reported with an efficiency of 4.5%.[14] The design most comparable to that of the current study is detailed in Ref. 13, where a photovoltaic effect was measured from vertically oriented GaAs NWs grown on n-GaAs (111)B substrates with a photoconversion efficiency of 0.83%. The lower efficiency values achieved on our CNT films, in comparison to the vertically oriented NWs, may be attributed to two main features. First, growth on CNT films results in NWs grown at a variety of dissimilar angles with respect to the film surface. During the contacting procedure, NWs oriented at more acute angles relative to the CNT film are likely to remain encapsulated by the photoresist layer used during the device processing. Consequently, only the NWs grown at relatively large angles to the substrate will be contacted, meaning that only an undetermined fraction of all NWs will have conductive pathways allowing for their photogenerated holes to be collected. Thus, the total contribution towards the quoted conversion efficiency is not necessarily a reflection of all NWs in the ensemble, but rather only the ones in contact with the ITO film.

Based on previous analysis,[19] we believe that an intimate, atomically abrupt interface exists between the carbon nanotube film and overlaying GaAs NWs. The distinct Au-nanoparticle decoration technique used in the present study is not expected to dramatically alter the atomic nature of the NW/CNT interface, since, in both cases, high temperature annealing results in removal of organic contaminants prior to growth. However, in view of the fact that the CNT film in the present study not only serves as the substrate, but also the electrical contact for the emitter layer of the solar cell, the conduction pathway at this junction requires further consideration. In fact, the second factor contributing to the noted efficiency degradation is the additional series resistance as a result of a barrier at the n-GaAs/CNT interface. Figure 4.5.A shows a one-dimensional band diagram, with respect to axial distance along a single group A NW, assuming a NW length of 2 μm, and derived using a SWNT film workfunction of 4.5 eV.[44] The band diagram was calculated using a one-dimensional Poisson-Schrödinger equation solver, based upon a finite-difference method, and is described in Ref. 46.[45] Here, the p-type GaAs segment is shown on the left side, the n-type GaAs segment in the middle, and the CNT substrate on the right. Conduction band and valence band energies are depicted by black and red lines, respectively, while the Fermi level is shown as a solid blue line. The solid lines represent the band structure anticipated from layers with the nominal doping concentrations, discussed previously. The dotted lines, on the other hand represent the energy bands that would result from acceptor and donor concentrations of 1×10^{17} cm^{-3}. This doping concentration is over one order of magnitude less than the quoted nominal level, and is shown as an expected lower limit of dopant incorporation within the nanowire core, according to Perea et al.[40] Figure 4.5.B shows a magnified view of the energy barrier present at the n-GaAs/CNT interface. The collection of photogenerated electrons is, therefore, preceded by either carrier tunneling from the n-GaAs NW segment to the underlying CNT film or by thermionic emission, dependant upon the concentration of dopants incorporated within the NW bulk.

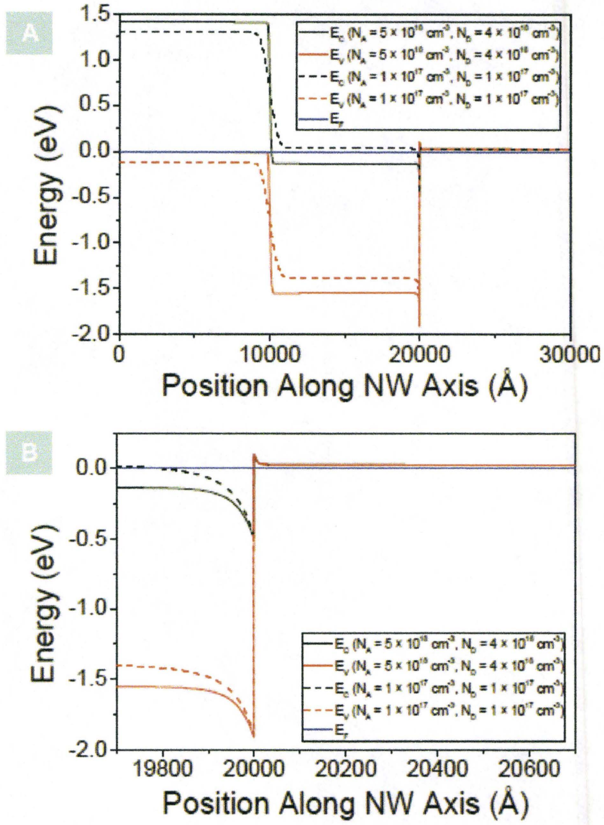

Figure 4.5. (A) One-dimensional energy band diagram as a function of axial position along a single, μm long group A NW. The p-type segment, n-type segment, and CNT film are shown from left to right. Black and red lines denote the conduction and valence bands, respectively. The solid lines represent the band energies according to nominal doping levels quoted in the manuscript, while the dashed lines represent energies at a reduced dopant concentration of 1 × 10^{17} cm^{-3}. The solid blue line represents the Fermi energy, E_F. (B) Magnified view of (A) at the n-GaAs/CNT interface, showing the presence of a small energy barrier.

We previously showed that the current-voltage characteristics of a collection of group A-type NWs exhibited asymmetric rectifications, and had attributed this diode-type behaviour directly to the pn-junctions incorporated within the NW structures.[19] Characterization of electrical junctions within composite films has subsequently been conducted to determine the electrical quality of the junctions and whether ideal current flow is inhibited by Schottky effects at the interfaces. In Figure 4.6, the current-voltage characteristics of group A and B NWs, contacted by opaque contacts, are compared. As seen here, the present study shows a similar current rectification from the group A NWs, while group B NWs exhibit a linear behaviour over the same voltage range. Similarly, group B NWs contacted with ITO also exhibited linear current-voltage characteristics. We present this distinguishing feature (rectifying behaviour of pn-junction NWs in sample A versus Ohmic behaviour of n-doped NWs in sample B) as the defining trademark of the desired dopant activation in our NWs, and evidence that the diode-type behaviour previously presented is not merely a manifestation of Schottky barriers at the n-GaAs/CNT interface. The low forward bias currents evident in the group A curve may be attributed to the partial depletion of the NWs. Furthermore, the aforementioned doping levels and NW density under each contact dot should exhibit resistance values on the order of tens of milli-Ohms, while the measured resistance is on the order of one hundred Ohms. This discrepancy may be ascribed to contact resistances suffered during the measurement process, as well as the effect of the GaAs/CNT interface.

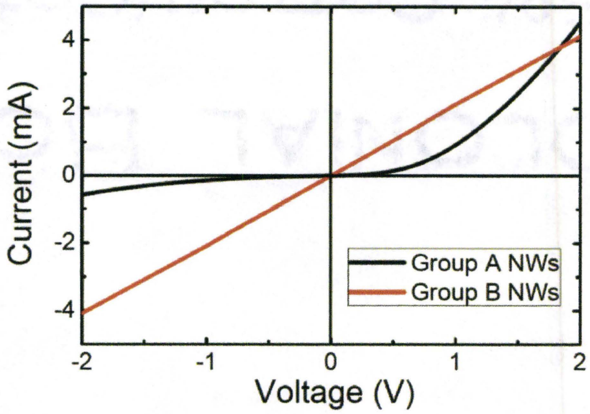

Figure 4.6. Comparison of current-voltage characteristics of group A (black curve) and group B (red line) NWs, contacted with opaque Ti/Pt/Au and Ni/Ge/Au layers, respectively. Rectification is exhibited by the pn-junction NWs while Ohmic behaviour is exhibited by the heavily n-doped NWs.

The influence of the planar GaAs layer, deposited alongside the NWs, upon the observed photovoltaic effect was also studied. As a lateral pn-junction exists in this layer, it is important to distinguish whether this element contributes to the measured conversion efficiency. To this end, the group C control samples were prepared with total film thickness chosen to mimic the average thickness of the planar GaAs layer in group A NW samples, as determined through cross-sectional transmission electron microscopy analysis. This film was subsequently contacted with ITO dots, equal to the thickness of that situated atop the processed group A NWs (as revealed through SEM inspection), such that optical absorption would be comparable between the control and test samples. Under the illuminated solar cell testing conditions described above, the group C control sample reproducibly exhibited an open circuit voltage of

$V_{OC} < 25\ \mu V$ and a short circuit current of $I_{SC} < 20$ nA, from all contact dots tested, representing negligible photovoltaic behavior. The lack of a photovoltaic response in the control sample is chiefly attributed to a high concentration of grain boundaries in the polycrystalline GaAs film, which act as sites for the recombination of any photogenerated electron-hole pairs. Thus, the planar GaAs layer makes no photovoltaic contribution and the energy conversion efficiency observed in group A samples can be attributed to the pn-junction NWs grown atop the CNT composite films. Similarly, the potential for photocurrent generation resulting from a Schottky contact at the ITO/p-GaAs NW interface can be dismissed. Havard et al. have shown that, under high temperature annealing conditions, the formation of Be-O complexes resulting from oxygen diffusion can compromise an Ohmic contact at the associated interface.[46] In the current study, however, the annealing temperatures are not sufficiently high to allow for significant oxygen inter-diffusion. Therefore, Ohmic behaviour is anticipated at the ITO/p-GaAs NW interface.

A final point of added interest is the degree of flexibility and operable range of the group A NW solar cells. The conversion efficiency of the fabricated devices was measured while being subjected to mechanical bending at various radii of curvature. Figure 4.7.A plots measured efficiency as a function of bend radius between 82.5 mm and 5 mm, for 4 particular contact dots. As the curvature of the devices increased (from right to left in Figure 4.7), it was noted that conversion efficiencies were stable to a bend radius of 30 mm. Increasing curvature, to a bend radius of 12.5 mm, resulted in the degradation of efficiency by approximately 25%. Further flexure beyond this point led to the onset of full device failure. Based on SEM analysis of samples intentionally curved past the critical radius of failure (Figure 4.7.B), we attribute the breakdown mechanism to fracture of the polycrystalline GaAs film and its detachment, along with the NWs, from the conductive substrate. Thus, beyond the critical curvature, the photogenerated carriers are no longer effectively collected.

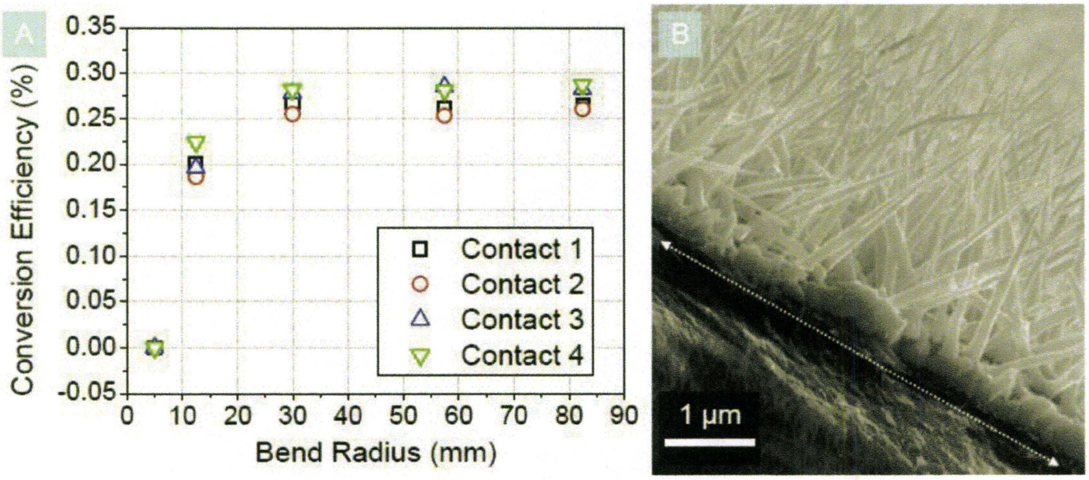

Figure 4.7. (A) Measured conversion efficiency as a function of device flexure at various bend radii (curvature increasing from right to left). A 25% decrease in efficiency is observed at a radius of 12.5 mm. Additional bending beyond this point results in device failure. (B) SEM image of sample curved beyond the critical radius of failure. The white, dotted line indicates the fracture plane where the GaAs NWs are separated from the CNT substrate.

4.3. Conclusions

In summary, a modified regime for the fabrication of Au nanoparticle-decorated SWNT films has been presented that requires no covalent functionalization and ensures the retention of the CNTs' electrical properties. Coaxial pn-junction GaAs NWs were grown upon these flexible, conductive substrates and subsequently employed in the fabrication of photovoltaic cells. Thus, the light harvesting potential of GaAs NWs on flexible CNT films has been demonstrated. The devices demonstrate photovoltaic behaviour when curved, up to a bend radius of 12.5 mm. Further curvature leads to failure due to mechanical fracture and detachment of the GaAs film deposited simultaneously between the NWs. We predict that the vacuum filtration method for SWNT composite film fabrication outlined in this work will be applicable to any nano-material having dimensions that enable their capture and immobilization upon the surface of SWNT membranes. We therefore envision that this scheme can lend itself to the deposition of a variety of inorganic nanoparticles and consequently to the incorporation of NWs composed of a wide range of semiconducting materials, and containing sophisticated heterostructures. This approach may be employed for the production of next generation flexible optoelectronic devices.

4.4. Experimental Section

4.4.1. General

Single-walled carbon nanotubes were purchased from Carbon Nanotechnologies, Inc. (Houston, TX). SWNTs were produced by the HiPCO process and were used as received. All other reagents and solvents were obtained from commercial suppliers and used without any prior treatment. Absorbance measurements were made using a Cary 50

Bio UV-Visible Spectrophotometer. Filtrations were carried out using VWR filtration apparatus with stainless steel support screen and Sartorius PTFE membranes (4.7 cm diameter, 200 nm pore size). Nanotube samples were dispersed in solvent using a Branson 1510 bath sonicator. Nanotube dispersions were centrifuged using a Beckman Coulter Allegra X-22 Centrifuge.

4.4.2. Preparation of SWNT dispersion in SDS solution

In a typical experiment, pristine SWNTs (10 mg) were added to a 125 mL Erlenmeyer flask containing sodium dodecyl-sulfate (SDS) solution (100mL, 1 wt%) and dispersed using sonication (20 minutes). Following sonication, the dispersion was subjected to centrifugation (2570 g, 20 minutes) after which the supernatant was removed and transferred to a 500 mL Erlenmeyer flask. The precipitate obtained during centrifugation was redispersed in 1 wt% SDS solution and this procedure was repeated until 500 mL of a dilute nanotube dispersion was obtained. This dispersion was then subjected to a second round of centrifugation (2570 g, 20 minutes). The supernatant was again removed and transferred to a clean Erlenmeyer flask. The concentration of SWNTs dispersed in solution using this procedure was determined to be approximately 10.5 mg L^{-1}. This value was obtained from UV-spectroscopy measurements for which a specific extinction coefficient at 700 nm (0.0235 L mg^{-1} cm^{-1}) was employed.[47]

4.4.3 Synthesis of Au Nanoparticles

Gold nanoparticles were prepared by citrate reduction of $HAuCl_4$[27-29] using the following procedure: $HAuCl_4$ solution (100 mL, 0.5 mM) in deionized water was added to a round bottomed flask equipped with a magnetic stir bar and condenser. The solution was heated to reflux while stirring rapidly. Upon reflux, a solution containing tri-sodium citrate (36.75 mg, 0.125 mmol) in deionized water (3 mL) was added rapidly to the solution. The solution was stirred at reflux for 10 minutes. The reaction flask was then allowed to cool to room temperature while stirring was continued. The nanoparticle solution was subsequently stored in a glass bottle at 4°C. Using scanning electron microscopy, the diameter of particles prepared using this procedure was determined to be 30 ± 5 nm.

4.4.4. SWNT-Au composite film preparation

SWNT films were prepared by vacuum filtration of SWNT dispersion in SDS solution through a PTFE membrane having pore size of 200 nm. 400 mL of nanotube dispersion, having concentration of approximately 10.5 mg L^{-1}, was filtered to produce each film. Deposition of Au nanoparticles was achieved by filtration of dilute nanoparticle solution through these SWNT thin films. For successful deposition of Au nanoparticles it is vital that the SWNT film does not become dry at any point during the filtration process. If this is allowed to occur, Au nanoparticles become localized in regions of high density and uniform coverage of nanoparticles across the film's surface is not obtained. The formation of SWNT films and deposition of Au particles must therefore be carried out as part of one continuous process. This was achieved by filtering four separate solutions in sequence. These solutions, in order of addition, were SWNT dispersion in SDS solution (400 mL), SDS solution containing no SWNTs (100 mL), pure distilled water (2 x 250 mL), and dilute Au nanoparticle solution (100 mL, 2 mM). Each solution was added when approximately 5 ml of the previous solution remained in the filtration apparatus, ensuring that the nanotube film remained submersed under solution at all times. Washing the nanotube film with distilled water, prior to Au nanoparticle deposition, ensures the removal of excess surfactant. The purpose of adding SDS solution between SWNT film formation and washing with distilled water is to prevent precipitation of SWNTs from the small volume of solution remaining in the filtration apparatus. In the final stage of composite film formation, the Au nanoparticle solution was allowed to pass completely through the filtration membrane. The SWNT-Au composite film was then dried, first overnight under air and subsequently in vacuo (24 hours, 50°C), during which time the film was kept intact upon the filtration membrane due to the mechanical support which this provided. Films were subsequently cut into small sections having dimensions of 5 x 10 mm and transferred, Au nanoparticle side up, to copper substrates. The samples were then subjected to a rapid thermal anneal (RTA) treatment (550°C, 10 minutes) under nitrogen atmosphere. The density of Au nanoparticles upon the surface of annealed SWNT-Au composite films, determined using SEM, ranged from between 20 and 86 nanoparticles per 1 μm^2, with an average value of 50 nanoparticles per 1 μm^2. These values were obtained from a total of 100 measurements made over 6 randomy selected regions in two sepearate composite film samples.

4.4.5. Growth of GaAs nanowires

The GS-MBE system used for NW growths was equipped with a solid elemental effusion cell, for the supply of Ga monomers, and a hydride (AsH_3) gas cracker operating at 950°C, for the supply of As_2 dimers. Prior to the commencement of the growth sequence, a degas procedure (15 minutes, 300°C) was performed, followed by an inductively coupled hydrogen plasma treatment (10 minutes, 550°C), under an As_2 overpressure. This procedure allowed for NW growth conditions that were consistent with prior growth experiments. A significant influence on the properties of the CNT film is not anticipated following this treatment. At a growth temperature of 550°C, NW growth was instigated by opening the shutter of the Ga cell. All growths were kept at a constant V/III flux ratio of 1.5 and nominal GaAs growth rate of 1 μmhr^{-1}. Upon the completion of growth, prompted by the termination of Ga flux, the samples were cooled under an As_2 overpressure.

For the purposes of investigations presented in this work, two NW groups were grown on CNT composite sheets, henceforth referred to as groups A and B. Group A NWs were designed to contain a pn-junction within a coaxial architecture, based upon diffusion-limited nucleation on the lateral NW facets, wherein an n-GaAs core segment was doped with Te, while a p-GaAs shell was doped with Be. Each segment of the group A NWs was grown for a duration of 15 minutes, resulting in a total growth period of 30 minutes. Group B NWs, in contrast, were entirely n-type doped with Te, also over a growth period of 30 minutes, yielding n-GaAs NWs. Nominal dopant concentrations were maintained at 4×10^{18} cm^{-3} and 5×10^{18} cm^{-3}, for Te and Be levels, respectively, based upon previous calibrations of epitaxial films on GaAs (100) substrates. The group A NWs were primarily used to assess the photovoltaic potential of such NW-CNT hybrid materials, while the group B NWs were employed in investigations into the nature of the photovoltaic response and the conduction pathways between the NWs and their underlying CNT substrates.

Additionally, a third growth was carried out, referred to as group C, wherein a planar pn-junction was incorporated into a thin film deposited upon a CNT composite film containing no Au-nanoparticles. This control sample was grown with the intention of mimicking the structure of the planar GaAs film deposited during the growth of, and situated adjacent to, the nanowires of the group A and B samples. The group C samples were prepared consisting of a 150 nm thick Be-doped GaAs layer overlaying a 150 nm thick Te-doped GaAs layer. Identical CNT film processing (surface decoration of Au-nanoparticles, notwithstanding) and GS-MBE growth parameters including temperature, nominal growth rate, III/V flux ratio, and nominal doping concentration where employed in the case of the thin film deposition and NW growths. Thus, the GaAs film of sample C was designed to duplicate the properties of the planar film concurrently deposited during NW growth.

4.4.6. Solar cell fabrication and contacting procedure

To prevent potential short circuit pathways between top contacts and the bottom CNT electrode, a previously reported processing method was employed.[13, 19] Starting with as-grown samples, SiO_x layers, approximately 1300 Å in thickness, were deposited through plasma-enhanced chemical vapor deposition (PE-CVD), to conformally coat the NWs (and the exposed surface of the GaAs films growing between the NWs) atop the CNT substrate. Subsequent spin-coating of S-1808 photoresist was carried out to encapsulate the oxidized NWs and GaAs film. Next, a O_2-plasma reactive ion etching (RIE) treatment (60 seconds) allowed for the removal of a thin photoresist film, thereby exposing the tips of the oxidized NWs. The oxidized tips were then chemically etched in a buffered-hydrofluoric acid solution and the remaining photoresist layer was removed in an acetone bath lift-off procedure. At this stage, the NW bases and adjacently situated GaAs film remained encapsulated by the previously deposited SiO_x layer, while NW tips were exposed as the sole semiconductor surface upon which electrical contacts could be deposited.

Two different conductive materials were employed as top contact layers in the present study. For experiments aimed towards investigations into photovoltaic behaviour, a 1000 Å thick transparent conductive film of indium tin oxide (ITO) was deposited via sputter coating. For direct comparison of the conductive behaviour of group A and B NWs, where optimal Ohmic contacts are required, opaque contacts were deposited on the processed samples. In this case, the commonly used Ti/Pt/Au and Ni/Ge/Au layers were deposited on group A and B samples, respectively, via electron-beam evaporation. In all cases, the depositions were made through shadow masks allowing for contact dots roughly 800 μm in diameter. Inspection of plan view scanning electron microscopy (SEM) images (not shown) indicated that each contact dot yielded the ensemble contribution of approximately 1.5 x 10^6 individual NWs. After the deposition of ITO or opaque contacts, the samples were subjected to a rapid thermal annealing (RTA) treatment (30 seconds, 400°C) for Ohmic contact formation.

SEM imaging was performed during pre-growth inspection of Au-decorated CNT films, during analysis of orientation and morphology of as-grown NWs, and during each stage of the device fabrication procedure. The SEM imaging was performed using a JEOL JSM-7000F SEM, equipped with a Schottky-type field emission gun filament. In addition, inspection of the CNT films were performed by focused ion beam (FIB) cross-sectioning using a Zeiss NVision SII Cross-Beam instrument.

4.4.7. Current-voltage characterization under dark and illuminated conditions

The current-voltage characteristics of the various samples were evaluated using a Keithley 2400 source meter. A Newport 96000 solar simulator with an A.M. 1.5 G filter yielding an incident power of roughly 2.6 Suns was used as the illumination source in measuring photovoltaic response. Conversion efficiencies and fill factors were calculated according to standard techniques.[48]

4.5. References

(1) M. Law, J. Goldberger and P. D. Yang. *Annu. Rev. Mater. Res.* **2004,** 34, 83-122.

(2) T. A. G. Eberlein, R. Jones, J. P. Goss and P. R. Briddon. *Phys. Rev. B* **2008,** 78, (4), 045403-045407.

(3) S. Y. Ju, A. Facchetti, Y. Xuan, J. Liu, F. Ishikawa, P. D. Ye, C. W. Zhou, T. J. Marks and D. B. Janes. *Nat Nanotechnol* **2007,** 2, (6), 378-384.

(4) K. Lee, Z. Wu, Z. Chen, F. Ren, S. J. Pearton and A. G. Rinzler. *Nano Lett.* **2004,** 4, (5), 911-914.

(5) M. C. McAlpine, R. S. Friedman, S. Jin, K. H. Lin, W. U. Wang and C. M. Lieber. *Nano Lett.* **2003,** 3, (11), 1531-1535.

(6) R. C. Tenent, T. M. Barnes, J. D. Bergeson, A. J. Ferguson, B. To, L. M. Gedvilas, M. J. Heben and J. L. Blackburn. *Adv. Mater.* **2009,** 21, 1-7.

(7) O. L. Muskens, J. G. Rivas, R. E. Algra, E. P. A. M. Bakkers and A. Lagendijk. *Nano Lett.* **2008,** 8, (9), 2638-2642.

(8) B. M. Kayes, H. A. Atwater and N. S. Lewis. *J. Appl. Phys.* **2005,** 97, (11), 114302-11.

(9) L. Tsakalakos, J. Balch, J. Fronheiser, B. A. Korevaar, O. Sulima and J. Rand. *Appl. Phys. Lett.* **2007,** 91, (23), 233117-233119.

(10) V. Sivakov, G. Andra, A. Gawlik, A. Berger, J. Plentz, F. Falk and S. H. Christiansen. *Nano Lett.* **2009,** 9, (4), 1549-1554.

(11) Y. J. Dong, B. Z. Tian, T. J. Kempa and C. M. Lieber. *Nano Lett.* **2009,** 9, (5), 2183-2187.

(12) B. Z. Tian, X. L. Zheng, T. J. Kempa, Y. Fang, N. F. Yu, G. H. Yu, J. L. Huang and C. M. Lieber. *Nature* **2007,** 449, (7164), 885-U8.

(13) J. A. Czaban, D. A. Thompson and R. R. LaPierre. *Nano Lett.* **2009,** 9, 148-154.

(14) C. Colombo, M. Heiss, M. Gratzel and A. F. I. Morral. *Appl. Phys. Lett.* **2009,** 94, (17), 173108-173110.

(15) C. Xu, X. Wang and Z. L. Wang. *J. Am. Chem. Soc.* **2009,** 131, 5866-5872.

(16) B. D. Yuhas and P. D. Yang. *J. Am. Chem. Soc.* **2009,** 131, (10), 3756-3761.

(17) M. Law, L. E. Greene, J. C. Johnson, R. Saykally and P. D. Yang. *Nat Mater* **2005,** 4, (6), 455-459.

(18) A. Nadarajah, R. C. Word, J. Meiss and R. Konenkamp. *Nano Lett.* **2008,** 8, (2), 534-537.

(19) P. K. Mohseni, G. Lawson, C. Couteau, G. Weihs, A. Adronov and R. R. LaPierre. *Nano Lett.* **2008,** 8, (11), 4075-4080.

(20) R. S. Wagner and W. C. Ellis. *Appl. Phys. Lett.* **1964,** 4, 89-90.

(21) V. G. Dubrovskii, N. V. Sibirev, G. E. Cirlin, J. C. Harmand and V. M. Ustinov. *Phys. Rev. E* **2006,** 73, (2), 021603-10.

(22) H. J. Fan, P. Werner and M. Zacharias. *Small* **2006,** 2, (6), 700-717.

(23) Z. C. Wu, Z. H. Chen, X. Du, J. M. Logan, J. Sippel, M. Nikolou, K. Kamaras, J. R. Reynolds, D. B. Tanner, A. F. Hebard and A. G. Rinzler. *Science* **2004,** 305, (5688), 1273-1276.

(24) F. Hennrich, S. Lebedkin, S. Malik, J. Tracy, M. Barczewski, H. Rosner and M. Kappes. *Phys. Chem. Chem. Phys.* **2002,** 4, (11), 2273-2277.

(25) L. Hu, D. S. Hecht and G. Gruner. *Nano Lett.* **2004,** 4, (12), 2513-2517.

(26) G. Lawson, F. Gonzaga, J. Huang, G. de Silveira, M. A. Brook and A. Adronov. *J. Mater. Chem.* **2008,** 18, (14), 1694-1702.

(27) J. Turkevich, J. Hillier and P. C. Stevenson. *Discuss. Faraday. Soc.* **1951,** 11, 55.

(28) J. Kimling, M. Maier, B. Okenve, V. Kotaidis, H. Ballot and A. Plech. *J. Phys. Chem. B* **2006,** 110, (32), 15700-15707.

(29) X. H. Ji, X. N. Song, J. Li, Y. B. Bai, W. S. Yang and X. G. Peng. *J. Am. Chem. Soc.* **2007,** 129, (45), 13939-13948.

(30) S. J. Park and D. G. Lee. *Carbon* **2006,** 44, (10), 1930-1935.

(31) A. S. Brady-Estevez, S. Kang and M. Elimelech. *Small* **2008,** 4, (4), 481-484.

(32) G. Viswanathan, D. B. Kane and P. J. Lipowicz. *Adv. Mater.* **2004,** 16, (22), 2045-2049.

(33) A. Srivastava, O. N. Srivastava, S. Talapatra, R. Vajtai and P. M. Ajayan. *Nat Mater* **2004,** 3, (9), 610-614.

(34) B. J. Hinds, N. Chopra, T. Rantell, R. Andrews, V. Gavalas and L. G. Bachas. *Science* **2004,** 303, (5654), 62-65.

(35) J. K. Holt, H. G. Park, Y. M. Wang, M. Stadermann, A. B. Artyukhin, C. P. Grigoropoulos, A. Noy and O. Bakajin. *Science* **2006,** 312, (5776), 1034-1037.

(36) X. F. Wang, X. M. Chen, K. Yoon, D. F. Fang, B. S. Hsiao and B. Chu. *Environ Sci Technol* **2005,** 39, (19), 7684-7691.

(37) M. Yu, H. H. Funke, J. L. Falconer and R. D. Noble. *Nano Lett.* **2009,** 9, (1), 225-229.

(38) E. T. Mickelson, C. B. Huffman, A. G. Rinzler, R. E. Smalley, R. H. Hauge and J. L. Margrave. *Chem Phys Lett* **1998,** 296, 188-194.

(39) C. Chen, M. C. Plante, C. Fradin and R. R. LaPierre. *J. Mater. Res.* **2006,** 21, (11), 2801-2809.

(40) D. E. Perea, E. R. Hernesath, E. J. Schwalbach, J. L. Lensch-Falk, P. W. Voorhees and L. J. Lauhon. *Nat Nanotechnol* **2009,** 4, (5), 315-319.

(41) J. E. Allen, D. E. Perea, E. R. Hemesath and L. J. Lauhon. *Adv. Mater.* **2009,** 21, 1-6.

(42) O. Gunawan and S. Guha. *Sol Energ Mat Sol C* **2009,** 93, (8), 1388-1393.

(43) T. Stelzner, M. Pietsch, G. Andra, F. Falk, E. Ose and S. Christiansen. *Nanotechnology* **2008,** 19, (29), 295203-295206.

(44) A. Benham, J. L. Johnson, Y. Choi, M. G. Estosun, O. A.K., P. Kapur, K. C. Saraswat and A. Ural. *Appl. Phys. Lett.* **2008,** 92, 243116-243118.

(45) I. H. Tan, G. L. Snider, L. D. Chang and E. L. Hu. *J. Appl. Phys.* **1990,** 68, (8), 4071-4076.

(46) E. Havard, T. Camps, V. Bardinal, L. Salvagnac, C. Armand, C. Fontaine and S. Pinaud. *Semicond Sci Tech* **2008,** 23, (3), -.

(47) A. Ikeda, K. Nobusawa, T. Hamano and J. Kikuchi. *Org Lett* **2006,** 8, (24), 5489-5492.

(48) J. Nelson, *The Physics of Solar Cells*. London: Imperial College Press: 2008.

Chapter 5: Growth of III-V Semiconductor NWs upon Highly Ordered Pyrolytic Graphite

Gregor Lawson, Parsian K. Mohseni, Alex Adronov and Ray R. LaPierre,

Work detailed in this chapter was carried out in collaboration with Parsian K. Mohseni and Dr. Ray LaPierre (Department of Engineering Physics and Centre for Emerging Device Technology, McMaster University, Hamilton, Ontario). Both Gregor Lawson and Parsian K. Mohseni contributed equally to the experimental planning of this work. Synthesis of Au nanoparticles, preparation of modified HOPG substrates and scanning electron microscopy analysis was conducted by Gregor Lawson. NW growth and characterization, including scanning electron microscopy, was conducted by Parsian K. Mohseni.

Abstract

Studies were conducted to determine whether epitaxial growth of GaAs nanowires (NWs) upon a highly ordered carbon substrate was possible. In this work, Highly Ordered Pyrolytic Graphite (HOPG), both unmodified and decorated with Au nanoparticles (NPs), was employed as a growth substrate. Under the conditions investigated, epitaxially initiated NWs, aligned normal to the substrate, were obtained in very low density. Analysis by electron microscopy and energy dispersive x-ray spectroscopy indicated that growth of orthogonally oriented NWs was Ga assisted. This observation was confirmed by growth of GaAs NWs in the absence of Au NPs. Attempts to improve nanowire density, using surface treatment techniques and modification of growth conditions proved unsuccessful. Based on the results of these studies, a mechanism for Ga assisted NW growth is outlined and additional experiments, that could help to confirm and refine this mechanism, are proposed.

5.1. Introduction

In the preceding chapters, procedures were developed for the preparation of single walled carbon nanotube (SWNT) composite films decorated by Au nanoparticles (NPs). These films were shown to be suitable substrates for the assembly of III-V semiconductor NWs using gas source molecular beam epitaxy (GS-MBE). As discussed, GaAs NWs obtained following these procedures were oriented at a variety of angles relative to the growth substrate, due to the disordered nature of the SWNT film, which resembled a network of randomly oriented nanotube bundles. Although it was speculated that the initial nucleation of GaAs could have occurred upon the sidewall of an individual CNT, the interfacial region at the base of several NWs, examined using TEM, was shown to extend over multiple SWNTs. It was therefore not possible to determine whether the initial nucleation had occurred via an epitaxial process.

The random orientation of NWs is problematic if the full potential of these materials as active components within functional electronic devices is to be developed. In work described in the previous chapter, the decreased efficiency of a solar cell device incorporating our SWNT-NW composite material relative to a similar device incorporating vertically aligned NWs, was explained, in part, by the observation that a percentage of wires, oriented at acute angles to the substrate, could not be effectively contacted. Consequently, these wires did not contribute to the overall photovoltaic response of the device. Additionally, non-orthogonal growth results in an increased number of defects, resulting from the merging of wires growing in close proximity to one another. Such defects may also have a detrimental effect upon the efficiency of devices and are therefore undesirable.

One manner by which orthogonally oriented NWs can be obtained is if growth occurs by an epitaxial process whereby a crystalline material acts as a template for the initial nucleation of adatoms. This can be promoted through the use of a highly ordered substrate which exhibits order extending over suitably sized area. In the case of carbon based substrates, the planar hexagonal array of carbon atoms found in graphite would provide the highest possible degree of order. Highly Ordered Pyrolytic Graphite (HOPG) is a high-purity grade of graphite which is widely used as a substrate for scanning tunneling microscopy. Given the lamellar nature of graphite, layers may be easily cleaved from an HOPG wafer to produce a relatively smooth substrate that will ideally contain very few defects or adsorbed contaminants. HOPG is also conductive, chemically inert and exhibits good stability at elevated temperatures. These properties make HOPG a potential candidate for investigation as a substrate for III-V semiconductor NW growth.

If aligned arrays of nanowires can be obtained upon HOPG it is possible that the approach could also be extended to graphene thin films. Significant interest has arisen in recent years regarding the potential of graphene in the development of novel conductive composite materials for use in electronic device applications.[1-6] Using aqueous suspensions of graphene oxide, films can be prepared by a variety of low cost room temperature techniques.[7-10] Subsequent reduction of graphene oxide by chemical or thermal means results in the formation of graphene thin films which exhibit a number of impressive properties similar to those of CNT thin films including low resistivity, high thermal stability and excellent flexibility.[5] Recently, a number of groups have reported improved methods for the production of highly pure graphene films by solution based methods. The investigation of high-purity graphene-based films as substrates for the growth of orthogonally aligned semiconductor NWs could therefore potentially enable the development of a new generation of flexible low-cost optoelectronic devices.

HOPG has previously been employed as a substrate for the deposition of a variety of materials. It has, for example, been used in the preparation of nanowires by step-edge decoration,[11-13] a technique by which a metallic or crystalline material is selectively deposited at the atomic step edges of a substrate to produce arrays of nanowires aligned parallel to the surface. Several groups have also reported the growth of vertically oriented NWs upon HOPG including those composed of ZnO,[14] In_2O_3,[15] InN,[16] and SiC,[17] as well as Co_5Ge_7[18] nanobelts. In the case of ZnO[14] and Co_5Ge_7[18] nanocrystals, an epitaxial relationship was shown to exist with the HOPG substrate, allowing the preparation of highly aligned nanocrystal arrays. In both examples, the authors attribute vertical growth, in part, to good epitaxial lattice match between HOPG and the material under investigation.

GaAs NWs grown in our previous work were shown to display a wurtzite crystal structure. The lattice parameter of wurtzite GaAs in the <1000> direction (3.912 Å)[19] is related the lattice constant of graphite (a = b = 2.46 Å) by a factor of 1.59 and has a lattice mismatch of + 8.92%. The corresponding lattice parameter in the <1120> direction (3.388 Å) is related to the carbon-carbon bond length (1.42 Å) by a factor of 2.38, resulting in a lattice mismatch of + 8.97%. For epitaxially grown films having thicknesses below a specific critical value, lattice mismatch values of up to 9% can be accommodated.[13] In the case of NWs, lateral constraints which are experienced by thin films are reduced considerably at narrow diameters, allowing NWs to relieve strain induced by lattice mismatch via lateral relaxation.[20, 21] This enables the epitaxial growth of NWs upon lattice mismatched substrates, provided that their diameter lies below a certain critical value. Previously, the heteroepitaxial growth of III-V NWs by MBE upon substrates with lattice mismatch values exceeding 11% has been reported.[22, 23] It is therefore feasible that epitaxial growth of GaAs NWs upon HOPG could potentially be achieved under the correct growth conditions.

At the time of writing, no examples could be found in literature describing the growth of GaAs NWs upon a graphitic substrate. Chu et al. previously reported the use of graphite as a substrate for deposition of GaAs thin films by chemical vapor deposition.[24, 25] In this work, graphite was selected as a substrate of interest, as it was chemically inert under the conditions used for film deposition and exhibited a thermal expansion coefficient similar to GaAs. Films prepared in this work were composed of crystallites 10 to 15 μm in diameter which displayed no preferred orientation. Authors cite the reversibility of the chemical reaction resulting in GaAs nucleation for the lack of observed order.

Here, we report the results of a model study designed to determine whether epitaxial growth of GaAs NWs upon an ordered carbon substrate is indeed possible. HOPG, both unmodified and decorated with Au NPs, was used as the substrate for nanowire growth under a range of different conditions. Although vertically aligned NWs were obtained, their density was very low. Data obtained using transmission electron microscopy (TEM) and energy dispersive X-ray spectroscopy (EDXS), indicate that NW growth was self-assisted, and these observations were confirmed by NW growths conducted with the absence of Au NPs. Subsequent attempts to promote nanowire formation using surface treatment techniques proved unsuccessful, indicating that epitaxial growth was not favored under the conditions investigated. Some discussion is provided as to the mechanism of GaAs NW growth upon HOPG, which may in part explain the low density of NWs which was obtained. Additionally, suggestions are made for future experiments that could be conducted to investigate the growth of III-V NWs upon HOPG and other carbon based substrates.

5.2. Results and Discussion

5.2.1. Preparation of Au NP modified HOPG substrates

HOPG samples used in this work were purchased from SPI supplies. Au NP decorated substrates were prepared by drop casting from a dilute solution (0.05 mM) of colloidal Au NPs in either water or ethanol. Prior to NP deposition, HOPG substrates were cleaved using the adhesive tape method, to produce a clean, uncontaminated surface. Following drop casting, samples were allowed to dry under air at room temperature for approximately 30 minutes or until no droplets were visible. The samples were then transferred to an oven and dried in vacuo overnight at 50°C.

Nanoparticle density upon modified substrates was evaluated using scanning electron microscopy (SEM). For samples prepared by drop casting from water, the outline of evaporated Au NP solution droplets, several hundreds of microns in diameter, were observed at low magnification. The density of Au NPs within these areas was not homogeneous and varied with their distance from the centre of each droplet. These areas did however contain regions in which a high density of NPs was observed. Figure 5.1.A shows a planar SEM image of one such region. Here it can be seen that discrete NPs are present upon the substrate, along with clusters of various sizes, which are composed of multiple NPs. The effect of pre-growth annealing conditions upon NP density and diameter was subsequently evaluated. In this study, Au modified substrates were subjected to conditions identical to those used prior to nanowire growth. Within the MBE system, a degas procedure under ultrahigh vacuum (15 minutes, 300°C) was first performed followed by treatment with an inductively coupled hydrogen plasma under As_2 overpressure (10 minutes, 550°C), the purpose of which was to remove possible surface contamination. The system was then cooled under As_2 overpressure. A planar SEM image of a Au modified HOPG substrate which has undergone this annealing procedure is shown in Figure 5.1.B. From this image it can be seen that some aggregation of NPs does occur under the annealing conditions described. It was however difficult to quantify the effect of this treatment on NP density, given the variability that existed in the sample prior to annealing. Regions could however be located exhibiting optimum density for NW growth within which the diameter of particles was measured to range between around 20 and 100 nm. In regions of higher density, large Au NP clusters with diameters of over 100 nm were also observed. If the purpose of this work were to prepare a highly ordered array of NWs, the polydispersity of Au NP diameters and inhomogeneous density would be problematic. However, as this was an initial study and the objective was to obtain a proof-of-concept result, confirming epitaxial growth of NWs upon an ordered carbon substrate, these samples were deemed suitable for use in subsequent experiments.

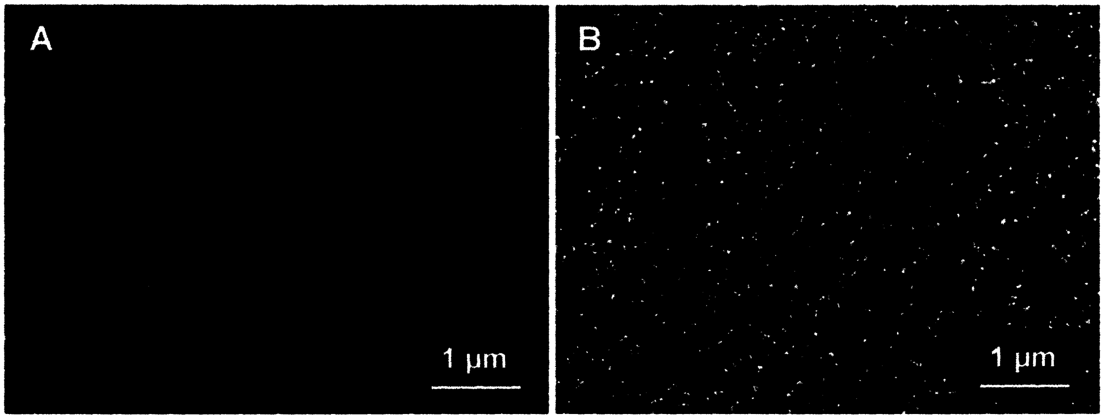

Figure 5.1. Planar SEM images of Au NP modified HOPG substrates, prepared by drop casting from dilute solution in water, before (A) and after (B) high temperature anneal within the GS-MBE system.

5.2.2. Nanowire Growth

NW growths were conducted using the same GS-MBE system described in previous chapters. Over the course of this study, a total of 5 different NW growths were conducted. The conditions employed for each growth, in addition to the substrates investigated are outlined in Table 5.1.

Table 5.1. Conditions of GS-MBE growths upon HOPG.

Growth	Temperature / °C	Structure			Total Growth Time / min	Sample #	Surface treatment
A	550	GaAs, pn-junction	n-GaAs [Te] = 5 x 10^{18} cm^{-3}, 15 mins	p-GaAs [Be] = 5 x 10^{18} cm^{-3}, 15 mins	30	1-3	31 ± 4 nm Au NPs
B	550	GaAs, Undoped	GaAs, 15 mins		15	1	25 ± 4 nm Au NPs
						2	-
						3	Ethanol treated
						4	5 nm SiO_x layer
						5	RIE, Oxygen plasma
C	550	GaAs, undoped	GaAs, 15 mins		15	1,2	1 nm Ga deposited at 550°C, prior to growth
D	600	GaAs, pn-junction	n-GaAs [Te] = 5 x 10^{18} cm^{-3}, 15 mins	p-GaAs [Be] = 5 x 10^{18} cm^{-3}, 15 mins	30	1,2	No treatment
E	400	InAs, pn-junction	n-InAs [Te] = 5 x 10^{18} cm^{-3}, 15 mins	p-InAs [Be] = 5 x 10^{18} cm^{-3}, 15 mins	30	1,2	25 ± 4 nm Au NPs
						3	No treatment

All Growths were conducted using a V/III ratio = 1.5 and nominal III-V Growth rate = 1 μm/hr.

5.2.2.1. Initial study

The conditions of Growth A were selected to mirror those of previous studies, in which p-n junction nanowires exhibiting a co-axial architecture were grown upon SWNT-Au NP composite films.[26] Figure 5.2 shows SEM images of a Au NP modified HOPG substrate, obtained at a tilt angle of 45°, following NW growth under these conditions. From the low magnification image (Figure 5.2.A) it can be seen that the majority of the surface was covered by islands of polycrystalline GaAs. Smooth features resembling droplets were also observed upon the sides of these islands and isolated upon the HOPG substrate. These features were determined using Energy Dispersive X-Ray Spectroscopy (EDXS) to be composed primarily of Ga (Appendix I, Figure 5.I.1). At higher magnification, GaAs NWs were also observed. While these wires were present in very low density and were surrounded by islands of GaAs, it can be seen from the images in Figure 5.2.C that these wires are aligned normal to the substrate and display a columnar structure typical of NWs grown via the standard bottom-up NW growth mechanisms. Additionally, it can be seen that these wires are growing directly from the surface of the HOPG substrate and not from islands of crystalline GaAs.

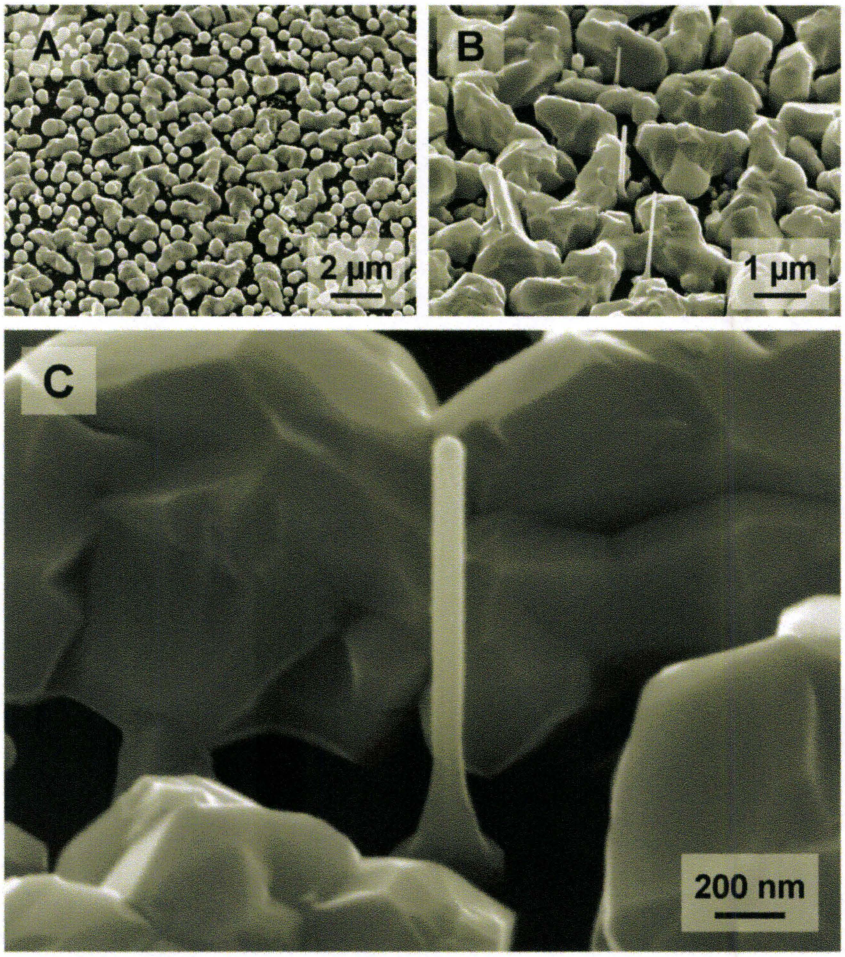

Figure 5.2. Tilted SEM images of Au modified HOPG substrate following NW growth A. Image (C) shows a typical example of a GaAs NW which was observed in low density upon the substrate.

Using focused ion beam (FIB) milling, an electron transparent lamella was prepared from this sample in which two NWs were embedded. The lamella was subsequently imaged using transmission electron microscopy (TEM), allowing investigation of the NW structures and the nature of the interface between the NW and the substrate. In Figure 5.3.A, a TEM image of one of these wires is shown. Material surrounding the nanowire in this image is carbon which was deposited during lamella preparation, to provide mechanical support preventing the NW from becoming detached during transfer of the lamella to the TEM grid. This image clearly shows that NW growth did indeed occur normal to the substrate. Examination of the base region of the wire (Figure 5.3.B) reveals a clean abrupt interface with the underlying HOPG. Selected area diffraction (SAD) patterns obtained from the base region indicated a zinc blende crystal structure with a [111] basal plane (Appendix I, Figure 5.I.2.). Analysis over the length of the wire revealed a high incidence of stacking faults and a predominantly 4-H polytype structured tip, resembling a wurtzite structure in SAD patterns.

A TEM image of the tip region of the same NW is shown in Figure 5.3.C, in which no Au nanoparticle can be observed. The catalyst free nanowire growth has previously been reported for a number of species including GaAs,[27-29] InAs,[30] and In_2O_3.[31] Substrates employed for Ga assisted nanowire growth typically contain a thin silicon oxide surface layer. Recently, Morral and coworkers proposed a mechanism for Ga assisted NW growth upon oxide modified substrates.[28] At high temperatures the sticking coefficient of Ga monomers upon the surface oxide is very low. Ga adatoms may therefore diffuse across the substrate until they reach a pore or defect which provides a suitable site for adatom nucleation.[28] At this point, following the model proposed by Morral and coworkers, reaction of Ga with the surface oxide, results in the expansion of the initial defect to produce a larger crater. Eutectic droplets that are formed by this reaction subsequently act as selective adsorption sites for As species, which alloy with Ga at the liquid solid interface to form GaAs. Nanowire growth subsequently occurs, with the Ga droplet at the nanowire tip being replenished by adatoms diffusing along the surface oxide and up the nanowire sidewalls. Epitaxial growth occurs when the deposited oxide is thin enough (< 30 nm) to allow adatom diffusion through porous regions to the ordered crystalline substrate below.[28]

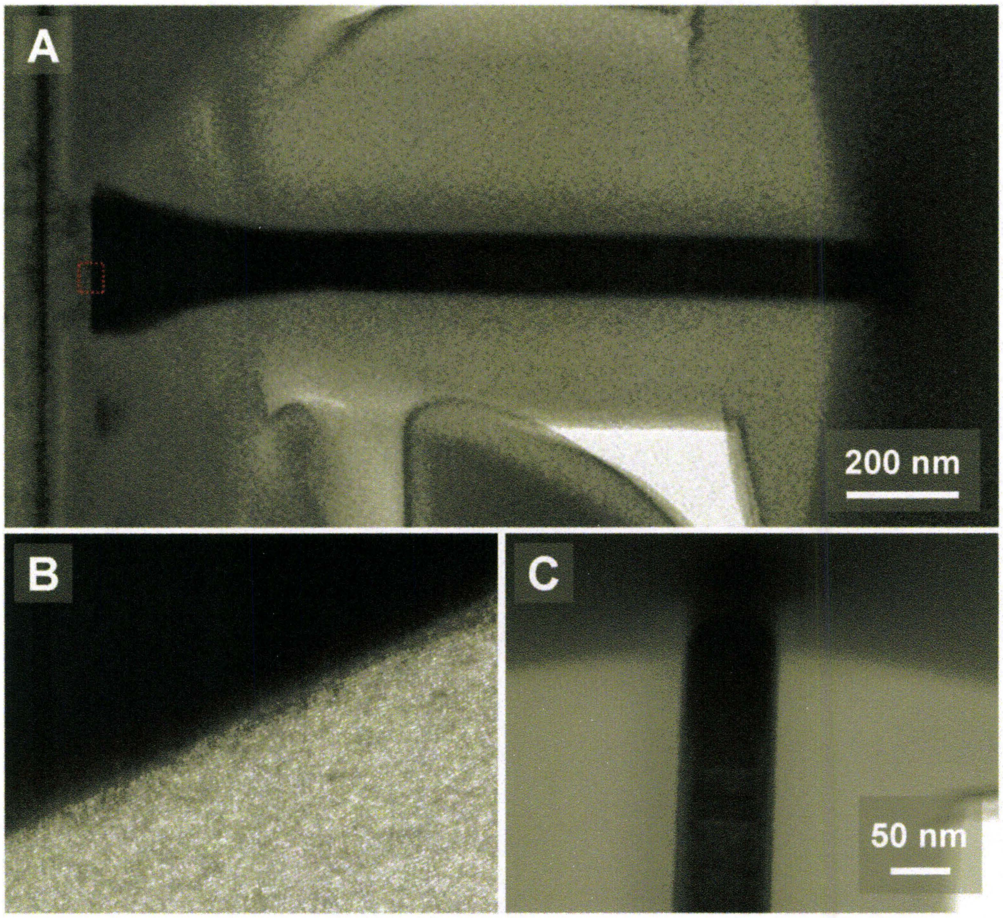

Figure 5.3. (A) TEM image of lamella containing GaAs NW, obtained using FIB milling, (B) High magnification image showing the interface between the base of the wire and HOPG substrate at the region indicated (C) TEM image of the nanowire tip showing the absence of a Au NP.

Figure 5.4 shows a high angle annular dark field (HAADF) image of the same nanowire described in the previous sections, with EDXS linescans superimposed along the length of the wire. From this image, it can be seen that Ga and As content was approximately equal at the base region and along the wires middle section. Approaching the tip region, As content was observed to decrease while Ga content increased notably. The high concentration of Ga at the tip region, relative to the rest of the wire, is in agreement with a Ga assisted nanowire growth mechanism. Under the conditions employed, samples were cooled under an As overpressure following the termination of NW growth. During this period, residual Ga will be consumed to form GaAs. Consequently, no Ga seed particle can be observed at the wires tip, although some excess Ga does remain. The absence of a Au particle, confirmed using EDXS, rules out the possibility of Au seed assisted growth. Despite thorough examination of samples from Growth A using SEM, no Au particle tipped NWs were observed.

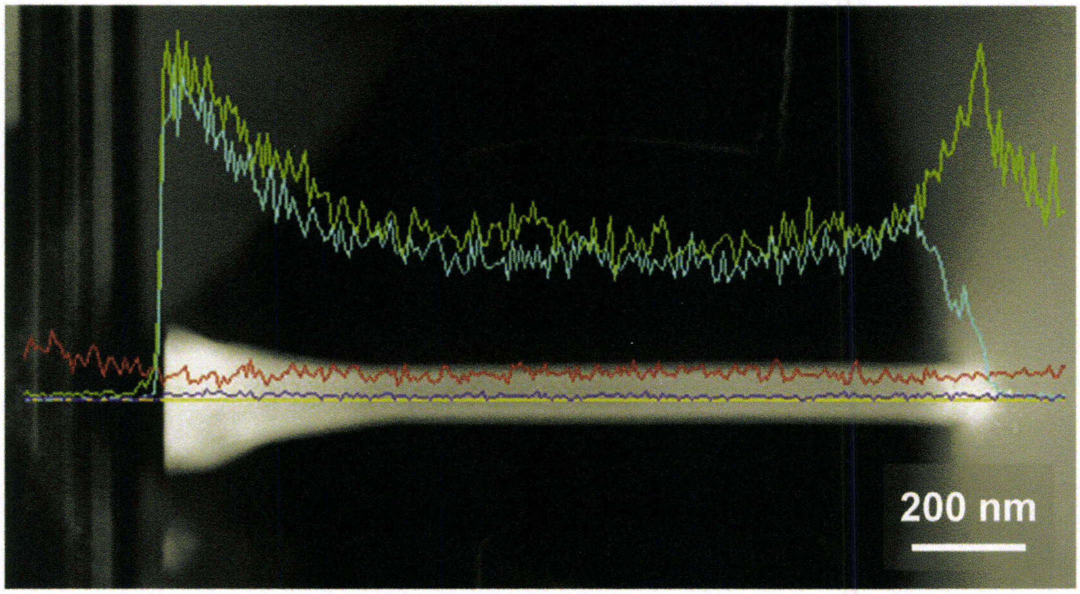

Figure 5.4. HAADF TEM image of lamella containing GaAs NW, obtained using FIB milling, and superimposed EDXS linescans showing the distribution of Ga (green), As (turquoise), C (red), and Au (blue).

5.2.2.2. Discussion

5.2.2.2.1. Mechanism of Ga assisted NW growth

An important topic of discussion is the mechanism or process by which GaAs NW growth proceeds upon HOPG. The presence of a Ga rich tip region, observed using EDXS, indicates that NW growth was likely Ga assisted, and did not proceed by self-organized vapour-solid growth.[32, 33] However, unlike SiO_x surfaces, employed in previously reported examples of Ga assisted growth,[27-29] the surface of HOPG is assumed to be atomically smooth and, excluding the presence of step edges, defect free. It should therefore offer no preferential sites, such as craters or pores, for Ga droplet formation. Furthermore, Ga is known to be chemically inert with respect to graphite, and does not wet the surface of HOPG.[34] For NW growth by the VLS mechanism, nucleation at the interface between the substrate and alloy droplet is disfavoured when a large wetting angle exists.[35] It is therefore unlikely that NW growth will proceed directly from a Ga droplet located upon the surface of an HOPG substrate.

The mechanism of NW formation is most likely similar to that reported by Vaddiraju et al. for the catalyst free growth of InN NWs by reactive vapor transport upon a range of substrates including HOPG.[16] In this example, the low sticking coefficient and consequent high diffusion path length of In adatoms upon the substrate is again important in the initial stages of NW growth. This allows the diffusion of In adatoms towards pre-existing InN crystals, which are formed upon the surface by a vapor-solid growth process. Indium droplets are preferentially formed upon these crystalline regions, promoted by the improved wetability of In upon InN, in comparison to the material from which the substrate is composed. The In droplets formed subsequently function as selective adsorption sites for NW growth. The formation of Ga droplets upon GaAs has been investigated, using a variety of methods including MBE.[36-39] In these studies, liquid Ga has been shown to display a low contact angle with GaAs. It is therefore probable that Ga droplets would be located preferentially upon GaAs islands over HOPG during the initial stages of NW growth.

A schematic representing the potential growth process is shown in Figure 5.5 alongside an SEM image of Growth B Sample 3, obtained at a tilt angle of 45°. This image was taken at a region which was partially masked by the sample holder during NW growth. Flux of growth species within this region was lower compared to the centre of the sample, and as a result the density of GaAs was significantly reduced. Features observed within these regions potentially resemble those occurring during the early stages of nanowire growth. It should however be noted that due to rotation of the sample holder during growth, flux of growth species within these masked regions was pulsed and alternated between Ga monomers and As_2 dimers. The V/III ratio therefore varied with respect to time and so the assumption that features observed are directly representative of those occurring at the centre of the sample in the early stages of growth may not be entirely accurate. The features shown in Figure 5.5.D do however appear to be in agreement with the proposed model. In this image, multiple small islands of GaAs can be observed in addition to which needle like structures aligned parallel to the surface can also be seen. Vertically aligned NWs were found within these regions, but as with the centre of the sample, were only present in very low density. Similar features were observed within holder masked regions of all other growths described within this chapter.

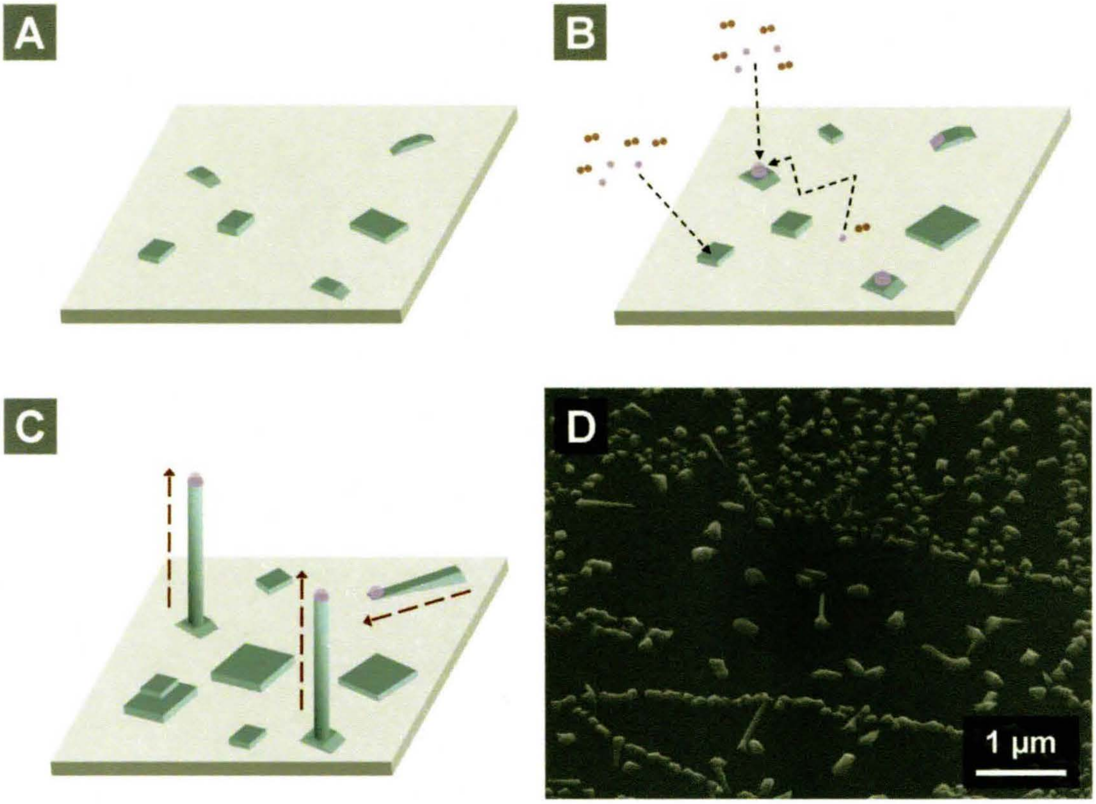

Figure 5.5. Schematic representing the proposed mechanism for Ga assisted growth; (A) In early stages of growth GaAs islands formed upon HOPG by vapor solid process. (B) Ga adatoms diffused across surface, coalescing upon the top and sides of GaAs islands to form droplets. (C) Ga droplets subsequently acted as selective adsorption sites for growth species resulting in NWs aligned both parallel and perpendicular to the substrate while vapor-solid growth of GaAs islands continues. (D) 45° tilted SEM of Growth B, sample 3 in a region partially masked by the sample holder during NW growth.

If the proposed mechanism is indeed correct, it may be asked why vertically aligned NWs are only obtained in low density? There are several possible explanations for this result. First, for aligned NW growth to occur, Ga droplets must form upon GaAs islands that exhibit a suitable crystal orientation extending over an appropriately sized area. This would require epitaxial crystal growth to occur upon HOPG via a vapor-solid mechanism. If this process is disfavoured under the selected growth conditions, the number of sites available for NW growth will be low and the resulting NW density will be negligible. Previous studies have shown that Ga adatom diffusion path length, sticking coefficients, and droplet formation upon III-V surfaces varies with both the crystal structure and surface reconstruction of the substrate.[33, 37-39] If an epitaxial relationship does not occur in the initial stages of growth, GaAs islands will exhibit a variety of different crystal structures and orientations. Droplet formation will not be favoured equally upon each island, and may only occur in a small fraction of cases. Again, this may partially explain the low density of NWs that was obtained

Second, for self-assisted growth to proceed, Ga within the droplet must be constantly replenished by adsorption of monomers from the vapor phase and by adatoms diffusing along the surface and up the side of NWs.[27] If the rate of Ga replenishment is lower than that of GaAs crystallization, the Ga droplet will be consumed and NW growth will cease. Formation of NWs would therefore be dependant upon the rate of diffusion of Ga adatoms. Careful control of V/III ratio and temperature would be required if optimum conditions for NW growth were to be determined.

Another possible explanation for why vertically aligned NWs are obtained in low density is that growth parallel to the surface is favored over vertical growth. A number of groups have previously reported procedures for the lateral growth of nanowires.[40-44] In several of these examples strain at the interface between the nanowire and the underlying substrate has been identified as potentially influencing the direction of nanowire growth.[41] Additionally, it was noted that wires growing from seed particles exhibiting small diameters are more likely to grow parallel to the surface than those originating from larger diameter particles.

Needle-like structures, observed in holder masked regions of HOPG samples (Figure 5.5.D), resemble those previously reported by Li and coworkers for Au assisted GaAs NW growth upon GaAs [111] substrates.[40] In this work, a mechanism for parallel growth was proposed in which Au-promoted VLS growth initially proceeded in the (111) direction, at a 35° angle to the substrate, but was quickly confined parallel to the surface due to growth upon the wires angled sidewall. In the case of Ga assisted growth upon HOPG, it is possible that Ga droplets, formed upon the angled facet of a GaAs island, become similarly confined. Subsequent VLS growth from the Ga droplet produces NWs oriented parallel to the substrate. Simultaneous vapour-solid growth upon the wires sidewall results in the triangular shaped structures which are observed. In the case of GaAs growth upon HOPG, wires growing parallel to the surface will eventually merge with other nanowires and islands, resulting in the formation of a polycrystalline GaAs film, covering the substrate.

Although experimental observations (Figure 5.5.D) appear to be in agreement with the proposed mechanism, there are several major points which require further investigation were the mechanism to be confirmed. In each of the growths described a V/III ratio of 1.5 was employed. Under As rich conditions Ga droplets would not be expected to form as they should immediately crystallize to form GaAs. Ga droplet formation under an As overpressure has previously been reported, in the Ga assisted growth of GaAs upon cleaved Si substrates.[45] Here, the authors speculate that droplet formation was promoted by surface roughness and the increased sticking coefficient of Ga adatoms upon Si in comparison to As terminated GaAs surfaces. Despite this previous example, the issue of Ga droplet formation upon HOPG under As rich conditions represents a significant problem with regard to the proposed mechanism, and as such requires further investigation. Additionally, if the majority of crystalline islands present in the early stages of growth do not display a preferred orientation, as was suggested, it may be asked why no NWs are observed that grow non-orthogonally relative to the substrate as a result of droplet formation upon the angled sidewall facets of these islands? In order to investigate the growth mechanism more fully a series of experiments would be required in which NW growth was terminated after various periods of time. By cooling samples under vacuum, as opposed to under an As overpressure, the presence and location of Ga droplets during the early stages of growth could potentially be confirmed, allowing the validity of the proposed mechanism to be evaluated.

5.2.2.2.2. Failure of Au assisted NW growth

Another point for discussion is the absence of Au NPs at the tips of GaAs nanowires. This result clearly indicates that metal particle assisted growth was not favoured in the direction normal to the substrate. One possible explanation for the absence of Au NPs is that growth proceeded in a direction parallel to the substrate, as discussed in the previous section with regards to Ga assisted NW growth. Here, the direction of growth will be determined by either lattice strain, induced by the underlying substrate, or by the drive to minimize interfacial surface energy. As NW growth proceeds, alloy droplets will progress across the surface, incorporating other alloy and Ga droplets in their path. A combination of solid vapour growth upon NW sidewalls and convergence of NWs with other GaAs structures will eventually result in the formation of large polycrystalline islands, such as those observed in Growth A (Figure 5.2). A mechanism, similar to that described, was proposed in a paper by Meyyapan and coworkers for the formation of a thin planar film during the growth of In_2O_3 NWs upon sapphire substrates[46]. If NW growth does indeed proceed in a direction parallel to the substrate there are two possible explanations as to why no Au NPs were located during analysis of samples by SEM and EDXS; (i) the NPs were present upon the substrate but became embedded beneath islands of GaAs and (ii) the metal became alloyed with Ga and was present in the large droplet like features which were observed by SEM (Figure 5.2), but only at concentrations below the detection limit of EDXS (0.1%), which was employed for elemental analysis of these samples. Further information regarding the fate of Au NPs following NW growth could potentially be obtained by investigation of the interface between polycrystalline GaAs and HOPG using FIB and TEM or by repeating the same experiments while reducing the total growth time, in the hopes that intermediate structures, such as planar nanowires, can be observed.

Other factors that may disfavour Au assisted growth of NWs include those related to the size of Au NPs present and the nature of their interaction with the HOPG substrate.

Au is unreactive with respect to graphite and consequently exhibits a high contact angle [47] upon graphite substrates (146° at 1373 K).[48] As mentioned previously, metal particle assisted growth is favoured when a strong interaction exists between the particle seed and the substrate. Given the low adhesion energy of both Ga and Au for graphite, alloys formed by adsorption of Ga into Au particles will likely not wet the surface of HOPG. This will disfavour NW growth by the VLS mechanism,[35] allowing competition from vapour-solid growth upon the substrate. Aggregation of Au NPs during high temperature annealing, results in an increase in the average particle diameter. The size of metal particles used in NW growth is known to affect a number of factors, including the diameter of the resulting nanowires as well as the rate of growth. For NWs grown upon lattice mismatched substrates, it is known that epitaxial growth of NWs will not occur if wires exhibit a diameter above a certain critical value.[21] As mentioned previously, the lattice strain between wurtzite-GaAs and HOPG was determined to be approximately 8%. This value is comparable to that of InP on Si(111) ($f = 8.1\%$), the critical thickness of which has been determined experimentally to be between 36 nm[23] and 39 nm.[22] These values were obtained from studies conducted by two separate groups using metal organic chemical vapour deposition (MOCVD) and MBE respectively. Cirlin and coworkers, cite the similarity of the critical thickness values obtain by these two different growth techniques as evidence of the importance of surface energy over kinetics in NW formation.[22] For GaAs NW growth upon HOPG, the critical diameter of NWs may be expected to lie within a similar range. Au particles exhibiting a diameter greater than this value would not be expected to yield epitaxial NWs.

5.2.2.3. Investigation of Ga assisted NW growth upon HOPG

A second growth was conducted (Table 1, Growth B), the objective of which was to increase NW density by promoting Ga assisted growth upon HOPG. To do this, the surfaces of two HOPG substrates were modified, one by deposition of a 5 nm thick SiO_x layer and another using reactive ion etching treatment (1 minute, inductively coupled oxygen plasma) to purposely introduce defects to the substrate. In both cases it was hoped that these treatments would increase the number of sites for Ga adatom nucleation and promote the formation of Ga droplets. Three other samples were also investigated; one pristine HOPG substrate, one Au NP modified substrate and a HOPG substrate that had been wet with ethanol and dried under air. The purpose of the last sample was to investigate whether the drop casting procedure used to deposit NPs contaminated the surface, resulting in reduced epitaxial nanowire growth relative to the pristine untreated HOPG substrate. Modifications were also made to the growth conditions. In both examples, the NWs grown were undoped as opposed to p-n junction type wires. The growth time was also reduced from 30 minutes to 15 minutes, to allow investigation of the behaviour of Au nanoparticles in the early stages of NW growth.

SEM images of samples from growth B, obtained at a tilt angle of 45°, are shown in Figure 5.6. In all cases the density of NWs was very low. GaAs NWs were observed in highest density upon the Au modified substrate, in which NPs were drop cast from a solution in ethanol (Figure 5.6.B). Analysis of this sample using SEM, revealed the presence of two types of nanowire, indicating that wire had proceeded by two separate mechanisms. The first type of NW resembled those obtained in the previous growth.

These wires displayed a columnar structure, were oriented normal to the substrate and did not have a Au particle at their tip, suggesting that NW growth was Ga assisted. In contrast, the second type of wire, displayed a tapered morphology with tips bearing Au NPs, confirming growth had proceeded by a Au seed assisted process. Here, it is likely that the improved wetting ability of ethanol upon HOPG, in comparison to water, decreases the extent of NP aggregation upon solvent evaporation. This in turn, results in a more homogeneous distribution of discrete NPs upon the HOPG substrate, ensuring that NPs remain within the diameter range required for NW growth. Although, Au particle assisted growth was obtained it was noted that the majority of tapered wires were oriented randomly with respect to the HOPG substrate, indicating that an epitaxial relationship did not exist with the underlying substrate. In contrast, wires grown upon the pristine HOPG sample which had not undergone any surface treatment were almost all oriented normal to the substrate (Figure 5.6.A). SEM analysis of the sample containing a SiO_x layer and that which had undergone RIE treatment (Figure 5.6, A and D respectively), revealed that they contained almost no nanowires. In each sample, the substrate was covered with a polycrystalline layer of GaAs. It is possible that in both cases the amorphous oxide layer and damaged carbon layer are thick enough to completely cover the underlying ordered substrate thereby preventing epitaxial NW growth, while simultaneously providing sites, such as craters and pores, for GaAs nucleation from the vapour phase.

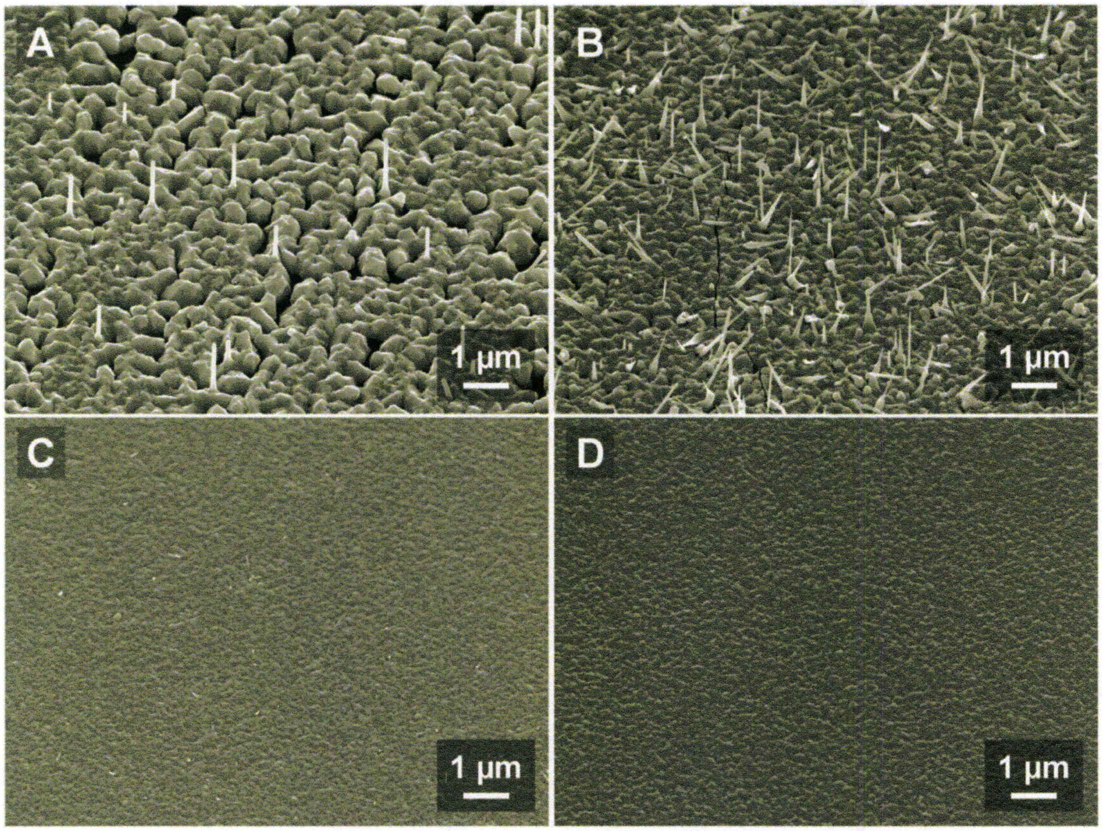

Figure 5.6. Tilted SEM images of samples following NW growth B; (A) pristine HOPG substrate, (B) Au NP modified HOPG, (C) HOPG with SiO_x surface layer (D) RIE treated HOPG

To summarize the results of growth B, orthogonally oriented wires were obtained upon both pristine HOPG substrates and also upon those modified by deposition of Au NPs by drop casting from ethanol solution. In both examples, SEM analysis indicated that orthogonally oriented wires primarily grew via a Ga assisted process. Au NP tipped wires were obtained following growth upon the Au modified HOPG surfaces, however in the majority of cases these were not oriented normal to the substrate. Results of growths conducted upon HOPG substrates modified by SiO_x deposition and reactive ion etching appear to indicate that any treatment which introduces defects to the HOPG substrate is likely detrimental to the epitaxial growth of GaAs NWs. This observation is in agreement with the mechanism for orthogonal NW growth discussed in the previous section, a requirement of which was the epitaxial growth of GaAs crystallite islands by a vapor solid mechanism prior to Ga droplet formation. Increasing disorder upon the substrate, by reactive ion etching or SiO_x deposition will disfavour epitaxial growth and consequently decrease the likelihood of a Ga island forming which is a suitable site for Ga droplet formation and in-turn for orthogonal NW growth.

Two subsequent growths (C and D) were conducted, using conditions outlined in Table 1. In growth C, a layer of Ga, approximately 1 nm thick was deposited upon a pristine HOPG substrate at 550°C, prior to introduction of As_2. Again, the objective of this growth was to promote the formation of Ga droplets and consequently the formation of NWs. A similar approach has been reported recently by Martelli and coworkers for the Ga assisted GaAs NW growth upon cleaved Si(100) substrates.[45] Conditions of growth D were comparable to those of growth A, except a higher growth temperature (600°C) was employed. It was speculated that an increase in substrate temperature would increase Ga adatom diffusion length on the surface and consequently increase the probability of adatoms finding a suitable site for nucleation. In both cases however, low nanowire density, comparable to that observed upon pristine HOPG samples in growth B, was obtained.

5.2.3. Growth of InAs NWs upon HOPG

A fifth study (Growth E) was conducted, the purpose of which was to investigate the effect of a reduction in growth temperature upon the density of NWs obtained by Au assisted growth. At lower temperatures, it was speculated that the migration and coalescence of Au nanoparticles would be limited, and therefore the average diameter of particles would potentially be maintained within a range suitable for NW growth. As growth temperature is lowered, the diffusion path length of adatoms upon the substrate decreases while adatom residence time increases as desorption becomes less favourable. Changes in substrate temperature are known to exert a strong influence upon the rate of growth and morphology of nanowires.[49, 50] Optimum temperatures for the growth of III-V NWs by metal particle assisted MBE is dependant upon both the eutectic temperature of the alloy seed and the vapour pressure of both the group III and group V species. For GaAs, temperatures within the range of 320 to 620°C can be employed, although temperatures between 470 to 570°C are typically used due to the favorable growth rates observed within this range.[51] In contrast, InAs NWs can only be grown at temperatures of between 380 and 430°C.[52]

As mentioned previously, an approximate indication of whether epitaxial nanowire growth is possible can be obtained using lattice fitting calculations. If the lattice parameter of a film is close to that of the underlying substrate, interfacial bond strain is minimal and defects such as edge dislocations are less likely to occur. In the case of NWs, improved lattice matching results in an increased critical diameter for which epitaxial nanowires can be obtained.[21-23] The lattice parameter of ZB-InAs[19] in the <110>

direction is related to the carbon-carbon bond length (1.421 Å) by a factor of 6.03 and exhibits a lattice mismatch value of only -0.49%. Additionally, the lattice constant of graphene (2.46 Å) is related to that of ZB-InAs in the <112> direction by a factor of 3.01, giving a lattice mismatch of -0.54%. These values suggest an excellent lattice match exists between InAs and HOPG (Appendix I, Figure 5.I.4.).

Samples investigated in Growth E included HOPG substrates that were both untreated and decorated with Au NPs. The conditions employed (Table 5.1.), were selected for the growth of p-n junction type InAs NWs and were based upon the results of prior experiments conducted by the LaPierre group. For unmodified HOPG samples (Figure 5.7.A), polycrystalline InAs was obtained, which covered the majority of the surface. Islands of polycrystalline material appeared to be aligned relative to one another in lines spaced approximately 1 μm apart. These features potentially result from preferential nucleation along step edge defects on the HOPG substrate. The image shown is representative of the entire surface of the sample. Thorough investigation of the sample by SEM determined that no preferential growth directed orthogonal to the substrate was observed under the growth conditions investigated.

In contrast to unmodified substrates, growth upon samples decorated with Au NPs resulted in a relatively high density of NWs, along with some triangular shaped nanoplates (Figure 5.7.B). InAs nanoplates of this kind, which result from anisotropy in the surface energies of nanowire crystal faces, have previously been reported by Lindelof and co-workers,[53] where GaAs was employed as a growth substrate. Although NWs grew at a variety of angles upon HOPG, examples of NWs aligned normal to the substrate could be observed at any region upon the substrate, indicating that an epitaxial relationship had potentially occurred for some percentage of the wires.

TEM, conducted upon NWs detached from the substrate indicated the presence of a Au NP tip upon both NW and nanoplate structures. The composition of these particles was confirmed using EDXS (Appendix I, Figure 5.I.4.). SAD of the base region of the NWs confirmed a [111] zinc blende structure along the basal plane, which corresponds to the lowest lattice mismatch previously calculated. The diameter of Au nanoparticle seeds measured by TEM (27.2 ± 3.6 nm), lies well below the critical thickness value required for epitaxial growth of NWs at the calculated lattice mismatch. As with previous growths, a high density of stacking faults was observed along the length of the NWs.

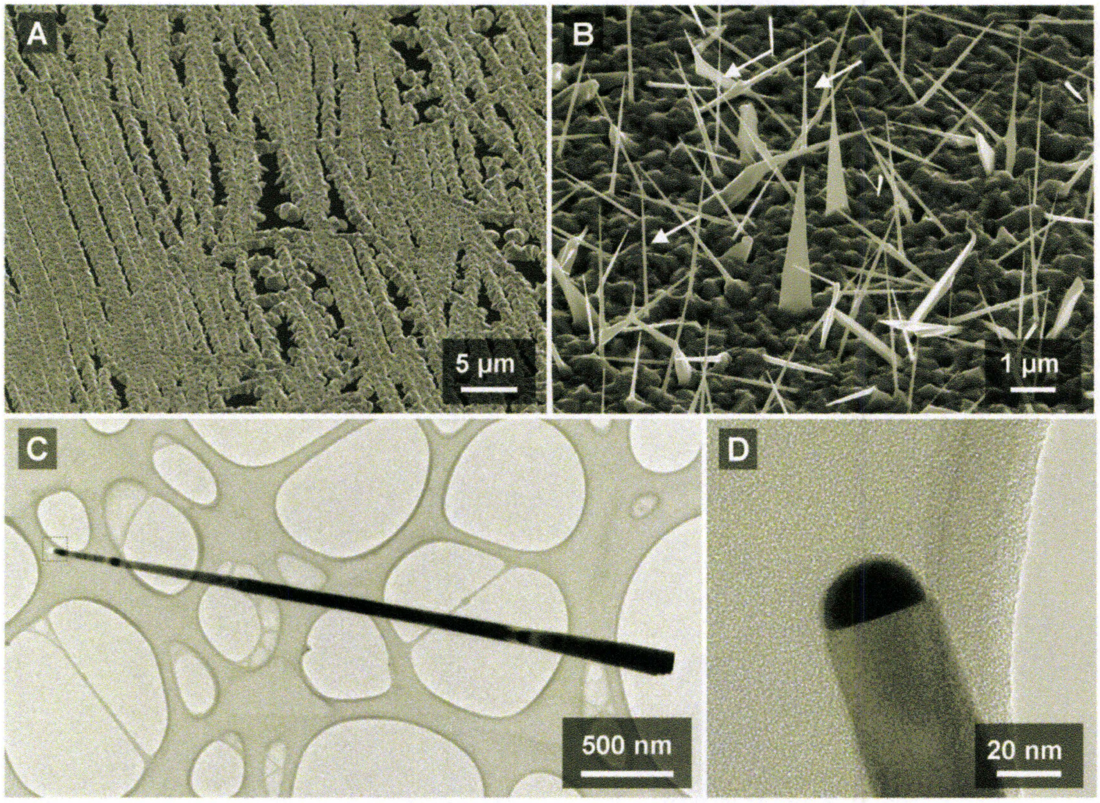

Figure 5.7. 45° tilted SEM images of samples following NW growth E; (A) pristine HOPG substrate, (B) Au NP modified HOPG. White arrows indicate NWs aligned normal to the substrate. (C) TEM image of a single InAs NW removed from an Au modified HOPG substrate and, (D) a close up of the tip region of the same NW that confirms the presence of an Au NP seed.

In summary, under the conditions investigated, growth of InAs NWs upon HOPG was shown to proceed via metal particle assisted growth. Attempted growth on NWs upon unmodified HOPG indicated that In assisted growth was not favoured under these conditions. Although these results may initially appear to be in contradiction to studies involving growth of GaAs NWs upon HOPG, it should be noted that the two studies are not directly comparable due to the number of variables that have been altered. It has been argued for example that Au assisted growth of InAs NWs may potentially proceed via the vapour-solid-solid mechanism in which the alloyed seed particle does not undergo a solid-liquid phase transition at growth temperatures.[52, 54-56] Other factors including lattice mismatch, adatom diffusion path length, and growth temperature will also exert a strong influence on nanowire growth processes.

5.3. Conclusions

In conclusion, growth of GaAs NWs upon HOPG using GS-MBE was investigated. NWs were obtained upon HOPG substrates, although only in very low density using the conditions investigated. Analysis by TEM and EDXS, indicated that growth of orthogonally oriented NWs was Ga assisted, allowing assembly of NWs upon pristine HOPG substrates which had not undergone any surface treatment. A mechanism for NW growth was proposed in which Ga droplets formed preferentially upon GaAs islands deposited via vapour-solid growth. It was speculated that droplets formed in this manner could subsequently act as selective adsorption sites for Ga and As species in the vapour phase, promoting the growth of NWs by the VLS mechanism. For this hypothesis to be confirmed, further experimental work would be required, conducting growths under similar conditions while reducing the total growth time. Analysis of samples from these experiments using electron microscopy and EDXS would reveal whether structures present during early stages of growth conform to those expected under the proposed mechanism. In order to increase NW density, optimization of V/III ratio and temperature would be required. If the proposed mechanism were found to be true, and GaAs islands were essential for the formation of selective assembly sites, NW density could also potentially be improved by altering growth conditions to first deposit a buffer layer of GaAs crystalline islands upon HOPG, then depositing a thin film of Ga prior to initiating NW growth. This could potentially increase the density of Ga droplets and consequently improve the density of NWs obtained. Growth of InAs upon HOPG was also investigated. Here, NW formation was shown to proceed by Au particle assisted growth resulting in wires which were oriented at a variety of angles relative to the substrate. The density of NWs obtained in this study was significantly greater than was observed for GaAs, and was potentially aided by improved dispersion of Au NPs and the use of lower growth temperatures which could help impede the detrimental aggregation of Au NPs into large clusters. As an initial experiment, the results of the InAs growth do appear promising and it is possible that improved results could be obtained through careful modification of growth conditions.

With respect to the assembly of III-V NWs upon graphene thin films, discussed in the introduction of this chapter, additional factors exist that could hinder the successful epitaxial growth. Unlike HOPG substrates, graphene thin films, which are composed of overlapping sheets with diameters ranging from several hundred nanometers to several microns, will not be atomically smooth. Defect sites will exist at points where graphene sheets converge and also potentially within the centre of sheets if introduced by the harsh oxidative treatment required for current solution processing methods. Delamination of graphene layers can also occur during thermal and chemical annealing of graphene oxide and this will significantly increase surface roughness of the film. The experiments outlined in this chapter indicate that a strong interaction does not exist between sp^2 hybridized carbon and metal particles required for growth of NWs by the VLS mechanism. It is therefore likely that for growth of NWs upon graphene, nucleation would occur preferentially at defect sites, and not upon areas of highly ordered carbon. An epitaxial relationship is therefore unlikely to exist. Graphene thin films may still however offer some advantages over carbon nanotube films as substrates for the growth of semiconductor NWs, specifically with regards to cost and ease of processing, provided that wires can be obtained in density equal to that reported for growth upon SWNT thin films.

5.4. Experimental Section

5.4.1. General

HOPG (Grade SPI-2) was purchased SPI Supplies, and cleaved prior to use using adhesive tape to produce a clean surface. All other reagents and solvents were obtained from commercial suppliers and used without any prior treatment. Scanning electron microscope (SEM) imaging was performed using a JEOL JSM-7000F SEM, equipped with a Schottky-type field emission gun filament. Focused ion beam (FIB) experiments were performed using a Zeiss NVision SII Cross-Beam instrument. Transmission electron microscopy (TEM) of individual NWs was conducted using a Phillips CM12 TEM. A

JOEL 2010F was employed for high resolution TEM (HRTEM) and analytical TEM (ATEM). FEI Titan 80-300 HB high resolution TEM. In Growth B, SiO_x was deposited plasma-enhanced chemical vapor deposition (PE-CVD), while reactive ion etching was conducted using an oxygen plasma.

5.4.2. Synthesis of Au NPs[57, 58]

100 ml $HAuCl_4$ solution (0.5 mM) in distilled water was added to a round bottomed flask equipped with a magnetic stir bar and condenser. The solution was heated to reflux while stirring rapidly. Upon reflux, a solution containing 36.75 mg tri-sodium citrate in 3 ml distilled water was added rapidly to the solution. The solution was stirred at reflux for 10 minutes. The reaction flask was then allowed to cool to room temperature while stirring was continued. The NP solution was subsequently stored in a glass bottle at 4°C. Using scanning electron microscopy the diameter of particles prepared using this procedure was determined to be 31 ± 4 nm.

5.4.3. Drop Casting of Au NPs upon HOPG

A dilute solution of Au NPs, in either water or ethanol was prepared, having a concentration of approximately 0.05 mM. Several small drops of this dilute solution were then applied a HOPG substrate which had been freshly cleaved using the adhesive tape procedure. The substrate was then allowed to dry at room temperature under air over a period of approximately 30 minutes. During this time the sample was gently agitated in an attempt to reduce the aggregation of NPs. The sample was then transferred to an oven and dried in vacuo overnight at 50°C.

5.4.4. Nanowire Growth

III-V semiconductor nanowire growth was conducted using GS-MBE, following the same general procedure as was described in the previous chapters where Ga and In were provided as monomers from resistively heated solid source effusion cells, while an AsH_3 gas-source equipped with a thermal cracker heated to 950°C acted as the source for As_2 dimers. Prior to nanowire growth, all samples were degassed by heating at 300°C for 15 minutes under ultra-high vacuum. Additionally, samples in growths A, B and E were subjected to an inductively coupled hydrogen plasma treatment (10 minutes) under an As_2 overpressure at the chosen growth temperature. The purpose of this step was to ensure removal of contaminants which may have been adsorbed upon the surface of the substrate prior to growth. This step was omitted from growths C and D in order to investigate whether plasma treatment had introduced defects to the HOPG substrate which could potentially have inhibited epitaxial growth.

NW growth was initiated by opening the shutter to the group III effusion cell. For the purposes of this study 5 different NW growths were conducted in which various parameters were modified, as outlined in Table 5.1. In all cases conditions yielded a nominal III-V growth rate of 1 $\mu m\ hr^{-1}$. NW growth was terminated by stopping flow of group III monomers from the effusion cell, after which the system was cooled under an As_2 overpressure.

Conditions for growths A, D and E were selected to produce p-n junction wires exhibiting a coaxial architecture, where Te and Be were employed as n and p type dopants respectively. The nominal concentration of both dopant species was maintained at 5 x 10^{-18} cm^{-3}, over a period of 15 minutes for each segment. A constant V-III flux ratio (A,D = 1.5, E = 2.3) was employed over the total growth period (30 minutes) during which time the temperature of the substrate was kept constant (A = 550°C, D = 600°C, E = 400°C). In contrast, NWs produced in growths B and C were undoped. In both examples the total NW growth time was 15 minutes, V-III ratio was held constant (B = 1.5, C = 2.3), and a substrate temperature of 550°C was maintained.

Prior to growth C a thin layer of Ga (1 nm) was deposited upon the substrate within the MBE chamber, at 550°C in the absence of an As_2 overpressure. The substrate was then annealed at 550°C for a period of approximately 3 minutes under vacuum, following which NW growth was initiated by simultaneously opening the shutters to both group III and group V sources. As in previous examples, NW growth was terminated by closing the shutter to the group III effusion cell. The samples were then cooled under an As_2 overpressure.

5.4.5. Lattice Matching Calculations

For epitaxially grown thin films, lattice strain can be calculated using the following equation:[13]

$$f = \frac{a_{substrate} - a_{crystal}}{a_{crystal}}$$

Where $a_{substrate}$ and $a_{crystal}$ equal the lattice parameters of the growth substrate and crystalline thin film respectively. Taking zinc blend [111] InAs upon HOPG as an example, the lattice parameter of ZB-InAs in the <112> direction (7.420 Å) is related to the lattice constant of graphene in the <1010> (a_{gr} = 2.46 Å) by a factor of 3.01. This means that the length of the ZB-InAs unit cell in the <112> direction is approximately equal to that of three graphene unit cells in the <1010> direction. Lattice strain experienced by InAs in the 112 direction can therefore be calculated as follows:

$$f = \frac{3a_{gr} - a_{112}}{a_{112}}$$

$$f = \frac{(3 \times 2.46) - 7.42}{7.42}$$

$$f = -5.3 \times 10^{-3}$$

5.5. References

(1) S. Stankovich, D. A. Dikin, G. H. B. Dommett, K. M. Kohlhaas, E. J. Zimney, E. A. Stach, R. D. Piner, S. T. Nguyen and R. S. Ruoff. *Nature* **2006,** 442, (7100), 282-286.

(2) Y. X. Xu, H. Bai, G. W. Lu, C. Li and G. Q. Shi. *J. Am. Chem. Soc.* **2008,** 130, (18), 5856-5875.

(3) Y. Si and E. T. Samulski. *Nano Lett.* **2008,** 8, (6), 1679-1682.

(4) M. Freitag. *Nat Nanotechnol* **2008,** 3, (8), 455-457.

(5) D. Li and R. B. Kaner. *Science* **2008,** 320, (5880), 1170-1171.

(6) J. Lu, I. Do, L. T. Drzal, R. M. Worden and I. Lee. *Acs Nano* **2008,** 2, (9), 1825-1832.

(7) L. J. Cote, F. Kim and J. Huang. *J. Am. Chem. Soc.* **2008,** ASAP.

(8) X. L. Li, G. Y. Zhang, X. D. Bai, X. M. Sun, X. R. Wang, E. Wang and H. J. Dai. *Nat Nanotechnol* **2008,** 3, (9), 538-542.

(9) J. T. Robinson, M. Zalalutdinov, J. W. Baldwin, E. S. Snow, Z. Q. Wei, P. Sheehan and B. H. Houston. *Nano Lett.* **2008,** 8, (10), 3441-3445.

(10) S. Biswas and L. T. Drzal. *Nano Lett.* **2009,** 9, (1), 167-172.

(11) R. M. Penner. *Modern Aspects of Electrochemistry* **2009,** 45, 175.

(12) E. C. Walter, M. P. Zach, F. Favier, B. J. Murray, K. Inazu, J. C. Hemminger and R. M. Penner. *Chemphyschem* **2003,** 4, (2), 131-138.

(13) M. Ohring, *The Materials Science of Thin Films*. Accademic Press, Inc.: 1992.

(14) H. T. Ng, J. Li, M. K. Smith, P. Nguyen, A. Cassell, J. Han and M. Meyyappan. *Science* **2003,** 300, (5623), 1249-1249.

(15) C. Li, D. H. Zhang, B. Lei, S. Han, X. L. Liu and C. W. Zhou. *J. Phys. Chem. B* **2003,** 107, (45), 12451-12455.

(16) S. Vaddiraju, A. Mohite, A. Chin, M. Meyyappan, G. Sumanasekera, B. W. Alphenaar and M. K. Sunkara. *Nano Lett.* **2005,** 5, (8), 1625-1631.

(17) C. C. Tang, Y. Bando, T. Sato and K. Kurashima. *J. Mater. Chem.* **2002,** 12, (6), 1910-1913.

(18) H. Yoon, K. Seo, N. Bagkar, J. In, J. Park, J. Kim and B. Kim. *Adv. Mater.* **2009,** 21, (48), 4979-4982.

(19) C. Y. Yeh, Z. W. Lu, S. Froyen and A. Zunger. *Phys. Rev. B* **1992,** 46, (16), 10086-10097.

(20) E. Ertekin, P. A. Greaney, D. C. Chrzan and T. D. Sands. *J. Appl. Phys.* **2005,** 97, (11), 114325-10.

(21) F. Glas. *Phys. Rev. B* **2006,** 74, (12), 121302-4.

(22) G. E. Cirlin, V. G. Dubrovskii, I. P. Soshnikov, N. V. Sibirev, Y. B. Samsonenko, A. D. Bouravleuv, J. C. Harmand and F. Glas. *Phys Status Solidi-R* **2009,** 3, (4), 112-114.

(23) L. C. Chuang, M. Moewe, C. Chase, N. P. Kobayashi, C. Chang-Hasnain and S. Crankshaw. *Appl. Phys. Lett.* **2007,** 90, (4), 043115-3.

(24) S. S. Chu, T. L. Chu and M. S. Lan. *J. Appl. Phys.* **1979,** 50, (9), 5805-5809.

(25) S. S. Chu, T. L. Chu, H. T. Yang and K. H. Hong. *J Electrochem Soc* **1978,** 125, (10), 1668-1671.

(26) P. K. Mohseni, G. Lawson, C. Couteau, G. Weihs, A. Adronov and R. R. LaPierre. *Nano Lett.* **2008,** 8, (11), 4075-4080.
(27) C. Colombo, D. Spirkoska, M. Frimmer, G. Abstreiter and A. F. I. Morral. *Phys. Rev. B* **2008,** 77, (15), 155326-5.
(28) A. F. I. Morral, C. Colombo, G. Abstreiter, J. Arbiol and J. R. Morante. *Appl. Phys. Lett.* **2008,** 92, (6), 149903.
(29) M. Heiss, A. Gustafsson, S. Conesa-Boj, F. Peiro, J. R. Morante, G. Abstreiter, J. Arbiol, L. Samuelson and A. F. I. Morral. *Nanotechnology* **2009,** 20, (7), -.
(30) B. Mandl, J. Stangl, T. Martensson, A. Mikkelsen, J. Eriksson, L. S. Karlsson, G. Bauer, L. Samuelson and W. Seifert. *Nano Lett.* **2006,** 6, (8), 1817-1821.
(31) D. Calestani, M. Z. Zha, A. Zappettini, L. Lazzarini and L. Zanotti. *Chem Phys Lett* **2007,** 445, (4-6), 251-254.
(32) G. R. Yazdi, P. O. A. Persson, D. Gogova, R. Fornari, L. Hultman, M. Syvajarvi and R. Yakimova. *Nanotechnology* **2009,** 20, (49), 495304-7.
(33) K. A. Bertness, A. Roshko, L. M. Mansfield, T. E. Harvey and N. A. Sanford. *J Cryst Growth* **2008,** 310, (13), 3154-3158.
(34) J. V. Naidich and J. N. Chuvashov. *J. Mater. Sci.* **1983,** 18, (7), 2071-2080.
(35) B. A. Wacaser, K. A. Dick, J. Johansson, M. T. Borgstrom, K. Deppert and L. Samuelson. *Adv. Mater.* **2009,** 21, (2), 153-165.
(36) J. H. Wu, W. Ye, B. L. Cardozo, D. Saltzman, K. Sun, H. Sun, J. F. Mansfield and R. S. Goldman. *Appl. Phys. Lett.* **2009,** 95, (15), 153106-3.
(37) T. Suzuki and T. Nishinaga. *J Cryst Growth* **1994,** 142, (1-2), 49-60.
(38) T. Suzuki and T. Nishinaga. *J Cryst Growth* **1994,** 142, (1-2), 61-67.
(39) Z. Y. AbuWaar, Z. M. Wang, J. H. Lee and G. J. Salamo. *Nanotechnology* **2006,** 17, (16), 4037-4040.
(40) S. A. Fortuna, J. G. Wen, I. S. Chun and X. L. Li. *Nano Lett.* **2008,** 8, (12), 4421-4427.
(41) B. Nikoobakht, C. A. Michaels, S. J. Stranick and M. D. Vaudin. *Appl. Phys. Lett.* **2004,** 85, (15), 3244-3246.
(42) A. Mikkelsen, N. Skold, L. Ouattara and E. Lundgren. *Nanotechnology* **2006,** 17, (11), S362-S368.
(43) B. Nikoobakht. *Chem. Mater.* **2007,** 19, (22), 5279-5284.
(44) B. Z. Tian, P. Xie, T. J. Kempa, D. C. Bell and C. M. Lieber. *Nat Nanotechnol* **2009,** 4, (12), 824-829.
(45) F. Jabeen, V. Grillo, S. Rubini and F. Martelli. *Nanotechnology* **2008,** 19, (27), -.
(46) P. Nguyen, H. T. Ng, T. Yamada, M. K. Smith, J. Li, J. Han and M. Meyyappan. *Nano Lett.* **2004,** 4, (4), 651-657.
(47) J. Lee, M. Nakamoto and T. Tanaka. *J. Mater. Sci.* **2005,** 40, (9-10), 2167-2171.
(48) U. Gangopadhyay and P. Wynblatt. *J. Mater. Sci.* **1995,** 30, (1), 94-100.
(49) S. A. Dayeh, E. T. Yu and D. Wang. *Nano Lett.* **2007,** 7, (8), 2486-2490.
(50) M. C. Plante and R. R. LaPierre. *J Cryst Growth* **2006,** 286, (2), 394-399.
(51) M. Tchernycheva, J. C. Harmand, G. Patriarche, L. Travers and G. E. Cirlin. *Nanotechnology* **2006,** 17, (16), 4025-4030.

(52) M. Tchernycheva, L. Travers, G. Patriarche, F. Glas, J. C. Harmand, G. E. Cirlin and V. G. Dubrovskii. *J. Appl. Phys.* **2007,** 102, (9), -.

(53) M. Aagesen, E. Johnson, C. B. Sorensen, S. O. Mariager, R. FeidenhanS'L, E. Spiecker, J. Nygard and P. E. Lindelof. *Nat Nanotechnol* **2007,** 2, (12), 761-764.

(54) K. A. Dick, K. Deppert, T. Martensson, B. Mandl, L. Samuelson and W. Seifert. *Nano Lett.* **2005,** 5, (4), 761-764.

(55) K. A. Dick, K. Deppert, L. Samuelson and W. Seifert. *J Cryst Growth* **2006,** 297, (2), 326-333.

(56) H. D. Park, A. C. Gaillot, S. M. Prokes and R. C. Cammarata. *J Cryst Growth* **2006,** 296, (2), 159-164.

(57) J. Kimling, M. Maier, B. Okenve, V. Kotaidis, H. Ballot and A. Plech. *J. Phys. Chem. B* **2006,** 110, (32), 15700-15707.

(58) J. Turkevich, J. Hillier and P. C. Stevenson. *Discuss. Faraday. Soc.* **1951,** 11, 55.

Chapter 6: Carbon Nanotube Thin Films as Substrates for the Controlled Flash Welding of Ultrathin Bismuth Sulfide Nanowires

Jordan W. Thomson, Gregor Lawson, Paul O'Brien, Richard Klenkler, Srebri Petrov, Michael Helander, Zheng-Hong Lu, Nazir Kherani, Alex Adronov and Geoffery Ozin

(Submitted to Advanced Materials, April 2010)

Work detailed in this chapter was carried out in collaboration with Jordan W. Thomson and Professor Geoffrey A. Ozin (Department of Chemistry, University of Toronto, Ontario). Contributions to experimental planning and writing were made equally by Gregor Lawson and Jordan W. Thomson. Composite film preparation, flash irradtiation experiments, raman spectrocopy and elecron microscopy analysis was conducted by Gregor Lawson. Nanowire synthesis, X-ray photoelectron spectroscopy, and powder X-ray diffraction was conducted by Jordan W. Thomson. Conductivity measurements were made by Paul O'Brien (Department of Chemistry, University of Toronto, Ontario). Measurements of camera flash intensity were made by Dr. Richard Klenkler (Xerox Research Centre Canada). Michael Helander and Srebri Petrov (Department of Chemistry, University of Toronto, Ontario) assisted with X-ray photoelectron spectroscopy and powder X-ray diffraction measurements respectively.

Abstract

Upon exposure to the high intensity pulsed emission of a conventional camera flash, thin films of light absorbing ultrathin bismuth sulfide (Bi_2S_3) nanowires were shown to undergo spontaneous vaporization. By incorporating these materials into a nanostructured assembly, in which a membrane composed of single-walled carbon nanotubes (SWNTs) acts as an underlying thermally conductive support, the photoresponse may be controlled allowing for the flash-welding of the nanowires into continuous crystalline thin films. The effect of flash irradiation upon the morphology, chemical composition and resistivity of these composite films was investigated using scanning electron microscopy, powder x-ray diffraction, X-ray photoelectron spectroscopy, Raman spectroscopy, and electrical conductivity measurements.

6.1. Introduction

Colloidal semiconductor nanocrystals show many interesting properties not seen in the corresponding bulk solid such as size-dependent fluorescence[1] and multiple exciton generation.[2] These properties make nanocrystals interesting from both a fundamental standpoint and also for technological applications such as biological labeling[3], solar cells[4], photodetectors[5], and light-emitting diodes.[6] The ability to synthesize colloidal nanocrystals in a bottom up fashion is appealing because of the potential to solution process thin films for device applications. Bulk metal chalcogenides (chalcogenide = S, Se, Te) such as CdSe or Bi_2S_3 are not soluble in common solvents, requiring the use of high vacuum deposition techniques such as CVD, which are costly and energy intensive. More recently, techniques such as chemical bath deposition[7] and hydrazine deposition of metal chalcogenides[8] have been used to produce thin films from solution, which have been shown to have good performance in photovoltaic devices and thin film transistors. In some applications, the advantages offered by solution phase processing may outweigh the benefits of quantum size effects that are potentially lost in the formation of polycrystalline films. For instance, Talapin and coworkers recently developed molecular metal chalcogenide ligands (MCCs) that act as 'electronic glue' allowing colloidal nanocrystals to be spincast and heat-treated at low temperature to produce polycrystalline films with good electrical mobility.[9] These films show the loss of nanoscale features such as surface plasmon resonance in metal nanoparticles and the strong red-shift of excitonic peaks in semiconductor nanocrystal films, however this method is especially attractive as it removes the insulating alkyl capping ligands present in most colloidal nanocrystals, examine the photothermal response to irradiation from a pulsed emission of a conventional camera flash. Beyond the fundamental nanoscience, the end goal of these experiments was to produce sintered nanowire films with improved electronic properties amenable to functional device fabrication.

Herein, we report the development of a novel nanostructured assembly in which a thin film of single-walled carbon nanotubes (SWNTs) functions as: (i) a flexible and conductive support for Bi_2S_3 nanowires, and (ii) a heat sink that prevents the overheating and vaporization of nanowires during flash irradiation and allows the formation of continuous crystalline thin films. The effect of flash irradiation upon these composite films was investigated using electron microscopy and powder X-ray diffraction (PXRD) aa well as X-ray photoelectron (XPS) and Raman spectroscopy. Electrical conductivity measurements indicate that bilayer film resistance decreases significantly following flash irradiation, provided the nanowire film is not too thick. From these observations, we propose that the composite materials produced in this work may be of interest in electronics applications such as photodetectors, photovoltaics and sensors and that the method could be generally applicable to any absorbing nanostructure exhibiting a suitable photothermal response.

6.2. Results and Discussion

Oleylamine stabilized Bi_2S_3 NWs were prepared in accordance with previously reported procedures and dispersed in THF to prepare dilute solutions.[17] SWNTs were dispersed by sonication in a 0.27 M solution of oleylamine in THF. Dispersion of carbon nanotubes in organic solvents has been reported previously, using a variety of amines.[18-20] Following sonication these dispersions were subjected to two rounds of centrifugation, which served to remove large nanotube bundles from solution. Thin films were fabricated using the vacuum filtration technique. This approach, which has been widely used in recent years for the preparation of carbon nanotube[21] and graphene oxide thin films,[22] offers a simple means by which homogeneous films can be produced with excellent reproducible control of film thickness. SWNT and Bi_2S_3 NW films were prepared by filtration of their respective dispersions in THF through membranes composed of either PTFE or hydrophilic polypropylene and having a pore diameter of 200 nm. Bilayer films were prepared by sequential addition of dilute SWNT and Bi_2S_3 NW dispersions to the same filtration apparatus. The porous SWNT thin film formed in the first step of this process effectively acts as a membrane upon which Bi_2S_3 NWs are deposited during the second step, forming a nanostructured film that contains two discrete layers. Alternatively, a nanowire solution could be dropcast onto the SWNT thin film, although the homogeneity and control of film thickness were inferior to the vacuum filtered films. The mechanical strength of films composed solely of Bi_2S_3 NWs proved insufficient to allow their removal from membranes using adhesive tape. In contrast, bilayer films were found to be relatively robust and could be easily peeled away to produce highly flexible free standing films. This enabled their transfer to carbon tape and subsequent imaging by scanning electron microscopy.

Initial flash irradiation experiments were conducted in air using a xenon flash lamp of a conventional compact camera. Typically, the flash component of the camera was positioned between 0.5 cm and 2 cm above the surface of the thin films, which were kept intact upon filtration membranes, due to the additional mechanical support which this provided. The dramatic response of Bi_2S_3 NW films to flash irradiation is shown in Figure 6.1.A and 6.1.B. It can be seen that following exposure to light from the camera flash, Bi_2S_3 NW films are completely vaporized, exposing the white surface of the underlying filtration membrane. In contrast, SWNT-Bi_2S_3 NW bilayer films, exposed under similar conditions, became smooth and shiny, exhibiting a silver-grey color similar to that of bulk Bi_2S_3 (Figure 6.1.C and 6.1.D). Cote et al. recently reported the preparation of graphene-polymer composite films, in which polystyrene microspheres functioned as a heat sink that prevented the overheating of graphene oxide nanosheets during flash reduction and photopatterning.[16] Individual carbon nanotubes are known to exhibit exceptional thermal conductivity,[23, 24] and have been investigated in heat management applications.[25, 26] Although the thermal conductivity of nanotube bundles and mats is considerably lower than that of individual nanotubes,[27-30] we propose that, in the case of our bilayer films, the underlying nanotube layer aids the dissipation of heat generated by Bi_2S_3 NWs during flash irradiation. This prevents overheating and vaporization of Bi_2S_3 NWs, which instead melt to form a continuous thin film in a process analogous to the previously reported flash welding of polyaniline nanofibres.[15]

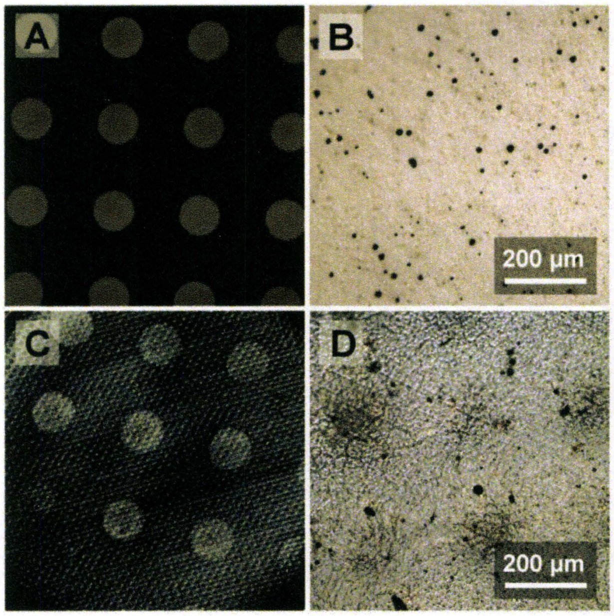

Figure 6.1. Photographs showing Bi_2S_3 NW (A) and SWNT-Bi_2S_3 NW bilayer films (C) following flash-irradiation through a photomask containing an array of circular holes 2 mm in diameter. Optical microscopy images of flash exposed regions of Bi_2S_3 NW (B) and SWNT-Bi_2S_3 NW bilayer films (D). In the case of Bi_2S_3 NW films, the material in exposed regions is almost completely vaporized revealing the underlying PTFE filtration membrane.

As Bi_2S_3 NWs display a broad absorption band,[17] the flash welding phenomenon reported was likely a response to light from across the visible spectrum, as opposed to that of a specific wavelength. Carbon nanotubes are also strongly absorbing, and have previously been shown to demonstrate a photothermal response when exposed to light emitted by a conventional camera flash.[11, 31-33] In the bilayer films described, carbon nanotubes located at the interface between the two materials are expected to absorb light transmitted by the upper Bi_2S_3 NW layer during flash irradiation. This could subsequently induce localized heating and melting of Bi_2S_3 NWs located at the interfacial region. Therefore, the underlying carbon nanotube layer may potentially function as a sensitizer in concert with the photothermal response of the nanowires, which aids the absorption of light over the entire visible spectrum.

Formation of continuous films by flash irradiation was confirmed using Scanning Electron Microscopy (SEM). Figure 6.2.A shows planar SEM images of a SWNT-Bi_2S_3 NW bilayer film that has not been subjected to flash irradiation. Prior to irradiation, the upper surface of this film, which consists of densely packed randomly oriented nanowires, appears highly smooth and displays very few observable surface features. Cross-sectional images of these films (Figure 6.2.C), obtained using Focused Ion Beam (FIB) milling within the SEM instrument, illustrate the well-defined bilayer architecture produced using the two step vacuum filtration approach described. The sample shown was prepared following a typical procedure in which filtration of 40 mL SWNT suspension in THF, having a concentration of 47 mg/L, resulted in the formation of a dense compact film with a thickness of approximately 2.5 μm. Addition of 100 mL Bi_2S_3 NW solution, having a concentration of 0.02 mM (1 mL of stock solution), in the second phase produced an upper layer approximately 330 nm thick. Figure 6.2.B displays a region of the bilayer composite film that has undergone flash irradiation at a distance of approximately 1 cm. Following flash treatment, the surface roughness of the nanowire layer can be seen to increase allowing surface features, resembling fused nanoparticles, to be observed. Figure 6.2.D shows a cross-sectional image of the same sample shown in Figure 6.2.C, taken from a trench milled in a region that has undergone flash irradiation. Following this treatment it can be seen that the thickness of the upper inorganic layer decreases by approximately 56% from 330 nm to 145 nm. At the elevated temperatures produced by flash irradiation the oleylamine ligand bound to the nanowire surface is likely evaporated along with traces of residual solvent, resulting in the observed decrease in film thickness and generation of free volume or pores, which appear as dark regions within the inorganic layer in FIB-SEM images of flash exposed films.

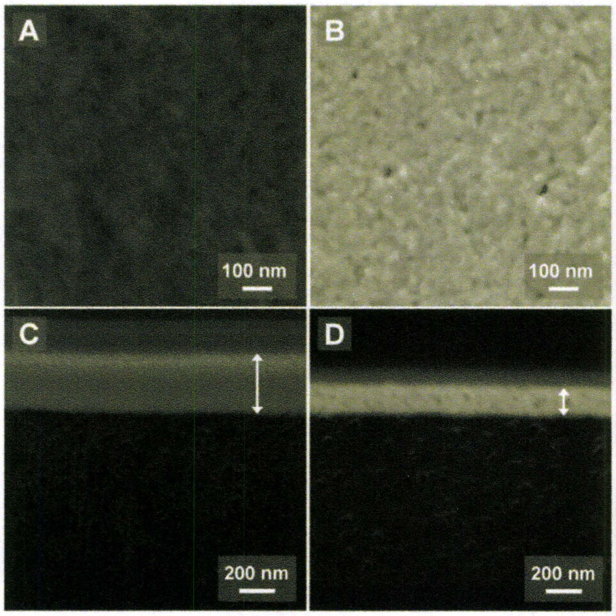

Figure 6.2. Planar SEM images of a SWNT-Bi_2S_3 NW bilayer film, before (A) and after (B) flash irradiation, and tilted SEM cross-sectional images of trenches milled within SWNT-Bi_2S_3NW bilayer films before (C) and after (D) flash irradiation. The grey region on the upper surface of the film, visible in (C) and (D), is a thin layer of carbon that was deposited on top of the sample prior to FIB milling, for the purposes of imaging. Double headed arrows indicate the thickness of the Bi_2S_3 layer.

Powder X-Ray Diffraction (PXRD) and X-Ray Photoelectron Spectroscopy (XPS) were utilized in the characterization of the nanowire layer. PXRD allows not only confirmation of the solid state structure of the nanowire layer, but can also provide information on the crystal size and amorphous content through Rietveld Refinement.

Figure 6.3 shows the comparison between a pre-flashed and post-flashed bilayer film, along with the corresponding bulk reference diffraction pattern.

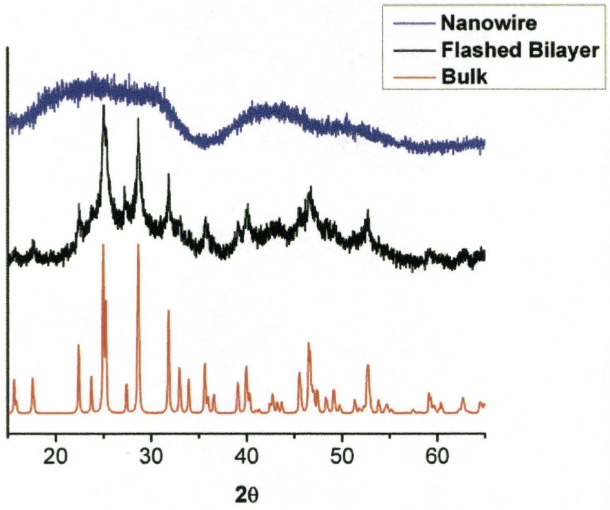

Figure 6.3. Powder X-Ray Diffraction of as-synthesized nanowires, flashed bilayer film, and bulk Bi_2S_3 reference.

The as-synthesized nanowires show a broad diffraction pattern due to Scherrer broadening caused by the small crystal size (previously calculated as 0.9 - 1.5 nm by Rietveld Refinement).[15] After exposure to a flash, the diffraction pattern became much sharper and well defined, indicating an increase in crystal size. Rietveld Refinement was performed and indicated 60% bismuthinite phase (Bi_2S_3) with an average crystal size of 9.2 nm, as well as the presence of 40% amorphous content (Appendices 6.I.1). Presumably the amorphous content of the PXRD pattern corresponds to uncrystallized nanowires, which show a very broad diffraction pattern. This represents an approximately eight to nine times increase in the crystal size. A similar increase in crystal size was also observed when heating a nanowire powder sample to 200°C for several hours under inert atmosphere (Appendices 6.I.2).

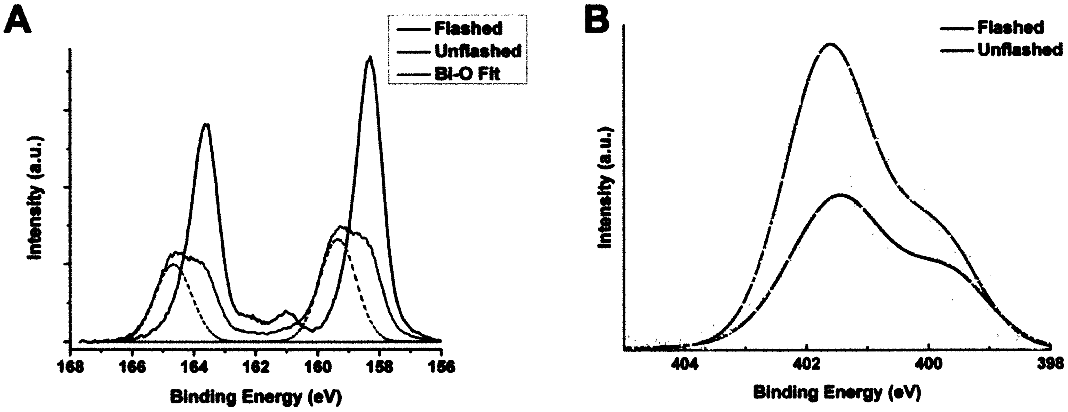

Figure 6.4. XPS of unflashed and flashed bilayer films: (A) Bi 4f and S 2p and (B) N 1s.

XPS was used to further characterize the bilayer and provide information on chemical species that could not be detected by PXRD. The pre-flashed and post-flashed bilayer spectra are shown in Figure 6.4. This analysis shows that there is a substantial amount of Bi-O present in the non-flashed sample (green traces). Note that dropcast nanowire films do not show the presence of any Bi-O species. The oxidation observed in the filtered bilayer samples is likely caused by the removal of excess oleylamine molecules that is necessary for stabilizing surface Bi atoms against oxidation. Furthermore, hydrolysis of Bi-S bonds to form Bi-O species and H_2S is also seen in the increase in Bi:S ratio from 0.39 in drop-cast films[34] to 2.2 in the filtered bilayer samples.

The removal of polysulfide/cyclooctasulfur impurities in filtered bilayer films also increases the Bi:S ratio compared to the dropcast films, where removal of these impurities is not possible without sacrificing colloidal stability. This provides an additional benefit to the vacuum filtration technique for film fabrication, as sample purity and homogeneity are both improved, in addition to achieving precise control of film thickness. Interestingly, upon flash exposure, the amount of Bi-O drops below the limit of detection, with only Bi-S and Bi-SO_x species remaining. This was observed flashing in an air atmosphere. Dropcast bilayer films showed a similar response to flash irradiation and XPS results confirm that no Bi-O species are formed upon flashing (Appendices, Figure 6.I.3). Such a result is very interesting as it shows that flash welding not only causes crystallization/sintering of the nanowires, but also their purification of surface bismuth oxide species.

The N 1s XPS was also acquired to determine the fate of oleylamine after flashing. Dropcast nanowire films show the presence of one broad peak at 399 eV, which likely contains two peaks corresponding to free and bound oleylamine.[34] The N 1s XPS of the filtered nanowire bilayer shows a large peak at 401.5 eV and a smaller shoulder at 400 eV. The larger peak at 401.5 eV can be attributed to protonated oleylamine, likely a byproduct of the hydrolysis/oxidation of the nanowire surface oxidation in which oleylamine is protonated by H_2S, while the peak at 400 eV is assigned to oleylamine bound to the nanowire surface. After flashing, a decrease in the amount of both protonated and uprotonated oleylamine is observed, with the majority of the weakly bound protonated amine being removed. The ratio of Bi:N increased from 2.1 to 5.5 upon flashing, which is consistent with the loss of oleylamine/protonated oleylamine. Similarly, the Bi:N ratio increased in dropcast films from 0.23 to 2.0. The decrease in the Bi:S ratio from 2.2 to 1.4 and increase in Bi:N ratio upon flashing suggests a mechanism in which surface Bi-O and oleylamine are ejected upon flash exposure, leaving a more pure sintered nanocrystal film, albeit with a small amount of oleylamine remaining. The atomic ratios pre and post-flash are shown in Table 6.1.

Table 6.1. Selected XPS atomic ratios for pre-flashed and post-flashed nanowire bilayer films.

Atom	**Pre-Flashed**	**Post-Flashed**	**Bulk**
Bi:S	2.2	1.4	0.67
Bi:N	2.1	5.5	N/A
Bi:O	0.69	1.8	N/A
Bi:C	0.08	0.14	N/A

The effect of flash irradiation upon the underlying carbon nanotube film was determined using Raman spectroscopy. The properties of carbon nanotubes are closely related to their structure. It is known that the introduction of defect sites within the sidewall of carbon nanotubes results in decreased electrical conductivity.[35, 36] It is therefore important that the structural integrity of carbon nanotubes be evaluated following flash irradiation. Figure 6.5 shows a comparison of an untreated SWNT film with a bilayer film before and after flash treatment. In each spectrum the characteristic radial breathing modes ($\omega_r \approx$ 100 - 350 cm^{-1}), tangential mode or G-band ($\omega_t \approx$ 1590 cm^{-1})

and disorder band ($\omega_d \approx$ 1290 cm^{-1}) associated with carbon nanotubes can be observed.[37, 38] The analysis of bismuth species using Raman spectroscopy has been reported previously.[39, 40] For Bi_2S_3, Raman active modes lie within the region of 100 to 260 cm^{-1} [39] and in the case of our bilayer film are not observed, due to overlap with the radial breathing modes of the nanotubes (Appendices 6.I.4). The spectrum of a SWNT film that has been purposely damaged by multiple exposures to flash irradiation at a distance of less than 5 mm is also included. Following this treatment, the disorder band increases significantly, indicating that a number of carbon atoms in the nanotube framework have undergone conversion from sp^2 to sp^3 hybridization, as a result of defect formation.[38] Additionally, broadening of the G-band and loss of features within the radial breathing mode are also observed. These results are comparable to those reported for carbon nanotubes that have been subjected to prolonged exposure to strong acids or high temperature annealing in an oxidative atmosphere,[38, 41] suggesting that high intensity flash exposure has damaged the nanotube structure. In contrast, the spectra of the bilayer film sample, which was irradiated at a distance of 1 cm, displays no significant changes in either the intensity of the disorder band or the shape of the G-band. From this result it can be concluded that, under the correct conditions, flash welding of NWs can be achieved in bilayer films without introducing significant structural damage to the underlying SWNT layer. The intensity of Raman peaks within the radial breathing mode of bilayer film samples was observed to decrease following flash exposure (Figure 6.5.C). It is known that signals within this region are sensitive to the environment of the carbon nanotubes and may be affected by factors such as the degree of nanotube bundling. As SWNTs located upon the upper face of the film, at the interfacial region, are expected to contribute strongly to the observed spectra, we speculate that the fusion of Bi_2S_3 nanocrystals to the nanotube surface may be responsible for the observed decrease in signal intensity.

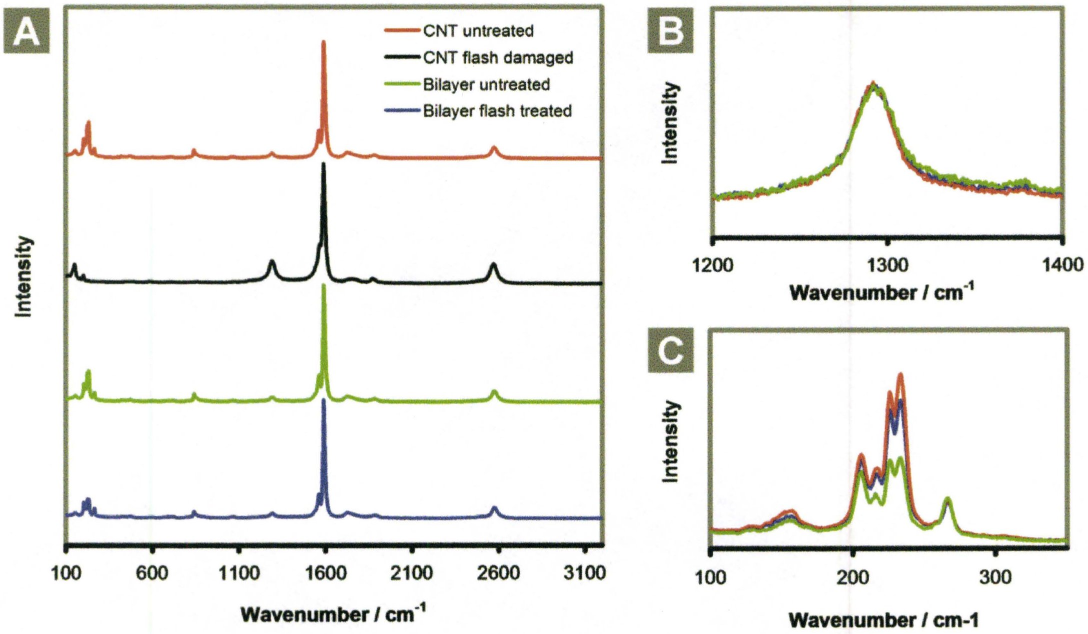

Figure 6.5. (A) Normalized Raman spectra of SWNT and bilayer film samples before and after flash irradiation (B) A close-up of the region surrounding the CNT disorder band ($\omega_d \approx 1290$ cm^{-1}) showing overlaid spectra. (C) A close-up of overlaid spectra showing radial breathing modes of SWNTs.

The electrical resistance of SWNT films and SWNT-Bi_2S_3 nanowire bilayer films measured before and after flash exposure are plotted in Figure 6.6. The irradiation from the camera flash causes the resistance of the bare SWNT films to increase from 26 Ω to

42 Ω, potentially due to the introduction of defects within the nanotube structure.[34, 35] Similarly, flashing a film of intimately mixed nanotubes and nanowires showed a similar increase in resistance. The resistance of the bilayer films is greater than that of the bare SWNT films and, unlike the SWNT films, show a significant decrease in resistance after being exposed to flash irradiation. For example, flashing the vacuum filtered bilayer film prepared from 0.5 mL of nanowire stock solution (3.7 mM) decreases its resistance from 150 Ω to 93 Ω, and flashing the sample prepared using 1 mL of stock solution reduces its resistance from 356 Ω to 124 Ω.

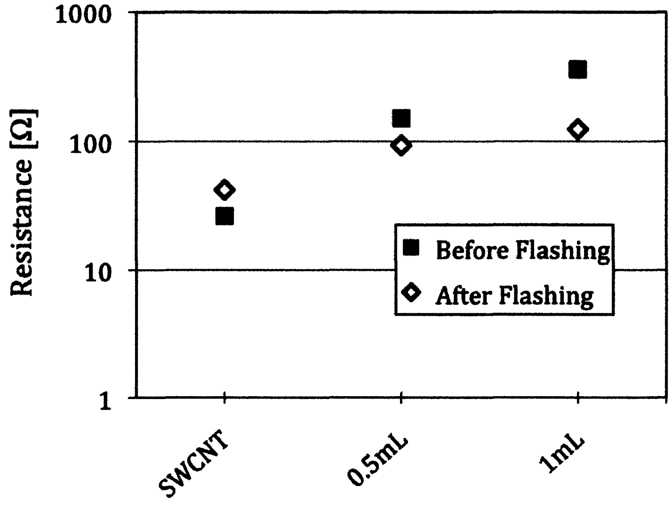

Figure 6.6. The resistance of SWNT and SWNT-Bi_2S_3 nanowire bilayer films measured before and after flash exposure.

A simple explanation for the decreased conductivity of flashed SWNT-Bi_2S_3 nanowire bilayer films can be provided with reference to Figure 6.7. Within a bilayer film, the underlying SWNT film is much more conductive than the upper Bi_2S_3 nanowire film. Consequently, for I-V measurements performed using a pair of coplanar contacts, the majority of the current flows through the underlying SWNT film while electron transport through the upper Bi_2S_3 nanowire film is negligible. However, as shown in Figure 6.7, in order to reach the SWNT film the electrons must first transverse the Bi_2S_3 nanowire film. Consequently, the resistance of the SWNT-Bi_2S_3 nanowire bilayer film is determined by the resistance across the upper Bi_2S_3 nanowire film. Thus, the resistance of the composite structure is reduced upon flashing because the upper Bi_2S_3 nanowire film undergoes rapid heating, thereby evaporating the oleylamine ligands and inducing a reduction of volume and increase in crystallinity. This decreases the distance the electrons have to travel and also reduces the amount of insulating material, both resulting in a decrease in resistance.

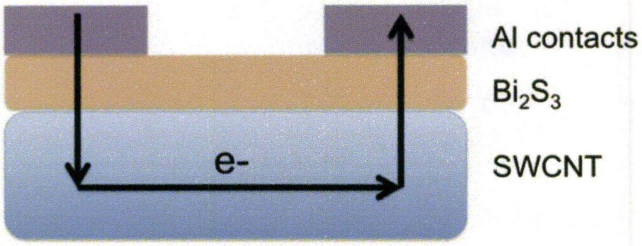

Figure 6.7. Electron transport along the planar direction in SWNT-Bi_2S_3 nanowire bilayer films.

Although the previous discussion provided with reference to Figure 6.7 explains the general trends observed in Figure 6.6, it should be noted that there are a number of other effects that may occur during flashing that would influence the electrical behavior of the composite films. For instance, it is expected that the transformations that occur in the composite film upon flashing depend on the thickness of the upper Bi_2S_3 nanowire film. If the upper nanowire film is too thin, then a greater portion of the flash radiation will reach the underlying SWNT film and may damage the carbon nanotubes. This was observed in the intimately mixed nanotube-nanowire films as a significant amount of light is absorbed by the nanotubes. On the other hand, if the upper Bi_2S_3 nanowire film is too thick, then most of the light may be absorbed in the upper portion of this film while the bottom portion of the film may prevent the SWNT film from functioning as an efficient heat sink. In this case the resistance of the composite film may increase upon flashing (Appendices 6.I.6). Nonetheless, the conductivity measurements reported herein demonstrate that charge transport can be enhanced in a nanostructured bilayer architecture by irradiation with a commercial camera flash.

6.3. Conclusion

Ultrathin Bi_2S_3 nanowires were shown to undergo a pronounced photothermal response to irradiation from a commercial camera flash. The use of SWNTs as a substrate controlled this response by acting as a heat sink and allowed the formation of a sintered nanowire film without causing damage to the underlying nanotubes. PXRD showed that the Bi_2S_3 nanowire layer increased its average crystal size to 9.2 nm, a large increase from the original size of less than 1.6 nm. XPS results confirmed the formation of Bi_2S_3 and also exhibited that the flashed bilayer films showed a decrease in both the amount of surface bismuth oxide species and oleylamine. The increase in crystal size and decrease in oleylamine, concomitant with the formation of a thinner and denser Bi_2S_3 layer as shown by FIB SEM is consistent with the observed decrease in the resistance of the NW-SWNT bilayer composite.

6.4. Experimental

6.4.1. General

Ultrathin Bi_2S_3 nanowires were prepared using previously reported procedures.[17] Purified grade SWNTs, purchased from Carbon Nanotechnologies, Inc. (Houston, TX), were produced by the HiPCO process[42] and used as received. All other reagents and solvents were obtained from commercial suppliers and used without any prior treatment. All absorbance measurements were made using a Cary 50 Bio UV-Visible Spectrophotometer. Laser Raman spectroscopy was performed using a Renishaw InVia Raman spectrometer equipped a 300 mW Renishaw 785 nm laser and 1200 l/mm grating. The Raman system is also equipped with a Leica microscope having 5 x, 20 x, and 50 x objectives as well as a USB camera for sample viewing. SEM imaging was performed using a JEOL JSM-7000F scanning electron microscope, equipped with a Schottky type field emission gun filament, with nanotube films attached to carbon tape upon SEM stubs. Energy Dispersive X-ray Spectroscopy (EDXS) was conducted using an Oxford instruments INCA Energy Dispersive Spectrometer X-ray microanalysis system equipped with HKL Electron Backscatter(ed) Diffraction (EBSD) system. Focused ion beam (FIB) experiments were performed using a Zeiss NVision SII, Focused Ion Beam/Scanning Electron Microscope Cross-Beam instrument. The first milling, used to produce the trench and the cross-sectional face, was conducted at 30 keV using a 1.5 mA probe. Damage created by this high energy beam was removed by a second milling at 30 keV using a 300 pA probe. A third milling at 30 keV with a 40 pA probe yielded a polished, smooth surface. Millings were carried out for a depth of 3 μm. Flash pulse energies were measured using a silicon photodiode (Hamamatsu S1337-BR) that was coupled to an electrometer (Keithley 6514). The current measured by the electrometer was recorded as a function time with the use of a GHz storage oscilloscope (Tektronix DPO 7104). Additionally, the spectrum of the flash was measured with an Ocean Optics HR4000CG spectrometer. X-Ray Photoelectron Spectroscopy was performed on a PHI 5500 Surface Analysis instrument using the underlying SWNT layer as a conductive support. High resolution scans were performed with a 0.1 eV step size. Powder X-ray diffraction was run on a D5000 diffractomter. A step scan mode was used for data acquisition with step size of 0.02° 2-theta and counting time of 2.5 s. per step. Rietveld analysis was carried out using Bruker AXS profile fitting software Topas v. 2.1.[43] The structure of orthorhombic Bi_2S_3[44] was used as an initial structural model. Electrical conductivity measurements were performed by evaporating Al metal through a mask to generate two contacts with a spacing of 1 mm and length of 5 mm. Filtrations were carried out using VWR filtration apparatus with stainless steel support screen and Sartorius PTFE membranes (4.7 cm diameter, 200 nm pore size). Nanotube samples were dispersed in solvent using a

Branson 1510 bath sonicator. Nanotube dispersions in solvent were centrifuged using a Beckman Coulter Allegra X-22 Centrifuge set at 5049 g for 40 min.

6.4.2. Dispersion of SWNTs in THF using oleylamine

15 mg SWNTs were added to a 200 mL round bottomed flask containing 20 g oleylamine (technical grade 70%) in 180 mL THF (approximate concentration = 0.27 M). The flask was then sonicated under nitrogen at 0 to 30°C for 2 hours after which the nanotube dispersion was subjected to centrifugation (45 minutes, 5049 g). Following centrifugation the supernatant was transferred to a round bottomed flask and allowed to stand for one day undisturbed, after which the solution was subjected to a second round of centrifugation (45 minutes, 5049 g). The supernatant was then transferred to 20 mL glass vials and stored at room temperature. The concentration of SWNTs dispersed in solution using this procedure was determined to be approximately 47 mg L^{-1}. This value was obtained from UV-spectroscopy measurements for which an specific extinction coefficient at 700 nm (0.0235 L mg^{-1} cm^{-1}) was employed[45].

6.4.3. Fabrication of ultrathin Bi_2S_3 nanowire thin films and SWNT-Bi_2S_3 bilayer films

All thin films described in this work were prepared using the vacuum filtration method. To prepare thin films of Bi_2S_3 nanowires, dilute solutions of these materials in THF were first prepared. These solutions were then filtered through a membrane composed of PTFE or cellulose nitrate and having a pore diameter of 200 nm. Between 0.9 to 3.8 mg of material was used in the preparation of each thin film. SWNT-Bi_2S_3 bilayer films were prepared by a two step process. In the first step, approximately 60 mL SWNT dispersion in oleylamine solution, was filtered through a PTFE membrane (200 nm pore diameter). The nanotube film formed was then washed with 300 mL THF to remove excess oleylamine ligand. The vacuum line was then disconnected from the filtration apparatus. A dilute solution of Bi_2S_3 nanowires in THF was added and the vacuum reapplied. Following fabrication, all films were dried under nitrogen and stored at room temperature under air. Films were kept intact upon filtration membranes due to the additional mechanical support that this provided.

6.4.4. Flash irradiation of Bi_2S_3 nanowire thin films and SWNT-Bi_2S_3 bilayer films

Flash irradiation experiments were conducted under air using the xenon flash lamp of a compact flash camera (Kodak Advantix 4700ix). In all cases, these films were kept intact upon filtration membranes during experiments due to the additional mechanical support which this provided. Typically the flash bulb was positioned between 0.5 and 2 cm from the sample which was being irradiated. At the distances employed, the energy of light to which samples were exposed was determined, to be between 0.15 and 0.17 mJ cm^{-1}.

6.5. References

(1) B. O. Dabbousi, J. RodriguezViejo, F. V. Mikulec, J. R. Heine, H. Mattoussi, R. Ober, K. F. Jensen and M. G. Bawendi. *J. Phys. Chem. B* **1997,** 101, (46), 9463-9475.
(2) R. J. Ellingson, M. C. Beard, J. C. Johnson, P. R. Yu, O. I. Micic, A. J. Nozik, A. Shabaev and A. L. Efros. *Nano Lett.* **2005,** 5, (5), 865-871.
(3) B. Dubertret, P. Skourides, D. J. Norris, V. Noireaux, A. H. Brivanlou and A. Libchaber. *Science* **2002,** 298, (5599), 1759-1762.
(4) I. Gur, N. A. Fromer, M. L. Geier and A. P. Alivisatos. *Science* **2005,** 310, (5747), 462-465.
(5) G. Konstantatos, I. Howard, A. Fischer, S. Hoogland, J. Clifford, E. Klem, L. Levina and E. H. Sargent. *Nature* **2006,** 442, (7099), 180-183.
(6) J. M. Caruge, J. E. Halpert, V. Wood, V. Bulovic and M. G. Bawendi. *Nat Photonics* **2008,** 2, (4), 247-250.
(7) J. Britt and C. Ferekides. *Appl. Phys. Lett.* **1993,** 62, (22), 2851-2852.
(8) D. B. Mitzi. *Adv. Mater.* **2009,** 21, (31), 3141-3158.
(9) M. V. Kovalenko, M. Scheele and D. V. Talapin. *Science* **2009,** 324, (5933), 1417-1420.
(10) D. Li and Y. N. Xia. *Nat Mater* **2004,** 3, (11), 753-754.
(11) P. M. Ajayan, M. Terrones, A. de la Guardia, V. Huc, N. Grobert, B. Q. Wei, H. Lezec, G. Ramanath and T. W. Ebbesen. *Science* **2002,** 296, (5568), 705-705.
(12) N. Braidy, G. A. Botton and A. Adronov. *Nano Lett.* **2002,** 2, (11), 1277-1280.
(13) J. Y. Chen, B. Wiley, Z. Y. Li, D. Campbell, F. Saeki, H. Cang, L. Au, J. Lee, X. D. Li and Y. N. Xia. *Adv. Mater.* **2005,** 17, (18), 2255-2261.
(14) N. Wang, B. D. Yao, Y. F. Chan and X. Y. Zhang. *Nano Lett.* **2003,** 3, (4), 475-477.
(15) J. X. Huang and R. B. Kaner. *Nat Mater* **2004,** 3, (11), 783-786.
(16) L. J. Cote, R. Cruz-Silva and J. Huang. *J. Am. Chem. Soc.* **2009,** ASAP.
(17) L. Cademartiri, R. Malakooti, P. G. O'Brien, A. Migliori, S. Petrov, N. P. Kherani and G. A. Ozin. *Angew Chem Int Ed* **2008,** 47, (20), 3814-3817.
(18) Y. Maeda, S. Kimura, Y. Hirashima, M. Kanda, Y. F. Lian, T. Wakahara, T. Akasaka, T. Hasegawa, H. Tokumoto, T. Shimizu, H. Kataura, Y. Miyauchi, S. Maruyama, K. Kobayashi and S. Nagase. *J. Phys. Chem. B* **2004,** 108, (48), 18395-18397.
(19) N. Choi, M. Kimura, H. Kataura, S. Suzuki, Y. Achiba, W. Mizutani and H. Tokumoto. *Jpn J Appl Phys 1* **2002,** 41, (10), 6264-6266.
(20) Y. Sun, S. R. Wilson and D. I. Schuster. *J. Am. Chem. Soc.* **2001,** 123, (22), 5348-5349.
(21) Z. C. Wu, Z. H. Chen, X. Du, J. M. Logan, J. Sippel, M. Nikolou, K. Kamaras, J. R. Reynolds, D. B. Tanner, A. F. Hebard and A. G. Rinzler. *Science* **2004,** 305, (5688), 1273-1276.
(22) G. Eda, G. Fanchini and M. Chhowalla. *Nat Nanotechnol* **2008,** 3, (5), 270-274.
(23) S. Berber, Y. K. Kwon and D. Tomanek. *Phys Rev Lett* **2000,** 84, (20), 4613-4616.
(24) K. Sun, M. A. Stroscio and M. Dutta. *J. Appl. Phys.* **2009,** 105, (7), 074316.

(25) H. Huang, C. H. Liu, Y. Wu and S. S. Fan. *Adv. Mater.* **2005,** 17, (13), 1652-1656.
(26) K. Kordas, G. Toth, P. Moilanen, M. Kumpumaki, J. Vahakangas, A. Uusimaki, R. Vajtai and P. M. Ajayan. *Appl. Phys. Lett.* **2007,** 90, (12), 123105.
(27) J. Hone, M. Whitney and A. Zettl. *Synthetic Met.* **1999,** 103, (1-3), 2498-2499.
(28) J. Hone, M. Whitney, C. Piskoti and A. Zettl. *Phys. Rev. B* **1999,** 59, (4), R2514-R2516.
(29) A. E. Aliev, G. K. Hemani, E. M. Silverman and R. H. Baughman. *Materials Research Society Symposium Proceedings* **2009,** 1142, 1142-JJ14-03.
(30) X. H. Yan, Y. Xiao and Z. M. Li. *J. Appl. Phys.* **2006,** 99, (12), 124305.
(31) B. Kang, Y. D. Dai, S. Q. Chang and D. Chen. *Carbon* **2008,** 46, (6), 978-981.
(32) D. H. Lien, H. F. Kuo and W. K. Hsu. *Appl. Phys. Lett.* **2006,** 88, (9), 093113.
(33) S. H. Tseng, N. H. Tai, W. K. Hsu, L. J. Chen, J. H. Wang, C. C. Chiu, C. Y. Lee, L. J. Chou and K. C. Leou. *Carbon* **2007,** 45, (5), 958-964.
(34) J. W. Thomson, L. Cademartiri, M. MacDonald, P. S., G. Calestani, P. Zhang and G. A. Ozin. *J. Am. Chem. Soc.* **2010,** (submitted).
(35) V. Georgakilas, K. Kordatos, M. Prato, D. M. Guldi, M. Holzinger and A. Hirsch. *J. Am. Chem. Soc.* **2002,** 124, (5), 760-761.
(36) J. Cabana and R. Martel. *J. Am. Chem. Soc.* **2007,** 129, (8), 2244-2245.
(37) T. Belin and R. Epron. *Mat Sci Eng B-Solid* **2005,** 119, (2), 105-118.
(38) R. Graupner. *J Raman Spectrosc* **2007,** 38, (6), 673-683.
(39) K. Trentelman. *J Raman Spectrosc* **2009,** 40, (5), 585-589.
(40) V. N. Denisov, A. N. Ivlev, A. S. Lipin, B. N. Mavrin and V. G. Orlov. *J Phys-Condens Mat* **1997,** 9, (23), 4967-4978.
(41) M. Zhang, M. Yudasaka and S. Iijima. *J. Phys. Chem. B* **2004,** 108, (1), 149-153.
(42) P. Nikolaev, M. J. Bronikowski, R. K. Bradley, F. Rohmund, D. T. Colbert, K. A. Smith and R. E. Smalley. *Chem Phys Lett* **1999,** 313, (1-2), 91-97.
(43) Topas. In 2.1 ed.; General profile and structure analysis softwars for powder diffraction data, User's Manual, Karlsruhe, Germany: 2003.
(44) K. Lukaszewicz, J. Stepien-Damm, A. Pietraszko, A. Kajokas and J. Grigas. *Pol J Chem* **1999,** 73, (3), 541-546.
(45) A. Ikeda, K. Nobusawa, T. Hamano and J. Kikuchi. *Org Lett* **2006,** 8, (24), 5489-5492.

Chapter 7: Thesis Overall Conclusions and Recommendations for Future Work

7.1. General Conclusions

The impressive strength, flexibility, and stability exhibited by carbon nanotube thin films make these materials ideal for use as scaffolds for the assembly of secondary structures such as polymers, inorganic particles, and biomaterials. The use of nanotube thin films as structural supports has therefore been investigated within a range of different applications including tissue engineering, catalysis and the development of photovoltaic devices. To date the majority of work investigating nanotube films as supports for inorganic materials has focused primarily upon the preparation of composite films containing spherical metallic or semi-conductor nanoparticles. In contrast, reports detailing the use of nanotube films as scaffolds for inorganic materials exhibiting larger or more complex structures, such as nanowires, nanoplates or nanoflowers, are at present relatively limited.

In Chapter 2 of this thesis, we outlined a simple method for the preparation of SWNT composite films containing Au nanoparticle clusters in high density. In this work it was shown that SWNTs functionalized covalently with poly(ethylene imine) displayed impressive solubility in aqueous solution enabling the fabrication of homogeneous thin films at room temperature using vacuum filtration. Au NP clusters were subsequently introduced to the surface of these films by in-situ reduction of $HAuCl_4$ under mild conditions. Here, PEI bound to the nanotube's suface was shown to play an active role as a reducing and stabilizing agent in the production of Au NPs. This work therefore demonstrated that modification of CNTs with polymers offered a means by which thin films bearing chemical functionalities could be produced, and harnessed to produce new composite materials.

In Chapter 3 we demonstrated that SWNT-Au NP composite films, prepared using the methods outlined in Chapter 2, could be used as substrates for the assembly of III-V semiconductor NWs using gas source molecular beam epitaxy (GS-MBE). Using this technique, GaAs NWs, aligned at a variety of angles, were obtained in high density across the surface of nanotube films. This work demonstrates the potential of CNT thin films to function as scaffolds for the support of inorganic nanostructures beyond simply spherical nanoparticles. Importantly, it was shown that nanotube films retained their impressive flexibility following nanowire growth, suggesting that these materials may hold promise in the development of lightweight flexible electronic devices.

The incorporation of SWNT-NW composites within a functional electronic device was described in Chapter 4 where core-shell pn-junction GaAs NWs grown upon a SWNT film served as the active light harvesting element in a photovoltaic cell. Devices incorporating these materials displayed conversion efficiencies up to 0.32% and were shown to function when bent up to a curve ratio of 12.5 mm, highlighting the potential of SWNT-NW composites in flexible device applications. A simplified method for the production of SWNT-Au NP composite films was also outlined in Chapter 4 whereby pre-formed Au NPs were deposited upon a SWNT thin film via vacuum filtration. This procedure did not require any chemical modification of carbon nanotubes and as such ensured that the structural and electronic properties of the SWNTs were not compromised in any way. Additionally, by reducing the number of steps that require chemical synthesis, the time required for SWNT-Au composite film fabrication was significantly reduced.

In Chapter 5, the growth of III-V semiconductor NWs upon highly-ordered carbon based surfaces was explored with the aim of producing ordered arrays of NWs oriented orthogonally to the growth substrate. In the experiments described, highly-ordered pyrolytic graphite (HOPG) decorated with Au NPs was employed as a substrate for the growth of GaAs NWs. Under the conditions investigated NWs were only obtained in low density. Analysis using electron microscopy and energy dispersive x-ray spectroscopy indicated that orthogonally oriented wires grew primarily by a Ga assisted process. This observation was confirmed by subsequent NW growths conducted upon unmodified HOPG substrates. A mechanism for Ga assisted growth of NWs upon HOPG was proposed, in which GaAs islands formed by a vapour-solid process acted as preferential sites for the formation of Ga droplets and subsequently for the growth of NWs by the vapour-liquid-solid mechanism. Attempts were made to improve NW density, through alteration of growth conditions and the use of various surface treatments, however none of these approaches proved to be successful.

In Chapter 6, the preparation of a different type of SWNT composite material was described. Using a two-step vacuum filtration process, similar to that utilized in Chapter 4, composite films were prepared exhibiting a well defined bi-layer architecture in which a film of randomly aligned Bi_2S_3 NWs was supported upon a SWNT membrane. Here, it was shown that the underlying SWNT film not only provided mechanical support for the Bi_2S_3 layer but also enabled the controlled welding of these nanocrystals by irradiation using an intense burst of light produced using the flash component of a conventional compact camera. It was speculated that during this process the SWNT film acted as a heat sink that prevented overheating and vapourization of the NWs and promoted the formation of a fused polycrystalline thin film. The effect of flash treatment upon the Bi_2S_3 NWs and underlying nanotube layer was characterized fully using techniques such as Raman Spectroscopy, Powder X-Ray Diffraction, X-ray Photoelectron Spectroscopy and Scanning Electron Microscopy. Additionally, the effect of flash irradiation upon the conductivity of composite films was also evaluated.

The most significant contribution of this thesis comes from the work detailing the growth of III-V semiconductors upon SWNT thin films using GS-MBE. This work demonstrates that, due to their exceptional stability, SWNT thin films are compatible with the high temperature conditions required for MBE, and may therefore be utilized as flexible, conductive substrates for the growth of semiconductor nanowires. We believe that the techniques developed in the work could potentially be applied to a range of different semiconductor materials and nanowire synthesis techniques, enabling the preparation of a new generation of composite materials combining the flexibility and conductivity of nanotube films with the novel optoelectronic properties of semiconductor nanowires. In Chapter 4 it was demonstrated that materials of this type could potentially find application in the development of flexible electronic devices such as light emitting diodes, chemical sensors, and solar cells. As mentioned previously, there are presently few publications that describe the use of nanotube films as scaffolds for the support of inorganic materials other than spherical nanoparticles. This thesis provides proof-of-principle examples demonstrating how bottom-up methodologies can be employed to construct complex nanoarchitectures incorporating carbon nanotube thin films.

7.2. Recommendations for Future Work

There are several directions in which research could proceed following the work described in this thesis. As a starting point, techniques developed for the growth of NWs upon SWNT thin films could be expanded to investigate other semiconductor materials. Although Au is widely used in metal particle assisted nanowire growth, various species of nanowire require the use of particles composed of other metals including Fe, Al and Ti. Although SWNT composite films containing nanoparticles composed of these metals would not be accessible using the self reduction method described in Chapter 2, the vacuum filtration approach which was later used to deposit pre-formed Au NPs, could potentially be applied to any nanomaterial having dimensions enabling their immobilization and retention upon the SWNT membrane. Any metal particles which can be prepared by solution based processes can therefore be deposited upon the surface of a CNT film.

One interesting opportunity that could be investigated is the preparation of nanotube films containing particles composed of the same material as the desired nanowire. Diffusion of metal atoms from seed particles during VLS growth and their subsequent incorporation within semiconductor materials is known to alter the electronic properties of the nanowires obtained. Additionally, the presence of a Schottky type contact between the metal particle and semiconductor wire creates a resistance barrier that contributes negatively to the efficiency of devices incorporating these materials. This is obviously undesirable and recently reported methods for the catalyst free growth of NWs have therefore captured significant attention. Stable dispersions of In NPs, having dimensions of approximately 30 nm, can be produced using solution based processes. SWNT-In NP composite films, prepared using procedures similar to those described, could in theory be utilized for the growth of InAs NWs using GS-MBE. The absence of a Au particle tip on these wires could potentially help to increase the photoconversion efficiency of solar cell devices incorporating these materials.

As mentioned in previous chapters, molecular-beam epitaxy (MBE) offers advantages over other available methods of NW synthesis with regard to the purity of materials obtained as well as the generation of well defined interfaces. This is of particular benefit in the preparation of doped pn-junction nanowires for photovoltaic applications. MBE does however require the use of both high temperatures and specialized equipment. This is seemingly at odds with some of the benefits which we cited for the use of nanotube films, namely the availability of low-cost solution based processing methods that can be conducted at room temperature. The preparation of similar composite materials through purely solution based methods under mild conditions would therefore be highly desirable. Previously, Chhowalla and coworkers, reported the growth of zinc oxide nanowires upon SWNT thin films via a hydrothermal process (Chapter 1, ref 248). A variety of inorganic nanowire species can also be prepared using template-free solution-based processes, including those composed of TiO_2, and In_2O_3, which have been identified as being of interest in chemical sensor and optoelectronic applications. The development of new techniques allowing the growth of nanowires upon CNT films via similar processes could potentially yield composite materials displaying useful properties, and, as such, warrants further investigation.

Appendix I

Chapter 2: Au–carbon nanotube composites from self-reduction of Au^{3+} upon poly(ethylene imine) functionalized SWNT thin films

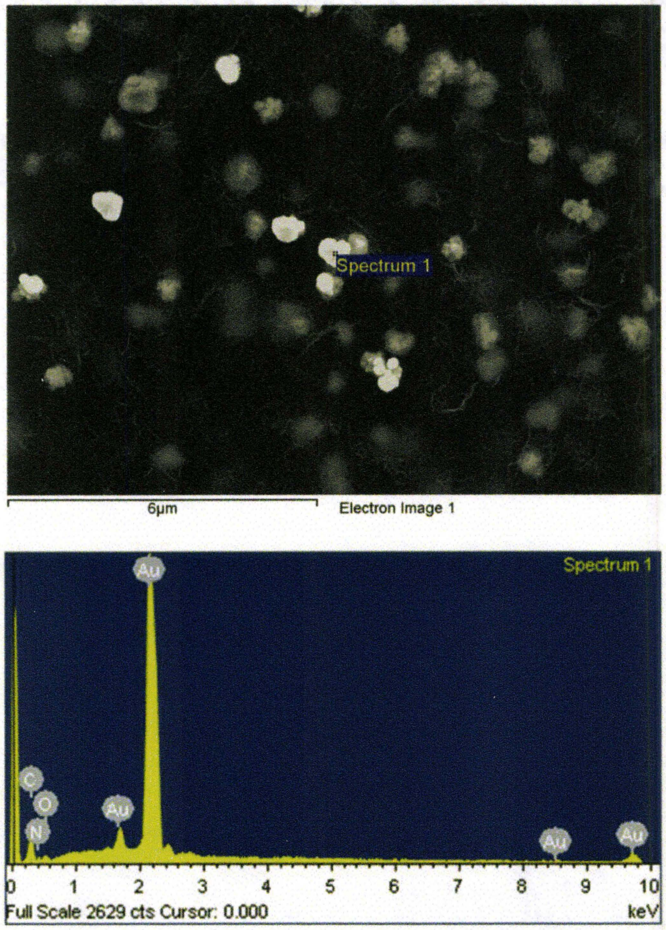

Figure 2.I.1. SEM image of PEI functionalized SWNT films following immersion and heating at 60°C in 2 mM $HAuCl_4$ solution for 1 hour and corresponding EDXS spectrum for the spot indicated.

Chapter 4: Hybrid GaAs-nanowire carbon nanotube flexible photovoltaics

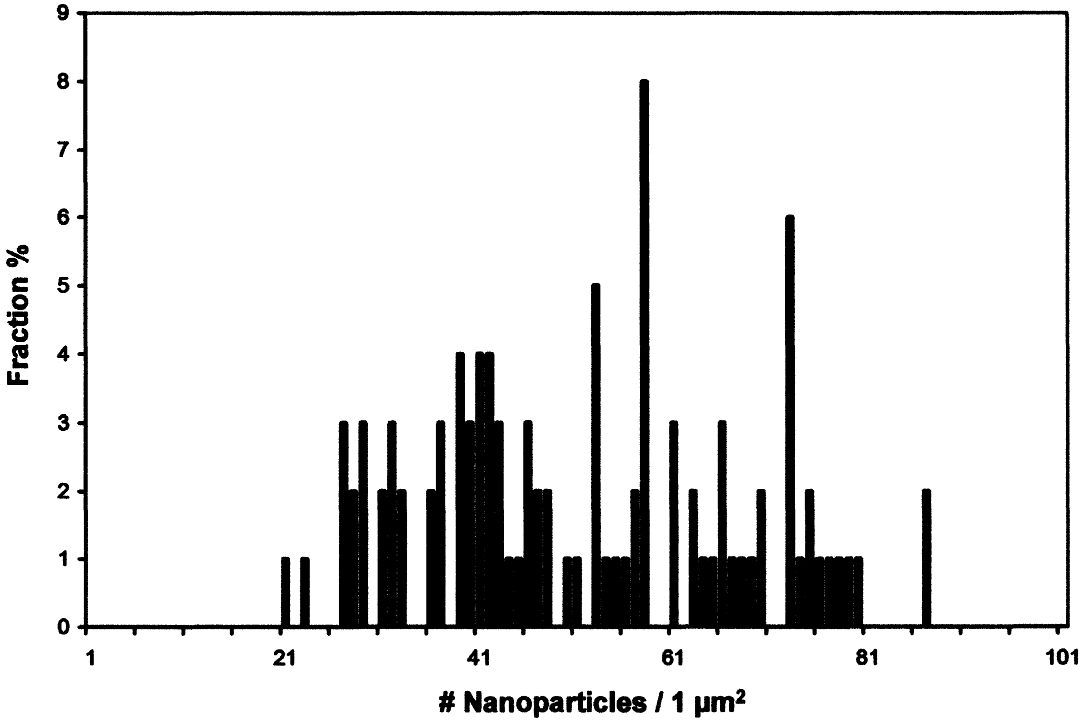

Figure 4.I.1. Histogram of Au nanoparticle density upon SWNT-Au composite film surface.

Chapter 5: Growth of III-V Semiconductor NWs upon Highly Ordered Pyrolytic Graphite

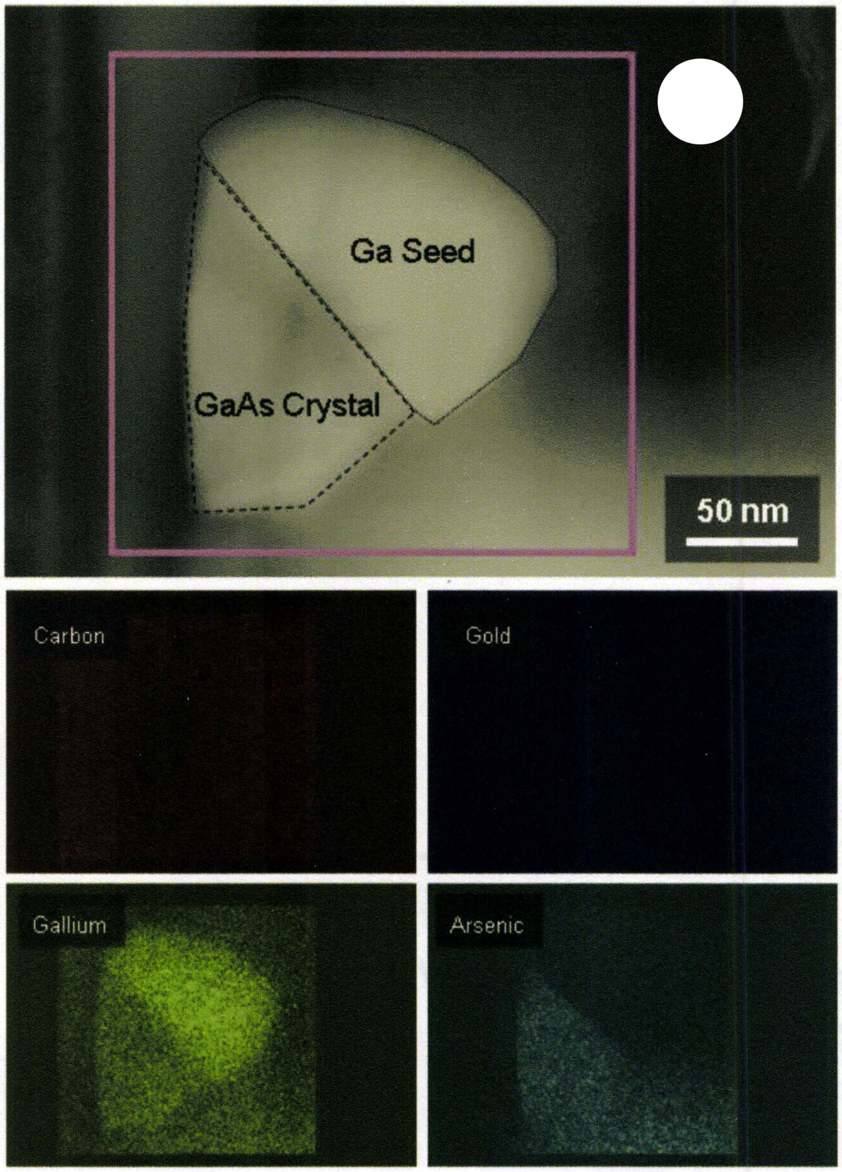

Figure 5.I.1. EDXS of droplet like structures observed upon Au modified HOPG substrates following growth A, indicating the presence of a Ga rich seed particle resting upon a GaAs crystalline base.

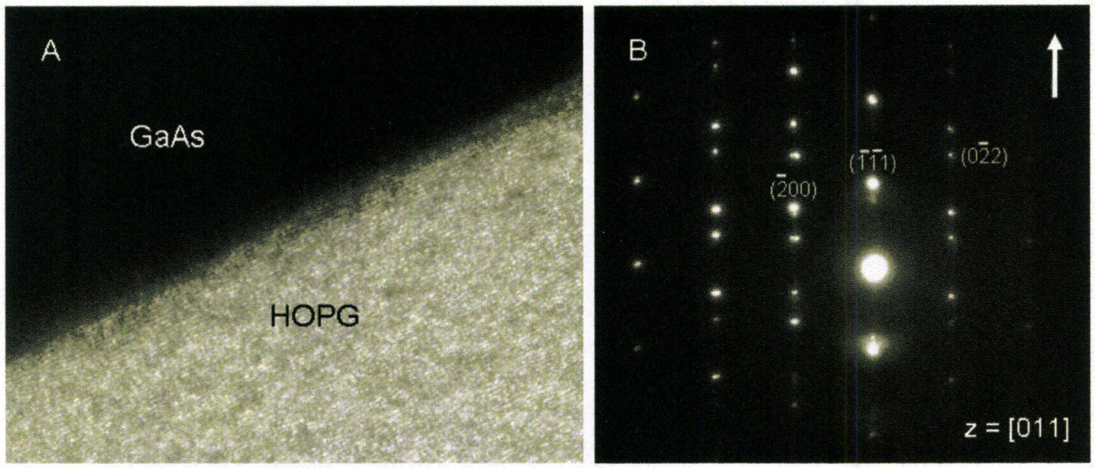

Figure 5.I.2. (A) TEM image showing the interface between the base of a wire and the HOPG substrate, obtained from a lamella prepared using FIB milling of a sample from growth A, and (B) select area diffraction (SAD) pattern obtained from the base region of the same wire indicating a zinc blende crystal structure with [111] basal plane where the white arrow indicates the direction of nanowire growth.

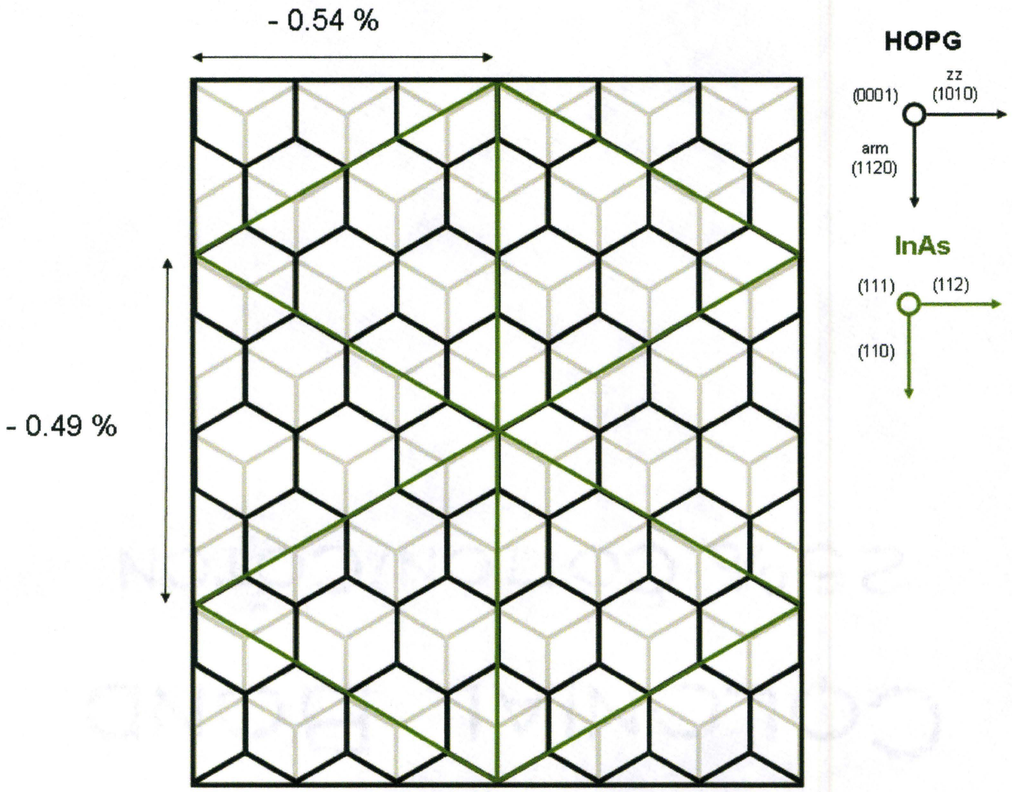

Figure 5.I.3. Schematic representing the lattice matching of (111) ZB InAs with HOPG

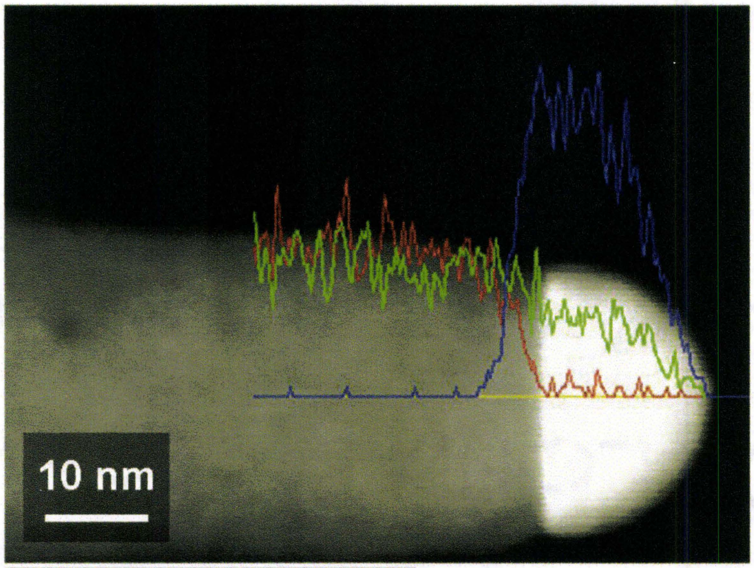

Figure 5.I.4. HAADF TEM image of lamella containing InAs NW and superimposed EDXS linescans showing the distribution of In (green), As (red), and Au (blue). The atomic composition of the seed particle was determined to be 71.05% Au and 28.95% In.

Chapter 6. Carbon Nanotube Thin Films as Substrates for the Controlled Flash Welding of Ultrathin Bismuth Sulfide Nanowires

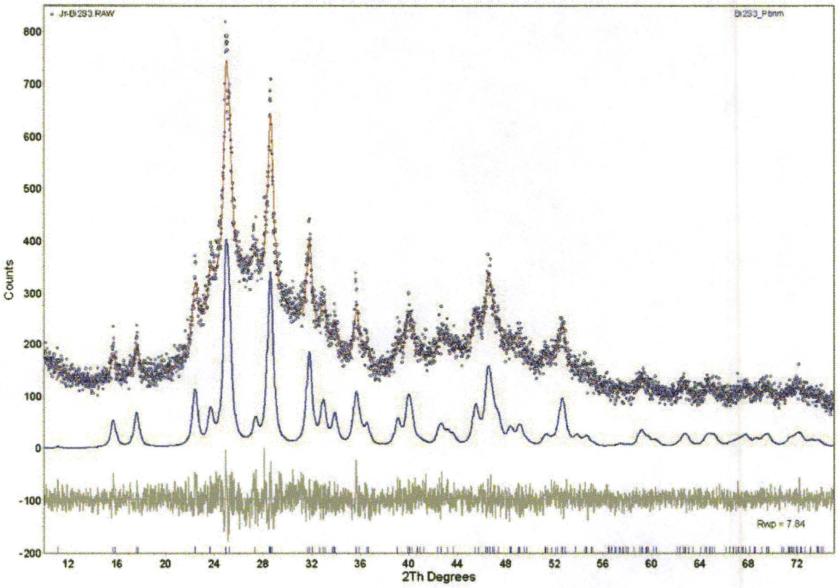

Figure 6.I.1. Rietveld plot: 159 reflections for orthorhombic Bi_2S_3 were fitted and extracted from the experimental pattern.

Table 6.I.1. Summary of the Rietveld analysis of Bi_2S_3*

General parameters	**Results**	**Sample's refined parameters**	**Bi_2S_3 - Pbnm**
Profile function	FPA – Topas**	Lattice parameters, Å	a = 11.147(11) c = 11.299(11)
Background	Chebychev, 10th	Cell volume, Å^3	502.7(9)
Sample preparation	From suspension	Crystalline: Amorphous, (% wt)	59:41
Zero, (mm)	0.02	Mean domain size, L_{vol}, nm	9.2 (1.1)
Sample displacement (mm)	-0.025	Microstrain (lattice disorder), e_0	0.01
Independent parameters	37	Linear Absorption Coeff. (cm^{-1})	1418(2)
Goodness of fit, χ^2	1.10	Calculated Density (g/cm^3)	6.79(1)
R_{wp}	7.84	Isotropic therm. parameters, B_{iso}	refined
R_p	6.22	Site Occupancy	Non-refined – 1.0
Weighted DW	1.79	Preferred orientation	Spherical 8th order
		Atomic coordinates	Non-refined

* Structural model for Bi_2S_3 obtained from Lukaszewicz, K. et al, *Polish Journal of Chemistry* 1999, 73, 541-546. The structure remains unchanged in its long-range structural order (the microstrain value, e_0, is 0.01). The mean crystallite (domain) size is around 9 nm. The sample contains about 40+ % wt. amorphous (ultrathin nanowire) material calculated as a ratio of the peaks/amorphous whole-pattern profile areas.

** Topas, v. 2.1, (2003) General profile and structure analysis software for powder diffraction data, User's Manual, Karlsruhe, Germany.

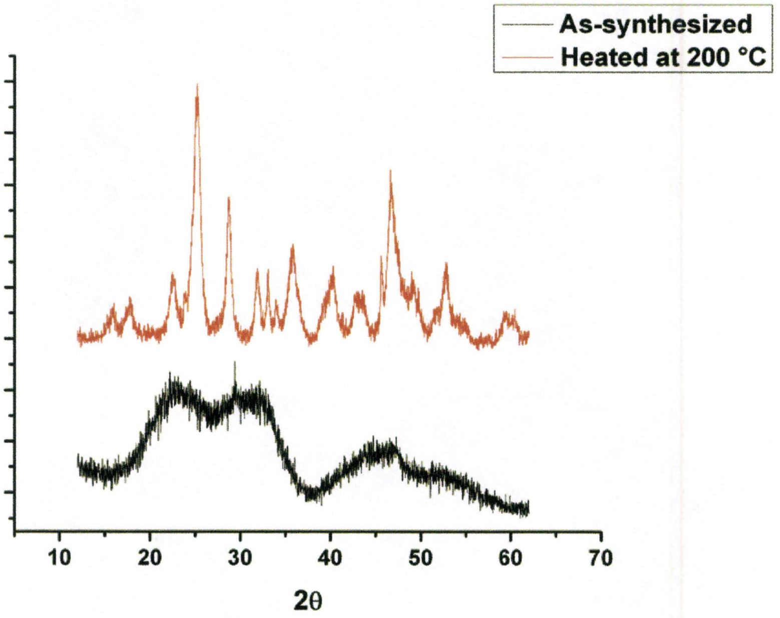

Figure 6.I.2. PXRD of Nanowires after heating at various temperatures for 4 hours.

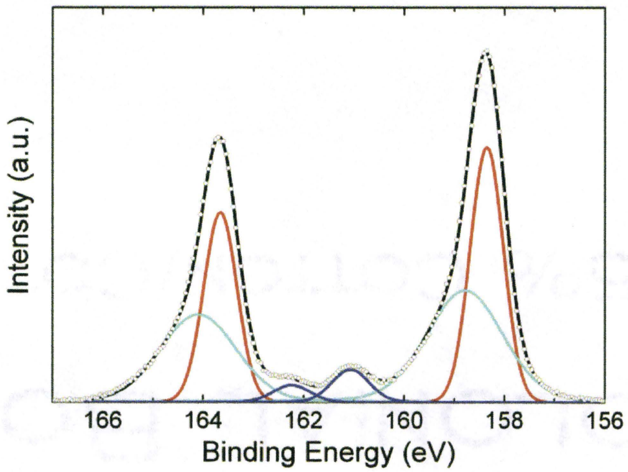

Figure 6.I.3.. Bi 4f XPS for flashed dropcast Bi_2S_3 bilayer film.

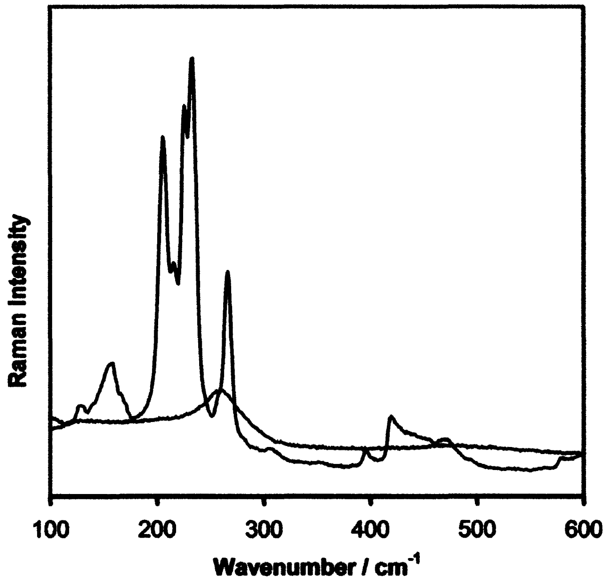

Figure 6.I.4. Un-normalized Raman spectra of a SWNT thin film prepared from oleylamine/THF solution (blue) and Bi_2S_3 nanowires obtained under the same conditions (red). The Raman intensity from Bi_2S_3 ultrathin nanowires is significantly less than that of carbon nanotubes within this region.

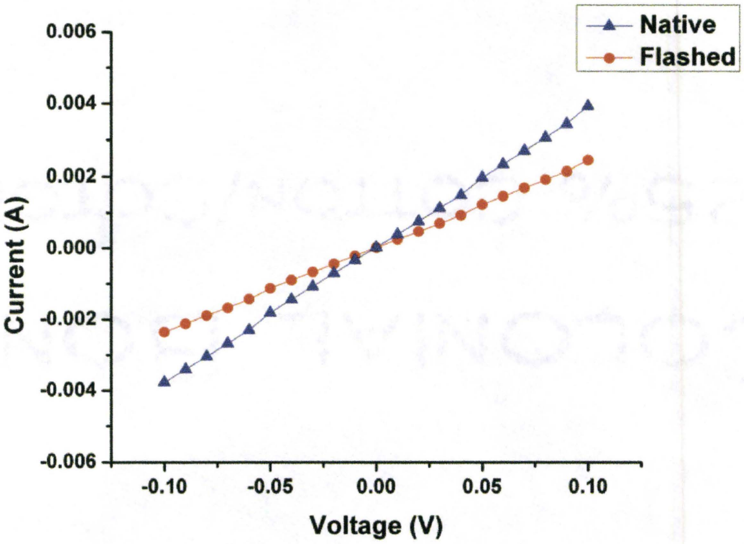

Figure 6.I.5. I-V curves for pre-flashed and post-flashed SWNT film on PTFE membrane.

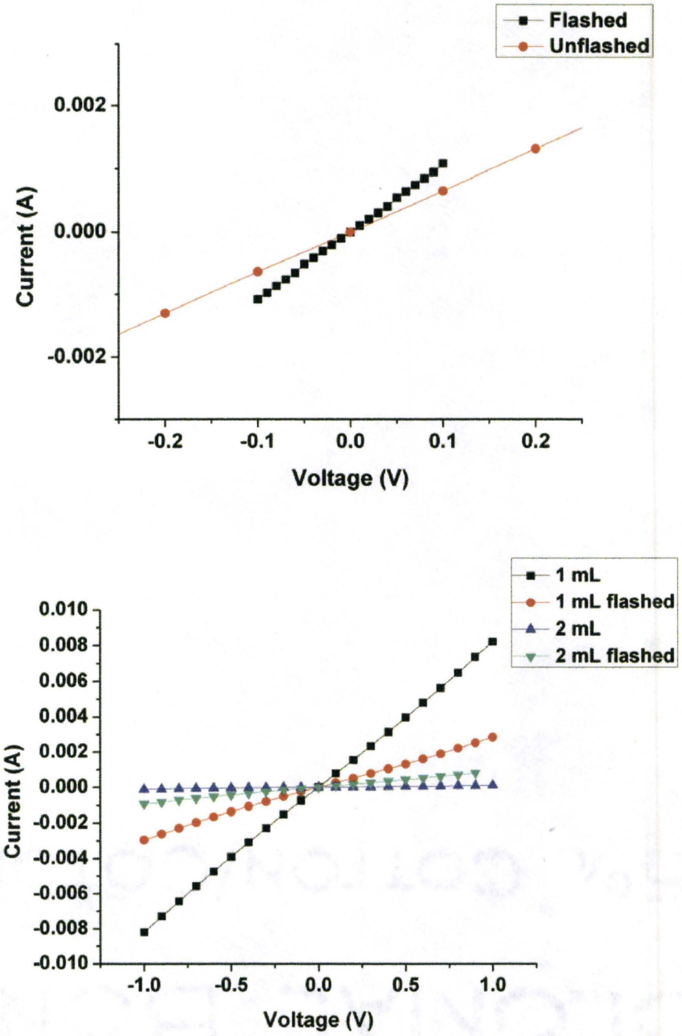

Figure 6.I.6. I-V curves for (A) 0.5 mL Bi_2S_3 bilayer film and (B) 1 mL and 2 mL Bi_2S_3 bilayer film (note scale difference).